BIOMECHANICS

American Society of Biomechanics

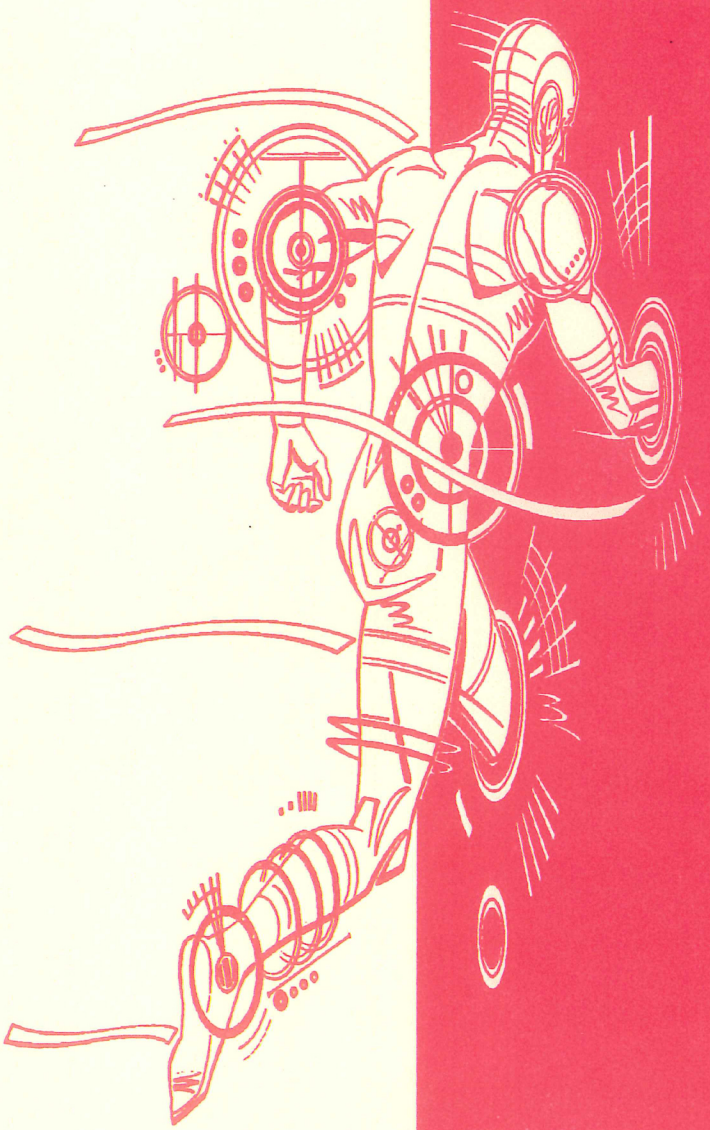

founded 1977

AMERICAN SOCIETY OF BIOMECHANICS

14th ANNUAL MEETING

University of Miami
Miami, Florida

November 14-16, 1990

Sponsors

American Society of Biomechanics

University of Miami

Department of Industrial Engineering

School of Continuing Studies
Office of Conferences and Institutes

PROCEEDINGS

AMERICAN SOCIETY OF BIOMECHANICS

14TH ANNUAL MEETING

BIOMECHANICS

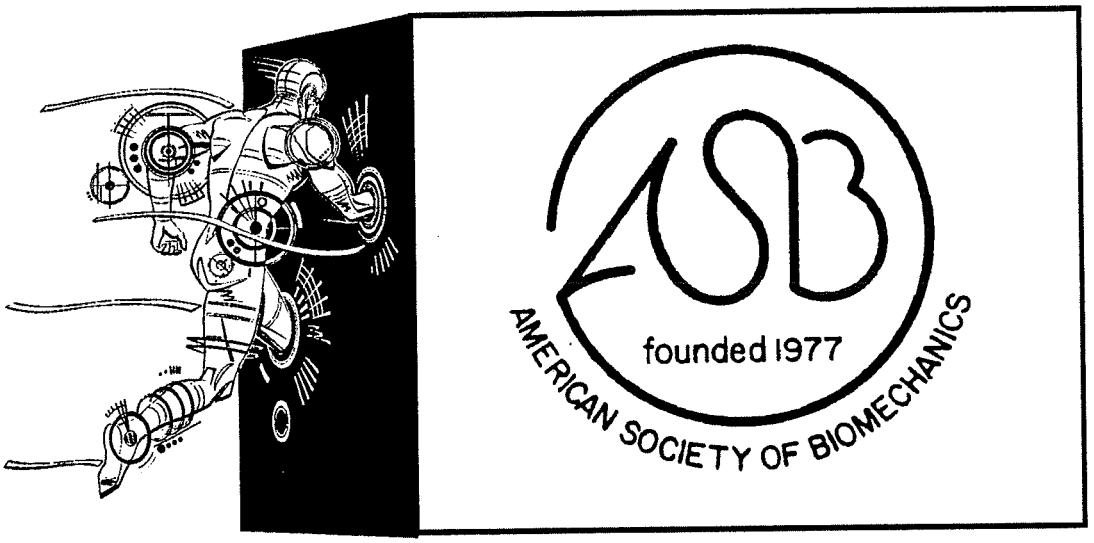

PROCEEDINGS FOR THE 14th ANNUAL M E E T I N G

University of Miami
Miami, Florida

November 14-16, 1990

Sponsors

American Society of Biomechanics

University of Miami

Department of Industrial Engineering

School of Continuing Studies
Office of Conferences and Institutes

TABLE OF CONTENTS

THE AMERICAN SOCIETY OF BIOMECHANICS

The American Society of Biomechanics was formed in 1977 to foster interaction among individuals in various disciplines in biomechanics research, such as anthropology, biology, engineering ergonomics, orthopedics, sport sciences, physiology, photogrammetry, rehabilitation, speech and hearing, sports medicine and zoology. In brief, Society members are persons applying the principles of mechanics to the study of biological systems. The Annual Meeting provides an opportunity to exchange information and to broaden perspectives on biomechanics in both formal and informal settings.

The Executive Board which has governed the Society during the past year comprises the following members.

President:
Roger M. Enoka
University of Arizona

Past-President
Nominating and Awards
Committees Chairperson:
Malcolm H. Pope
University of Vermont

President-Elect:
George T. Rab
University of California, Davis

Secretary/Treasurer:
Melissa G. Hoy
Palo Alto, VA Medical Center

Meeting Chairperson:
Tarek M. Khalil
University of Miami

Program Chairperson:
Edmund Y.S. Chao
Mayo Clinic

Program Chair-Elect:
Christopher L. Vaughan
Kluge Children's Rehabilitation Center

Membership Committee Chairperson:
Thomas D. Brown
University of Iowa

Education Committee Chairperson:
Mary M. Rodgers
Wright State University

Program Overview

14th Annual Meeting of the American Society of Biomechanics

WEDNESDAY, NOVEMBER 14

12:00-5:00 p.m.	Registration	Outside Ashe Auditorium/Third Level
2:00-6:00 p.m.	Poster/Exhibits set-up	Merrick I & II/Third Level
12:00-2:00 p.m.	Executive Committee Meeting	Gautier/Third Level
1:00-3:00 p.m.	Tutorial Session/ Muscle Modeling	Pearson I&II/Third Level
3:00-5:00 p.m.	Tutorial Session/Biomechanics Research...	Pearson I&II/Third Level
1:00-5:00 p.m.	Lab Tours	
1:00-3:00 p.m./3:00-5:00 p.m.	UM/Comprehensive Pain & Rehabilitation Center (CPRC)	
1:00-3:00 p.m./3:00-5:00 p.m.	UM/The Miami Project to Cure Paralysis	
	UM/RMSB Biomechanics Research Laboratory	
2:00-5:00 p.m.	Miami Children's Hospital/The Motion Laboratory	
	UM-Division of Physical Therapy/Steven J. Rose Center for Clinical Research	
	UM-Department of Industrial Engineering/Ergonomics Laboratory	
6:00-8:00 p.m.	Welcome Reception and cash bar	Promenade/Terrace Level

THURSDAY, NOVEMBER 15

6:30 a.m.-5:00 p.m.	Registration	Outside Ashe Auditorium/Third Level
6:30-7:50 a.m.	Posters/Exhibits set-up	Merrick I&II/Third Level
7:50-8:45 a.m.	Opening Session	Ashe Auditorium/Third Level
8:45-9:00 a.m.	ASB Young Scientist Award—Post-Doctoral	Ashe Auditorium/Third Level
9:00 a.m.-5:00 p.m.	Posters and Exhibits open	Merrick I&II/Third Level
9:00-10:15 a.m.	POSTER SESSION 1/EXHIBITS (All posters)	Merrick I&II/Third Level
10:15-10:30 a.m.	Coffee Break	Ashe Auditorium pre-function area/Third Level
10:30-11:30 a.m.	Session 1—BIOFLUID MECHANICS	Pearson I&II/Third Level
	Session 2—BONE #1	Ashe Auditorium/Third Level
11:30-1:00 p.m.	LUNCH - BORELLI LECTURE	Tuttle and Monroe/Terrace Level
1:00-2:45 p.m.	Session 3—LOCOMOTION	Pearson I&II/Third Level
	Session 4—MATERIALS AND DEVICES	Ashe Auditorium/Third Level
2:45-3:00 p.m.	Coffee Break	Ashe Auditorium pre-function area/Third level
3:00-3:45 p.m.	Plenary Session	Ashe Auditorium/Third Level
3:45-4:45 p.m.	Session 5—MUSCLE AND CONTROL	Ashe Auditorium/Third Level
	Session 6—EXERCISE AND SPORTS	Pearson I&II/Third Level
4:45-5:30 p.m.	POSTER SESSION 2/EXHIBITS (All posters)	Merrick I&II/Third Level
6:30-10:00 p.m.	Reception/Banquet	
6:30 p.m.	Meet in hotel lobby to board buses	
6:45 p.m.	Buses depart for banquet site, Crawdaddy's Restaurant	
10:15 p.m.	Buses return to hotel	

FRIDAY, NOVEMBER 16

7:00 a.m.-2:00 p.m.	Registration	Outside Ashe Auditorium/Third Level
8:00-8:45 a.m.	Plenary Session	Ashe Auditorium/Third Level
8:45-9:00 a.m.	ASB Young Scientist Award—Pre-Doctoral	Ashe Auditorium/Third Level
9:00-10:15 a.m.	Presidential Address and Business Meeting	Ashe Auditorium/Third Level
10:15-10:30 a.m.	Coffee Break	Ashe Auditorium pre-function area/Third Level
10:30-11:45 a.m.	Session 7—MEASUREMENT	Ashe Auditorium/Third Level
	Session 8—SPINE #1	Pearson I&II/Third Level
11:45 a.m.-1:00 p.m.	Lunch on your own	
12:00-1:00 p.m.	Executive Committee Meeting	Orchid C/Terrace Level
1:00-2:30 p.m.	Session 9—REHABILITATION	Ashe Auditorium/Third Level
	Session 10—SPINE #2	Pearson I&II/Third Level
2:30-2:45 p.m.	Coffee Break	Ashe Auditorium pre-function area/Third Level
2:45-4:45 p.m.	Session 11—MODELING	Ashe Auditorium/Third Level
	Session 12—ERGONOMICS	Pearson I&II/Third Level

END OF CONFERENCE

MATHEMATICAL MODELING OF TRANSPORT EXCHANGE IN THE MICROCIRCULATION

Keynote Address by
Eric P. Salathé
Director

Institute for Biomedical Engineering and Mathematical Biology
Lehigh University

EFFECT OF DEFECT SIZE ON THE STRESS CONCENTRATION AND FRACTURE CHARACTERISTICS FOR A TUBE WITH A TRANSVERSE HOLE UNDER TORSION

ASB Young Scientist Award—Post-Doctoral

By
R.F. Kuo

Biomechanics Laboratory
Mayo Clinic
Rochester, Minnesota

THE EFFECT OF DEFECT SIZE ON THE STRESS CONCENTRATION AND FRACTURE CHARACTERISTICS FOR A TUBE WITH A TRANSVERSE HOLE UNDER TORSION

R.F. Kuo, E.Y.S. Chao, K. Rim*, J.B. Park*
Biomechanics Laboratory, Department of Orthopaedics,
Mayo Clinic Rochester, MN 55905
*Department of Biomedical Engineering,
University of Iowa, Iowa City, IA 52242

INTRODUCTION

In the present study, tubular models with transverse circular defects were carefully examined by both experimental and finite element techniques. Both single and double-cortex penetration were considered. The torsional fracture pattern and fracture torque were obtained from torsional fracture tests; stress concentration factors were calculated by finite element analyses. The effect of defect size on the location of the maximum stress point was examined from the resulting fracture path. By incorporating the strain energy density criterion in the finite element analysis, the fracture toughness associated with a unique defect was explored.

METHODOLOGY

Experimental Model A commercially available cast acrylic rod was machined into tubular structures with six defect ratios (d/D) from 10 to 60%. The outer and inner tube diameters were 31.75 mm and 19.05 mm, respectively. To eliminate residual stress, all specimens were annealed in an oven before testing at a temperature of 160°F for 24 hours, followed by slow cooling. Fracture testing of the acrylic specimens was then performed on an MTS machine under a high of twisting, 10°/sec. Prior to the mechanical testing, a 45° helical curve was marked on each tube to provide a reference line to determine the location of the fracture path for a particular defect ratio, d/D. To identify the shifting of the maximum stress location, elastic torsional strain measurements were designed for the d/D = 60% specimen using six 120° strain gage rosettes along two 45° spiral helix paths on the tube surface. Tensile tests were performed on the acrylic specimens to generate elastic material properties for finite element modeling, Young's modulus (E=2.25 GPa), Poisson's ratio (v=0.34) and data for the critical strain energy density. The critical strain energy density was obtained by integrating the area under the true stress and strain curve.

Finite Element Model The range of the defect ratios included in the linear elastic finite element analysis were 10, 20, 30 and 40%. Models were composed of twenty node quadratic isoparametric solid elements with a model length of 99.75 mm.

A) Global modeling - Stress concentration factors were determined by applying a 1 N-m torque to the top of the model while the bottom remained fixed. Evaluation of the fracture toughness was performed by application of the failure torques obtained from mechanical testing as the model loading conditions.

B) Local modeling - Utilizing the specified boundary displacement method, stress recovery was performed on a localized portion of the model centered around the defect.

Strain Energy Density Criterion(1) For a linear isotropic material the critical strain energy density factor S_c was defined as $S_c = r_c * (dW/dV)_c$...(a). The length parameter, r, represents the arc length along the fracture path with its origin at the defect. By incorporating the known value of $(dW/dV)_c$ from tensile testing along with its associated SED distribution along the fracture path determined by finite element analysis, the value of critical length r_c was determined. Solving for the unknown S_c in equation (a) and substituting S_c into equation (b), one can solve for K_{IC}, $K_{IC} = 2*\Pi*E*S_c/(1+v)(1-2v)$...(b).

RESULTS AND DISCUSSION

The location of the maximum stress point shifts parallel to the 45° helix with increasing defect size. An illustration of the shift in the fracture helix path is shown in Figure 1. By measuring the shift angle associated with each unique defect size, a linear relationship, $\Delta\theta = -6.28+0.55*(d/D)$, was determined. The threshold value of d/D at which shifting was initiated in the acrylic tubular models was calculated as 11.3%. Results from elastic torsional strain measurement support the initial findings; the shift in location of the peak stress is strongly influenced by defect size. This indicates that the amount of parallel shifting is proportional to the amount of material loss which is directly related to the defect size. The amount of helical shifting as a function of the wall thickness still remains unanswered. Table 1 shows the stress concentration factor, Kg, as a function of defect size. Enlarging the defect size results in a direct increase of Kg. It is also interesting to note that no significant change in Kg was determined in the comparison of single and double-cortex tube defects. Finally, fracture toughness values were obtained based on a selected deformation rate of 100 mm/min. In Table 1 finite element results show the increasing trend of the K_{IC} values associated with the four defect sizes demonstrating a greater resistance to crack growth for larger defect sizes. This may be due to the curvature of the hole which is related to the material loss associated with defect size.

Table 1

	Single-Cortex		Double-cortex	Fracture Torque
d/D	Kg	K_{IC}	Kg	Tmax (N-m)
0.1	3.78	61.8	3.75(3.71)*	230.2±3.6**(n=3)
0.2	4.39	74.5	---	204.4±10.4 (n=5)
0.3	4.95	78.8	4.99(4.59)*	184.6±10.3 (n=5)
0.4	5.28	89.7	---	178.3±4.7 (n=4)

* Data in Parentheses are from Jessop's results.(2)
** Values presented as mean±S.D.

Figure 1

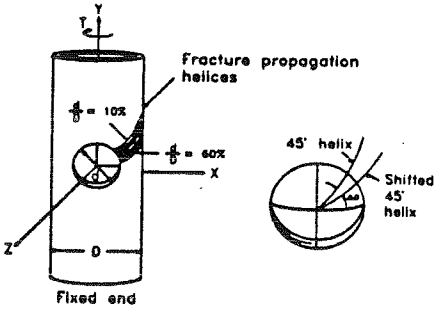

REFERENCES

1.Sih G.C. and Oliveria Faria Lde (1984) Fracture Mechanics Methodology. Martinus Nijhoff Publishers, The Hague.
2.Jessop H.T., Snell J. and Allison J.M. (1959) The Stress Concentration Factors in Cylindrical Tubes with Transverse Circular Holes. Aeronaut. Q. 10, 326-344.

SESSION 1

BIOFLUID MECHANICS

AN EXPERIMENT SHOWING LATERAL DRIFT OF PLATELET-SIZED BODIES IN FLOWING BLOOD

C.-J. Yeh and E.C. Eckstein
Department of Biomedical Engineering, P.O. Box 248294
University of Miami, Coral Gables, FL 33124

INTRODUCTION

The scale and nature of platelet transport depend greatly upon whether the suspension contains red cells. The use of augmented diffusion coefficients for blood flows is a well-known illustration of this point. Near-wall excesses of platelets or platelet-sized latex beads are observed during the flow of blood suspensions through small tubes; these also occur because of lateral motions induced by red cells. Such excesses are limited by the diffusion of material away from the peak. To form a near-wall excess, some lateral platelet motions must have a preferential direction. The purpose of this paper is to show an experimental technique that illustrates the scale of the directed lateral motions of platelets that are caused by flow-induced interactions with the red cells.

REVIEW AND THEORY

Platelet transport in blood flow is highly influenced by interactions of platelets with red cells. The importance of such interactions to diffusive motion of platelet is well recognized; see, e.g., the review of hemorheology by Goldsmith and Turitto (1). Commonly, interactions with blood cells cause a diffusion coefficient that is two or more orders of magnitude greater than the Brownian diffusivity. Since diffusive motions are small, studies of transport of dilute suspensions often emphasize the non-random, directed lateral motion of the species. A particularly classic example for rigid particles is the tubular pinch effect (aka the Serge-Silberberg effect) that describes the tendency of particles in flows with small amounts of inertia to accumulate at a position located 60% of the radius from the central axis. For flexible particles, the centerline is the preferred position for accumulation in tube flow. Blood, being a suspension of particles of different properties (flexible red cells and smaller, relatively rigid platelets), exhibits a more complex effect. Near-wall excesses of platelet-sized particles occur for many rheological conditions (2).

METHODOLOGY

Major elements of the freeze-capture method (2) were used for the experiments reported here. Briefly, a flow of blood suspension was established, and the tube and blood were rapidly frozen by pouring liquid nitrogen over the tube. Segments of frozen tube were mounted in a cryomicrotome on a fluorescence microscope and sectioned; images of the freshly exposed surface were collected. The platelets or platelet-sized latex beads were readily found in the images because they were the only fluorescent objects in the blood suspension. The least distance from the tube wall to each fluorescent object was measured and added to a list. A kernel estimate technique was used to determine the radial probability density of fluorescent objects from the list of measured distances. The concentration profile was calculated from the probability density.

To allow flow of suspension with marker particles into a tube that previously conveyed suspension without marker particles, a two chamber stirred reservoir was used. The reservoir walls included resealing rubber diaphragms. The end of the tube through which blood flowed was mounted in a short length of needle. Initially the needle and tube passed through the diaphragms and the near chamber so that the tube entrance was in the far chamber, which was filled with suspension without fluorescently platelet analogues. The near chamber contained suspension with the analogues. The two chambers had suspensions of identical hematocrit. Note that this chamber/flow protocol avoids any transient effects

due to difference of hematocrit. The suspension characteristics are equal except for the presence of the fluorescent tracer particles. Suspensions of zero hematocrit were used as a control. The flow rate in the tube was set by a syringe pump operating in withdrawal mode; a wall shear rate of 800 s^{-1} was used. Tubes of approximately 200 μm i.d. and 55 cm length were used. Steady flow from the far chamber without platelet analogues was allowed for a period of 30 minutes. The needle and tube were then pulled into the near chamber and the tube was frozen after 15 to 25 seconds of flow. This time of flow permitted a tongue of labelled suspension to move into the tube. Segments of tube were collected at axial locations that corresponded to deciles of the maximum distance the tongue could extend into the tube (marked on the figure as % tube length). Concentration profiles were determined in a fashion similar to our prior work (2).

RESULTS AND DISCUSSION

Typical profiles for three locations are shown in the adjacent figure. Without red cells (dashed lines), the expected events occur: the tongue moves in, and at stations further from the entrance, the tongue has not had enough time to diffusively spread to the wall. When there are red cells (solid lines), a much different set of profiles occurs. These profiles exhibit near-wall excesses. The tongue of labelled fluid extends a shorter distance into the tube when the suspension contains red cells; this outcome is due to a combination of blunted velocity profile, red-cell-enhanced diffusion, and the directed lateral motions that cause the near-wall excess.

CONCLUSION

The experiments indicated that flow-induced interactions of platelets with red cells caused directed as well as random lateral motions. These motions are directed to the site of the peaks observed in the steady flow of similar suspensions through similar tubes.

1. Goldsmith HL, Turitto, VT Thromb. and Haemostasis 55:415 1986
2. Bilsker DL, et. al. Biorheology 26:1031 1989

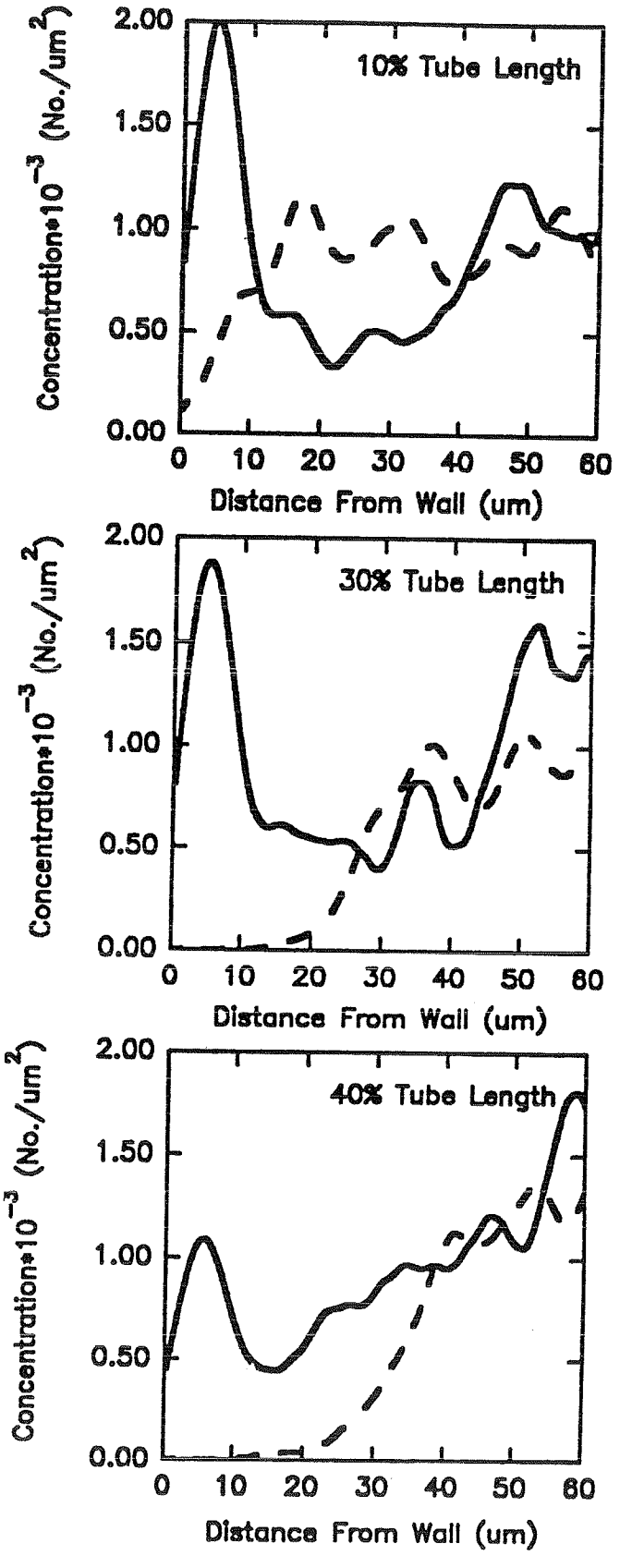

COMPARISON OF MARROW FLUID PRESSURES VS TIME IN CORED AND UNCORED FEMORAL HEADS - AN ANALYTICAL SOLUTION

R.H. Kufahl and S. Saha
Department of Orthoapedic Surgery, LSU Medical Center
P.O. Box 33932, Shreveport, LA 71130

INTRODUCTION

One possible cause of avascular necrosis of the femoral head is an increase in the fat cell volume in bone marrow. The subsequent increase in pressure within the femoral head can cause the collapse of the veins draining the femoral head. This loss of blood supply causes bone cell death. High femoral head pressures are relieved by drilling a hole through the femoral neck into the femoral head.

THEORY

The equation governing fluid pressure (P) in bone marrow is derived and solved analytically for the cases of a cored and uncored femoral head. The laws which govern fluid pressure in the marrow are: (1) conservation of volume for an incompressible fluid: $-dq/dx = de/dt$ where q = flow rate/(total) area and e = fluid vol./(total) vol., (2) Darcy's law: $q = -k/\mu\, dP/dx$ where K = permeability and μ = fluid viscosity, (3) Stress-strain relation: $de = \phi\varepsilon$ where $\varepsilon = \Delta L/L$ (longitudinal) strain and ϕ = percent of total cross sectional area occupied by the fluid. Replacing ε by Hook's law $\sigma = \varepsilon/E$ where E = longitudinal stiffness of the cancellous bone and σ is the longitudinal stress in the cancellous bone. Even though the fluid is incompressible, e can increase at the expense of collapsing the small veins in the marrow. (4) Equilibrium: $s = (1-\phi)\sigma + \sigma P$ where S is the applied compressive stress. Combining these four relations the equation governing fluid pressure is obtained:

$$-dP/dt = (1-\phi)KE/(\phi^2\mu)d^2P/dx^2 \qquad (5)$$

This equation is solved for two geometries: (A) an uncored cylinder impervious to fluid flow on all sides except for the bottom face which is maintained at 0 pressure and (B) a cored cylinder whose hole along the cylinder axis is maintained at 0 pressure. For an applied compressive stress S, the inital pressure developed in the incompressible fluid is given by: $P(t=0, x>0) = \phi S/3$. The solution to eq. (5) for the pressure in an uncored cylinder is (A):

$$P(X,t) = \frac{4S\phi}{\pi} \sum_{n=odd}^{\infty} 1/n \; EXP(-n^2 t/t_c) \; SIN(n\pi X/(2L)) \qquad (6)$$

L = cylinder height and $t_c = 4L^2\mu\phi^2/(\pi^2 KE(1-\phi))$

The solution for the pressure in the cored cylinder is expressed in terms of Bessel functions (J_0, J_1, Y_0) and is given by (B):

$$P(r,t) = \pi \sum_{n=1}^{\infty} \frac{J_1^2(\lambda_n m) V_o(\lambda_n r/r_i)}{J_o^2(\lambda_n) - J_1^2(\lambda_n m)} \text{EXP}(-\lambda_n^2 at/r_i) \qquad (7)$$

where $V_o(\lambda_n r) = J_o(\lambda_n r)Y_o(\lambda_n r_i) - J_o(\lambda_n r_i)Y_o(\lambda_n r)$

and λ_n are the roots of

$$J_1(\lambda r_o)Y_o(\lambda r_i) - J_o(\lambda r_i)Y_1(\lambda r_o) = 0$$

and $m = r_o/r_i$ and $a = (1-\phi)KE/(\mu\phi^2)$

RESULTS

Figure 1 compares the maximum bone marrow fluid pressure vs time in the cored and uncored femoral heads. The maximum fluid pressure occurs at the impervious cortical bone, which corresonds to the clinical finding that the blockage of veneous drainage occurs near the cortical bone. The much faster rate of decay of fluid pressure in the cored femoral head is due to the shorter distance (L) from the cortical shell to the low pressure core. The solution (6) shows that the time constant t_c is a sensitive functin (L^2) of the distance from the cortical bone to the closest low pressure region. A clinical application of this finding would be to replace a single large core in the femoral head by smaller diameter holes.

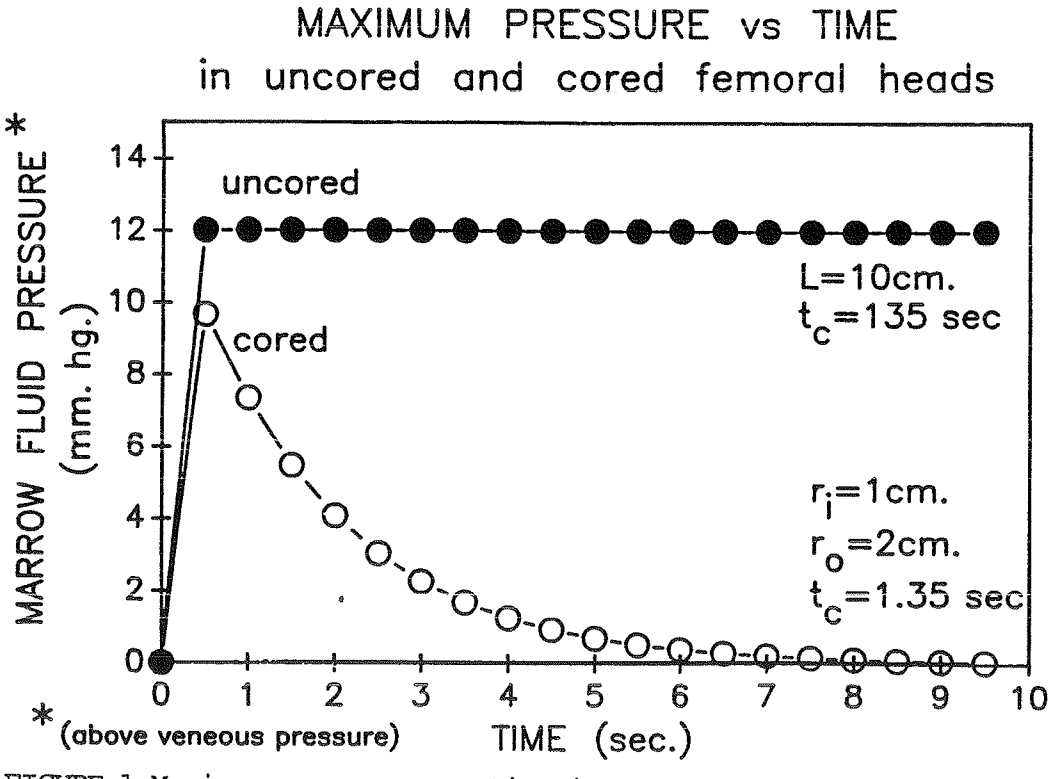

FIGURE 1 Maximum pressure vs. time in cored and uncored femoral heads

A FLUID MECHANICAL MODEL OF CYTOKINESIS IN ANIMAL CELLS

Metin Ger and Nuri Akkas
Department of Engineering Sciences
Middle East Technical University, Ankara, Turkey

INTRODUCTION

The cortical layer, enveloping cells, contains microfilaments and microtubules. It is treated as an elastic or viscoelastic membrane (Akkas 1980,1981). Yoneda (1973) treats the cell as a liquid drop. There are tension elements uniformly distributed over the cell surface before cleavage begins (Greenspan 1977). As the uniformity of the surface tension is disturbed, the elements move towards the equatorial surface and cleavage starts. Once triggered, it is completed without further stimulus. Greenspan's work is concerned with cleavage initiation. Here we will study if a fluid disc can be divided into two completely by a constricting agent applied around its equator.

METHODOLOGY

A disc of incompressible viscous fluid is immersed in another viscous fluid. The disc's peripheral zone (PZ), with a thickness of 5% of the disc radius, separates the interior zone (IZ) from the exterior zone (EZ). The viscosity of the IZ is twice that of the EZ. Effect of the viscosity of the PZ will be studied. The penalty-finite element method is used to analyse the disc subjected to a constant equatorial rate of strain. The total area of the dividing disc remains constant in accordance with the well-accepted fact in animal cell cleavage. The finite element grid is shown in Fig. 1. The pressure is constant on the outermost boundary. The numerical results do not differ significantly when the EZ is discarded and the constant pressure condition is applied at the surface nodes of the PZ.

RESULTS AND DISCUSSION

Figure 2 shows the dividing disc when the PZ has a uniform viscosity which is six times that of the EZ. Figure 3 is for the same problem; now the uniform PZ viscosity is ten times that of the EZ. The general trend of the shapes in Figs. 2 and 3 is named the "pointed form". This form becomes more pronounced as the uniform PZ viscosity increases. For a flatter shape, a nonuniform viscosity must be given to the PZ. The case in which the viscosity of the polar region of the PZ is ten times that of the EZ and the viscosity of its equatorial region is six times that of the EZ is shown in Fig. 4. The case in which the viscosities of the polar and equatorial regions of the PZ are interchanged is shown in Fig. 5. The general trend of the shapes shown in Figs. 4 and 5 is named the "rounded form". A dividing animal cell has a rounded form. The pointed and rounded forms are compared in terms of their polar displacements in Fig. 6. The rate of polar displacements is almost constant for the cases with rounded form. The polar displacements demonstrate a stepwise increase in time, implying an instability phenomenon, for the cases with pointed form.

Ackowledgement. The second author acknowledges the NATO grant 87/342.

REFERENCES

Akkas,N., J.Biomechanics, 13, 977-988, 1980.
Akkas,N., J.Biomechanics, 14, 621-631, 1981.
Greenspan,H.P., J.theor.Biol., 65, 79-99, 1977.
Yoneda,M., Adv. Biophys., 4, 153-190, 1973.

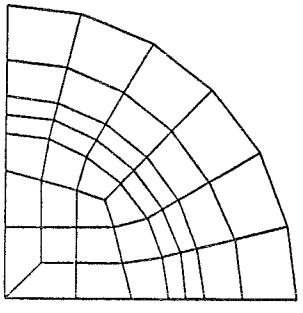

Fig.1

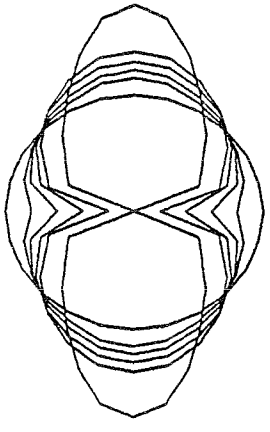

Fig.2

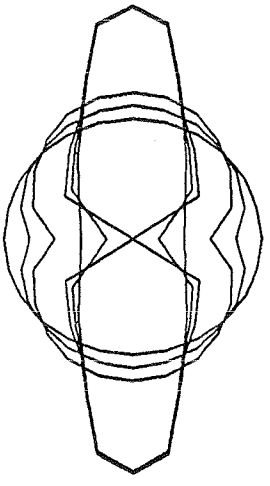

Fig.3

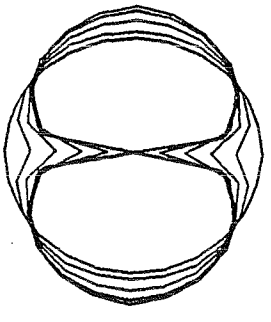

Fig.4

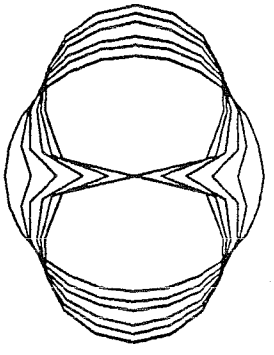

Fig.5

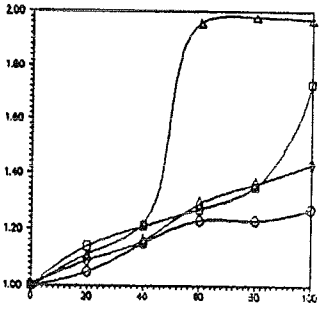

Fig.6

Fig. 1. The finite element grid.
Fig. 2. The uniform PZ viscosity is six times that of the EZ.
Fig. 3. The uniform PZ viscosity is ten times that of the EZ.
Fig. 4. The PZ has nonuniform viscosity. The ratio between the viscosities of the polar and equatorial regions is 10/6.
Fig. 5. The PZ has nonuniform viscosity. The ratio between the viscosities of the polar and equatorial regions is 6/10.
Fig. 6. The polar displacements of the pointed and rounded forms as a function of time.

HYDRODYNAMICS OF TURTLES

W.R. Krause, A.J. Beaudoin, C. Krause, and J. Keinath
Medical College of Virginia and VA Institute of Marine Science

Introduction

The turtle is one of the oldest living species of animals on the earth today. The turtle's longevity results from its hard outer skeletal structure that has protected this species from its enemies and predators over millions of years. The shell's primary function is for protection, however it must also be hydrodynamic. A hydrodynamic shape helps the turtle move through the water with ease and mobility whether the turtle is escaping from oncoming death by predator or traveling to another area to feed or migrate. The shell of a turtle plays a role in the turtle's way of survival and its way of travel. Having the shell in a shape designed to give lift may help reduce the energy expenditure of the turtle as it moves through the water.

Davenport, Munks, and Oxford [1] performed an experiment comparing the swimming forces of marine and freshwater turtles. The average thrust over five seconds was 0.67±0.21 N for the marine Green turtle (Chelonia mydas), 0.45±0.22 N for the freshwater Caspian terrapin (Mauremys caspica), and 0.26±0.20 N for the freshwater Red Eared Slider (Chrysemys scripta). They hypothesized that the shell has a hydrofoil characteristic and functions to some extent as a lifting body.

Wyneken [2] studied the comparative and functional considerations of locomotion in six hatchling Green turtles (Chelonia mydas) and four hatchling Loggerhead turtles (Caretta caretta). Each turtle was attached to a brass rod which was attached to an aluminum force beam in a flow tank to determine the lift and drag forces. Analysis of the results showed that slight differences in body design can result in significant hydrodynamic differences. Green turtles had significantly higher lift and drag coefficients than did loggerheads.

Methods and Materials

Shells from a Yellow Bellied Slider (Trachemys Scripta Scripta) and a Red Bellied Turtle (Pseudemys Rubrivetris Rubrivetris) were obtained. Molds were made from both the carapace (top) and plastron (bottom) shells and a clay model of the turtle was made. A preserved male Red Bellied Slider (Pseudemys Rubriventris Rubriventris) was also obtained for evaluation. The turtle shell model was placed on a force transducer in a flow tank at two water velocities (0.23 and 0.46 m/s) and six angles of attack (-5,0,5,10,15,20 deg). The transducer was connected to an A/D board in a IBM PC/AT computer. The lift and drag forces were measured at two velocities, 0.23 and 0.46 m/s.

An FEM model of the preserved Red Bellied Slider was made and run using the FIDAP program [3]. The pressure distribution and velocity vectors and streamlines about the turtle were determined for the experimental conditions.

Results and Conclusion

Both the Yellow and Red Bellied Slider models showed an increasing lift force as the angles increased at the higher velocity of water (0.461 m/s), Figure 1. At the lower velocity (0.229 m/s) the results of the lift force gradually decreased as the angles increased. The drag force increased at the higher velocity (0.461 m/s) from 10.0 to 16.0 N as the angles increased. At the slower velocity (0.229 m/s) the drag force gradually increased slightly with an increase in angle.

The results for the preserved male Red Bellied Slider also showed similar trends. The lift force at the higher velocity (0.461 m/s) increased as the angle increased. At the slower velocity (0.229 m/s) the lift force showed an erratic variation but had an overall increase with increasing angle. The drag force gradually increased at the higher velocity (0.461 m/s) in a curve from 1.0 to 17.5 N. At the slower velocity (0.229 m/s) the drag force gradually increased. The results from the FEM analysis, Fig. 2, shows a negative pressure (shaded area) and higher velocities along the carapace and generally a positive pressure and lower velocities along the plastron.

The conclusions of this study, supported with an FEM analysis, indicate that the turtle shell does act as a hydrofoil creating lift.

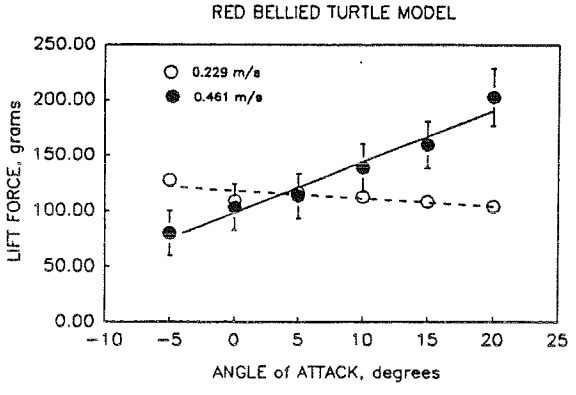

Fig. 1 Lift forces of the Red Bellied Slider.

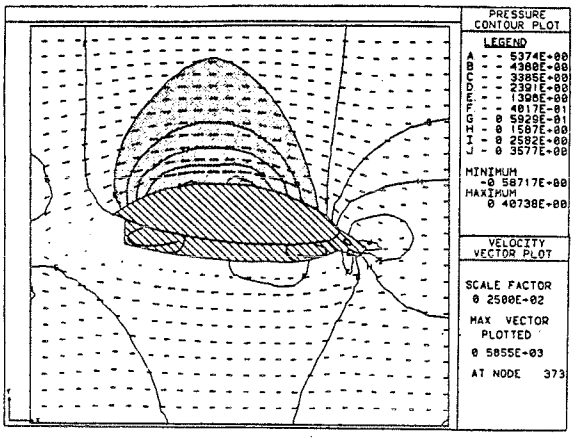

Fig. 2 Velocity and Pressure Distributions

References:

1. Davenport, J., Munks, S.A., and Oxford, P.J.: A Comparison of the swimming of Marine and Freshwater Turtles. Proc. Roy. Soc. Lond. B. 220:447-475, 1984.

2. Wyneken, J.: Comparative and Functional Considerations of Locomotion in Turtles. Ph.D. Thesis, Univ of Illinois at Urbana-Champaign, 1988.

3. FIDAP, Fluid Dynamics Int., Evanston, IL

SESSION 2

BONE #1

PREDICTING TRABECULAR BONE INGROWTH PATTERNS USING A STRUCTURAL TOPOLOGY OPTIMIZATION SCHEME

S.J. Hollister, N. Kikuchi*, K. Suzuki*, and S. A. Goldstein

Biomechanics, Trauma, & Sports Medicine Laboratory, Section of Orthopaedic Surgery, and *Department of Mechanical Engineering & Applied Mechanics, The University of Michigan, Ann Arbor, MI 48109

INTRODUCTION: Porous coating has become increasingly popular as an alternative to cement for total joint fixation. While it is widely believed that the interface mechanics will influence bone ingrowth, little is known about how trabecular bone adapts to the mechanical environment in the porous coated interface. The purpose of this paper is to present predictions of bone ingrowth using a recently developed structural topology optimization program developed by Bendsoe and Kikuchi (1988).

BACKGROUND: The physiological processes of the interface region are generally considered to be similar to a fracture healing response. The large changes in bone structure during fracture healing have been hypothesized to follow a structural optimization scheme (Wolff 1892). Based on this hypothesis, the structural topology optimization scheme of Bendsoe and Kikuchi was used to predict bone ingrowth patterns in two dimensional models of porous coated implant interfaces. This scheme assumes that the structure is composed of small microstructural voids which determine the average or apparent structural compliance. The structural compliance, calculated from a finite element model, is updated by changing both the density and orientation of the microstructure. The final shape of the structure is shown by plotting a density map on the original finite element mesh of the structure.

METHODS: Predictions of bone ingrowth patterns using the topology optimization program were performed for two different animal models. The first was the *in vivo* remodeling implant model of Goldstein and associates (1986) which has a cylindrical geometry with a flat porous coated loading surface. The second animal model utilized a prothesis with multiple porous coated cone projections implanted in the canine tibia (Goldstein et al, 1989). The initial meshes modeled the implants as symmetric. The surrounding trabecular bone was modeled as idealized struts with fixed displacements and the implants were loaded under uniform compression. Parametric studies of boundary stiffness and loading conditions were performed to assess how these variables affected bone ingrowth.

RESULTS: The results for the prosthesis are shown in Fig. 1 along with an SEM photograph of the experimental ingrowth. The optimization program predicted general bone apposition along the bottom of the cone and some bone ingrowth within the porous layer along the lower one third of the cone side. The predicted ingrowth shows very good agreement with experimental results where bone appostion and ingrowth is seen primarily in the bottom one third of the cone. The prediction of ingrowth for the flat cylindrical loading piston were also consistent with experimental results (Fig. 2), although the model did not predict as much depth of ingrowth as was found experimentally. Changing the boundary conditions from being fixed to elastic springs changed the distribution of bone apposition, although the general pattern remained the same. For the instancone model, reduction in boundary stiffness caused ingrowth to be distributed along a greater portion of the cone. The effect of boundary stiffness was much less significant for the flat piston. Different loading conditions also changed the ingrowth pattern slightly, but their effect was not as significant as either the implant geometry or trabecular boundary conditions for the two models.

DISCUSSION: The good agreement between predicted and experimental ingrowth patterns suggest that trabecular bone adaptation in the porous coated region may follow some

structural optimization scheme. Validation with experimental ingrowth results adds confidence that this microstructural modeling procedure may be used to evaluate the potential of different implant designs for inducing bone ingrowth. Initial evaluation of two implant designs shows that implant geometry is the most important mechanical variable for determining ingrowth pattern. The cone interface of the instacone prosthesis imposes multiaxial stress fields on the surrounding bone which is more conducive to bone ingrowth than the more uniaxial stress fields imposed by the flat ended implant geometry. Stiffness of the surrounding trabecular bone and implant loading conditions play a secondary but nonetheless important role in determining bone ingrowth. The results of both models showed that boundary conditions may moderately effect ingrowth distribution, which suggests that the density of the surrounding trabecular bone may influence the ingrowth patterns in different parts of the implant. The loading conditions had the least effect of the three variables on the predicted ingrowth pattern.

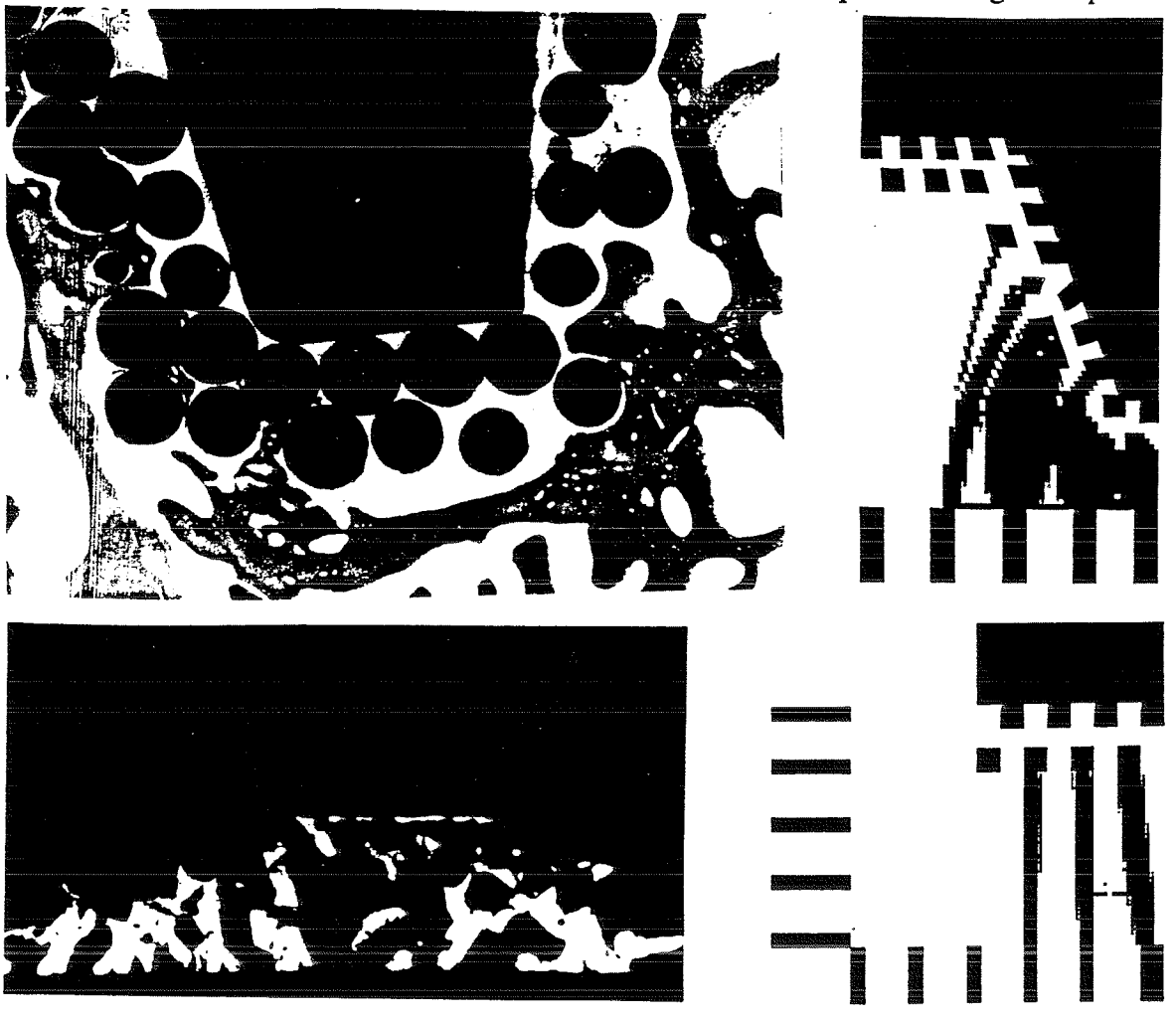

Figures 1 and 2. Figure 1 above shows the experimental and predicted ingrowth patterns for the conic prosthesis. Figure 2 shows the experimental and predicted ingrowth patterns for the flat ended implant. In the plot of predicted ingrowth, dark areas are solid material and white areas are fibrous tissue.

REFERENCES: 1) Bendsoe, MP & Kikuchi, N (1988), Com. Meth. App. Mech. Eng., 71:197 - 224; 2) Goldstein SA et al (1986), Trans 32nd ORS, p. 432; 3) Goldstein SA et al, ASME AMD-48, p. 289-290. 4) Wolff, The Law of Bone Transformation,1892. **Acknowledgements:** We wish to thank Fred Champlain and Rob Goulet for their assistance. Support was provided by the NIH(AR 34399, AR 31793, AR 20557).

EFFECTS OF AGE AND SEX ON THE STRENGTH AND CROSS-SECTIONAL GEOMETRY OF THE FEMUR SHAFT IN RHESUS MONKEYS

R.B. Martin
Orthopaedic Research Laboratory
University of California at Davis
Davis, CA 95616

INTRODUCTION: Macaque mulatta monkeys, being primates, may be especially useful as models for human skeletal problems. This possibility has not been fully tested, however, and there is relatively little data on macaque bone physiology and biomechanics. This study analyzed the bending strength of 54 macaque femurs as a function of age and sex. It was found that female femurs are weaker than male femurs, and that femur strength is well correlated with body weight. The bending strength and cross-sectional moment of inertia of male femurs peaks at 6 years of age, then declines significantly with age. This senile diminishment in strength is contrary to the situation in modern American men, raising some question as to the suitability of this species for studies of senile osteoporosis, and underscoring the importance of using age-matched controls in various experiments involving the rhesus femur.

REVIEW AND THEORY: It has previously been established that the cross-sectional geometry of the human femur shaft changes with age in ways which significantly affect the diaphyseal bending and torsional strength [2]. For example, in modern American men, periosteal apposition causes cross-sectional moment of inertia (CSMI) to increase with age, effectively compensating for endosteal resorption and diminished material strength of the cortical bone. Such compensation is not sufficient in the female cohort because resorption on the endosteal surface is too great to be balanced by periosteal apposition. In other populations, compensatory radial expansion may or may not maintain bone strength in aging men [3,4,5]. Whether or not such effects occur in rhesus monkeys is of interest to physical anthropologists, and because these animals are often suggested as a superior experimental model for human skeletal biology because the two species are primates. In order to properly plan and interpret the data from such experiments, it is important to understand the relationships between age, sex, and femoral geometry and strength in this animal. The limited amount of information available for the macaque femur is not sufficient to answer these questions [1].

METHODOLOGY: Fifty-four femurs were obtained from 16 male and 22 female rhesus monkeys ranging in age from newborn to 20.8 years. Four of these animals had been controls in experiments at the NASA/Ames Research Center and the remainder were obtained from the California Primate Center at Davis. Each femur was tested to failure at the midshaft in quasistatic three point bending. Subsequently, the fractured bone was reassembled and a 100 micron thick cross-section was prepared and stained with tetrachrome. This cross-section was digitized and its CSMI was computed with respect to the antero-posterior (I_{AP}) and medio-lateral directions (I_{ML}); the

mean of these values was also computed (I_{AV}). These variables were related to age and sex using analysis of variance and regression analysis.

RESULTS: Figure 1 shows the relationship between femoral shaft bending strength and age. There was a sigmoidal increase in femoral strength as the juvenile animals aged. The male femurs were stronger than the female femurs at intermediate ages, exhibiting maximum strength at about six years of age. After age 6, there was a significant decline in male femoral yield ($r = 0.72$, $p < 0.01$) and failure ($r = 0.64$, $p < 0.05$) strength, as well as mean CSMI ($r = 0.68$, $p < 0.05$). There was not a significant age-related change in work-to-failure.
When male and female animals were pooled, yield and failure strengths correlated similarly with I_{AP}, I_{ML}, and I_{AV} (r about 0.90, $p < 0.01$). Body weight was nearly as good a predictor of bending strength as CSMI ($r \geq 0.85$). CSMI and body weight were poor predictors of work-to-failure, however.

DISCUSSION: It is important to remember that three point bending of whole bones involves large shear stresses; however, such data may serve as an index of strength with respect to species, sex, and age.
The lack of female specimens at intermediate ages makes it impossible to know whether the female strength-age curve also peaks at about age 6, or increases more linearly with age. It is certain, however, that male femoral strength and CSMI diminish with age in adult macaques. This behavior appears to be contrary to that found in the femurs of modern American men, and more similar to that seen in the their female counterparts, who experience excessive endosteal resorption [3]. At this point it is unclear whether this difference, or that between modern American men and Eskimo men, is determined primarily by endosteal resorption or another factor, and by genetic or epigenetic influences. Correlated studies of macaque femoral biomechanics and remodeling may help to resolve these questions and the extent to which rhesus monkeys may serve as models for human skeletal problems.

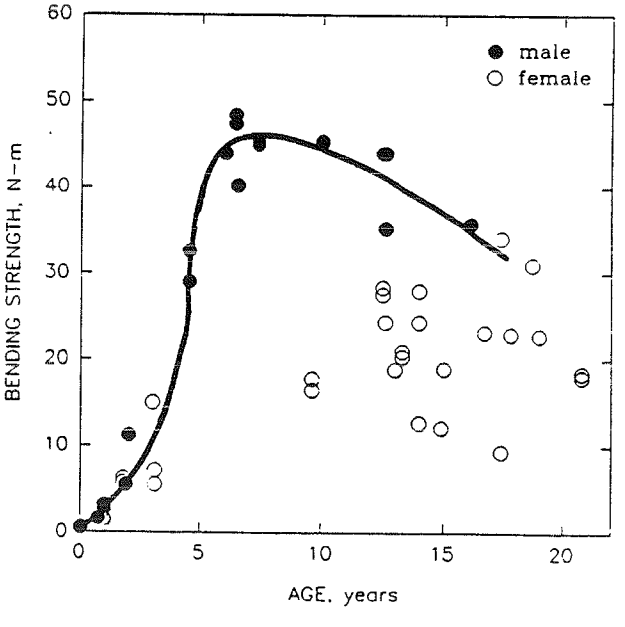

REFERENCES: **1.** DeRousseau, CJ, Amer J Phys Anthrop, 68:157-17, 1985. **2.** Martin, RB, et al, Clin Orthop, 149:268-282, 1980. **3.** Martin, RB, et al, Amer J Phys Anthrop, 67:371-380, 1985. **4.** Ruff, CB, & Hayes, WC, Amer J Phys Anthrop, 60:383-400, 1983. **5.** Ruff, CB, & Hayes, WC, J Orthop Res, 6:886-896, 1988.

Fluoride ion effect on interfacial bonding and mechanical properties of bone.

W.R. Walsh and N. Guzelsu
University of Medicine and Dentistry of New Jersey-SOM Biomechanics
Rutgers University Biomedical Engineering 675 Hoes Lane
Piscataway, NJ 08854

The mechanical properties of a composite material rely on the properties of the individual constituents as well as the interfacial bonding between constituents. Interfacial bonding forces, which reflect quality, are due in part to the adsorption forces between the constituents. These forces include electrostatic (coulombic), Van der Waals', hydrogen bonding and hydrophobic interactions. The adsorption forces between the mineral and organic constituents of bone are related to the interactions between the lattice ions of bone mineral (Ca, PO4 and OH) and the ionic domains of the organic constituents.

Bone is porous fluid containing composite of a mineralized matrix containing inorganic bone mineral (hydroxyapatite (HA) and organic constituents (type I collagen and non-collagenous proteins). The porosity of bone consists of micropores in the matrix and the organic lined vascular channel system (Haversian and volkmann's canals). The organic linings of the vascular channel system functions like a diffusional barrier to ions and separates bone fluid spaces.

Electrostatic interactions between the mineral and organic constituents of bone can be influenced by the composition, ionic strength and pH of the fluid they are equilibrated in. The organic linings of the vascular channel system must be removed to some degree to allow ions access to the mineral-organic interface through diffusion. Nonionic detergent treatment (Nonidet P40, NP40) removes enough organic layers to permit ions access to the mineral organic interface. Previous mechanical testing in our laboratory on phosphate ion treatment of NP40 treated samples reduces the interfacial bonding forces and lowers the mechanical properties compared to control samples. Phosphate ions compete with the anionic domains of organic consituents for cationic bonding sites of the mineral (Ca++). This study examines the effect of fluoride ions, the effect on interfacial bonding forces and the reversibility of the effect on the mechanical properties. Fluoride is specifically adsorbed by HA and has been used in osteoporosis therapy.

MATERIALS AND METHODS: 18 adult femur tension samples were prepared through wet grinding and milling with an aluminum templated submersed in treatment solution. Uniaxail tension experiments were performed on an Instron testing machine at a strain rate of 2.65 x 10-3 sec-1. Samples were treated with 0.1 % NP40 for 24 hours at room temperature. Detergent treatment removes some of the organic linings present in the vascular channel system allowing ions access to the mineral-organic interface. Treatment solutions used were, 2.0 M NaCl pH 7.5 and 2.0 M NaF initial pH 7.5. Samples were separated into three groups following detergent treatment as follows;

Group 1; NP40 (1 day) + 2.0 M NaCl (pH 7.5) (3 days)
Group 2; NP40 (1 day) + 2.0 M NaF (pH 7.5) (3 days)
Group 3; NP40 (1 day) + 2.0 M NaF (pH 7.5) (3 days) +
2.0 M NaCl (pH 7.5) (3 days).

Elastic modulus and ultimate stress were calculated for all samples. Student t-tests were performed on the means to assess statistical significane.

RESULTS: Previous mechanical testing performed in our laboratory has shown the use of nonidet does not alter the mechanical properties. Electrokinetic studies reveal that ions are able to access the mineral-organic interface following detergent treatment. The pH of NaF

solutions (group 2 & 3) rose from 7.5 to 10.1 following three days equilibration. The pH of group 1 did not vary during equilibration. The pH of 2.0 M NaCl of group 3 rose to 7.95 after equilibration. The mechanical results are summarized in table 1. Elastic modulus and ultimate stress were determined for all samples.
The elastic modulus and utlimate stress for fluoride treated samples were statistically lower than control samples (group 2 vs 3). Equilbration in 2.0 M NaCl after NaF equilibration did not bring the mechanical parameters back to control values (group 1 vs 3). Fluoride treated groups (group 2 and 3) were not statistically different.

DISCUSSION:
The rise in pH of detergent treated samples equilibrated in fluoride buffer indicates that fluoride ions were able to access the mineral surface. Fluoride ions can exchange with hydroxyl ions (OH) on the bone mineral surface. The exchange of F and release of OH accounts for the increase in pH.

The reduction of interfacial bonding and mechanical properties with fluoride ion treatment may be multi-fold. The exchange of fluoride ions for hydroxyl may effect organic bonding to mineral due to an alteration in surface energy. The release of hydroxly ions will create an unfavorable electrostatic environment at the mineral-organic interface due to a local rise in pH. An increase in pH will shift the bone mineral above its isoelectric point of pH 8.5 (IEP is defined as the pH where species has zero zeta potential; a species will be positive at a pH below its IEP and vice versa). This will cause a charge reversal for the bone mineral from positive to negative. The organic constituents have very low IEP and a rise in pH will increase their negativity. Finally, the negatively charge fluoride ions may function like phosphate ions and compete with anionic domains of organic constituents for cationic bonding sites on the bone mineral surface (Ca++.) The reduction in interfacial bonding forces between the mineral and organic constituents results in an alteration in the mechanical properties of bone.

Samples were equilibrated in 2.0 M NaCl (pH 7.5) after 2.0 M NaF (group 3) to determine if the action of fluoride was reversible. The pH of 2.0 M NaCl rose slightly from 7.5 to 7.95. However, the mechanical properties remain reduced as in the fluoride treated samples (group 2). The local unfavorable electrostatical condition between the mineral and organic constituents may still exist even though the pH of the bulk is no longer high. The organic layers remaining on the mineral "shields" the mineral-organic interface from pH changes in the bulk. However, ions which preferentially adsorb to bone mineral can cause a local change in pH or electrostatic conditions at the mineral-organic interface. Fluoride ions exchange with OH and become part of the lattice of bone mineral and may not simply desorb from the surface with a shift in concentration gradient.

Fluoride treatment reduces the interfacial bonding forces between the mineral and organic constituents of bone and lowers the mechanical properties. This change in bone quality (mineral-organic interfacial bonding) may play a role in the aged and diseased (osteoporosis) properties of bone.

Table 1:

Sample	Ultimate (MPa)	Elastic Modulus (GPa)
Nonidet + 2.0 M NaCl (pH 7.5)	121.5 (9.9)	23.4 (1.2)
Nonidet + 2.0 M NaF (pH 10.1)	107.4 (10.8)	19.1 (1.3)
Nonidet + 2.0 M NaF (3 days) + 2.0 M NaCl (3 days)	100.5 (3.7)	20.8 (0.5)

Acknowledgment: This work was supported by the NIH-National Institute of Health Arthritis, Musculoskeletal and Skin Disease, Ortho. Grant # R23-AR26951.

STRUCTURAL QUALITY OF THE PROXIMAL FEMUR IN DIABETIC RAT TREATED WITH MINOCYCLINE

Edward P. Lanigan, Steven D. Bain and Clinton T. Rubin
Musculo-Skeletal Research Laboratory
Department of Orthopaedics, SUNY at Stony Brook, NY 11754-8181

INTRODUCTION:

The structural quality of the bone organ is a product of its morphological and material properties. Biochemical, cellular, or tissue abnormalities which are observed at microscopic levels may or may not produce significant risk to the bone structure. In the case of diabetes, defective collagen metabolism has been implicated as a mechanism which exacerbates diabetic osteopenia (1,2,3). Recent studies suggest that low dose tetracycline prophylaxis reduces collagenolytic activity (4,5) and thereby normalizes bone formation in the tibia of diabetic rats (6). However, even though these biochemical, cellular, and tissue level studies suggest the potential of tetracyclines as a treatment for this connective tissue disorder, studies at these levels neglect the responsibility of bone as a structure. Therefore, the purpose of this study was to identify changes in the structural quality of the proximal femur due to the effects of experimental diabetes, as well as diabetes plus tetracycline prophylaxis, and compare them to the structural properties achieved in normal controls.

METHODS:

Twelve adult (350g) male Sprague-Dawley rats were randomly assigned to control (C), diabetic (D), or minocycline treated diabetic (MTD) groups. To induce diabetes, animals were injected with 70mg/kg of streptozotocin. Criteria used to establish the diabetic state included glycosuria, polyuria, and weight loss. Minocycline (20mg/day) suspended in 2% carboxymethyl cellulose vehicle was administered daily via oral gavage to the MTD group while control and diabetic rats were gavaged with vehicle only. After a four week experimental period, the animals were anesthetized with halothane and sacrificed by cervical dislocation. The right and left femora were excised while leaving soft tissue intact. The bones were then wrapped in 0.9% saline solution soaked gauze, stored in a plastic bag, and then frozen at -20°C until testing. Prior to testing, the femora were put in a bath of 21°C normal saline and allowed to thaw (2 hours). The soft tisue on the distal end was dissected off and the bones embedded up to the mid-diaphysis in a 2cm cube of methylmethacrylate. Soft tissue was left on the proximal end of the femur. Care was taken to keep the specimen moist during all procedures. Whole bone testing was utilized to assess rigidity and ultimate load to failure of the femoral neck. Rigidity gives an indication of the structure's resistance during deflection, and in this case, was defined as force as a function of displacement within the elastic region. In this study, a linear displacement transducer was used to measure the deflection and a load cell measured the resistance. The peak load, measured at the point of absolute failure, was recorded to characterize the ultimate strength of the femoral neck. The specimen was mounted such that the long axis of the femur was parallel with the axis of the actuator, and aligned with the femoral head under the load cell. The soft tissue was retracted to expose the cartilage of the head to assure proper visual alignment. Using an interactive microcomputer package, a hydraulic testing machine (MTS, 442 controller) was driven under stroke control at a constant rate of 10 mm/sec onto the femoral head until absolute failure occured. Displacement and force were digitally recorded at a 500 Hz sampling rate.

RESULTS:

The average calculated rigidity of the diabetic group (165N/mm ±36) was significantly lower than that of the normal control group (220N/mm ±27; $p<0.05$). Although no significant difference was found between the treated diabetic group (187N/mm ±40) and either control or diabetic animals, the average calculated rigidity for the treated group was greater than the untreated group (Figure 1). The average ultimate strength, defined as the peak load to absolute failure, was greatest for the control group (124N ±33) and least for the diabetic group (81N ±18), with the peak load of the treated diabetic group falling in between (93N ±17).

DISCUSSION:

By testing the whole bone structural properties of the proximal femur, this study demonstrates the diabetic state will result in a statistically decreased rigidity of the bone organ. Although the potential for tetracyclines to inhibit this structural deterioration is not statistically supported, strong trends were evident. Further study of this unique prophylaxis, from the biochemical through the structural level, may identify an optimal treatment regimen.

REFERENCES

1. Schneir, M, et al., Biochim. Biophys. Acta, 583, 95-102, 1979.
2. Goodman, WG, et al., Diabetes, 33, 825-831, 1984.
3. Rico, H, et al., Calc. Tiss. Intl., 45, 71-73, 1989.
4. Golub, LM, et al., J. Periodont. Res., 18, 516-524, 1983.
5. Golub, LM, et al., J. Dental Res., 65, 516, 1987.
6. Bain, SD, et al., Trans. 36th Orth. Res. Society, 47, 1990.

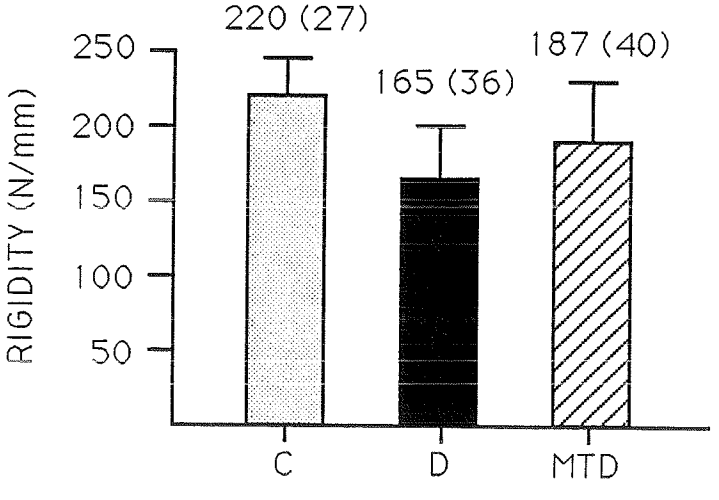

Figure 1. Mean (S.D.) rigidity across treatment groups. Control group was significantly more rigid than the diabetic group at $p=0.05$.

OPTIMIZATION METHODS FOR BONE REMODELING AND HIPPROSTHETIC DESIGN

Borelli Lecture By

Rik Huiskes, Ph.D.
Director

Biomechanics, Katholieke Universiteit Nijmegen
Nijmegen, The Netherlands

SESSION 3

LOCOMOTION

VERTICAL QUADRIPODAL STANCE ASSSESSMENT IN ROCK CLIMBING

Patrice ROUGIER
RE.S.ACT.SPORT, UFR.APS
Université Joseph Fourier
BP 53-X, 38041 Grenoble
FRANCE

Paul ALLARD
Dept. of Physical Education
University of Montréal
Montréal, PQ, H3C 3J7
CANADA

Jean-Pierre BLANCHI
RE.S.ACT.SPORT, UFR.APS
Université Joseph Fourier
BP 53-X, 38041 Grenoble
FRANCE

INTRODUCTION

This paper describes a system to study the interaction between posture and movement in vertical human quadrupedy. The forces exerted during vertical stance on an artificial climbing wall are used to test the climber's level of expertise.

REVIEW

Standing equilibrium following body movement (Bouisset et al., 1987) or random postural perturbations (Nashner, 1971) has retained much attention in man. Similarly, quadripodal equilibrium following these types of perturbations has been mostly studied in animals (Rushmer et al., 1983; Dufossé et al., 1982). Yet, quadripodal equilibration in man has retained little attention and has been limited essentialy to the horizontal posture (Dunbar's et al., 1986). Although recently, Dee and Adrian (1989) studied the loads and speeds on the kinematics of climbing, little is known about vertical quadripodal equilibrium situations; eventhough, this situation is quite common during the practice of some sport activities such as rock and ice climbing. This paper presents an original dynamometric device for measuring the hands and feet reaction forces while the subject maintains a vertical quadripodal stance on an artificial climbing wall.

METHODOLOGY

The measuring device consists of a fixed and movable 0,60 m by 2,20 m vertical wall-mounted rigs to which adjustable hand and foot plates are independantly instrumented by means of a load cell. The right vertical rig can be moved laterally to adapt itself to different body breath while the four plates can be adjusted according to body height. In all, 8 competion artificial holds are mounted at four different levels not exceeding 2,20 m in height. Each instrumentated plate has 2 holds, the lowest one always being the starting point while one of the upper one can chosen as the target hold. The hand holds allow a cling prehension while the feet holds allow only medial shoe border support. These have been particularly selected to force the climbers close to the wall.

Sixteen male rock climbers participated in this study. Six are occasional climber of level 5.7; five are experienced climbers of level 5.10c/d and the last five are high level climbers, of level 5.12b. Subjects wear climbing shoes with rigid soles and were allowed to use magnesia powder on their hands. Subject were instructed to climb on the lower foot and hand holds of the measuring device. Load cell data are displayed on a four chanel oscillocsope and stored on a Olivetti M 380 micro-computer. Once a stable signal is obtained, they were asked to move either their right or left hand or foot to the target hold located just above it, on the same plate. The choice is randomized to avoid learning effects. After the signal is again stabilized, the subject dismounted the instrument and rested for one minute. In all the subject carried out 24 trials, six for each different limb displacements.

To quantify the load distribution, we used the diagonality index, D (Dufossé et al., 1982; Gahéry et al., 1980), defined as $D = 1-(|\Delta FL - \Delta HR| + |\Delta FR - \Delta HL|) / (|\Delta FL| + |\Delta HR| + \Delta FR| + |\Delta HL|)$, where HR, HL, FR and FL are the load variations occuring at the right and left hand and foot respectively. Fig 1 illustrates a load variation observed for a right foot displacement. The D index provides an estimate of the hands and feet contibution to the diagonal postural adjustment which takes place during limb displacement. It has a value of 1 when the load variations are identical but of opposite sign on the diagonals. For values increasing towards unity, the D index reflects a

diagonal behaviour. When it tends towards zero, the load transfer is done by the contra-lateral limb.

RESULTS AND DISCUSSION

The hand displacement results are quite variable and as such are not of immediate interest; while the right and left foot displacements results are quite similar. Consequently, only the right foot displacement results are presented here. The mean (S.D.) diagonality index for the Occasional, Experienced and High Level groups are 0,29 (0,03), 0,23 (0,03)and 0,19 (0,04) respectively. Using a Mann and Whitney U test, significant differences were found between all groups ($\alpha \leq 5\%$)

The mean D values are generaly close to 0,25, indicating a non-diagonality behaviour. The index appears to decrease as the ability level increases; whereas, its standard deviation remains constant regardless of the level of expertise.

As found in cat studies for horizontal quadrupodal posture (Dufossé et al., 1982; Gahéry et al., 1980), the training effect is also present in man for a limb displacement, while maintaining a vertical quadrupodal posture. After training begins, they indeed observed a shift from diagonal to non-diagonal behaviour. This change permits the animal to have a more stable support while the non-diagonal behaviour implies a lateral shift of the position of the center of mass. Additionaly, they showed that this type of support behaviour was more energy efficient than that of the diagonal one. We could think that the same evolution is present in our climbers, the expertise level inducing a shift to a more non-diagonal behaviour.

ACKNOWLEDGEMENTS

This work was funded by a French, Rhône-Alpes regional grant. The holds were freely provided by the manufacturer Entreprises. We wish to thank Mr. R. Billat, Mr. G. Blouis and Mr. A. Cividino from Physical Spectrometry Laboratory of Joseph Fourier University for their technical assistance and Mr. C. Dupuy, from Ecole Nationale de Ski et d'Alpiniste (Chamonix) for his helpfull comments.

REFERENCES

Bouisset S. et al. J. Biomech.20(8):735-742,1987.
Dee, L and Adrian, M. Absract 158, XII I.S.B. Congress, Los Angeles, CA, USA, 1989.
Dufossé M. et al. Exp. Brain Res. 45:38-44, 1982.
Dunbar D.C. et al. Am. J. of Physical Anthropology 69:93-105,1986.
Gahéry Y. et al. Acta Neurobiol. Exp. 40:741- 756,1980.
Nashner L.M. Acta Oto-Laryngol. 72:429-436,1971.
Rushmer D.S. et al. Exp. Brain Res. 50:45-61,1983.

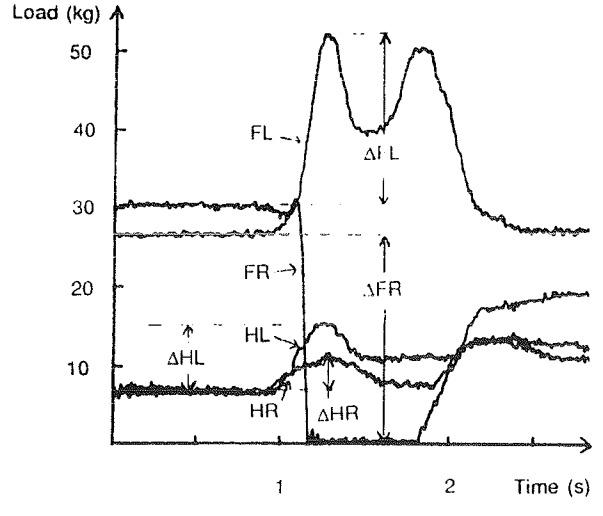

Figure I: Typical load variations during a right foot limb displacement

THREE-DIMENSIONAL KINEMATICS AND KINETICS OF THE ANKLE AND KNEE DURING LEVEL AND GRADE WALKING

Frank L. Buczek †, *Peter R. Cavanagh* ‡, *and H. Joseph Sommer III* ‡

†National Institute of Arthritis and Musculoskeletal and Skin Diseases
Biomechanics Laboratory, Bldg. 10, Rm. 6S235, Bethesda, MD 20892, USA

‡Center for Locomotion Studies and Mechanical Engineering Department, respectively
The Pennsylvania State University, University Park, PA 16802, USA

INTRODUCTION

Joint power and work were calculated at the ankle complex and knee relative to three-dimensional (3D), anatomically meaningful axes during the stance phase of barefoot walking over level, uphill, and downhill (8.3%) grades. Taking a simple situation, with a predictable outcome (increased power generation and positive work with increased grade, increased power absorption and negative work with decreased grade), parameters for axes often neglected showed results similar to those for primary axes.

METHODOLOGY

The kinetic analysis required the combination of information from three basic areas. Body segment parameters were estimated from cadaver studies and from geometric modeling. Kinematic parameters were calculated using screw-axes [1,2] with global position data obtained through cinematography. (The accuracy of the kinematics software was determined through analysis of a machine with known translation and rotation.) Ground reaction forces were measured using a piezoelectric force plate. Data were combined in custom FORTRAN software on a laboratory-based microcomputer. Nine adult males were studied.

RESULTS AND DISCUSSION

Comparison of the level data (patterns and magnitudes) to results reported in the literature [3] served to validate the kinetic analysis. Results from primary axes (ankle dorsiflexion/plantarflexion; knee flexion/extension) showed the ankle complex to be critical in propulsion, with the knee's function being primarily shock absorption and control. The peak plantarflexion moment, peak power generation, and positive work performed at the ankle were significantly increased with grade ($p \leq 0.05$). Figure 1 shows corresponding graphs for a typical subject. Results at the knee were not consistent across grades, but shock absorption at heel-strike seemed more important than control at mid-stance for uphill and downhill walking, while the reverse was true for level walking (Figure 2). Results for secondary axes were similar for both joints, though magnitudes were often less than 33% of primary axis values.

CONCLUSION

Data indicated that all three anatomical axes can show biomechanically relevant effects, such as those due to grade. Although magnitudes for parameters along secondary axes are relatively small, it seems unwise to disregard them as unimportant.

REFERENCES

[1] Lenox, J.B. and Cuzzi, J.R. (1978) Accurately characterizing a measured change in configuration, ASME publication 78-DET-50.

[2] Sommer, H.J. and Buczek, F.L. (1990) Experimental determination of the instant screw axis and angular acceleration axis, presented at the 16th Annual Northeast Bioengineering Conference, IEEE, March 26-27, The Pennsylvania State University, University Park, PA, USA.

[3] Apkarian, J., Naumann, S., and Cairns, B. (1989) A three-dimensional kinematic and dynamic model of the lower limb, *J. Biomechanics* 22(2), 143-155.

The work reported in this abstract was conducted at the Center for Locomotion Studies, The Pennsylvania State University, USA.

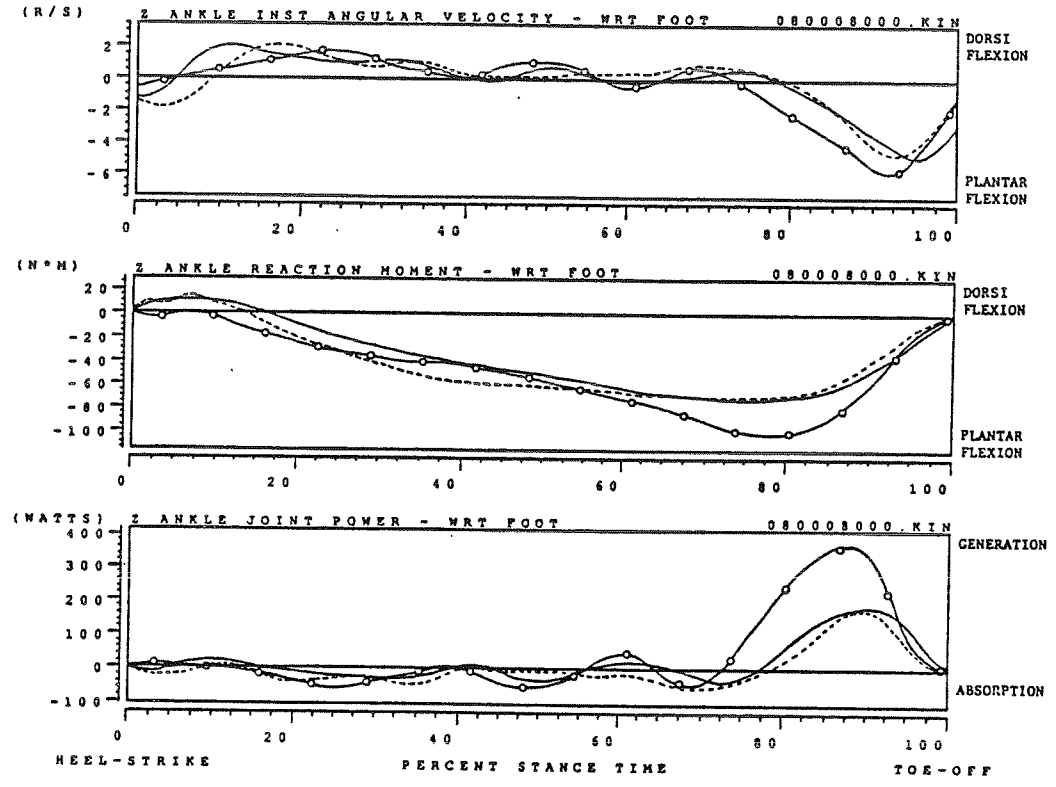

Figure 1 Composite of Ankle Instantaneous Angular Velocity, Reaction Moment, and Joint Power Curves for Uphill (open circles), Level (solid), and Downhill (dashed) Walking.

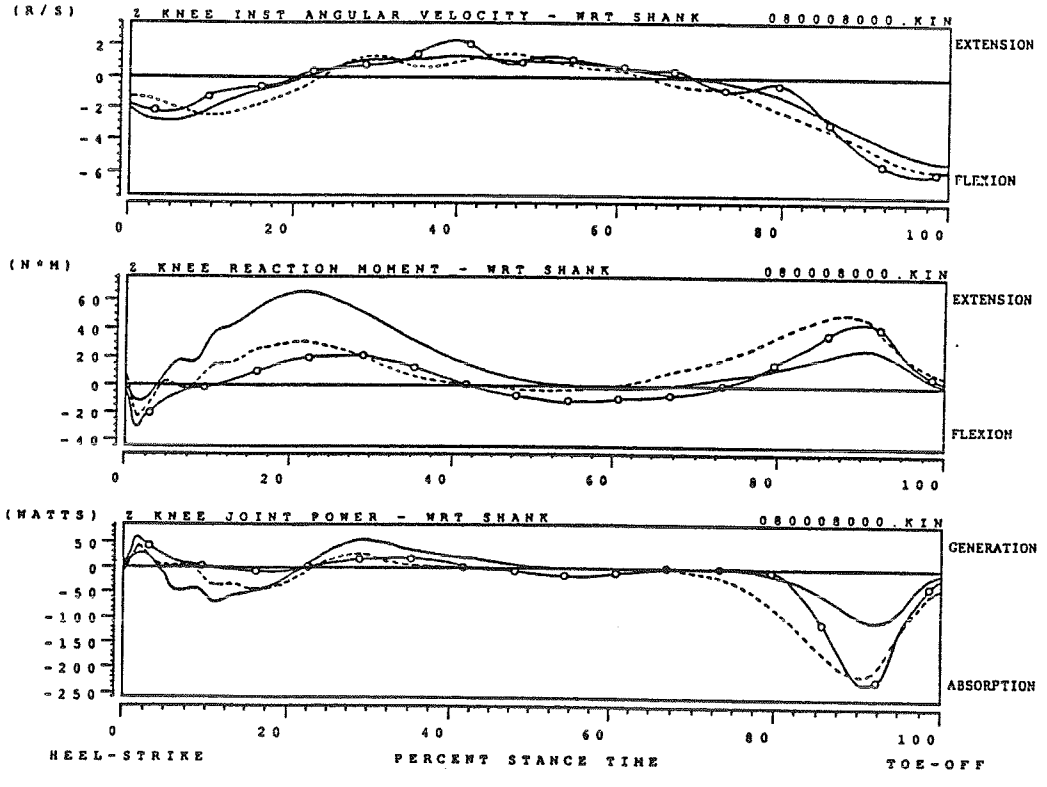

Figure 2 Composite of Knee Instantaneous Angular Velocity, Reaction Moment, and Joint Power Curves for Uphill (open circles), Level (solid), and Downhill (dashed) Walking.

AN INTRINSIC PARAMETER FOR THE STUDY OF COMPLEX THREE-DIMENSIONAL HUMAN MOTION

Raymond R. Brodeur and Robert W. Soutas-Little
Department of Biomechanics, Michigan State University,
East Lansing, MI 48824

INTRODUCTION

A complete understanding of joint kinematics is essential to the diagnosis of joint disorders, athletic training, and for assessing treatment and/or training progress. However, most joint motions involve complex three-dimensional rotations and translations, making it difficult to compare joint motions within and between subjects. The motion of two relative body segments is best characterized by the instantaneous screw axis (ISA). The path created by a line moving in space is called a ruled surface. The moving line is called the generator of the ruled surface. Thus, the motion of the ISA creates a ruled surface with the ISA as its generator. A ruled surface can be completely described in three-dimensional space using five scalar quantities (1). However, a single intrinsic parameter can describe the first order equivalency (defined below) of two generators. Thus, for a given instant in time, the generators of two ruled surfaces can be compared by a single scalar quantity. In addition, there exists a kinematically defined coordinate system called the generator trihedron, which, by itself, provides significant insight to the motions taking place at a joint. The purpose of this presentation is to provide the theoretical background and to discuss the ramification of the application of the above theory to the study of human motion.

THEORETICAL BACKGROUND

Figure 1 shows the instantaneous screw axis (ISA) of a rigid body at time t. Define a coordinate system:

$$\mathbf{e}_w = \mathbf{w}/|\mathbf{w}|$$
$$\mathbf{e}_k = \mathbf{w} \times \alpha/|\mathbf{w} \times \alpha|$$
$$\mathbf{e}_T = \mathbf{e}_k \times \mathbf{e}_w$$

where $\mathbf{w}$ and α are the angular velocity and angular acceleration of the rigid body. Locate the origin of the coordinate system at the center point, A, of the ISA. The center point, A, is defined as the point on the ISA where the acceleration in the $\mathbf{e}_k$ direction is zero (2). It should be noted that the center point cannot be uniquely defined if α is parallel to $\mathbf{w}$. The above coordinate system is called the generator trihedron. It describes both the first and second order motion of the rigid body. First order motion (velocity) is the screw motion of the body about the $\mathbf{e}_w$ axis. Second order motion (acceleration) has two components: (i) a screw motion of the body about the ISA ($\mathbf{e}_w$) and (ii) a screw motion of the ISA about the line $\mathbf{e}_k$.

At time t + dt the ISA moves to ISA′, as shown in Figure 1. In general the ISA and ISA′ are two non-intersecting lines in space. The shortest distance, ds, between ISA and ISA′ occurs at the center point of the ISA, along the line $\mathbf{e}_k$. The line $\mathbf{e}_k$ is perpendicular to both ISA and ISA′. Between the time t and t + dt, the ISA translates along $\mathbf{e}_k$ by a distance ds and rotates about $\mathbf{e}_k$ by an angle $d\theta$. The ratio:

$$p = ds/d\theta$$

is called the distribution parameter of the ISA. P is an intrinsic variable that describes the geometry of the ruled surface. The distribution parameter, p, can be defined relative to the kinematics of the point A:

$$ds/dt = (a_A \cdot e_T) / |w| - (\alpha \cdot e_T)(V_A \cdot e_w) / (w \cdot w)$$
$$d\theta/dt = \alpha \cdot e_T / |w|$$
$$P = ds/d\theta = (ds/dt)(dt/d\theta) = a_A \cdot e_T / \alpha \cdot e_T - V_A \cdot e_w / |w|$$

where a_A is the acceleration of A, and V_A is the velocity of A. Two ruled surfaces are said to have zero order equivalency when their generators coincide. For first order equivalency, the coinciding generators must have the same distribution parameter (1). Higher order equivalence exists (1-3) however, it requires higher order differentiation, making it more difficult to accurately apply to human motion.

There are two special cases for p: (i) If the motion of the rigid body is conical, then p = 0. This is equivalent to motion about a fixed point. (ii) If α is parallel to w, the motion of the body is cylindrical. For cylindrical motion $p = \infty$. Although the center point cannot be defined for cylindrical motion, the generator trihedron can still be defined:

$$e_w = w/|w|$$
$$e_k = w \times a_Q / |w \times a_Q|$$
$$e_T = e_k \times e_w$$

where a_Q is the acceleration of any point, Q, that lies on the ISA. The above definition allows the generator trihedron to be defined for planar motion.

DISCUSSION

Intrinsic parameters of rigid body motion have been used in robotics and mechanism design for several years (4). The theory described in this presentation relates to only the first order equivalency of two generators. Equivalency to the n^{th} order can be shown to exist, but derivatives of the n + 1 order are necessary to describe n^{th} order motion, making equivalency of 2 and higher difficult to apply to human motion. However, even first order equivalency provides a powerful tool for describing and comparing the motions taking place at a joint. It also provides a new avenue of approach for developing and studying more advanced prosthetics.

1) Yang, A.T., Kirson, Y., Roth, B. (1975). On a Kinematic Curvature Theory for Ruled Surfaces. Proc. of 4th World Congress on the Theory of Machines and Mechanisms, pp737-42.

2) Siddhanty, M.N., Soni, A.H. (1979). Intrinsic Invariants of Rigid Body Motion and Higher Path Curvature Theory in Spatial Kinematics. Proc. of the 5th Congress on Theory of Machines and Mechanisms, pp1440-43.

3) Kirson, Y., Yang, A.T. (1978). Instantaneous Invariant in Three Dimensional Kinematics. J. of Applied Mechanics, 45:409-14.

4) Lipkin, H., Duffy, J. (1982). Analysis of Industrial Robots Via the Theory of Screws. 12th Int. Symp. on Ind. Robots and 6th Int. Conf on Ind. Robot Tech., pp359-70.

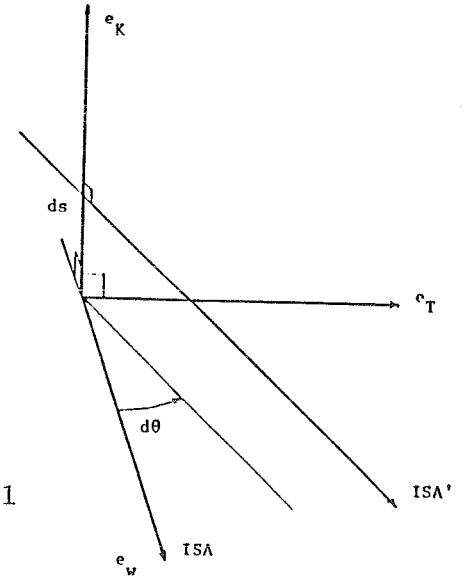

Figure 1

THREE-DIMENSIONAL KNEE JOINT REACTION FORCES DURING WALKING AND STAIR CLIMBING

J.Li, U.P. Wyss, K.J. Deluzio, P.A. Costigan
Clinical Mechanics Group and Department of Mechanical Engineering
Queen's University, Kingston, Ontario, Canada, K7L 3N6

INTRODUCTION

Accurate prediction of bone-to-bone reaction forces at the knee joint during level walking and stair climbing has many applications in prosthetic design and rehabilitation. Most previous investigations were two-dimensional since only sagittal plane forces and moments were evaluated (1,2). Although there were a few three-dimensional (3D) mathematical knee models available (3,4), data of 3D joint reaction forces was limited. The purpose of the current study was to develop a 3D dynamic algorithm which incorporates information from gait analysis, EMG and Questor Precision Radiography (QPR, 5) to calculate the bone-to-bone reaction forces at the proximal tibia during walking and stair climbing. This paper focuses on the dynamic aspects.

REVIEW AND THEORY

In order to describe the motion of the tibia in 3D space, three orthogonal, body-fixed coordinate axes are defined based on properly placed surface markers attached directly on the skin. The tibia orientation in space is defined by a set of Cardan angles which may be determined from the following equations:

$$\beta = arc\ \sin(-\vec{j} \cdot \vec{K})$$

$$\alpha = arc\ \sin(\vec{i} \cdot \vec{K} / \cos\beta) \qquad \alpha = \alpha \quad \text{if} \quad \vec{k} \cdot \vec{K} > 0$$

$$\alpha = 180 - \alpha \quad \text{if} \quad \vec{k} \cdot \vec{K} < 0$$

$$\gamma = arc\ \sin(\vec{j} \cdot \vec{I} / \cos\beta) \qquad \gamma = \gamma \quad \text{if} \quad \vec{j} \cdot \vec{J} > 0$$

$$\gamma = 180 - \gamma \quad \text{if} \quad \vec{J} \cdot \vec{J} < 0$$

where $\vec{i}$, $\vec{j}$, $\vec{k}$ and $\vec{I}$, $\vec{J}$, $\vec{K}$ are the unit vectors of the body fixed coordinate system and the global coordinate system, respectively. Anatomically, α, β and γ correspond to the clinical definitions of flexion-extension, abduction-adduction and internal-external rotation angles. The angular velocity and acceleration of the tibia can be expressed in terms of Cardan angles and Cardan angle velocities (6). Since the position of the center of mass of the tibia can be determined as well, the net joint reaction forces and net moments at the proximal tibia can be calculated using the classical dynamics equations.

METHODOLOGY

A two-camera 3D WATSMART system and an AMTI force platform were utilized for

the data collection. A foot switch was taped on the subject's heel to record the heel strike. A total of fourteen young, healthy subjects (8f, 6m) were tested. Five walking and five stair climbing trials were collected for each subject and the results averaged.

RESULTS AND DISCUSSION

Figure 1 shows the average net joint reaction forces for fourteen subjects during level walking. In figure 2 are the average net forces for the same group during stair climbing. As expected, large forces existed in the sagittal plane in both trials. Forces in the medio-lateral direction were relatively small in comparison to those in other two directions. Results of net moments also showed the largest moment in the sagittal plane, which was about ten times of those in the frontal and transverse planes. With the addition of muscle forces and their lines of action based on EMG and QPR data, the actual bone-to-bone reaction forces at the knee joint could be estimated in three dimensions with adequate accuracy.

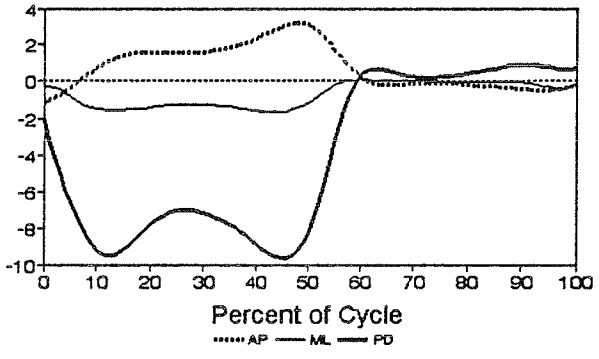

Figure 1. Average net joint reaction forces at the proximal tibia for 14 subjects during walking.

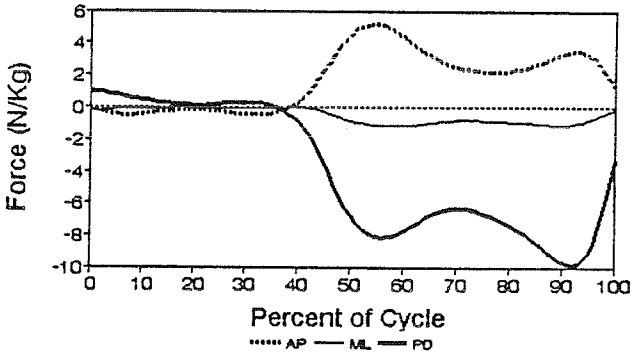

Figure 2. Average net joint reaction forces at the proximal tibia for 14 subjects during stair climbing.

REFERENCES

1. Johnson, F. & Waugh, F. 1979. Med. & Biol. Eng. & Comput.. 17:145-154.
2. Harrison, R.N. et al. 1986. J. Sports Science. 4:201-218.
3. Morrison, J.B. 1970. J. Biomech. 3:51-61.
4. Wismans, J. et al. 1980. J. Biomech. 13:677-685.
5. Wevers, H.W. et al. 1982. J. Biomed. Eng. 4:319-324.
6. Tupling, S.J. & Pierrynowski, M.R. 1987. Med. & Biol. Eng. & Comput.. 25:527-532.

ACKNOWLEDGEMENT

This work was supported by the National Sciences and Engineering Research Council of Canada, and the Medical Research Council of Canada.

Relationships Among Ankle Muscle Moments and Joint Kinetics During the Stance Phase of Locomotion in the Cat

E.G. Fowler, R.J. Gregor, J.A. Hodgson and R.R. Roy
Department of Kinesiology and Brain Research Institute, UCLA Los Angeles, CA 90024-1568

INTRODUCTION - Control of joint motion depends on the production of appropriate moments over a sufficient time period. The moment required about the joint is determined by environmental factors such as movement speed, gravitational forces, and ground reaction forces. Joint moments may be quantified by modeling the segments as a rigid body system and using principles of inverse dynamics (Bresler and Frankel, 1950). Using this approach, a generalized muscle moment (GMM), the sum of all active and passive tissues acting about the joint may be determined (Hoy et al., 1985). The contribution of individual muscles to the GMM may be determined using tendon transducers, implanted in freely moving animals (Walmsley et al., 1978, Gregor et al., 1988, Fowler et al., 1988). The purpose of this study was to quantify the relative contribution of individual muscles to the GMM, acting about the cat ankle joint, during locomotion.

METHODS- Three adult male cats (3.6-5.0 kg, body weight) were trained over a two month period to locomote within a plexiglass enclosed walkway. Tendon force transducers were placed on the soleus (SOL) in one hindlimb of each animal, under sterile conditions, such that mechanical interference was prevented. In the contralateral hindlimb, a transducer was placed on the PLT or MG and LG tendons. Lead wires were passed subcutaneously to an amphenol connector secured to the skull with dental cement.

Force recordings and high speed filming occurred approximately one week post operatively. Both hindlimbs were shaved and markers placed on the iliac crest, greater trochanter, approximate knee joint center, lateral malleolus, base of the fifth metatarsal, and head of the third distal phalanx. An external multilead shielded cable wired to recording equipment was attached to the amphenol connecter on the skull. The hindlimb was filmed at 100 fps by a cine camera, placed orthogonal to the plane of movement. The animal was coaxed to walk across the walkway. Limb position data, tendon forces, and ground reaction forces were synchronized using a DC pulse and light in the camera field of view. Tendon force transducers were calibrated *in situ*. The limb was secured by pins and clamps and the force transducer left undisturbed on the tendon which was connected distally to a force lever. A calibration factor was determined by comparing tendon transducer output to calibrated lever output during a series of isotonic contractions.

Muscle moment arms, about a instantaneous center of joint rotation, were obtained using a photographic method proposed by Lieber and Boakes (1988). Individual muscle moments were computed by multiplying muscle forces by their corresponding moment arms for each trial. Coordinates (x,y) of skin markers were obtained from serial film frames. Kinematic data were smoothed using a 4th order zero lag digital filter.

Vertical components of the ground reaction forces were used to calculate the point of force application on the plantarsuface of the paw. Anthropometric data were obtained for each segment using regression equations with cat mass and segment lengths as predictor variables (Hoy et al., 1985). The cat's shank, tarsals, and digits were modeled as a planar, three-segment, rigid body system. Equations of motion were formulated using Newtonian mechanics and the ankle GMM determined.

RESULTS/DISCUSSION - A direct relationship was found between moments produced by individual muscles and the ankle GMM. Peak MG, LG, and PLT moments increased as a

function of peak ankle GMM during level locomotion ($p<.05$), while peak SOL moments were relatively constant (Fig. 1). These results indicate that changes in peak ankle GMM were due to increased force output in fast twitch extensor muscles. Changes in the ankle GMM-time integral; however, were positively related to changes in SOL and PLT moment-time integrals ($p<.05$) (Fig. 2). These results demonstrate that while fast extensors are important in determining the maximum output in a limited region of the moment-time curve, the SOL and PLT output continues throughout the period of moment production. The SOL role can be explained by its slow twitch fiber composition while the PLT moment contribution may be explained by its role as both a primary ankle and metatarsalphalangeal joint extensor. Exemplar data, obtained from different trials of similar peak GMM, show that the sum of muscle moments was similar to the average GMM curve, for these same trials.

Fig. 1

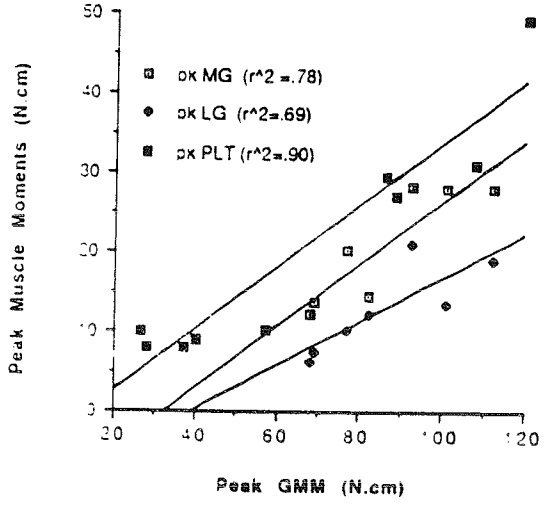

Fig. 2

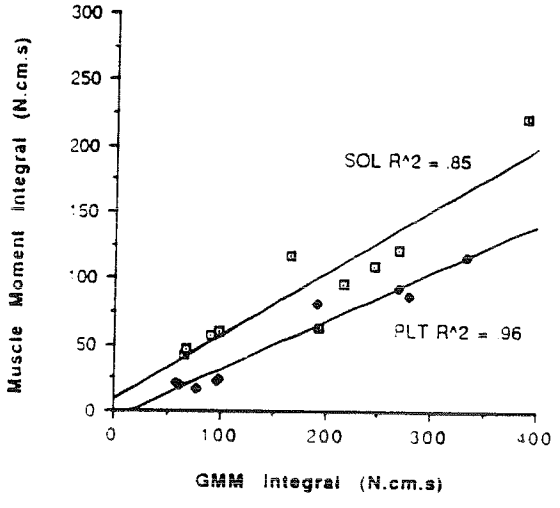

REFERENCES

Bresler, B. and Frankel, J.P. (1950) *Trans. Amer. Soc. Mech. Engrs.* 72, 27.

Fowler, E.F., Gregor, R.J., Hodgson, J.A. and Roy, R.R. (1989) The contribution of individual muscles to the ankle moment produced in the cat hindlimb. *J. Biomech.* 22:1101.

Gregor, R.J., Roy, R.R., Whiting, W.C., Lovely, R.G., Hodgson, J.A. and Edgerton, V.R. (1988) Mechanical output of the cat soleus during treadmill locomotioon: *in vivo* vs *in situ* characteristics. J. Biomech. 21:721-732.

Hoy, M.G. and Zernicke, R.F. (1985) Modulation of limb dynamics in the swing phase of locomotion. *J. Biomech* 18:49-60.

Lieber, R.L. and Boakes, J.L. (1988) Sarcomere length and joint kinematics during torque production in the frog hindlimb. *Am. J. Physiol.* 254 (Cell Physiol. 23) C759-C768.

Walmsley, B., Hodgson, J.A. and Burke, R.E. (1978) Forces produced by medial gastrocnemius and soleus muscles during locomotion in freely moving cats. *J. Neurophysiol.* 41:1203-1216.

KINETIC ANALYSIS OF LOAD SHARING BETWEEN ANKLE EXTENSORS OF THE CAT HINDLIMB DURING WALKING AND JUMPING

K. L. Perell, R. J. Gregor, J. A. Tjoe and R. R. Roy
Department of Kinesiology and Brain Research Institute, UCLA, Los Angeles, CA 90024-1568

INTRODUCTION. Load sharing among ankle extensors of the cat hindlimb has been indirectly estimated using EMG and information concerning the physiology of these muscles, particularly cross-sectional area, P_O, and fiber type. Muscle forces, however can be measured directly using chronically implanted force transducers. Previous studies demonstrate load sharing between the medial gastrocnemius (MG), a relatively fast-twitch muscle and the soleus (SOL), a slow-twitch muscle (Walmsley, *et al.*, 1978) during walking and jumping or the SOL and the lateral gastrocnemius (LG) using EMG (Smith, *et al.*, 1977) during locomotion. The purpose of this study is to evaluate the load sharing relationship between four ankle extensors (SOL, MG, LG, and PLT) using direct force measurements during jumping and walking.

METHODS. Two normal adult male cats (weight = 4.65 $\pm$ 0.35 kg) were trained to vertically jump to a platform height of 0.62 m and to walk through an enclosed plexiglass walkway. Force transducers were implanted, under sterile conditions, on the SOL, MG, plantaris (PLT) and LG tendons (Sherif, *et al.*, 1983).

Force recording and high speed filming occurred approximately one week following surgery. Markers were placed bilaterally on the iliac crest, greater trochanter, approximate knee joint center, lateral malleolus, base of the fifth metatarsal, and base of the distal phalanx of the third toe. The plexiglass walkway contained two concealed force platforms placed in succession on the side of the walkway floor closest to the camera. (Fowler, *et al.*, 1989) For the jumping trials, the cats were placed directly upon one force plate and rewarded for jumping up to the platform. Film speed was at a rate of 100 fps and the camera lens placed orthogonal to the plane of movement. Film, tendon forces, and ground reaction forces were synchronized using a DC pulse and light in the camera field of view. A calibration factor was obtained for each tendon transducer during a terminal experiment *in situ* (Sherif, *et al.*, 1983).

Paw contact (PC) and paw off (PO) were signaled using the vertical component of the ground reaction forces and synchronized to digitized film frames. Coordinates (x,y) of skin markers were obtained from serial film frames. Kinematic data were smoothed using a fourth order zero lag Butterworth digital filter and first and second derivatives computed (Whiting, *et al.*, 1984). The beginning of the jump was defined as the point in time when an increase in angular acceleration at the ankle joint occurred, while take off (TO) was signaled by zero ground reaction force. Ground reaction force records were acquired on line to an IBM PC, multiplied by appropriate conversion factors, and point of force application on the paw calculated. Anthropometric data (segment mass, center of mass, and moment of inertia) were obtained for each segment using regression equations with cat mass and segment lengths as predictor variables (Hoy, *et al.*, 1985). Standard rigid body mechanics were employed to calculate the generalized muscle moment about the ankle (Fowler, *et al.*, 1989).

RESULTS AND DISCUSSION. Mean data are shown in Table 1 for both cats. During the stance phase of walking the SOL assumed a large proportion of the load sharing as the other muscles singularly produced only a quarter to a half of that produced by the SOL. During the terminal phase of jumping, however, the MG, LG, and PLT showed approximately 2x the force production relative to the SOL force due to a 6-fold increase in MG, a 10-fold

increase in LG, and a 4.5-fold increase in PLT peak force. The SOL peak force decreased slightly (8%) from walking to jumping. In additon, force curves for the LG showed that the muscle contributed little after mid stance during walking. The SOL force curves demonstrated unloading of the muscle during the terminal phase of the jump, while MG, LG, and PLT were still producing substantial forces.

The timing characteristics of peak force showed differences primarily between the LG and PLT from walking to jumping. In walking the LG peak force occurred prior to that of the PLT (19.7 ± 3.3 % vs. 36.3 ± 2.2 % of the stance phase relative to PC) and the LG force decreased to almost zero by mid stance. During jumping, however, the peak forces of these muscles occurred at the same time relative to TO (76.7 ± 11.5 ms). For the jumping trials the timing of peak force for all four muscles showed consistency within a cat, but not necessarily between cats as different strategies could be utilized by different cats.

These findings are supported by Walsmley, *et al.* (1978) for changes in peak SOL and MG force during the two conditions. Predictions based on architecture, histochemical profiles and EMG of the LG and PLT also support these data.

Table 1. Mean peak forces, percentages of maximum tetanic tension, and timing of peak force as a percentage of stance time during walking and jumping.

	SOL	MG	LG	PLT
Peak Force (N)				
Walking	33.1 ± 4.4	11.0 ± 3.3	8.4 ± 2.3	14.1 ± 1.0
Jumping	30.6 ± 3.6	70.8 ±20.7	89.2 ± 2.0	55.6 ±10.6
% P_0 (%)				
Walking	95.2 ±12.6	9.1 ± 2.6	7.8 ± 2.1	16.3 ± 1.1
Jumping	87.6 ± 9.7	66.7 ±32.2	82.6 ± 1.8	64.0 ±12.2
Timing of Peak Force--Walking (% stance time)	31.4 ± 7.0	23.5 ±12.7	19.7 ± 3.3	36.3 ± 2.2
Timing of Peak Force--Jumping (ms prior to TO)	126.7 ±16.3	115.0 ±20.7	76.7 ± 11.5	76.7 ± 11.5

REFERENCES

Fowler, E.G., Gregor, R.J., Hodgson, J.A., Roy, R.R., and Broker, J.P. (1989) The contribution of individual muscles to the ankle moment produced in the cat hindlimb. *J. Biomechanics.* 22(10):1011.

Hoy, M.G. and Zernicke, R.F. (1985) Modulation of limb dynamics in the swing phase of locomotion. *J. Biomechanics.* 18(1):49-60.

Sherif, M.H., Gregor, R.J., Liu, L.M., and Roy, R.R. and Hager, C.L. (1983) correlation of myoelectric activity and muscle force during selected cat treadmill locomotion. *J. Biomechanics.* 16(9):691-701.

Smith, J.L., Edgerton, V.R., Betts, B., and Collatos, T.C. (1977) EMG of slow and fast ankle extensors of cat during posture, locomotion, and jumping. *J. Neurophysiol.* 40(3):503-513.

Walmsley, B., Hodgson, J.A. and Burke, R.E. (1978) Forces produced by medial gastrocnemius and soleus muscles during locomotion in freely moving cats. *J. Neurophysiol.* 41:1203-1216.

Whiting, W.C., Gregor, R.J., Roy, R.R. and Edgerton, V.R. (1984) A technique for estimating mechanical work of individual muscles in the cat during treadmill locomotion. *J. Biomechanics.* 17(9):685-694.

ENERGY OPTIMAL TRAJECTORY DURING UNIDIRECTIONAL TRUNK FLEXION AND EXTENSION

Mohamad Parnianpour, Ph.D. & Gerardo Lafferriere, Ph.D.
CIOC, Hospital for Joint Diseases Orthopaedic Institute
Robotics Laboratory, New York University, N.Y. 10003

INTRODUCTION: Evaluation of trunk performance must include not only the strength and endurance but also analysis of the strategy of performance. In order to establish a physical basis for such evaluation, optimal control theory is used to predict the optimal trajectory of trunk movement with respect to different cost functions (strategies).

METHOD: In a first stage we use the classical inverted pendulum model for the study of the flexion/extension movement on the sagittal plane. For this first approximation we assume that all the trunk muscles combine to generate a resultant torque τ about, the L5/S1, an axis perpendicular to the sagittal plane. The motion will be described using as a variable the angle θ that the trunk forms with the vertical. The dynamic equation of the motion is given by

$$A\frac{d^2\theta}{dt^2} - B\sin\theta = \tau \quad L \leq \tau \leq U$$

where $A = I_c + ml^2$, $B = mgl$ and m is the mass of the trunk, I_c is the moment of inertia of the trunk at its center of mass, l is the distance from the center of mass of the trunk to the axis of rotation, g is the gravitational acceleration, and τ is the torque generated by the muscles. While this is a simplified model it is already fully nonlinear in its characteristics. Equating $\sin\theta$ with the θ is a valid approximation for values of θ near 0° and is used in studying the behavior of an inverted pendulum near the vertical (Hemami and Golliday, 1977). However, our interest is in studying the trajectory profiles of the upper trunk during flexion/extension. Such motions include full flexion where the approximation above is no longer valid. It is assumed that human motion trajectories satisfy some additional optimization criteria. Model will be verified by comparing optimal trajectories corresponding to various cost functions predicted by our nonlinear model to actual position and velocity of normal subject performing trunk flexion and extension using B200 Isostation, a triaxial dynamometer. The energy optimal trajectory will be the function $\theta(t)$ that satisfy the derived nonlinear differential equation of motion and minimizes the following cost function:

$$\frac{1}{2}\int_0^T |\tau(t)|^2 dt = \frac{1}{2}\|\tau\|_2^2$$

The optimal trajectory $\theta(t)$ is approximated by a third degree polynomial plus a linear combination of Fourier terms with weighting coefficients

$$\theta(t) = p(t) + \sum_{i=1}^{k} C_i\phi_i(t).$$

The polynomial is used to match the boundary conditions and the Fourier terms ϕ_i are chosen so that they vanish at the end points. In that way the resulting trajectory satisfies the boundary conditions (Schmitt *et al* 1985). Using the equation of motion we obtain the torque τ corresponding to the given trajectory as a function of the linear combination of the coefficients C_i. The cost is then a function of the coefficients C_i and the final time T. This function of several variables (the coefficients and the time) is optimized using the

Nelder-Meade nonlinear optimization technique. We use the method in two stages. First using one approximating function ϕ_i we found the time T that minimized the energy. Then, with the time fixed we added more terms to converge to the optimal energy trajectory. After two more terms the improvements were minimal (less than 10^{-4}).

RESULTS: The results of optimization procedure provided some qualitative properties of the optimal trajectories. Both for flexion and extension the velocity profile is unimodal (Figure 1). An analysis of the model shows that the total time remains constant, however, the time to peak velocity is different depending on whether flexion or extension was performed, the longer time occuring during flexion. Moreover there is no overshoot in the position. The results of the theoretical prediction correspond qualitatively with the experimental data. We are currently in process of validation of the model and using other cost functions.

CONCLUSION: The comparison of the results of the mathematical model and the experimental data collected using B200 allows us to develop a physical basis upon which to evaluate the dynamic trunk movement. This will be an advancement over the existing emphasis on the range of motion measurement.

REFERENCES:

Hemami H, Golliday GL: The inverted pendulum and biped stability. Mathematical Biosciences 34: 95-110, 1977.
Schmitt D, et al.: Optimal motion programming of robot manipulators. J Mechanisms, Transmissons, and Automation in Design, 107: 239-244, 1985.

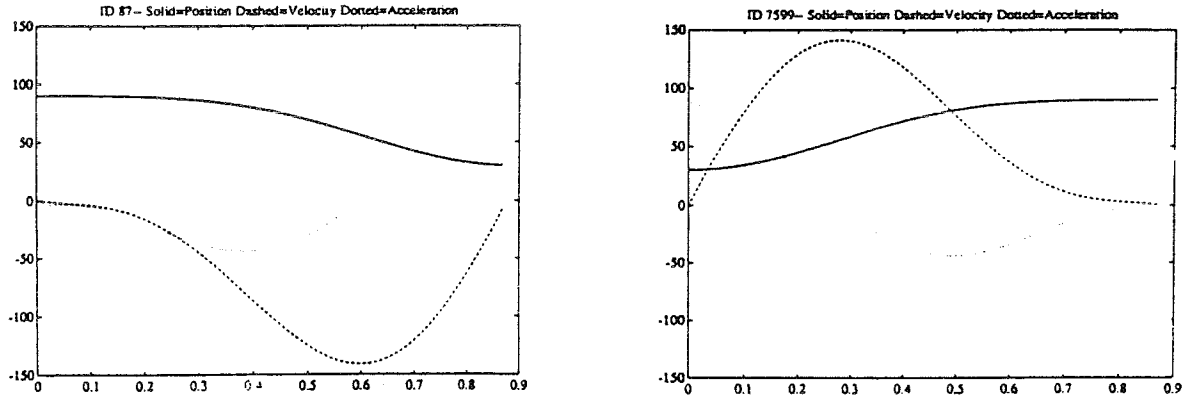

Fig. 1 The predicted energy optimal trajectory for the simulation of an unidirectional trunk extension and flexion. Solid= Angular Position (with respect to horizontal) (Deg) Dashed= Angular Velocity (Deg/sec); Dotted= Angular Acceleration (Deg/sec^2)

SESSION 4

MATERIALS AND DEVICES

THE MECHANICAL STABILITY OF POROUS COATED ACETABULAR COMPONENTS IN TOTAL HIP ARTHROPLASTY

J. B. Stiehl, D. A. Skrade, Dept. of Orthopaedic Surgery, Medical College of Wisconsin, Milwaukee, WI 53226 USA

Introduction: Five different porous coated acetabular prosthetic configurations underwent invitro testing to assess mechanical stability in embalmed cadaver hemipelves: Harris Galante II cup with three cancellous screws; Biomet Universal cup; Whiteside cup with peripheral pegs; Whiteside cup with two cancellous screws; and Whiteside cup plain. Following implantation in a neutral frame, cyclic load testing was done using 33 specimens at 100 kilogram load for 100,000 cycles using an MTS machine. Subsequently, static load to failure testing was done in all specimens. Subsidence and micromovement were determined for each specimen using linear variable differential transformers.(LVDT's) Relative bone mineral density studies were done using thin slice high resolution computed axial tomography. With cyclic testing, overall cup subsidence revealed a significant increase ($p < .0001$) from 500 to 100,000 cycles. Overall cup micromovement revealed a significant decrease ($p < .002$) and all cup groups demonstrated less than 125 microns of average mean micromotion at the completion of cyclic testing. The best cup configuration was a one millimeter over-sized press fit cup using two 6.5 cancellous screws for additional fixation which revealed an average mean of 60 microns of micromovement. Static load testing revealed unacceptable micromovement over 150 microns in most cups with 300 kilogram loads. Relative bone mineral density was not a factor in fixation.

Review and Theory: Clinical experience has shown the need for rigid initial fixation in order to achieve bony ingrowth into porous coated acetabular components. Pilliar suggested that micromovement of 28 microns is compatible with biologic ingrowth but movement over 150 microns was not compatible with ossification. (1) Previous authors have shown that invitro micromovement and subsidence measurement offers an effective means to study initial implant fixation. (2, 3)

Methodology: Embalmed cadaver hemipelves were mounted to a neutral frame and each acetabular component was inserted according to the manufacturer's protocol. Load transmission was done to approximate neutral single leg stance with the hip in extension. Three dimensional subsidence and xmicromovement of the acetabular components with respect to bone were measured with two pods of three LVDT's attached to the anterior and posterior rim of each cup. Cyclic loading was done on an MTS machine with load of 100 kilograms for 100,000 cycles with frequency of 5 Herz. Static load to failure was done at successive loads of 150, 200, 250 and 300 kilograms performing 5 cycles at each increment. All data from LVDTs was recorded simultaneously with information from the load cell and integrated with a computer. Statistical analysis was completed using the ANOVA method. Indirect mineral density was done. A new technique called thin slice high resolution computed axial tomography was utilized which is accurate to within 5% of actual ashed bone mineral density.

Results: Mean micromotion values diminished significantly for all cup groups ($p < .002$). The average mean for anteromedial and posterolateral transducer

placement was nearly identical. The best cup configuration was a 1.0 mm pressfit using two cancellous screws. Subsidence demonstrated a significant crease for all cups tested ($p < .0001$). Anteromedial and posteriorlateral transducer placement gave nearly identical results for subsidence, similar to to micromovement.

ACETABULAR CUP MICRO-MOTION
500 and 100,000 Cycles

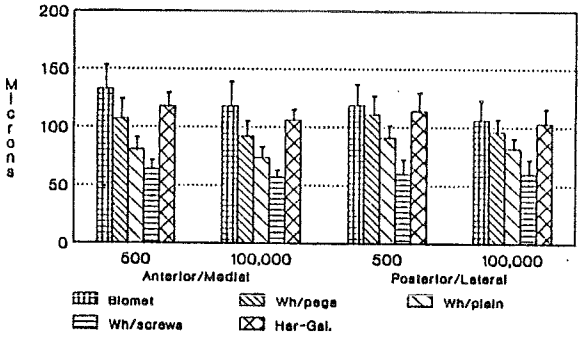

ACETABULAR CUP SUBSIDENCE
500 and 100,000 Cycles

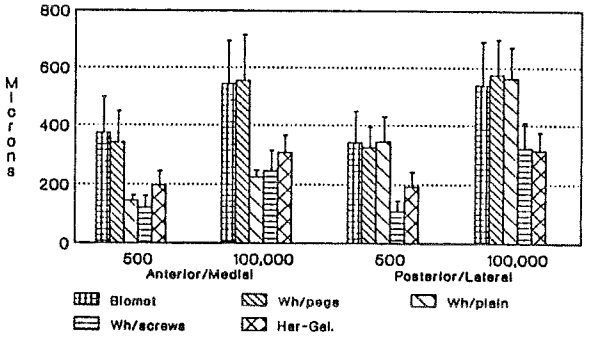

Load to failure demonstrated incremental increase for both micromovement and subsidence. No statistical difference was seen with these trends and rates of increase were similar for both. All cup groups except one millimeter press fit with two screws revealed over 150 microns average micromovement at 300 kilogram load. There was no statistical trend seen with bone mineral density values which varied from 847 to 1078 mg./cc.

MICRO-MOTION FAILURE TESTS

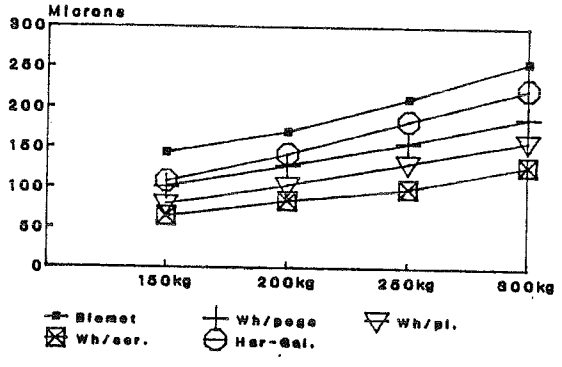

SUBSIDENCE FAILURE TESTS

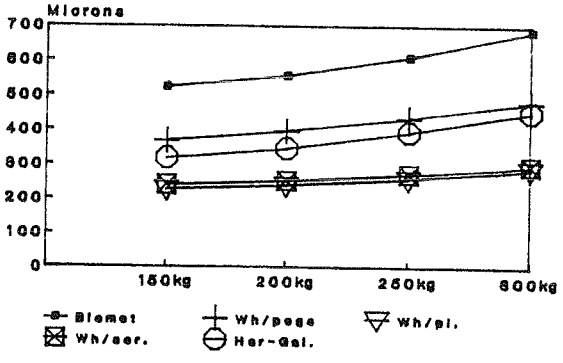

Discussion: This study has shown that excellent initial fixation can be achieved with existing porous coated acetabular designs. With progressive seating of the implant, micromovement actuall decreased and the average mean for all cup groups was below 125 microns. Static load testing demonstrated potentially unacceptable micromovement for biologic ingrowth if exaggerated (2-3 x body weight) forces are applied to the implant. Bone density did not appear to affect acetabular implant fixation as long as the subchondral plate was preserved.

References:

1. Pilliar, R.M., et al: Clin Orthop 156:249, 1981
2. Lachiewicz, P.F. et al: J. Arthro 4:201, 1989
3. Volz, R. G., et al: Clin. Orthop. 226:38, 1988

ASSESSMENT OF STRENGTH AND STABILITY OF PEDICLE SCREW FIXATION

Narayan Yoganandan, Frank A. Pintar, Dennis J. Maiman, Anthony Sances, Jr.

Department of Neurosurgery, Medical College of Wisconsin
8700 West Wisconsin Avenue, Milwaukee, WI 53226
Marquette University, Milwaukee, WI and
Veterans Administration Medical Center, Milwaukee, WI

INTRODUCTION

Although many biomechanical investigations have been conducted to evaluate the effectiveness of pedicle screws for posterior lumbar spine stabilization, alterations in the strength and stability of the spine under increasing compression-flexion forces on human cadaveric spinal columns have not been addressed. Therefore, this study was undertaken to determine the biomechanical strength and motion analysis of transpedicular fixation to the lumbar spine.

MATERIALS AND METHODS

Seven fresh human cadavers with ages ranging from 38 to 75 years, height ranging from 157 to 185 cm, and weight ranging from 59 to 86 kg were used. The T12-L5 column was fixed at the proximal and distal ends according to standard techniques. The specimen was placed on an x-y cross table firmly positioned on the platform of an electrohydraulic testing device. Retroreflective spherical targets were placed on the bony landmarks of the specimen at each level of the spinal column. Four targets at the vertebral body, two in the anterior and two in the posterior regions near the endplate, one in the facet column, and one at the tip of the spinous process were used. A total of 20 to 30 targets were used to span the entire thoracolumbar spine. To insure that the specimen is injured with anterior vertebral compressions accompanied by posterior element distractions so that the spine can be appropriately instrumented with pedicle screws, the continuity of the vertebral cortex was disrupted using an osteotome. This procedure not only permitted a specific injury for applying the implant, but also served as its own control for evaluating the efficacy of the instrumentation technique. Following this procedure a radiograph was taken to document the position of the retroreflective targets and spinal configuration.

The specimens were tested under increasing compression-flexion forces. Three cycles of force application were conducted on each specimen: intact, injured, and stabilized. The specimen was loaded to failure in the first cycle. At the point of failure, the piston was held in place, a radiograph was taken with the specimen still experiencing the failure load. Failure was defined as the point on the biomechanical response at which an increasing compression resulted in a decrease of the applied force. The second cycle of force application (injury cycle) was conducted by limiting the applied compressions to the maximum deflection achieved at failure during the intact cycle. Following this, the spine was radiographed and transpedicular screws were inserted in the pedicle bilaterally at one level proximal and one level distal to the level of injury. Two or three slot spine plates were fixed to the pedicle screws using standard surgical procedures. A radiograph was taken to insure proper placement of the implant. To this instrumented spine, the final cycle of loading (stabilized cycle) was applied using the procedure adopted in the previous cycle.

RESULTS AND DISCUSSION

The biomechanical strength data included the force and displacement histories from the force gauge and the linear variable differential transformer attached to the piston on the testing device, and generalized force histories from the distal six axis load cell. Localized kinematic data were retrieved from RS170 video signals and a video motion analyzer. The biomechanical strength response for the intact cycle indicated nonlinear and sigmoidal characteristics with continuously changing resistance. This behavior is typical of biological materials. Failure forces and deformations ranged from 2.2 to 5.4 kN and 7.6 to 18.2 mm, respectively. At these forces, compressions at the vertebral body routinely occurred at the middle of the spinal column accompanied by distraction of the posterior elements. In the injury cycle, forces ranged from 0.5 to 2.2 kN for deformations of 14.8 to 25.4 mm. These increases in the deformation together with the decrease in the load represents a relatively flexible structure. The load-deflection response was primarily bilinear with initial and final stiffnesses ranging from 25 to 78 N/mm and 161 to 500 N/mm, respectively. For the stabilized specimen the forces ranged from 0.8 to 3.1 kN with accompanying deformations of 14.6 to 24.6 mm. These load-deflection responses were also bilinear with initial and final stiffnesses of 48 to 124 N/mm and 186 to 526 N/mm, respectively. The significant ($P<0.001$) increase in initial stiffness by as much as 100 percent in the stabilized specimen compared to the injured specimen is indicative of the strength added to the posterior part of the spinal column due to fixation. However, the relative insignificant change in the final stiffness between the stabilized and the injured cycles corresponding to the load share by the anterior column (portion of the structure anterior to the instantaneous center of rotation) may support the hypothesis that above a critical strain level in the posterior column, the anterior column absorbs the majority of the external load. Beyond this level little stability and strength is imparted to the structure. Therefore, in order to enhance the strength of the column, it may be necessary to fixate the anterior column using bone graft or fusion of the vertebral body.

Localized kinematic data indicated decreased motion between the fixated levels (anterior compressions and posterior distractions compared to the injured specimen). Steffee plate fixation significantly decreased the superior-inferior movements of the posterior portion of the vertebral body as measured by the relative motion between the two posterior vertebral body targets. However, anterior vertebral compressions were not significantly reduced suggesting that the fixation contributes primarily in stabilizing only the posterior column. In addition to this increased rigidity between the fixated levels, in general, motions were more pronounced at levels proximal and distal to the fixation indicating an added flexibility at these neighboring levels. Increased motions may lead to other spinal disorders such as hypermobility and degeneration during repeated *in vivo* loading of the spine.

ACKNOWLEDGMENT

This research was supported in part by PHS CDC Grant R49CCR502508, DOT NHTSA Grant DTNH22-89-Z-07305, and Veterans Administration Medical Research Funds.

THE ORGAN RESPONSE OF BONE TO THE REMOVAL OF FUNCTIONAL STIMULI

Ted S. Gross and Clinton T. Rubin
Musculo-Skeletal Research Laboratory
Department of Orthopaedics, SUNY at Stony Brook, Stony Brook, NY 11794

INTRODUCTION

Bone is unique among structural materials as it possesses the ability to alter its mass and morphology in response to new functional demands. If the functional environment does, in fact, act as the controlling mechanism to maintain skeletal mass, removal of this stimulus should engender an organ wide adaptive bone loss. Previous work has demonstrated bone loss in response to reduced mechanical stimulus at various trabecular and cortical sites in both humans and animal models (1,2,3,4), but the extent and uniformity of the adaptive process has not been determined. The purpose of this study was to determine how bone, as an organ, adapts to the removal of functional stimuli.

METHODS

Under general halothane anesthesia, the right radius of three adult male turkeys were isolated from functional stimuli with parallel metaphyseal osteotomies. Delrin caps were filled with 5cc of methylmethacrylate bone cement and placed over the exposed diaphyseal bone ends to insure that the radius remained unloaded through the experiment. The musculature, vasculature, and innervation of the diaphyseal shaft was left undisturbed. The radii were isolated from their normal functional environment for a period of eight weeks, after which the adaptive response of each isolated radius was contrasted with its intact, contralateral control. Fluorescent labels were administered at two week intervals during the protocol. Three transverse sections were extracted at 1.5cm intervals spanning the middle 3cm of the diaphysis of the experimental and control radii. The sections were ground to 100 microns, microradiographed, and digitized to determine areal properties. The area bounded by the endosteal envelope and intractortical porosities were subtracted from the periosteal envelope area to determine total bone area for a given cross section. The ground sections were then examined under ultraviolet light, and sites of intracortical fluorescent labeling were counted as an indication of the level of cellular activity.

RESULTS

Eight weeks of isolation from functional stimuli precipitated a loss of bone tissue in all experimental cross sections. When compared to the intact, contralateral control, the isolated sections demonstrated an average (S.D.) 13.8(6.3)% reduction in bone area. Mean bone loss varied between turkeys (Figure 1). However, within each animal, bone loss was more uniform in magnitude (Figure 2). The loss of bone was achieved primarily via expansion of the endosteal envelope, with the experimental radii demonstrating a mean 13.5% increase versus the contralateral control. Increased intracortical porosity accounted for 16% of the bone loss. The experimental periosteal area was within 2.0% of the control area indicating the absence of periosteal adaptation. Fluorescent labeling confirmed that the removal of mechanical stimulus activated an otherwise quiescent skeleton, as the average (S.D.) number of active intracortical remodeling sites increased from 21.7(15.4) in the intact control, to 80.4(46.5) in the functionally isolated radius.

DISCUSSION

Similar to that observed in humans (5), the adult turkey radii responded to the removal of functional stimuli by activating quiescent cellular populations which, in turn, reduced bone mass primarily by expansion of the endosteal envelope. Although each of the three turkeys lost bone during the eight week isolation protocol, the extent of the loss varied between turkeys. The magnitude of bone loss varied to a smaller extent across the three sampling sites, suggesting a drive toward a uniform adaptive response within each bone. As bone loss precipitated by the removal of functional stimuli appears to be an organ response, future research will examine whether adaptation to increased functional stimuli is site specific, or is mediated by some, as yet undefined, organ imperative.

REFERENCES

1. Donaldson, CL, et al., Metabolism, 19, 1071-1084, 1970.
2. Minaire, P, et al., Calc. Tissue Research, 17, 57-73, 1974.
3. Jaworski, ZFG, et al., Bone, 7, 431-439, 1980.
4. Young, DR, et al., Calc. Tissue Intern., 33, 631-639, 1981.
5. Dequeker, J, Ann of the Rheum. Dis., 34, 100-115, 1975.

ACKNOWLEDGEMENT

This work was supported by NIH grant #AR38714.

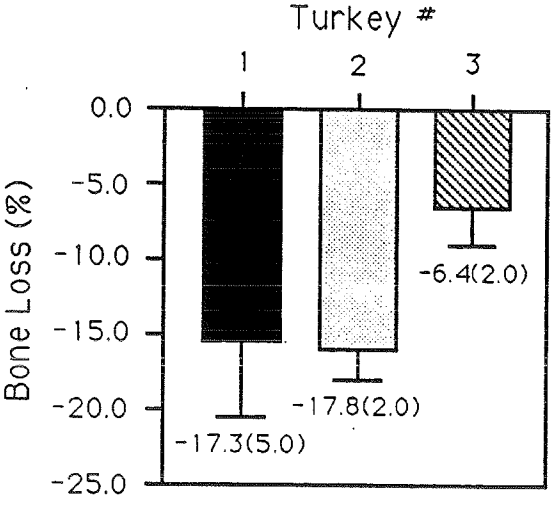

Figure 1. Mean (S.D.) bone loss.

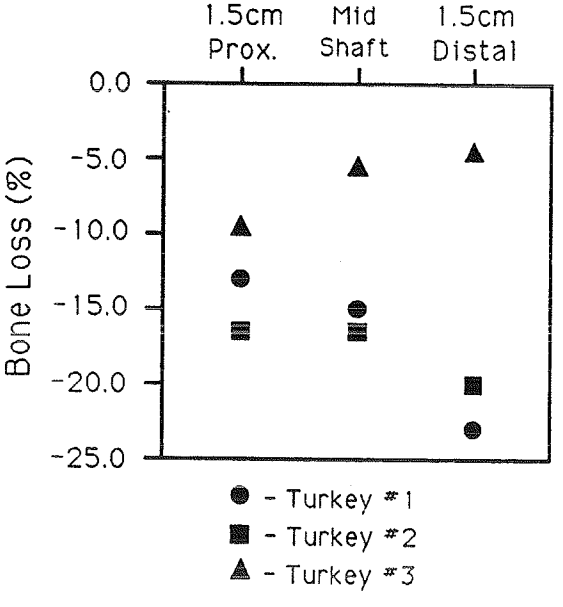

Figure 2. Bone loss across sites.

THE EFFECTS OF COMPONENT DESIGN VARIATIONS ON MECHANICAL PERFORMANCE OF PROPHYLACTIC KNEE BRACES

B.J. Daley, J.L. Ralston, T.D. Brown, and R.A. Brand.
Biomechanics Laboratory, Department of Orthopaedics
University of Iowa, Iowa City,IA 52242

INTRODUCTION: Prophylactic knee braces (PKBs) are widely employed to reduce major knee morbidity, despite the lack of scientific concensus on their efficacy. Several studies of commercial braces reported reductions in severity and number of injuries (4,5). However, a larger series in 1987 failed to find braces effective (7). The most recent and rigorously controlled epidemiological study showed a reduction in number, but not severity, of injuries (6). Biomechanical testing cannot be done in vivo, and the manifold problems of cadaveric specimens discourage their use. A new surrogate leg (8) provided a limited but reproduceable setting for valgus forces simulating a lateral blow to the knee, resulting in medial collateral ligament (MCL) injury. This surrogate was validated with cadaver studies. Tests of commercially available braces have been reported (9).

The surrogate has now been augmented to include muscle forces, simulated by pneumatic actuators connected to cables tethered to anatomic insertion points. (Muscular forces are probably the greatest stabilizers of the knee (2)). Individual component design parameters were studied to find if one or more aspects of brace design correlated with MCL strain relief. Baseline and perturbation ranges of the design variables were chosen from a survey of commercially available PKBs. A modular generic brace (Figure 1) was constructed with interchangeable components, facilitating a systematic approach to design variable testing.

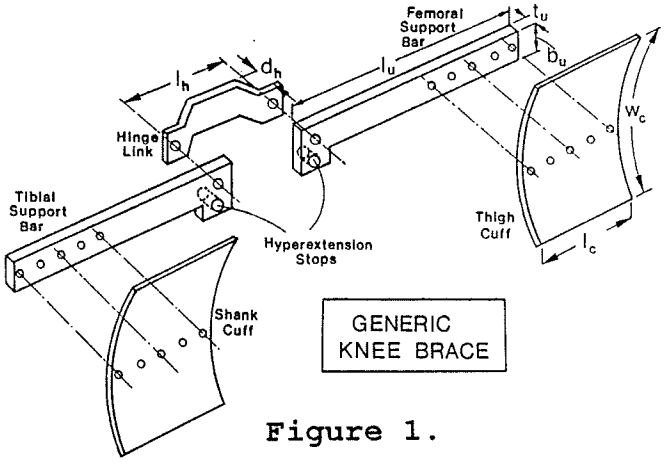

Figure 1.

METHODS: Design variables studied included hinge length, hinge offset, upright thickness, upright breadth, upright length, and cuff configuration. Fit of thigh and calf cuffs was controlled by instrumented tension bands. Generic brace placement was centered on the joint line in all cases. The surrogate is based on anatomically representative components, assembled with interchangeable ligament blanks made of polybutylene, a polymer with tensile properties mimicking those of ligament. Femur and tibia are aluminum rods casted in PMMA to anatomic likeness. The soft tissues are simulated by a latex foam rubber. The gastroc, medial and lateral hamstrings, and the quadriceps muscle forces were simulated at 50% of the values calculated from Cheng (3) and Andriacchi (1). A proximal actuator provided a 350 newton hip contact force. The distal tibia is held in a SACH prosthesis within a running shoe bolted to the baseplate. MCL analogs were tested to failure and then replaced with unused blanks. Liquid metal strain gauges (LMSG) were used to measure MCL analog distension.

A massive steel indentor was driven abruptly into the lateral side of the surrogate by the servohydraulic actuator of an MTS model 810, operating under stroke control. A valgus preload of 150 newtons was implemented to overcome static weight of the horizontally suspended limb. Command signal, actuator deflection, valgus load uptake,and LMSG ouput were recorded on a storage oscilloscope. After each impact, the surrogate was disassembled, MCL analog replaced, and a new brace configuration assembled.

RESULTS: Addition of muscle forces more than doubled the gross stiffness and load at failure of both the unbraced and braced surrogate, from 450N to 1100N, and 625N to 1400N, respectively. Compared to the unbraced case, the standard generic braced surrogate showed a statistically significant increase in the load at failure (32%), gross stiffness (23%), and MCL strain relief (19%). The Anderson-Omni brace also showed significant increases in all these parameters over the unbraced leg, (as was observed in the unmuscled case (9)), but not to the extent seen for the baseline generic brace. Load at failure and gross stiffness are greater for the stiffer mechanical constructs; e.g. tripling hinge offset from 0.5 to 1.8cm increases load at failure by 300N. Thicker components and upright breadth increases had similar effects. But, importantly, no individual component was found to produce statistically significant increases in load to failure. Permanent angular deformation (2-25 degrees) of the brace occured in all cases, in a manner dictated by the shape of the soft tissues.

DISCUSSION: Rule changes, shoe and surface changes, and improved player conditioning have been implemented to reduce knee injuries in football. Another approach to protection is bracing, but with the violent nature of the game it is obvious that bracing needs to be substantial. Therefore, protection comes at the cost of speed, agility and comfort. We have found that very substantial increases in component size and weight are necessary to achieve even small gains in mechanical protection

The present data do demonstrate that the muscle forces about the knee contribute very substantialy to valgus stability. In the surrogate, simulation of 50% of the physiologic maximum muscle force more than doubled the stiffness and load to failure, a far greater increase than any PKB has yet demonstrated. The generic modular design concept was found to be a rapid and efficient means for evaluating individual comnponent contributions.

REFERENCES:

(1)Andriacchi TP, et al.JOR 1(1984) 266-275.
(2)Branch TP, et al. Am. J. Sports Med. 17(1989) 35-41.
(3)Cheng C. Doctoral Thesis, University of Iowa 1987.
(4)Hansen BL, et al. Phys. and Sports Med.13(1985) 75-81.
(5)Randall F, et al. Orthotics and Prosthetics 37(1984) 54-57.
(6)Sitler et al. Transactions of the ORS. Vol. 15(1990) 224.
(7)Tietz CC, et al. JBJS 69A(1987) 2-9.
(8)Van Hoeck JE, et al. Proc. 11th. ASB. (1987a) 37-38.
(9)Van Hoeck JE, et al. Clinics in Sports Med., in press.

THE EFFECT OF SUBCHONDRAL PLATE INVOLVEMENT ON STRESSES IN SEGMENTAL FEMORAL HEAD OSTEONECROSIS

Kelly J. Baker, Thomas D. Brown, and Richard A. Brand
Biomechanics Laboratory, Department of Orthopaedic Surgery
The University of Iowa, Iowa City, Iowa, 52242.

Introduction: In osteonecrosis of the femoral head, an often-used clinical sign is a crescent-shaped fracture, typically present at the interface between subchondral and cancellous bone. The close proximity of the subchondral plate to the site of potential crescent fracture suggests that its structural integrity may be important in crescent sign genesis. The structural role played by the subchondral plate, potentially influenced if necrosis or fracture has ensued, has not been explicitly investigated. We have included a subchondral plate in an existing three-dimensional femoral head model, to investigate the influence of plate integrity on dangerous stress levels existing in a segmental lesion. Insight into the structural importance of the crescent sign may provide useful diagnostic information.

Methods: Our existing finite element model (Baker et al., 1989) was modified in order to study the importance of the subchondral plate. The present isotropic model, as shown in Figure 1, includes a subchondral plate of parametrically-variable thickness, and the number of elements has been increased in the head proper, yielding about 13,200 degrees of freedom. Material properites of subchondral bone of the femoral head were extracted from existing literature (Brown and Vrahas, 1984). Lesion geometry, modelled as a uniform 75% stiffness deficit, was mapped directly from MRI scans of a typical segmental lesion patient.

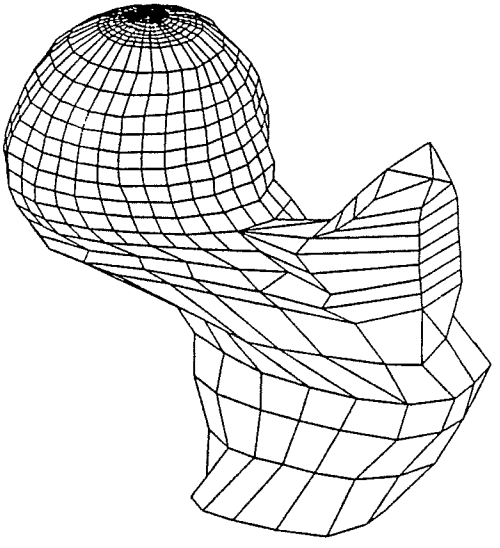

Figure 1.

To evaluate the role of the subchondral plate viability, seven specific cases were created in which the geometry and loading were identical, except for the 'peripheral' extent of lesion involvement. Case 1 is an intact head; cases 2-7 have an MRI-defined lesion with a central region of necrosis, but varying necrotic involvement of the associated 1mm-thick subchondral bone and underlying dense cancellous bone (subjacent): (2) both subchondral and subjacent regions necrotic, (3) viable subchondral plate but necrotic subjacent region, (4) both subchondral and subjacent regions viable, (5) necrotic subjacent layer and viable subchondral plate but low modulus peripheral rim (to mimic crescent sign initiation), (6) viable subchondral plate, but compliant tissue between the plate and lesion (to imply a developed crescent sign), and (7) necrotic subjacent layer subchondral plate with the inner 50% of lesion subtended arc viable and the outer 50% necrotic (to simulate necrotic invasion). A coronal midsection view of the MRI-defined lesion as well as the associated subchondral plate and subjacent region, specifically case 2, are illustrated in a Figure 2.

Results: Juxta-articular stress distributions in the entirely necrotic segmental lesion (case 2) were similar to the fully intact femoral head (case 1). For a subchondral plate modelled as intact (case 3), principal stresses increased three-fold from those seen with a necrotic plate (case 2). However, these primarily tangentially-elevated stresses were not accompanied by any stress concentrations at the necrotic/viable interface, or at the subchondral periphery of the lesion. Figure 3 shows shear stress to yield strength ratios at specific sites from the subchondral plate down through cancellous bone (sampled points indicated in Figure 2). Stress/strength ratios in this region are considerably higher at the subjacent/cancellous interface. Simulation of fracture initiation at the subchondral plate periphery (case 5) exhibited minimal stress deviation from the case of an intact plate. The fully-developed crescent sign condition (case 6) also failed to produce a substantial redistribution of stresses.

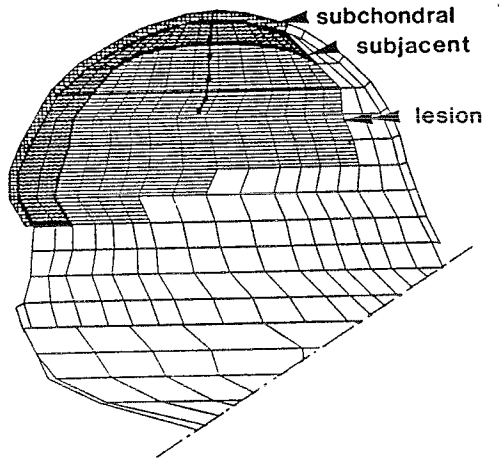

Figure 2.

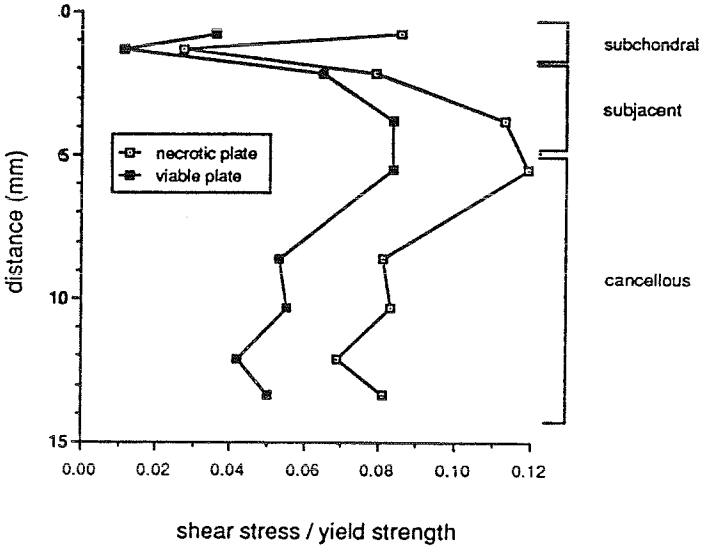

Figure 3.

Discussion: When the subchondral plate remains viable and elevated tangential compressive stresses develop in the plate, the associated transverse shear stresses peak in the underlying subjacent layer where crescent fractures commonly occur. This phenomenon may indicate that crescent sign development occurs via Mode II (shear) crack propagation. Since the arch effect of passing load through the strongest material (subchondral bone) is only responsible for a small portion of load transmission in the head, the presence of a crescent fracture does not appear to interfere with longitudinal compression through the underlying lesion. However, while global mechanics do not change, local mechanics probably do; the fracture line compacts and articular congruity is progressively lost, leading to degenerative changes.

References:

Baker, K.J., Brown, T.D., and Brand, R.A., Clin. Orthop. 249:183-198, 1989.
Brown, T.D., and Vrahas, M.S., J. Orth. Res. 2:32-38, 1984.

Acknowledgement: Financial support by NIH Grant AR-35788.

EXPERIMENTAL DETERMINATION OF BREAKING STRENGTHS OF LIVE REEF CORALS

Brent R. Constantz*
Earth Sciences, University of California, Santa Cruz, CA 95064 USA and
Discovery Bay Marine Laboratory, University of the West Indies, Discovery Bay, Jamaica and
Bellairs Research Institute of McGill University, St. James, Barbados, W.I.
*Present address: Norian Corporation, 1025 Terra Bella Avenue, Mt. View, CA 94043 USA.

Reef building scleractinian corals inhabiting reef crest habitats in tropical coral reefs fracture during storms (Woodley 1980). Scleractinians propagate asexually via fragmentation (Highsmith et al. 1981). Live storm-generated fragments of reef crest scleractinian species are recovered several hundred meters leaward of the reef crest following major storms (Porter et al. 1981, Knowlton et al. 1981, Turnicliffe 1981). Immunocompatibility studies have shown that individual asexual propagate lineages may survive thousands of years and predominate over extensive areas. Reproduction via fragmentation appears to be a very important reproductive mechanism for these species.

The Caribbean scleractinian coral, *Acropora cervicornis*, has a prolific occurrence on and surrounding reef crest habitats where wave energy during storms is greatest (Graus et al. 1976). *A. cervicornis* has a skeletal microarchitecture where pores are organized as serial planes that are particularly susceptible to shear fracture (Constantz 1984). Two differing selective forces appear to be relevant to the biomechanical adaptive strategy of this coral species. First, routine exposure to tidal and wave force would require a skeletal structure able to withstand the routine mechanical stresses the reef crest habitat. Second, skeletal fracture would have to be common enough during certain periodic high mechanical stress regimes (storms) to generate fragments for asexual propagation.

The fracture strength of *A. cervicornis* was measured with whole pieces of skeleton. Since published past studies of coral skeleton mechanical properties have used bleached or dried skeletons, identical testing was performed on live and bleached specimens to evaluate the importance of the hydrated skeletal organic matrix in approximating *in vivo* skeletal mechanical properties (Chamberlain 1978). Figures 1 and 2 diagram cantilevered and tensile test set-ups and the results of testing with both live and bleached specimens.

Observations of skeletal fracture surfaces are consistent with the precise failure plane noted in the microarchitecture of *A. cervicornis* (Constantz 1984). Mechanism of failure appears to have been the same in both bleached and live groups. Strengths between the bleached and live groups are not statistically significant.

These findings indicate that the strength of *A. cervicornis* are is quite low. Significant similarity of breaking strength with and without the hydrated skeletal organic matrix correlates with earlier findings on its quantitative significance, despite its qualitative similarity to other skeletal organic matrices (Constantz et al. 1988). The predominant mechanism of failure is along a preferential plane of fracture in the skeleton's microarchitecture.

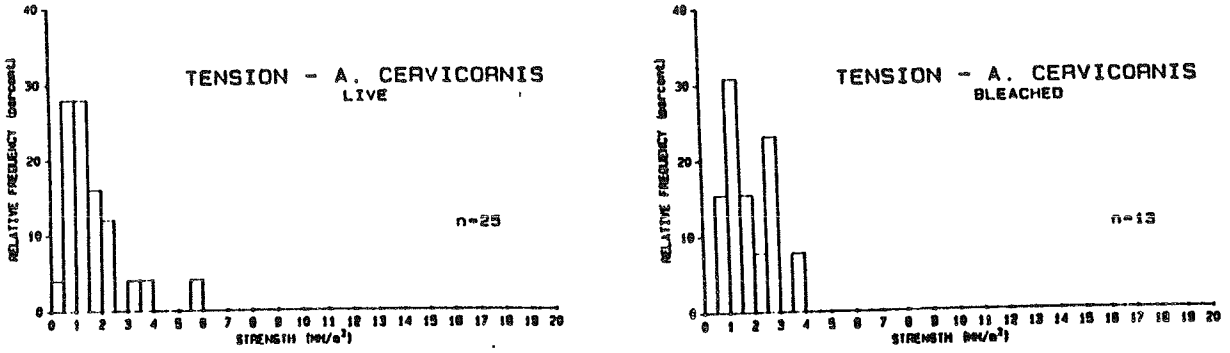

Figure 1: Both tests are shown statistically significant by calculating the Student's t distribution for the four experimental groups of *A. cervicornis* and analyzing the variance with a single-factor ANOVA. The median value for the bleached tensional breaks was 2.3 MN/m^2. The 99% confidence interval for the mean of the tensional strength (bleached), 1.0 MN/m^2, was between 1.0 to 2.8 MN/m^2. The median value for the live tensional breaks was 3.0 MN/m^2. The 99% confidence interval for the mean of the tensional strength (live), 1.6 MN/m^2, was between 0.9 to 2.3 MN/m^2. The calculated F-value for the two groups is 1.92 and the critical value for F at the 99% confidence interval is 7.08. The test fails to reject the null hypothesis that there is no difference in the tensile strength of *A. cervicornis* branches measured in tension when alive versus when bleached.

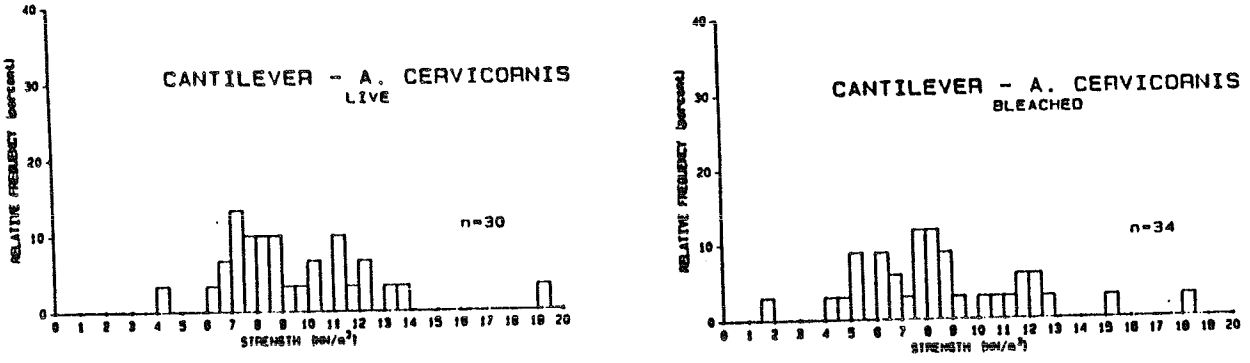

Figure 2: The median value for the bleached cantilevered breaks was 10.0 MN/m^2. The 99% confidence interval for the mean of the cantilevered strength (bleached), 9.6 MN/m^2, was 8.9 to 10.3 MN/m^2. The median value for the live cantilevered breaks was 11.0 MN/m^2. The 99% confidence interval for the mean of the cantilevered breaks (live), 10.2 MN/m^2, was 9.4 to 11.0 MN/m^2. The calculated F-value for the two groups is 0.5 and the critical value for F at the 99% confidence interval is 7.31. The test fails to reject the null hypothesis that there is no difference in the tensile strength of *A. cervicornis* branches measured as a cantilever when alive versus when bleached.

Chamberlain, J.A., Paleobiology, 4(4), pp. 419-435, 1978.
Constantz, B., et al., J. Exp. Zool., 248, pp. 253-258, 1988.
Constantz, B.R., Palaeont. Amer., 54, pp. 548-552, 1984.
Graus, R.R., et al., Science, 193, pp. 895-897, 1976.
Highsmith, R.C., et al., Oecologia, 46, pp. 322-329, 1980.
Knowlton, N., et al., Nature, 294, pp. 251-252, 1981.
Porter, J.W., et al., Nature, 294, pp. 249-250, 1981.
Tunnicliffe, V., Proc. Natl. Acad. Sci. USA, 78(4), pp 2427-2431, 1981.
Woodley, J.D., Nature, 287, p. 387, 1980

EFFECTS OF FREEZE-DRYING ON THE MECHANICAL BEHAVIOR OF PATELLAR LIGAMENT

L. Latta
Department of Orthopaedics & Rehabilitation, University of Miami, Miami, FL
T. Milne
University of Miami Orthopaedics Biomechanics Laboratory at Mt. Sinai Medical Center, Miami Beach, FL
T. Malinin
Department of Surgery University of Miami, Miami, FL

INTRODUCTION

The purpose of this study was to determine the effects of freeze-drying on the mechanical properties of various candidate materials for anterior cruciate ligament replacement and to identify materials with the appropriate strength for this application.

REVIEW AND THEORY

It is now well known that untreated anterior cruciate ligament tears lead to knee instability, meniscal tears, degeneration of the articular cartilage and eventually degenerative osteoarthritis[1,2]. Because of this natural history, attempts have been made to substitute the anterior cruciate ligament with biologic grafts fashioned from the patients own patellar ligament, other tendons or fascia or by bovine xenografts. The biomechanical analysis of these substitutes is, as yet, incomplete.

Several studies have established standards for testing techniques using ligaments[3,4,5] :

1. Rate dependence of soft tissue testing; 100% strain/sec. best simulates injury conditions and mode of failure;
2. End conditions: ligament must remain attached to bone at both ends during testing;
3. Direction of the load: parallel to the orientation of the collagen fibers;
4. Testing conditions: specimens must be kept moist and tested fresh.

Testing to date has established a tensile strength for normal anterior cruciate ligament to be 1730 ± 269 Newtons for young healthy humans. Several allografts [frozen (FF) or freeze-dried (FD)] have been used with success in the reconstruction of anterior cruciate ligament (patellar tendon, anterior cruciate, and Achilles tendon.) However, information is not available in the literature on the mechanical properties of all of these materials and particularly the effects of freeze-drying on them. The purpose of this study was to determine the effects of freeze-drying on the mechanical properties of patellar tendon ligament.

METHODOLOGY

Fresh patellar ligament harvested from cadavers were kept cool (<50) until processing by one of two methods: 1) quick freezing and 2) freeze-drying.

Whole patellas and at least 2 cm X 2 cm X 4 cm of the tibial tubercle were left attached to the patellar ligament specimens. Freezing was in liquid nitrogen vapor. Freeze-drying with a condensor was at -70°C, shelf at 30-40°C and vacuum in the chamber at mtorr or less.

Mechanical testing took place after 24 hours of reconstitution of the freeze-dried specimens in normal saline. The bone attachments were embedded in methylmethacrylate and gripped with standard mechanical wedging jaws. Load was applied at a constant displacement rate of one ligament length (100% nominal strain rate) per second to failure. The load and displacement were monitored so that load to yield, ultimate load, stiffness and energy to failure were measured or calculated.

RESULTS

Twenty-nine specimens were tested. Eight were FF and 21 were FD. Most specimens failed at the ligament-bone junction or by avulsion of bone from the attachment point. This study showed that patellar ligament was significantly stronger than ACL ($P < .005$), see Fig. 1. There was no significant difference in the strength or mechanical behavior apparent between FD and FF specimens, see Fig. 2. The weak link in the patellar ligament-bone complex, the interface, is not significantly different from the ACL in strength.

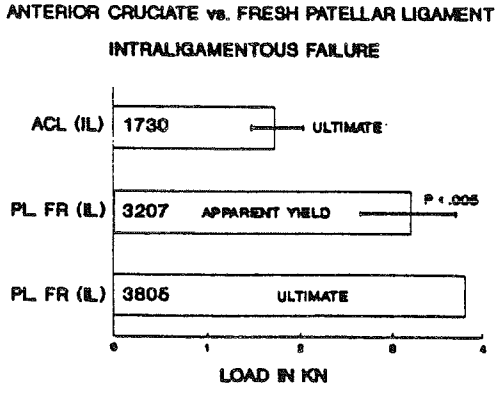

Figure 1. FF whole specimens compared to ACL, all with intraligamentous failure.

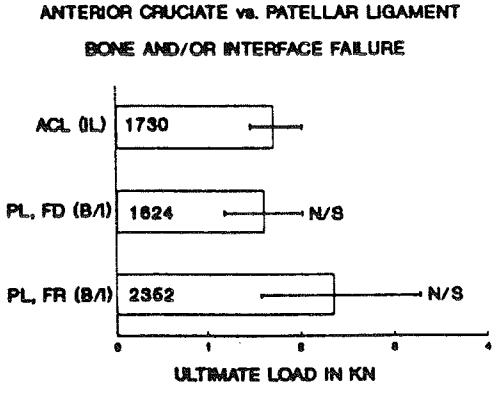

Figure 2. Whole and partial FD and FF specimens with bone-interface failure.

CONCLUSION

This study showed freeze-drying did not alter the biomechanical properties of human patellar tendons.

REFERENCES

1. Grove, T.P. J. Bone Joint Surg., 65A:184, 1983.
2. Kennedy, J.C. J. Bone Joint Surg., 56A:223, 1974.
3. Noyes, F.R. J. Bone Joint Surg., 56A:236, 1974.
4. Noyes, F.R. J. Bone Joint Surg., 58A:1074, 1976.
5. Noyes, F.R. Clin. Orthop., 172:71, 1983.

SPEECH PRODUCTION BIOMECHANICS

Keynote Address By

Thomas J. Hixon, Ph.D.
Professor and Head

Department of Speech and Hearing Sciences
The University of Arizona

SESSION 5

MUSCLE AND CONTROL

THE EFFECT OF NON-SYNERGISTIC ELBOW FLEXOR ACTIVITY ON THE ESTIMATION OF ISOMETRIC ELBOW FLEXION TORQUE

Marc Van Leemputte and Graham E. Caldwell
Institute of Physical Education, Katholieke Universiteit Leuven,
Tervuursevest 101, 3030 Heverlee, Belgium

INTRODUCTION

Quantification of raw EMG, from which the degree of muscular activity is derived, is often used to estimate muscle force. For isometric contractions, linear relations have been reported between a weighted sum of muscle activities and the torque around the joint, suggesting that the force per unit of muscle activity is constant. However, non-linear relationships have also been reported and it is the purpose of this paper to address this inconsistency.

METHODOLOGY

Subjects were seated on an inclined chair (30 degrees back from the vertical), with the shoulder constrained and the upper arm supported horizontally. A handgrip was positioned such that the rotation of the forearm was in midposition and the angle at the elbow was 90 degrees.

The static torque about the transverse axis (flexion -extension) and about the longitudinal axis of the forearm (supination - pronation) was measured. The raw EMG of m.biceps brachii, m.brachialis, m.brachioradialis and m.triceps were recorded using surface electrodes. These two torques and four EMG's were recorded (500 Hz) for 4 seconds.

19 male subjects performed 9 different tasks, all starting from rest. The first 3 tasks involved a gradual increase to maximum effort for extension, flexion and co-contraction (between flexors and extensors). In task 4, 5 and 6 the subject performed a flexion torque at 30%, 70% and 100% of maximum flexion, and maintained this flexion while adding maximal supination. In trial 7, 8 and 9 the same flexion torques were performed, but maximal pronation was introduced.

Flexion and extension torques were expressed as a percentage of the maximum flexion torque. Supination and pronation torques were expressed as a percentage of the maximum supination torque. The raw EMG's are quantified using a differentiation technique (Van Leemputte 1987) and then normalized to the maximum activity in trial 1 or 2.

RESULTS

Table 1 presents the mean (n=19) and standard deviations of the two normalized torques and the four muscle activities for the 9 trials (the mean is based on steady state values near the end of the recorded contractions). RMS1 and RMS2 represent the root means square error of a linear regression between a weighted sum of 4 activities and the normalized flexion-extension torque. RMS1 is based on individual trials, allowing the weight factors to change from trial to trial. RMS is calculated from one

regression line and one set of weight factors over 3 trials. The root mean square error with one set of weight factors over the 9 trials is 8.3.

DISCUSSION

The mean activity levels of the 9 tasks show the expected trends: high flexor activity in flexion and high extensor activity in extension, with a co-contraction of about 20 % in both cases. In the co-contraction trial, activity levels of only about 50 % were found in all muscles, although maximal activation was requested. With respect to the activity of m. brachialis, the activity of m.biceps is higher and brachialis lower in supination, and the reverse in pronation.

Of significance is that the RMS1's of trials 4 to 9 are significantly higher than for trials 1 to 3. This can be explained by the dual function of biceps and brachioradialis (Caldwell and Van Leemputte 1990). However, RMS2 for trial 1 to 3 is not significantly different from the other RMS2's. The introduction of a factor representing the amount of non synergistic flexor activity significantly reduces the RMS error not only for the combined tasks but also for the pure flexion and pure extension trials. It is suggested that the force per unit of activity decreases with the amount of non-synergy between the flexor muscles.

Trial	FE	SP	A1	A2	A3	A4	RMS1	RMS2
1	-82.1	0.0	18.9	43.2	30.3	95.5	4.2	
	(10.6)		(9.4)	(9.3)	(10.9)	(7.1)		
2	96.6	0.0	92.9	93.0	91.4	21.7	3.4	7.6
	(19.6)		(21.1)	(19.4)	(17.8)	(8.7)		
3	0.3	0.0	47.7	52.1	43.4	57.6	3.7	
	(3.2)		(23.2)	(23.0)	(14.6)	(16.2)		
4	29.3	91.2	89.0	73.7	37.2	29.1	8.6	
	(6.6)	(13.0)	(24.0)	(32.2)	(10.5)	(11.5)		
5	70.5	88.7	102.7	93.1	65.5	26.9	8.2	8.1
	(12.2)	(23.7)	(24.8)	(32.1)	(15.7)	(10.1)		
6	82.0	78.1	112.7	103.0	78.0	28.2	7.9	
	(17.3)	(29.9)	(32.3)	(34.5)	(14.1)	(8.4)		
7	28.0	-68.4	15.5	37.9	48.4	15.6	7.9	
	(6.5)	(21.0)	(13.3)	(16.8)	(14.2)	(10.6)		
8	70.0	-72.8	55.1	70.2	76.8	17.6	8.0	8.0
	(9.0)	(17.9)	(21.0)	(18.6)	(11.3)	(5.9)		
9	79.3	-78.7	69.3	79.7	81.9	19.9	8.0	
	(15.9)	(22.0)	(25.0)	(19.2)	(13.4)	(5.0)		

Table 1. Mean and standard deviation of normalized flexion-extension torques (FE), normalized supination-pronation torques (SP), activities of m Biceps (A1), m Brachialis (A2), m Brachioradialis (A3), m Triceps (A4).

REFERENCES

Caldwell G.E., Van Leemputte M., Elbow Torques and EMG Patterns of Flexor Muscles during Different Isometric Tasks, Submitted for publication

Van Leemputte M. (1987) EMG Quantification and its Application to the Analysis of Human Movement, Medicine and Sports Science Vol 25, pp 177-194

THE CALCULATION OF LOWER LIMB SUPPORT MOMENT DURING STANCE IN GAIT USING A FIVE-SEGMENT MODEL*

Andrew W. Smith, PhD, School of Physical and Health Education, University of Toronto, Toronto, Ontario, Canada M5S 1A1

INTRODUCTION

The purpose of the present study was to determine what effect using a five-segment model has on the overall lower limb support moment of force (Winter, 1980) during normal gait. Data averaged from eight subjects were used in a comparison of the support moment calculated using Winter's four-segment model to that of the five-segment model. A strong correlation between the two models was indicated with respect to lower limb support during gait.

REVIEW AND THEORY

In 1980, Winter introduced the concept of the overall lower limb support moment of force. The support moment of force demonstrates a pattern of positive (or extensor) during stance and either slightly negative or zero during swing. The equation used by Winter (1980) was:

$M_s = M_k - M_h - M_a$ *where:* M_s *= support moment of force;* M_k *= knee moment of force;* M_h *= hip moment of force;* M_a *= ankle moment of force*

Winter felt that the support moment of force demonstrated the possibility that the entire lower limb was being controlled by an overall pattern of either extension (stance) or flexion (swing) which permitted compensations to occur between the lower limb joints (typically the hip and knee).

METHODOLOGY

The eight subjects used in the present study were college students who volunteered to participate. The subjects were screened for any neuromuscular dysfunctions and were informed of the purpose of the study. Informed consent was obtained from each subject prior to testing. The subjects, all males, each made one visit to the laboratory and had four trials of data recorded. These were obtained from both the right and left sides of the body (two trials from each side).

Specific details of the methodology used appear in the literature (Smith, 1990). In summary, kinematic data were collected using a video camera. Video has been shown to be sufficiently fast for gait analyses (Winter, 1982). These data were synchronised with force platform data collected during each stride of walking. Analysis of the data included calculating segmental kinematics and kinetics along with the overall support moment of force. In the case of the second model which used a two-segment foot, Winter's (1980) equation was adjusted to include a fifth term on the right hand side, - M_m, i.e., the moment of force at the metatarsophalangeal (MTP) joint.

*The author wishes to acknowledge the assistance of **Paul Donovan** in the collection and analysis of these data. This study was partially supported by a *Cumberland College of Health Sciences (Sydney, Australia) Research Grant.*

RESULTS AND DISCUSSION

Joint moment of force data were time-normalised to 100% of stride and ensemble averaged at each 2% of the gait cycle prior to the support moments being calculated for each of the two models. To quantify the amount of variability within each model, a percent coefficient of variability (CV) was calculated which represented the root mean square variability across the 32 strides (Winter, 1987; Smith, 1990). The CV calculated for the four-segment model was 52% while the corresponding CV for the five-segment model was 62%. A correlation coefficient was also calculated between the two models, with a r^2 value of 0.977 being determined for the entire stride and an r^2 value of 0.955 for stance (i.e., 0-60% of stride).

In addition to the above analyses, a linear regression was calculated for the average knee moment during stance compared to the corresponding hip moment for both models (Winter et al., 1987). The regression analysis revealed r^2 values of 0.692 and 0.308 for the four-segment and five-segment models, respectively.

The principle of overall lower limb support was proposed by Winter (1980) in order to explain why, of the three main joints in the lower extremity, only the ankle joint displays a consistent moment of force pattern. The hip and knee are quite variable, with the knee especially being rather unpredictable, often demonstrating a flexor pattern during single support. The algebraic summation of hip, knee and ankle moments revealed a highly consistent trend resembling the vertical ground reaction force pattern in shape. The question addressed in the present paper concerned the effect of including an additional joint moment in the calculation of the overall support moment. Theoretically, further partitioning of the total moment of force acting in the lower extremity into another component should not have made any difference; however, no attempt to do this has previously ever been done.

Results of the present study revealed two interesting findings: first, the algebraic summation of four lower limb joint moments of force produced a very similar support moment pattern to that calculated using four joint moments. Thus, the theory of the existence of a single control pattern in gait for lower limb support is strengthened by these data. Second, the inclusion of a MTP joint in the model did reduce the predictability of the relationship between hip and knee moments found by Winter et al. (1987). This finding may have to do with the fact that, in the four-segment model, most compensations occurred between the hip and knee joints while in the five-segment model, the MTP joint would also be able to make contributions to this mechanism of compensation.

REFERENCES

Smith, A.W. **Int J Sport Biomech, 6(3)**, in press, 1990.

Winter, D.A. **J Biomech, 13**, 923-927, 1980.

Winter, D.A. **Med & Biol Eng & Comput, 20**, 408-412, 1982.

Winter, D.A. **The Biomech. & Motor Cont. of H. Locomotion.** Waterloo: U. of Waterloo Press, 1987.

Winter, D.A. et al., **Biomech. X-A**, 363-368, 1987.

Mechanical Output of the Cat Medial Gastrocnemius: In-situ vs In-vivo Characteristics During Locomotion & Jumping

R.J. Gregor, K. Perell, J. Tjoe, J.A. Hodgson and R.R. Roy
Department of Kinesiology and Brain Research Institute, UCLA, Los Angeles, CA 90024-1568

INTRODUCTION - The ability of skeletal muscle to contribute to a joint moment depends, in part, on its mechanical characteristics as measured in isolation. By design the force-velocity properties of skeletal muscle are measured under conditions of maximal stimulation and represent the force production capabilities of the cross bridges. During normal movements however, it is the properties of the muscle-tendon unit that are important to movement control. Consequently any measurements of force, length and velocity changes in muscle during normal movements represent the output characteristics of the muscle-tendon unit. Additionally, this output is typically under submaximal activation. The purpose of this investigation was to compare the force output of the medial gastrocnemius in the cat during walking and jumping, ie. accelerating motion, to its maximal force-velocity properties measured in isolation, *in-situ*.

METHODS - One adult male cat (weight 4.9 kg) was trained to walk and jump (0.62m) within a plexiglass enclosed walkway with food reward. Tendon force transducers were implanted, under sterile conditions, on the individual tendons of the medial gastrocnemius (MG) and soleus (SOL) muscles (Sherif. *et al.*, 1983).

Force recordings and high speed cinematography were employed approximately one following surgery for data collection of all trials. Joint markers were placed on the iliac crest, greater trochanter, approximate knee joint center, lateral malleolus and base of the fifth metatarsal for kinematic analysis. The cat was placed in the walkway containing two consealed force platforms possessing two piezoelectric load washers capable of measuring three components of the ground reaction force. Limb movements were filmed at a camera rate of 100 fps with the optical axis of the lens placed orthogonal to the plane of movement. Film, tendon force and ground reaction force data were synchronized using a DC pulse and a light in the camera field of view.

Coordinates (x,y) of the segment endpoint markers were obtained via serial film frame digitization (Numonics). Ground reaction force records were acquired on-line by an IBM PC, multiplied by the appropriate conversion factors, and point of force application on the paw calculated. Joint kinematic data were subsequently used as input to a muscle length algorithm (Goslow, 1973) for calculation of length changes in the MG and SOL muscles during all trials. Lengths were smoothed using a 4th order zero lag Butterworth digital filter (10 Hz) with velocities calculated using finite differences.

Each tendon transducer was calibrated during a terminal experiment, *in-situ*, where the buckle was left undisturbed on the tendon, connected distally to an isotonic lever. The tendon transducer output was then compared to the calibrated lever and a calibration factor determined. All procedures for determining maximum isometric tetanic tension (P_o) and maximum shortening velocity (V_{max}) in situ (36^0C +/- 1^0 C) have been reported previously (Roy *et al.*, 1984).

RESULTS AND DISCUSSION. Exemplar data for one walking trial and one jump are presented below. It is clear during the walking trial that the SOL output is well above that of the MG both in force and velocity. It is also speculated that there was no *enhancement* of the SOL at this slow speed. and that the data are comparable to those previously reported for the SOL muscle (Gregor *et al.*, 1988). Although this type of information has not been reported previously for the MG it appears that as the environmental demands increase the MG output increases (jumping). Peak MG force and velocity markedly increased while SOL velocity increased and peak force remained essentially the same.

The more interesting comparison, however, is between the output of the MG *in-vivo* and its maximum output capabilities as measured *in-situ*. The third figure presented below illustrates this relationship. It appears that the MG did not exceed its maximal capabilities during this jump. As previously reported, the SOL did exceed its maximal F/V capabilities during treadmill locomotion (Gregor et al., 1988) Since the jump height used in this current investigation was only 0.62m we do not rule out the possibility of the MG *in-vivo* F/V curve exceeding the *in-situ* curve at greater heights or in other cats.

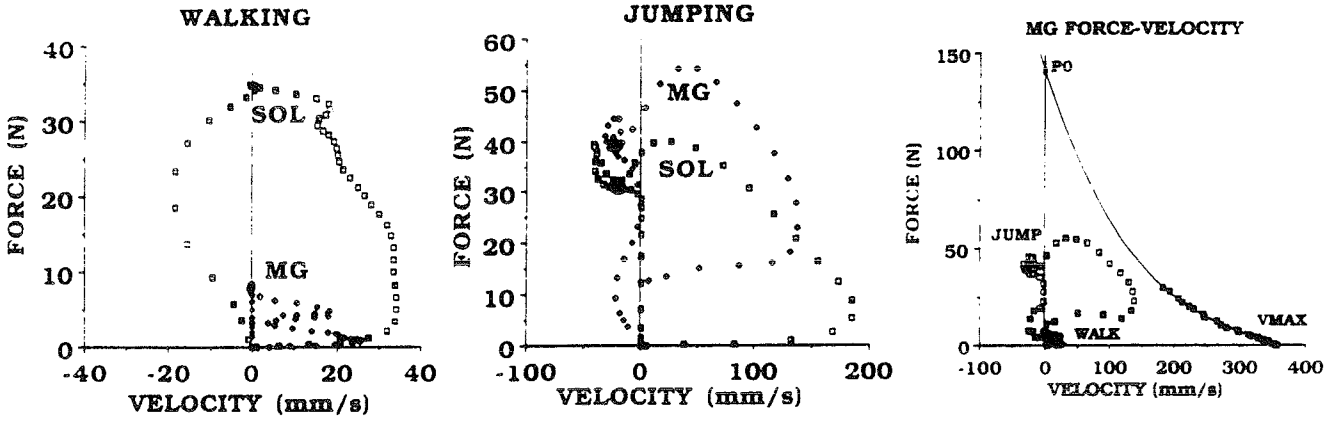

REFERENCES

Goslow, G.E., Reinking, R.M., and Stuart, D.G. (1973) The cat step cycle: hindlimb joint angles and muscle lengths during unrestrained locomotion. *J. Morphol.* 141,1-42.

Gregor, R.J., Roy, R.R., Whiting, W.C., Lovely, R.G., Hodgson, J.A. and Edgerton, V.R. (1988) Mechanical output of the cat soleus during treadmill locomotion: in-vivo vs in-situ characteristics. *J. Biomech.* 21, 721-732.

Roy, R.R., Sacks, R.D., Baldwin, K.M., Short, M., and Edgerton, V.R. (1984) Interrelationships of contraction time, V_{max} and myosin ATP_{ase} after spinal transection. *J. Appl. Physiol.* 56, 1594-1601.

Sherif, M.H., Gregor, R.J., Liu, L.M., and Roy, R.R. (1983) Correlation of myoelectric activity and muscle force during selected cat treadmill locomotion. *J. Biomech.* 16, 691-701.

FROG SEMITENDINOSUS TENDON MECHANICAL PROPERTIES DURING PASSIVE LOADING AND ACTIVE MUSCLE CONTRACTION

Richard L. Lieber, Christine L. Trestik and Margot E. Leonard

Division of Orthopaedics and Rehabilitation, Department of Surgery
University of California and V.A. Medical Center
San Diego, California 92161

INTRODUCTION: The mechanical properties of tendons have been studied by a variety of investigators (*c.f.* Butler *et al.* 1979). An understanding of the relationship between muscle and tendon properties is important in understanding the biomechanical basis of movement. Muscle-tendon interaction may be very complex with the tendon providing more than simply a muscle force conduit (Zajac, 1990).

We recently measured the relationship between muscle and joint properties in the frog semitendinosus (ST) muscle during isometric force generation (Lieber and Boakes, 1988). We then modelled the system in order to investigate ST function during conditions other than isometric (Mai and Lieber, 1990). As a first approximation, we assumed that tendon compliance was negligible. We have now explicitly measured tendon properties in order to check the validity of our previous assumptions. In addition, we measured tendon properties during passive loading and isometric muscle contraction.

METHODS: The entire pelvis-tendon-ST muscle-tendon-tibia complex (BTMTB complex) was isolated from 10 grassfrogs (Rana pipiens). Dye lines were applied to mark regions of the tendon, aponeurosis, and muscle. The pelvic and tibial bones were clamped into a testing jig which was immersed in physiological saline (21°C). The muscle was maximally activated at a frequency of 100 Hz for 400 ms at a supramaximal stimulation intensity in order to measure maximum contractile tension (P_O). The BTMTB complex was then loaded at a constant rate of about 3% P_O/s while measuring force and videotaping the applied dye lines. The muscle was then stimulated to P_O while again measuring the same parameters.

Muscle physiological cross-sectional area (PCSA) was calculated according to the methods of Sacks and Roy (1982) and tendon cross-sectional area was calculated by direct microscopic measurement of 8 μm slices of tendons fixed in 10% buffered formalin and embedded in Paraffin using standard histological procedures.

Using load-time, strain-time (as measured off line using a video-dimensional analyzer, Woo, 1982), and cross-sectional area values, tendon and muscle load-

strain and stress-strain relations were generated (Fig. 1). These properties were also generated for the tendon during active contraction (Fig 1A, open symbols).

RESULTS AND DISCUSSION: Tendon strain corresponding to P_o was approximately 6% (Fig. 1A). Tendon stress at P_o was approximately 2 MPa (Fig. 1B). These values are higher and lower respectively than the values calculated by Zajac (1990) based on data from a variety of sources. In addition, at physiological contraction velocities, the tendon was relatively stiffer suggesting that the viscoelastic properties were significant, even during isometric contraction (Fig. 1A open symbols). The results also demonstrate that tendon compliance is sizeable even in the physiological range and cannot be assumed to be negligible. Current efforts are underway to develop a model which predicts the effects of tendon compliance on the physiological properties of the muscle itself.

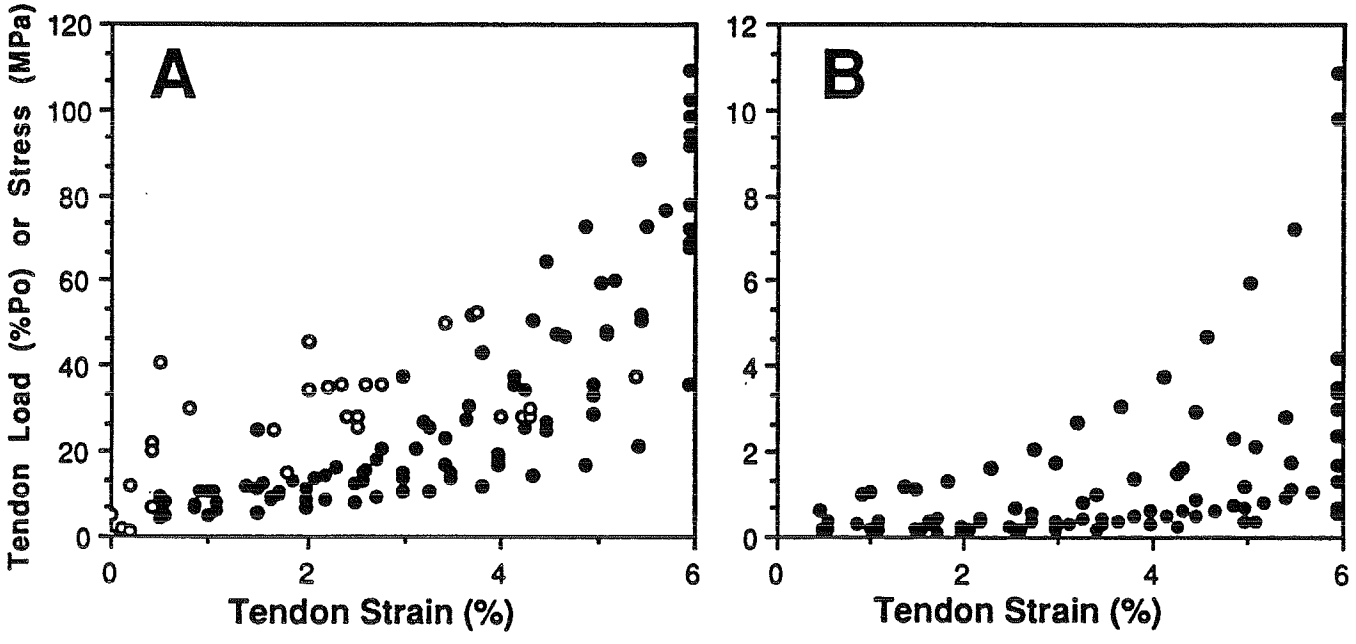

Figure 1: Tendon load-strain (A) and stress-strain (B) properties. Open symbols in (A) represent those measured during isometric contraction. Tendon strain at P_o was approximately 6%. Tendon stress at P_o was approximately 2 MPa.

REFERENCES:

Butler, Grood, Noyes, and Zernicke (1979) Ex. Sport Sci. Rev. 6:125-181.
Lieber and Boakes (1988) Am. J. Physiol. 254:C759-C768.
Mai and Lieber (1990) J. Biomech. (in press).
Sacks and Roy (1982) J. Morphol. 173:185-195.
Woo (1982) Biorheology 19:385-393.
Zajac (1990) CRC Crit. Rev. Bioeng. 17:359-411.

SESSION 6

EXERCISE AND SPORTS

EVALUATION OF RUNNING SURFACES: THE *IN VIVO* APPROACH

Wangdo Kim and Arkady S. Voloshin
Department of Mechanical Engineering and Mechanics

Lehigh University
Bethlehem, PA 18015

INTRODUCTION

The main objective of this experiment was to determine the running surface that produces the least amount of impact loading on a runner. The impact generated during foot strike may cause footaches, headaches, lower back pain and even bone fractures. Many lower extremity injuries have been associated with 'overuse phenomena' resulting from the repeated impact loading of the foot[1]. Most of these degenerative disorders more commonly affect the lower extremity, particularly the knee[2]. Studies have been conducted to rate the performances of the running shoes, but little has been done to compare different running surfaces[3].

METHODS AND MATERIALS

An accelerometric technique[4,5] was employed to obtain quantitative values necessary to evaluate the amplitudes of the shock wave invading the human musculoskeletal system while running on different surfaces. In order to collect the data, a 2 gram accelerometer was placed on a specially designed holder, which was then attached to the tibial tuberosity with a velcro strap below the knee. Thin wire ran up the subject's leg into a bag secured around the waist containing an FM recorder to store the accelerometer's response. Three surfaces were evaluated: asphalt road, which is the most accessible surface, 2 inch thick grass, and a polyurethane over concrete - a race track. The subject's average running velocity during these tests was adjusted to approximately 0.75 sec/step. Approximately 70 heel strikes of the right foot per surface were recorded for each subject and sampled at 1000 Hz. Six males and three females, all in good health, averaging 21 years of age were chosen from a student population to serve as test subjects. Each subject ran on all three surfaces consecutively to avoid influences caused by removing the accelerometer and replacing it.

RESULTS AND DISCUSSIONS

Frequency histograms in Figures 1 through 3 represent the average values and standard deviations of acceleration (g) for nine subjects on the asphalt (13.66 ± 3.12), grass (17.07 ± 4.32) and track (14.36 ± 2.78). ANOVA showed that there are significant differences between surfaces, with grass being the worst, since running on a grass resulted in the highest dynamic loading on the runners' musculoskeletal system. The graphs in Figures 1 - 3 show the normal distribution curves fit to the histograms. It is obvious that the spread of data for grass is higher than that for the asphalt and the track. For grass surface two percent of heel strikes were observed as having values more than twice higher than its mean.

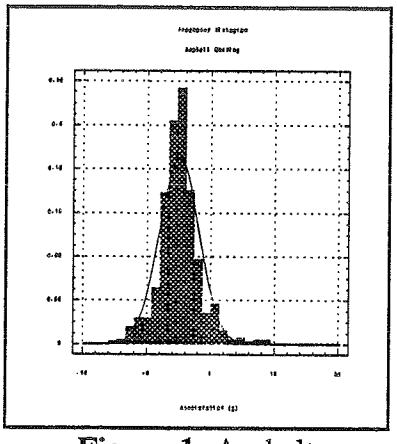

Figure 1. Asphalt

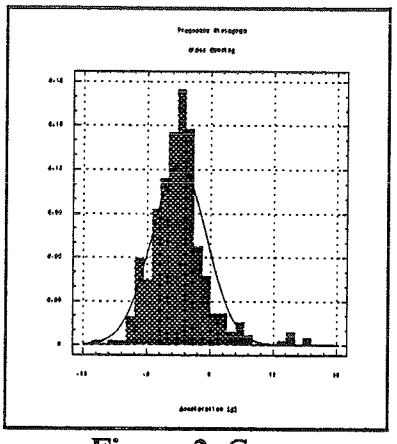

Figure 2. Grass

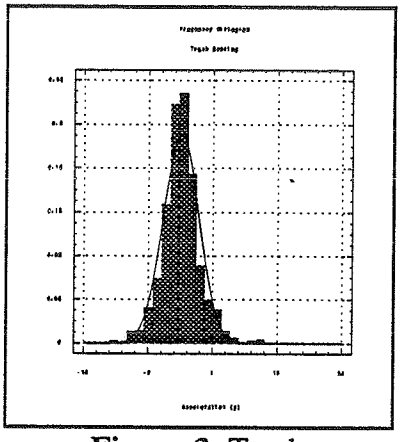

Figure 3. Track

This means that running on grass results not only in higher average values, but also in a larger amount of higher heel strikes than other two surfaces. Grass was concluded to be the worst of the three surfaces because it is uneven, and results in higher dynamic loading.

CONCLUSION

The results of the study show that running on grass results in higher impact loading on the runner's musculoskeletal system than running on the track or on the asphalt surfaces. Because running on asphalt for extended time probably will lead to sidewalks, curbs, inclines and potholes, it is recommended that track surface be used to avoid unnecessary injuries. Grass should be avoided as far as possible, as it causes the highest impact on the runner, as well as the largest standard deviation. Further testing should include additional surfaces such as turf and basketball or tennis courts that are widely used in college and professional sports.

REFERENCES

1. James, S.L., et al., Am. J. Sports Med., 6, 40-50, 1978.
2. Clancy, W.G., Am. J. Sports Med., 8, 287-289, 1980.
3. Kolitzus, H.L., Sport Shoes and Playing Surfaces, Human Kinetics, Champaign, IL, 98-118, 1984.
4. Light, L.H., et al., J. Biomech., 13, 477-480, 1980.
5. Voloshin, A.S., J. of the Amer. Podiatric Med. Assoc., 78, 295-299, 1988.

ADJUSTMENTS IN KINEMATICS AND KINETICS DURING MODIFIED LANDINGS

Jill L. McNitt-Gray, David D. Anderson, Carolyn A. Barbieri, and Kevin W. Cvengros
Biomechanics Laboratory, Department of Exercise Sciences
University of Southern California, Los Angeles, CA, 90089-0652

INTRODUCTION

The large reaction forces experienced during landings may be modified voluntarily by selectively controlling the joint motion (Nigg, 1985, McNitt-Gray, 1989). Landing strategies which use greater degrees of knee and hip flexion reduce the impact peak force (Lees,1981), however, the effect of the modified landing strategy on the net joint moments and the temporal relationship between the kinematics of the lower extremity joints is unknown. This study compares the kinematics and kinetics of landings performed by recreational athletes using landing strategies softer and stiffer than their preferred style. Examination of these parameters characterizing modified landings provides additional insight as to the mechanical consequences of alternate landing strategies.

METHODOLOGY

Seven males, actively participating in recreational athletics, volunteered to serve as subjects. Prior to collection, each subject practiced stepping from a platform and landing onto Kistler force plates. Each subject was also asked to modify their preferred landing strategy and practice landing as soft and as stiff as possible. The platform was positioned at a medium height (.72 m) to permit a range of landing strategy modifications. During data collection, each subject performed four trials using their preferred, soft, and stiff strategies in a randomized order. The segmental movement patterns were recorded using high speed film (100 fps). The reaction forces applied to each foot during the landing were quantified simultaneously using two Kistler force plates (825 Hz). Muscle activation patterns of the medial gastrocnemius, tibialis anterior, vastus lateralis, and the rectus femoris were monitored simultaneously using surface electromyography (1800 Hz). The high speed film was transferred to video format and manually digitized using a video data acquisition system (Peak Performance, Inc.). Each coordinate of the digitized body landmarks (Zatsiorsky & Selyanov, 1982) were digitally filtered using a second order Butterworth Filter (Saito & Yokoi, 1982) with a cut-off frequency derived by the method of Jackson (1979). The kinematic and reaction force data was synchronized and net joint moments were calculated using Newtonian mechanics. The ground reaction force data for each foot were normalized by body weight of the individual and expressed as a multiple of body weight (BW). The interval of interest, identified as the landing phase, was defined as the time required to bring the vertical velocity of the total body center of mass to zero. Statistical comparisons of the impact peak forces, joint kinematics, and net joint moments were made between landing strategies using ANOVA ($p<.05$).

RESULTS AND DISCUSSION

The soft landings were characterized by significantly smaller minimum knee and hip angles than the preferred and stiff landings. No significant differences in minimum ankle joint angle was noted across strategies which is consistent with the findings of McNitt-Gray (1989). Data from McNitt-Gray (1989) also confirms that peak knee angular velocities exceed the peak hip joint angular velocities during landings from this height. The mean reaction force data indicates that the impact peak force experienced during landing was significantly reduced (>20%) when subjects used a soft landing strategy as compared to the preferred or stiff strategies (Table 1). Despite significant differences in

minimum knee and hip angles between the preferred and stiff landings, no significant difference in impact peak magnitudes were noted. The lack of significant difference in impact peak magnitudes between the preferred and stiff strategies suggests that subjects are reluctant to voluntarily modify their strategy towards stiffer strategies. Significantly greater peak hip extensor moments were observed for the stiff landings as compared to the preferred and soft landings, however, no significant differences in peak knee extensor moments were noted across strategies. Temporal characteristics indicate that joint angles, joint angular velocities, vertical force, and the net joint extensor moments peaked earlier during the stiff landings than the preferred and soft landings, respectively (Table 2). The increase in knee and hip flexion, the peak hip extensor moment, and the temporal shift towards earlier peaks demonstrated during the stiff landings are similar to those encountered when landing at higher impact velocities (McNitt-Gray, 1989).
In conclusion, soft landing strategies provide a means to reduce the impact peak experienced, however, the neuromuscular control implications of the temporal and joint moment modifications warrant further investigation.

Table 1: Mean kinematic and kinetic characteristics of preferred, soft, and stiff landings performed by male recreational athletes.

LANDING STRATEGY	IMPACT PEAK(BW)*	MIN. ANGLE(rad) KNEE*	MIN. ANGLE(rad) HIP*	MAX. ANG. VEL.(rad/s) KNEE	MAX. ANG. VEL.(rad/s) HIP	PK.EXT.MOMENT(Nm/kg) KNEE	PK.EXT.MOMENT(Nm/kg) HIP*
Soft	7.7	1.28	1.84	-9.91	-4.84	2.83	3.44
Preferred	9.8	1.51	2.20	-9.99	-4.53	3.66	4.38
Stiff	10.0	1.65	2.34	-10.30	-4.79	3.30	6.21

Table 2: Mean temporal characteristics of preferred, soft, and stiff landings performed by male recreational athletes.

LANDING STRATEGY	TIME OF IMPACT(s) PEAK	TIME OF MIN ANGLE (s) KNEE*	TIME OF MIN ANGLE (s) HIP*	TIME OF MAX ANGULAR VELOCITY (s) KNEE	TIME OF MAX ANGULAR VELOCITY (s) HIP	TIME OF PEAK EXTENSOR MOMENT (s) KNEE	TIME OF PEAK EXTENSOR MOMENT (s) HIP*
Soft	.038	.236	.261	.048	.074	.050	.072
Preferred	.032	.166	.204	.051	.072	.037	.050
Stiff	.032	.101	.139	.042	.044	.032	.036

* Statistically significant difference between strategies ($p<.05$)

References

Jackson, K.M. (1979) Fitting of mathematical functions to biomechanical data. IEEE Transactions on Biomedical Engineering, 26, 122-124.

Lees, A. (1981). Methods of impact absorption when landing from a jump.Engineering in Medicine, 10, (4), 207-211.

McNitt-Gray, J. L. (1989). Kinematics and Kinetics of Drop Landings, Doctoral Dissertation, The Pennsylvania State University, University, Park, PA.

Nigg, B. M. (1985). Biomechanics, load analysis and sport injuries in the lower extremities. Sports Medicine, 2, 367-379.

Saito, S., & Yokoi, T.(1982). Basic programs of cubic spline smoothing and digital filtering. Bulletin of Health and Sports Science, University of Tsukuba, 5, 201-206

Acknowledgements: The authors thank Takashi Yokoi, Dawn Irvine, Isolina Pommier, Len Perkinson, Anil Wadiawani, and Zareh Kouyoumdjian for their assistance in this project. Funding was provided by USC Faculty Research and Innovation Fund.

MECHANICS OF SPRINT VELOCITY DECLINE WITH AGE IN ELITE MASTER'S SPRINTERS*

Nancy Hamilton
School of Health, Physical Education and Recreation
University of Northern Iowa, Cedar Falls, IA 50614-0241

INTRODUCTION

To date there have been few investigations of the decline in sprint speed which occurs with age in older runners. With the inceased interest in the Master's level of competition (ages 35 to 90+) there is an increasing need to understand the changes in stride mechanics which contribute to performance decline. The purpose of this study was to investigate those changes in sprint stride pattern between ages 35 and 90+ and to examine the relationship between changes in stride pattern and the kinematics of both upper and lower extremity motion. The data reported in this study are preliminary findings concerning the correlation between changes in stride pattern and changes in joint range of motion.

THEORY AND REVIEW

That sprint speed declines with age is an accepted fact. Moore, in 1974, compiled records to show that past the age of 30 running speed deteriorates steadily. Factors contributing to the decline in sprint speed per se have not yet been studied, but it has been reported that declines in distance running speed may be due to loss of muscle strength, loss of aerobic power, or loss of neuromuscular function (Roberts et al, 1986; Kavanagh & Shepard, 1976; Spirduso, 1984).

The combination of the above factors does not examine or explain the variations in sprint stride velocity which might be a function of movement pattern or mechanics. The only data on the biomechanics of stride in older runners is a small sample study of the swing leg in Master's distance runners done by Roberts et al. These investigators reported a decline of up to 3.6 m/s in speed and up to 4.44 m in stride length between the ages of 20 and 65. They also reported no clear differences in kinematic or kinetic variables for segment motion between older and younger runners.

METHODOLOGY

Subjects for this study were 65 male Master's sprinters between the ages of 35 and 94. All subjects were participants in either the TAC/USA National Master's Track and Field Championships (San Diego, 1989) or the World Veterans Games (Eugene, 1989). Subjects chosen were those with the fastest sprint times in the 100 meter dash at either meet. Where possible data was collected on a minimum of five runners, although in the older age groups there were fewer subjects. Data was collected at the two meets during competition. All heats, semifinal, and final races were videotaped using a Panasonic AG120 camcorder with a 2000 Hz shutter. Videotape data were then input into a computer using Peak Performance Motion Measurement Systems software, which digitizes at a frame rate of 60 Hz. From the digitized data

measures of stride length (SL), stride duration (SD), swing time (SWT), support time (SPT) and air time (AT) were derived. Further, measures of range of motion were calculated for the knee (KROM), hip (HROM) and shoulder (SROM), along with total trunk motion (TROM) and shank angle at foot strike (SHANK). A Pearson correlation was used to establish covariance and significant correlations. A Tukey's post hoc test was used to establish significant differences for each measure within the range of ages.

RESULTS AND DISCUSSION

With the exception of SD, SWT and TROM all measures varied significantly with age. SL, AT, KROM, HROM and SROM all showed a significant decrease with an increase in age while SPT and SHANK increased with age. The actual change in stride length was from a mean SL of 4.72 meters at age 35 to 2.84 meters at age 90+ ($p \geq .01$), which accounted for 80% of the variation in stride velocity. Stride duration changed very little, from a mean of .462 seconds to a mean of .578 seconds across ages, not statistically significant ($p \geq .10$). Since stride length and stride duration are the two components of stride velocity the decrease in velocity with age can therefore be said to be primarily a function of the change in stride length.

Range of motion in the lower extremity decreased significantly across ages, with the 75-90 age range being significantly lower than all others. The decline in ROM for both knee and hip was not linear, showing some variation at both ends of the age spectrum. There was a positive correlation between the range of motion and stride length. The strongest correlation was found to exist between HROM and SL ($r=.55$, $p \leq .01$) with KROM correlated at $r=.45$ ($p \leq .01$).

The range of motion results and the correlation with stride length strongly suggest that it is decreasing range of motion which produces a decrease in stride length. From 35 to 90 years of age SPT increases from 23% to 35% of the stride cycle. AT decreases from 26% to 15% of the cycle. Although stride duration does not vary significantly more time is spent in support and less time bringing the free leg through, implying less angular motion in the lower extremity. At this point it is not possible to state an absolute cause and effect relationship between range of motion and stride length. Further investigation must be done to determine whether decreasing range of motion is the result of the relative decrease in swing time and slower limb motion or if decreased range of motion leads to decreased stride length because the lower extremity cannot travel through as great an arc.

REFERENCES

Kavanagh, T. & Shepard, R. Med. & Sci. in Sport. 8(1):76, 1976.
Moore, D.H. Nature. 253: 264-265, 1976.
Roberts, E.M. et al. Proceedings North Amer. Cong. on Biomech., 1986.
Spirduso, W.W. Limits of Human Performance. AAPE, Hum. Kinetics Pub., 1984.

* Supported in part by a grant from the College of Education and NSF Grant #USE-8853326

KINETIC ANALYSIS OF FEMALE RUNNERS WITH A HISTORY OF STRESS FRACTURE

S.K. Grimston, J.R. Engsberg, #D.A. Hanley, and J.L. Patterson. Human Performance Lab. and #Dept. of Medicine, Univ. of Calgary, Calgary, CANADA.

INTRODUCTION: Low bone mineral density (BMD), or osteopenia, at the lumbar vertebrae (L2-L4) has been associated with athletic amenorrhea (1,2). This relationship, together with reports of higher stress fracture incidence in runners with athletic amenorrhea, has lead to the general association of osteopenia and stress fracture in female runners. However determination of an individual's propensity for stress fracture requires evaluation of the relative contribution of both intrinsic (e.g. BMD) and extrinsic (e.g. running mechanics) factors (3).

Extrinsic factors associated with stress fracture in female runners have received limited attention from researchers. Responses to questionnaires lead Barrow and associates (4) to propose biomechanical parameters as a risk factor for stress fracture. In a recent investigation the area moment of inertia of the tibia was found to have a statistically significant correlation with the incidence of tibial, femoral and total stress fracture incidence in male army recruits. However BMD was not significantly related to stress fracture incidence.

The purposes of this investigation were to compare 1) the external loading patterns of female runners with a history of stress fracture to those of runners with no stress fracture history, and 2) the relative contribution of menstrual status, BMD and external running kinetics to stress fracture incidence.

METHODS: All female runners recruited for this study were injury free at the time of the investigation. Three runners reported a history of stress fracture (SF) and 6 runners reported no stress fracture history (NSF). As a group SF reported a total of 5 stress fractures, 2 tibial and 3 femoral neck. All SF subjects were regularly menstruating (11-12 menses/year), while 2 of 6 NSF subjects had athletic amenorrhea (0-3 menses/year). Bone mass was measured at the lumbar vertebrae (L2-L4), the femoral neck (FN), and the medial diaphysis of the tibia (T), using dual photon absorptiometry (DPA).

Four trials (2 trials each foot) of force plate data for each subject were collected using a Kistler force plate (1000 Hz). Subjects wore standard shoes and ran across the force plate at a standard speed of 4 m/sec$\pm$10%. All data were normalized to a 100% of support time, and force data were normalized to a ratio of body weight. Two peak force values in the vertical, and peak forces in the medial, lateral, anterior, and posterior directions were determined from the force time curves. Impulses relevant to each force determination were calculated from the area under each curve.

Student's T-test was used to determine any significant differences between variables. All references to significant differences imply a probability at or below $P<0.01$.

RESULTS: There were no significant differences in BMD between SF and NSF at any site. Results for BMD L2-L4 are given in Figure 1. Menstrual status was not related to stress fracture incidence in these women. Peak vertical force, maximum anterior, posterior, and peak medial force were significantly greater for SF than for NSF (Figures 2-4).

DISCUSSION: In this preliminary study we have attempted to establish the relative contribution of BMD and external loading patterns to the incidence of stress fracture in female runners. Our results suggest that BMD and/or menstrual status may not be the underlying cause of stress fracture. However the external loading patterns of female runners were shown to contribute to their propensity for stress fracture. The magnitude of these higher forces combined with the repetition with which a long distance runner experiences these loads may be of greater importance than BMD L2-L4 with respect to stress fracture incidence.

Our results cannot address the issue of changes in running kinetics occuring as a consequence of prior stress fracture. A prospective study following NSF subjects until they incurred a stress fracture would be required for this analysis. Our results do suggest that running mechanics may be extremely critical in terms of the loading patterns chronically experienced by the cortical bone of the femur and tibia.

It was concluded that runners with a history of stress fracture in the tibia may experience greater impact and propulsive forces than those runners with no stress fracture history. Whether these higher loading patterns may be a cause or a consequence of stress fracture requires further investigation. The independance of these loading patterns from BMD and/or current menstrual status suggests their significant contribution to the etiology of stress fracture.

REFERENCES:

1. Drinkwater et al., N Engl J Med 5:277-281, 1984
2. Marcus et al., Ann Intern Med 102:158-163, 1985
3. Milgrom et al., J Biomech 22(11/12):1243-1248, 1989.
4. Barrow et al., Am J Sport Med 16(3):209-216, 1988.

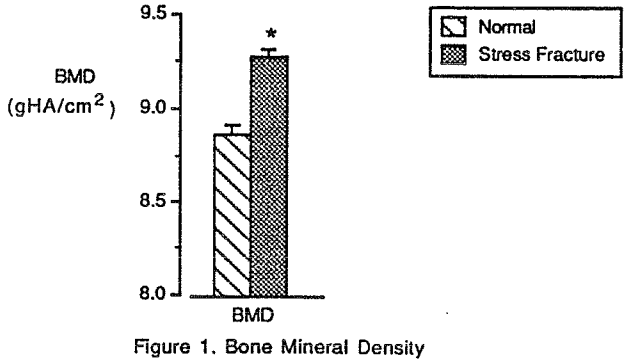

Figure 1. Bone Mineral Density

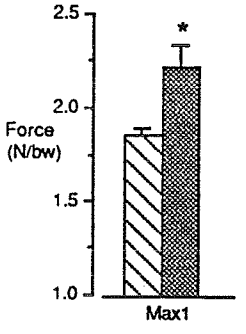

Figure 2. Vertical Impact Force

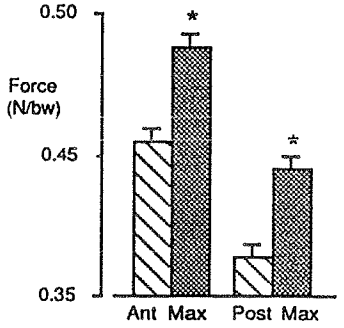

Figure 3. Anterior and Posterior Peak Forces

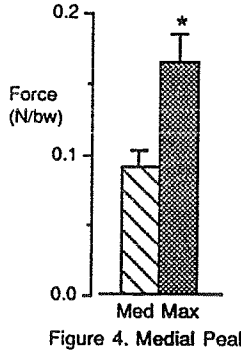

Figure 4. Medial Peak Force

* Significantly different from normal ($p < 0.01$)

FROM BIOMECHANICAL MODELING TO BIOMECHANICAL SIMULATIONS

Keynote Address By

M.M. Ayoub, Ph.D.,P.E.
P.W. Horn Professor

Institute for Ergonomics Research
Department of Industrial Engineering
Texas Tech University

LUMBAR EMG ACTIVITY DURING STATIC ASYMMETRIC LOADING OF THE TORSO

ASB Young Scientist Award—Pre-Doctoral

By

Richard E. Hughes

Center for Ergonomics
University of Michigan

LUMBAR EMG ACTIVITY DURING STATIC ASYMMETRIC LOADING OF THE TORSO

Richard E. Hughes and Don B. Chaffin
Center for Ergonomics, University of Michigan, Ann Arbor, MI 48109-2117

INTRODUCTION

Asymmetric lifting activities require complex combinations of torso muscle contractions. While contralateral muscle activity has been predicted by various models, co-contraction of ipsilateral muscles is not as well understood. This is especially true in situations in which there is no clear antagonist muscle due to the three-dimensional nature of realistic models of the lumbar trunk. An experiment was performed to explore the ability of two optimization models to predict co-contraction of ipsilateral muscles during asymmetric loading of the torso.

REVIEW AND THEORY

The minimum intensity-compression model for predicting muscle forces from intervertebral moments developed by Schultz *et al.* (1983) and reformulated by Bean *et al.* (1988) has been extensively compared to measured EMG activity and found to be much better at predicting contralateral muscle activity than ipsilateral muscle activity. It sequentially solves two linear programs to find the minimum upper bound on muscle contraction intensity (forces/cross sectional area) that allows the moment equilibrium conditions to be satisfied and then chooses the muscle forces to minimize spinal compression force. An extension of the eigenvector-based model of Gielen and van Zuylen (1986) to the torso does at least as well at predicting contralateral muscle forces as the minimum intensity-compression model on existing data sets. The eigenvector-synergy model minimizes co-contraction after choosing a set of muscular synergy levels to satisfy the moment conditions. The two models predict qualitatively different behavior during loadings in which the sagittal plane moment ranges from flexion to extension with a fixed but small level of frontal plane moment. The eigenvector-synergy model predicts increased left erector spinae force as the attempted flexion moment increases while the minimum intensity-compression model predicts zero force during attempted flexion. Such qualitative model behavior can be investigated without making assumptions about the muscle force-EMG relationship beyond the fact that it is monotonically increasing for static exertions.

METHODOLOGY

Eight male subjects were studied using surface electromyography in an erect static posture. Loads were applied to the torso at the level of T5 using a padded harness which was attached to ropes leading over pulleys to free hanging weights. The distance from the L3/L4 spinous interspace was measured so that the weights could be chosen for each subject to give combinations of -10 and -20 N.m of frontal plane moment and -45, -30, -15, 0, 15, 30, and 45 N.m of sagittal plane moment about the L3/L4 motion segment. Negative frontal plane moments involve attempted right bending; positive sagittal plane moments are attempted flexion. All 14 combinations were used and four replications of each loading combination were performed with a minute rest between trials. Each subject's posture was controlled to within $\pm$ 1 cm in the AP direction at L3, C7 and forehead levels and in the lateral direction at C7 at the beginning of each trial. Six muscles were monitored using arrays of six 4-mm diameter Ag-AgCl electrodes arranged into 3 pairs over a 2x3 cm rectangle: left and right erector spinae at L3, rectus abdominus at umbilicus, and external oblique 6 cm dorsal to ASIS. The signals were amplified and passed through RMS circuits with time constants of 55 msec before being sampled at 100 Hz for 3 seconds by a microcomputer. The mean of the three electrode pairs for each muscle was computed to give the estimated activity level.

RESULTS

Table 1 gives coefficients of simple determination for linear regressions between predicted force for the two models and measured EMG. Mean EMG values and standard deviation error bars for the left erector spinae (LES) muscle are presented in Figure 1. Note the LES activity appears to increase as the flexion moment increases. Analysis of variance shows that LES force is not constant across flexion moments ($p<0.001$).

Table 1. R^2 Values Between EMG and Predicted Force

Model	LES	RES	LRA	RRA	LEO	REO
Min. Intensity-Compression	0.860	0.968	0.954	0.922	0.723	0.816
Eigenvector-Synergy	0.863	0.925	0.969	0.925	0.413	0.894

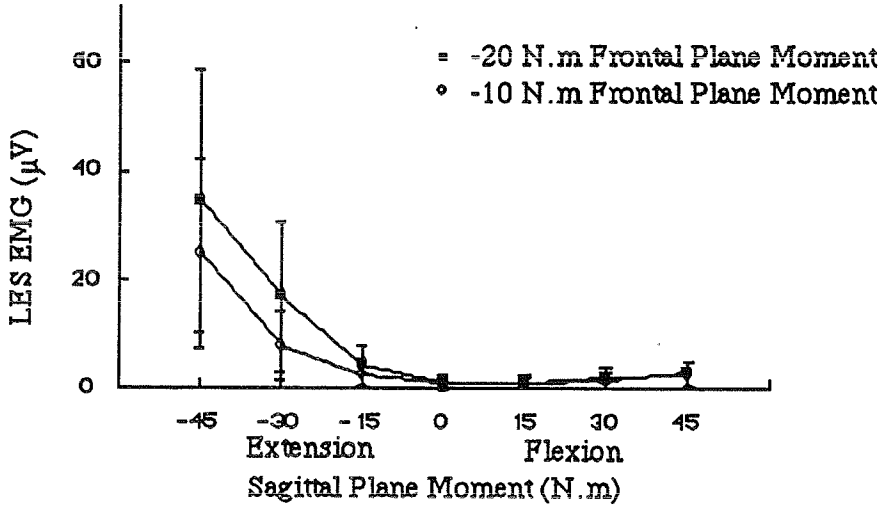

Figure 1. Left Erector Spinae EMG vs. Sagittal Plane Moment

DISCUSSION

The data supports the prediction of the eigenvector-synergy model that antagonist activity in the left erector spinae during attempted right lateral bending and flexion increases as the flexion moment increases. While good correlations between model predictions and EMG results are obtained for the erector spinae and rectus abdominus muscles, the eigenvector-synergy model does not predict left external oblique activity during extension as well as the minimum intensity-compression model does. This is due to an over-prediction of left external oblique antagonist activity during extension. Both models show higher correlations for the right erector spinae and external oblique muscles than for the corresponding left side muscles, suggesting the continued need to find improved methods for predicting co-contraction.

REFERENCES

1. Bean, J. C. *et al.* (1988) *J. Biomechanics* **21**: 59-66.
2. Gielen, C. C. A. M. and van Zuylen, E. J. (1986) *Neuroscience* **17**: 527-539.
3. Schultz, A. B. *et al.* (1983) *J. Ortho. Res.* **1**: 77-91.

This research was supported by NASA grant NGT-23-005-802 and NIH-AR39599.

SESSION 7

MEASUREMENT

CALIBRATION OBJECT MEASUREMENTS AND THREE DIMENSIONAL RECONSTRUCTION ACCURACY OF THE DLT ALGORITHM

Bernard André, M.Sc. eng.[1,3]; Jean Dansereau, Ph.D. eng.[2,3] and Paul Allard, Ph.D. eng.[1,3]

1: Dept. of Phys. Ed., Univ. of Montréal, P.O. Box 6128 St. "A", Montréal, Canada, H3C 3J7
2: Dept. of Mech. Eng., Ecole Polytechnique., P.O. Box 6079, St. "A", Mtl., Canada, H3C 3A7
3: Research. Center, Ste-Justine Hosp., 3175 Côte Ste-Catherine, Mtl, Canada, H3T 1C5

Introduction: As for the Direct Linear Transformation (DLT) algorithm [3], many sophisticated three dimensional (3D) reconstruction techniques use a calibration object for implicit calculation of their reconstruction parameters. In many papers, the accuracy of this calibration object is not reported. Most of these 3D reconstruction algorithms include calculation for estimating the reconstruction error. This estimate is known as the standard error or standard deviation [1, 3, 4, 5], the RMS error [6] or the RMS residual [2]. As presented in many studies, this estimate could be interpreted as the actual accuracy of the reconstruction technique. The aim of this study was to investigate the relation between the measurement accuracy of the calibration object and the 3D reconstruction accuracy using the DLT algorithm.

Material and method: A computer program was developped in order to generate a "pure" theoretical 3D calibration object (63 points uniformly distributed in a volume of 762mm x 300mm x 300mm) and 2D projections of it on different planes. These projections were used as digitized images of the object, allowing 3D reconstructions. Three biplanar stereo setups were simulated (the angles between the two projected planes were 20°, 45° and 90°). Randoms errors were imposed on the 3D theoretical object coordinates for ten sets ranging between ±0.01mm and ±5.0mm, producing 10 calibration objects of different accuracies. The stereo setups and the reconstruction algorithm were validated by reconstructing the theoretical object (no measurement error) with the 2D projections.

Using each of the ten calibration objects generated previously, the theoretical object (no error) was reconstructed . The reconstruction error was defined as the absolute difference between the 3D reconstructed coordinates and the known 3D coordinates. The DLT error was the name used for representing the estimation on the reconstruction error.

Results and discussion: The three setups investigated gave reconstruction results of the same order of magnitude but the biplanar orthogonal installation was sligthly more accurate than the others, as predicted by the theory [3]. Validation of the three stereo setups gave the same results: 3D real reconstruction errors of 0.000 ± 0.000 mm.

The "digitized" images used in this study were simply mathematical projections of the theoretical calibration object (obtained with the colinear equations of photogrammetry [3]). Therefore, validation results show that the DLT algorithm is exact, as far as double precision computer arithmetic is concerned.

Figure 1 shows that the mean 3D reconstruction errors (middle curve) increased almost linearly with the simulated measurement errors and were of a magnitude between 30% and 35% of these measurement errors. The maximum 3D reconstruction errors (upper curve) ranged between 50% and 100% of the measurement error magnitudes. On the other hand, the DLT error (lower curve) was always very small when compared with the measurement errors (< 10%).

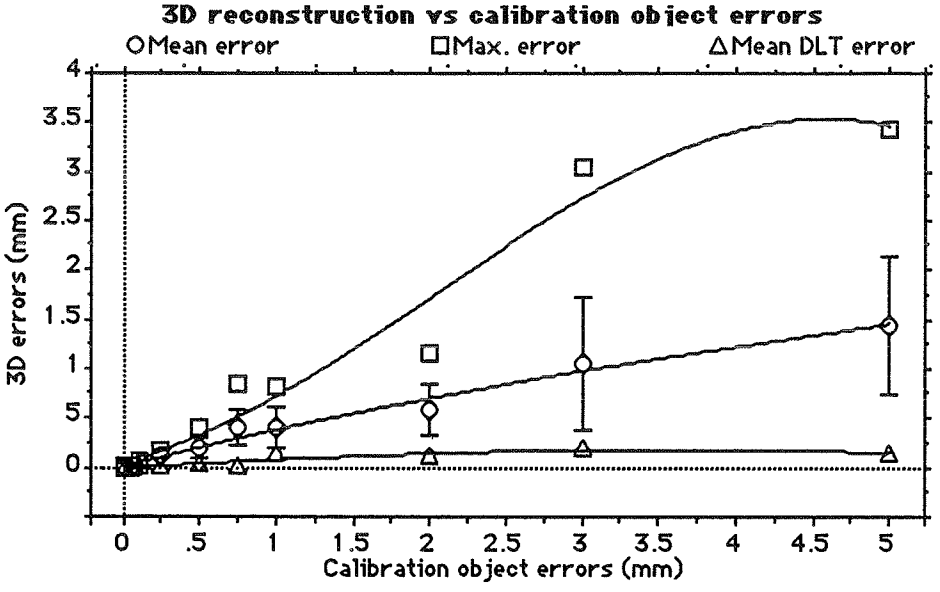

Figure 1: *Effects of calibration object measurement error on real 3D reconstruction error and on 3D DLT error (estimation of the real error given by the DLT algorithm).*

Results presented above emphasized the importance of the calibration object accuracy on the reconstruction results. Since the calibration object is so critical, great care should be taken in the design of these objects in order to facilitate the measurements and to provide structural rigidity as high as possible. This is particularly important for large calibration objects that have to be moved, as those used for gait analysis [6] or radiographic studies [4].

For the range of errors studied, it is clear that the estimation of the 3D reconstruction errors (DLT error) is not representative of the real 3D errors (figure 1). Therefore, reconstruction results should always be presented in relation with the accuracy of the calibration object.

Conclusions: According to this study, the following conclusions can be drawn:

1 - the real 3D reconstruction error increases markedly with the measurement error made on the calibration object;
2 - for the stereo setups studied, the estimation of the 3D reconstruction error given by the DLT algorithm (DLT error) is not representative of the real 3D reconstruction error;
3 - 3D reconstruction accuracy results should always be presented in relation with the accuracy of the calibration object.

References: 1. de Lange, A. et al.; J. of Biomech.; 23;259; 1990
2. Fioretti, S., et al.; J. of Biomech.; 18; 831; 1985
3. Marzan, G.T et al.; Symp. on Close-Range Photogram. Syst.; 420; 1975
4. Stokes, I.A.F., et al.; Med. & Biol. Eng. & Comput.; 18; 694;1980
5. Stokes. I.A.F., et al.; J. of Biomech.; 18; 1; 1985
6. Wood, G.A. et al.; J. of Biomech.;19; 781; 1986

Acknowledgements: Health and Wellfare (Canada) and NSERC (Canada).

A METHOD FOR THE INTRAVITAL MEASUREMENT OF INTERSPINOUS KINEMATICS

Allison M. Kaigle, Malcolm H. Pope, Braden Fleming, *Tommy Hansson

VT REC, McClure Musculoskeletal Research Center, Univ of Vermont, Burlington, Vermont
*Dept of Occupational Orthopaedics, Sahlgren Hospital, Gothenburg, Sweden

INTRODUCTION

A non-radiographic method for quantifying in vivo segmental motion is needed. By accurately measuring the degree of normal and abnormal motion, a better understanding of the general kinematics of the motion segment can be obtained and hopefully give insight into the mechanics of spinal instability. The design and preliminary testing of the Intervertebral Motion Device (IMD) which is capable of measuring quasi-static and dynamic two-dimensional sagittal plane motion of the lumbar spine is presented. Preliminary in vivo testing on normal subjects has included static sitting, flexion/extension, compressive loading, and exposure to vibration.

REVIEW AND THEORY

The condition of spinal instability has been cited as a low-back pain producing entity. From both clinical and experimental standpoints, there is no consensus on the definition of instability[1]. Pope and Panjabi[2] have proposed a definition of instability as loss of stiffness under known loads. Segmental instability is generally diagnosed from clinical symptoms and radiographic techniques. Although biplanar radiographic studies have distinguished the intervertebral motion of normals from that of individuals with low-back pain, significant clinical correlatins have not been identified. Excessive exposure to ionizing radiation limits radiographic methods. There are many applications in research where in vivo motion segment kinematics are of interest: disc creep under external loads, postural kinematics, evaluation of spinal fixation devices, and segmental motion under whole body vibration. Knutsson[3] suggested an association between anterior-posterior shear in flexion-extension and disc degeneration. Although spinal motion is coupled, the amount of axial rotation, lateral rotation or lateral translation occurring during flexion-extension is said to be minimal.[4,5] Experimentally, it is practical to study sagittal plane motion.

METHODOLOGY

The stainless steel IMD is an instrumented linkage transducer system (Figure 1). The trapezoidal linkage consists of two columns (11-gage tubing). Three sliding rods, A, B and C, (20-gage tubing) are allowed to rotate sagittally at their respective origins on the columns. At the other intersection of the rods with the columns, both sliding and sagittal plane rotation can occur. It is rods A and C which make up the parallel sides of the trapezoid while rod B forms a diagonal. Under local anesthesia, two intraosseous threaded Steinman pins (2.38mm D, 112mm L) are inserted approximately 8-10 mm into the spinous process of each vertebrae. Using an image intensifier, the locations of the pins within the vertebrae are established. The two columns of the IMD slide onto the pins and are secured at both ends, thereby forming a rigid fixation with the motion segment. The IMD employs the use of three custom-built strain gaged extensometers to fully quantify the planar motion. The extensometers, which attach to the IMD at ball-and-socket junctions, will either compress or extend due to the sliding of rods A, B, and C. Depending upon the application, different extensometers can be used to allow for full range read-out and maximize the signal-to-noise ratio (e.g. full range of motion vs. static sitting). Because of the rigid bone-pin interface, the movements of each vertebrae are imposed upon the IMD, thereby changing the lengths of the three calibrated extensometers. A post-processing computer algorithm can then use initial measurements and the sampled voltages from the extensometers to compute the spacial coordinates of points of interest and determine axial, shear and rotational segmental motion.

RESULTS AND DISCUSSION

The IMD was calibrated both statically and dynamically to determine the system accuracy using an ENCO 92068 Milling Machine, MTS 810 Materials Testing System, Compaq II portable computer and a digital caliper. Calibration results showed the individual extensometers to be linear within the +/-5mm operating range. The worst-case noise measured for vibration inputs was 0.018mm for 5Hz/0.2grms and 0.035mm for 8Hz/0.1grms. Preliminary in vivo testing has included static sitting, flexion/extension, compressive loading, and sitting vibration. For example, the axial compression at the L4/L5 level of an upright sitting normal subject with controlled posture was found to be 1.062mm over a five minute period. During this same time interval, the L4 vertebra sheared 0.048mm posteriorly with respect to the L5 vertebra. Table 1 contains peak-to-peak axial displacements of a sinusoidally vibrated (vertical) normal sitting subject.

Table One

Frequency/Acceleration (Hz) / (grms)	Axial Displacement (mm)
5.0 / 0.03	0.152
5.0 / 0.10	0.471
5.2 / 0.17	0.964

CONCLUSION

Many studies aimed at quantifying the movements of a lumbar motion segment have been conducted. These studies used cadaveric specimens and/or radiographic techniques. Results from preliminary testing indicate that the IMD is an accurate device for measuring in vivo quasi-static or dynamic two-dimensional sagittal plane motion of a spinal motion segment. Clinically, the IMD could be a useful tool for measuring segmental motion and corroborating these intravital measurements with symptoms of the low-back pain patients.

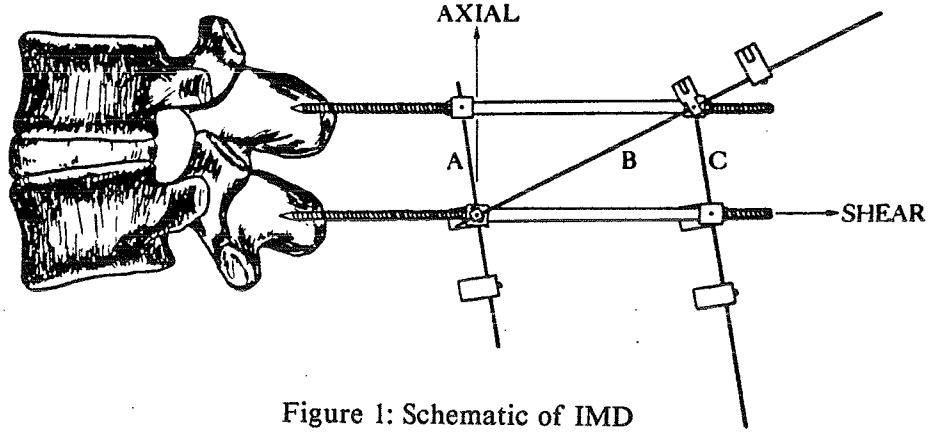

Figure 1: Schematic of IMD

REFERENCES

(1) Nachemson, Spine 10:290-291, 1985.
(2) Pope and Panjabi, Spine 10:255-256, 1985.
(3) Knutsson, Acta Radiol 25:593-609, 1944.
(4) Gertzbein et al., Spine 10:257-261, 1985.
(5) Panjabi and White, Neurosurg 7:76-93, 1980.

CONTACT STRESS GRADIENT DETECTION LIMITS OF PRESSENSOR FILM

Joseph E. Hale and Thomas D. Brown
Biomechanics Laboratory, Department of Orthopaedic Surgery
The University of Iowa, Iowa City, IA 52240, USA.

INTRODUCTION: Fuji Pressensor film has been widely used in studies of the contact mechanics of articular joints. Although there has been relatively little direct study of the film's performance characteristics, contact stress measurement errors are reported to lie in the range of approximately 10 to 15 percent [1,2]. While this level of accuracy is acceptable for many applications, the lack of suitable alternatives has led to Pressensor use in problems which clearly challenge the film's spatial resolution capabilities. The purpose of the present investigation was to evaluate the limits of Pressensor film's ability to detect contact stress gradients when analyzed using state-of-the-art digital imaging technique.

METHOD: Standardized contact stress distributions for analysis by Pressensor film were obtained experimentally by means of MTS-driven cylindrical indentations of a compliant polyurethane sheet adhesively bonded to a rigid substrate (Fig. 1). Right circular cylinders of various radii (2, 3, 4, 6, 9, 12 and 20 mm) and a polyurethane sheet (4.8 mm thick; 95A durometer hardness) gave an appropriate range of contact stress gradients.

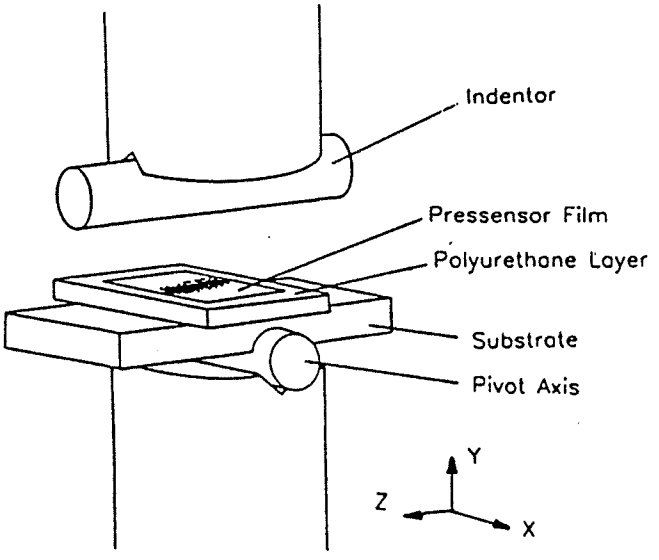

Figure 1. Experimental test configuration.

A new digital image analysis protocol was used to quantitate the Pressensor contact stress distributions. Preliminary image captures were performed under transmitted backlighting using an Eikonix digital camera. Data were stored as a 512 by 512 array of eight bit grey levels. Reference points for full background illumination intensity and for an in-field 10 percent neutral density filter permitted direct conversion from grey scale to optical density. Subsequent conversion from optical density to contact stress was based on a series of known pressure/optical density standards. Transverse variation of pixel contact stresses was sampled at a large number of ostensibly equivalent stations, and then ensemble averaged. The transverse contact stress distribution ideally present was estimated by finite element analysis and by a closed-form analytical solution [3].

RESULTS: Comparison of analytical versus measured contact stress distribution across a nearly 100-fold range of stress gradient variation showed that the ensemble averaged Pressensor profiles consistently underestimated the peak contact stress magnitude, and consistently overestimated the contact zone half-width. These discrepancies diminished as the gradient severity decreased. The analytically-predicted spatial maximum contact stress gradient occurred at the contact periphery, and ranged from 283 MPa/mm (R = 2 mm) to 29.9 MPa/mm (R = 20 mm). The spatial mean contact stress gradient, indicative of overall contact stress nonuniformity, varied from 39.6 to 4.5 MPa/mm. Experimentally detected gradients were consistently smaller than those predicted analytically (Fig. 2). The relative difference again progressively diminished as the contact stress distribution became more uniform, with the spatial mean gradient being more accurately transduced throughout the series. The experimental and analytical estimates of spatial mean gradient became reasonably convergent (<15 percent error) at approximately 9 MPa/mm (R = 9 mm).

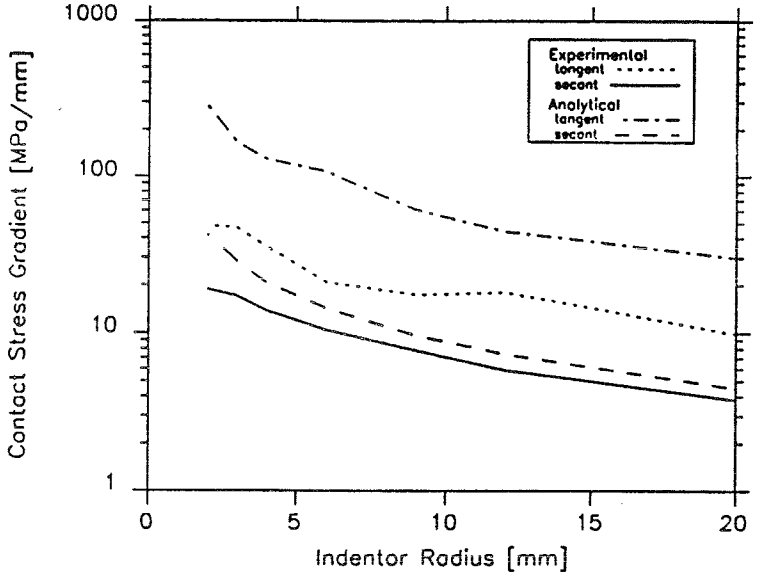

Figure 2. Contact stress gradients as a function of indentation cylinder radius.

DISCUSSION: The present results substantiate medium grade Pressensor film's capability to transduce gradients reliably up to approximately 9 MPa/mm. At its upper extreme, the film was capable of registering a local contact stress gradient of approximately 48 MPa/mm. While this falls well short of the theoretically-present value of 283 MPa/mm, the 48 MPa/mm reading nevertheless occurred at an appropriate site in a reasonably-shaped profile which, upon integration, yielded a resultant load that was only 8 percent less than the physically applied load. Even conservatively interpreted, the film's capability to transduce contact stress gradients of up to approximately 9 MPa/mm is more than sufficient for most local incongruity applications in articular joints (contact stress gradients < 2 MPa/mm). [4]

REFERENCES:

1 Fukubayashi & Kurosawa, Acta. Orthop. Scand. 51:871-879, 1980.
2 Brown et al., J. Orth. Res. 6:851-862, 1988.
3 Meijers, Appl. Sci. Res. 18:353-383, 1968.
4 Huber-Betzer et al., J. Biomech., in press, Feb. 1990.

Supported by NIH grant AR38916.

VALIDATION OF A THREE DIMENSIONAL MOTION AND FORCE ASSESSMENT SYSTEM

K.J. Deluzio, U.P. Wyss, J. Li, P.A. Costigan
Clinical Mechanics Group and Department of Mechanical Engineering
Queen's University, Kingston, Ontario, Canada, K7L 3N6

INTRODUCTION

In the evaluation of human motion, systems based on different principles are used to collect kinematic data. Recent advances in electronics have made available optoelectric systems to acquire this data (1). The objective of this study was to determine the accuracy of three dimensional (3D) knee motion and force analysis based on an optoelectric system, which is used to assess knee loading during walking and stair climbing. Two simple mechanical models with known behaviour were used to assess the system performance. Both models simulated elements of the human knee: the first represented the three clinical rotations of the knee, while the second allowed accurate force measurements of a single degree of freedom link. Flexion and longitudinal rotation could be measured within 2° with the error in adduction slightly higher. Force measurements were found to be within 8.0%.

REVIEW

Optoelectric systems require active markers (LEDs) to be placed on the subject at known landmarks. Cameras record the position of the markers from which 3D coordinates, velocities, accelerations, and forces are calculated. The automation these systems provide has lead to a much wider use of motion assessment systems; whereas, little has been reported about the accuracy of a given set-up for a particular study. The accuracy depends on many factors such as LED-camera configuration and control of reflections.

METHODOLOGY

The test conditions were kept as close as possible to those used in the knee motion analysis study. The test site was a portion of the walkway about the force plate. The two cameras were mounted on tripods in such a way that their field of view covered one cycle of gait. As reflections result in the erroneous location of LEDs, care was taken to minimize them.

Model 1: This model consists of two segments representing the tibia and the femur with the possibility of three rotations at the knee joint (flexion, longitudinal rotation, and ab/adduction). The three axes were instrumented with potentiometers to accurately record the angles. These angles were simultaneously calculated using the floating axis method (2). The accuracy to which the three angles could be determined over the entire range of motion in each degree of freedom was found.

Model 2: This model consists of a freely moving compound pendulum with one degree of freedom. The dimensions and mass moment of inertia were chosen to simulate the shank and foot of a 70kg person (3). The pendulum was instrumented with a strain gauge transducer calibrated to yield the axial load. The model was positioned at various distances from the centre of the walkway as well as at various angles to the cameras. It was decided to vary the cutoff frequency from about 3 to 9 Hz to assess the sensitivity of the system to data smoothing.

RESULTS

The errors in calculating the three rotations of model 1 are shown in table 1. There was no significant difference between the static and the free motion trials. A typical graph of the free motion trial is shown in figure 1. The results from model 2 indicated the average error over all the trials was 3.4 N or 7.6%. Figure 2 shows a typical result for one cycle of the pendulum.

Table 1: Floating Axis Angles - Potentiometers
(error in degrees)

		Adduction	Flexion	L.Rotation
Static	Avg.	3.8	0.9	1.5
	S.D.	2.2	0.5	1.1
Free Motion	Avg.	3.2	0.5	1.5
	S.D.	2.0	0.4	1.1

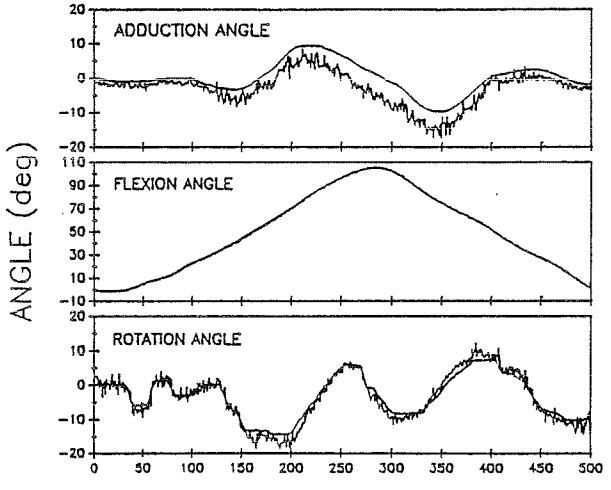

Figure 1: 'Knee Rotations'

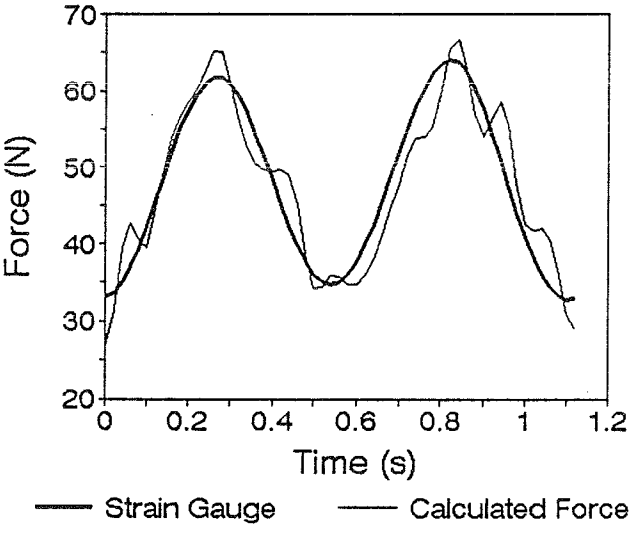

Figure 2: Dynamic forces

DISCUSSION

The results reveal that the knee assessment system performs well and the accuracy of the system could be determined. The clinical rotations were calculated within 2 degrees with the exception of adduction during high flexion angles. Movement of the model within the cameras' calibrated volume did not affect the force calculation.The filtering cutoff frequency was the most significant effect: reducing it by 1 Hz lowered the error by 0.25 N.

References

1. Chao, E.Y.S. in *Frontiers in Biomechanics* Schmid-Schoenbien (ed) pp. 225-244, 1986.
2. Grood, E.S., et al. J. Biomech. Eng. 105:136-144, 1983.
3. Winter, D.A. *Biomechanics of Human Movement*, John Wiley & Sons, Inc. 1979.

Acknowledgements

This work was supported by the National Sciences and Engineering Research Council of Canada and the Medical Research Council of Canada.

THE SPECTRA OF ENDOGENOUS STRAINS IN THE CRANIUM: EVIDENCE FOR FUNCTIONAL ADAPTATION IN MINIMALLY LOADED BONES

John Tashman, Kenneth J. McLeod and Clinton T. Rubin
Musculo-Skeletal Research Laboratory
Department of Orthopaedics, SUNY at Stony Brook, NY 11794-8181

INTRODUCTION

The spectral distribution of strain energy in the cranium has been estimated from accelerometer recordings obtained during normal functional activities (chewing, speaking). The accelerometer provides sufficient sensitivity to evaluate endogenously induced strains up through 100 Hz. Specific frequency regimes of strain energy can be clearly defined as increasing activity results in the appearance of high frequency strain components with little alteration of the lower frequency components. The magnitude of these high frequency strain components rarely exceeds 10 microstrain at 10 Hz, and decrease to .1 microstrain at 100 Hz. Investigations on the frequency response characteristics of bone adaptation suggest that strains even of this low magnitude may be physiologically significant.

REVIEW AND THEORY

The maintenance of bone mass is known to be dependent on the dynamic mechanical strains engendered in bone due to normal functional activity. However, the specific components of functional strain which are most critical to this adaptation remain unknown. This is exemplified by the fact that bone mass is maintained at bone sites which rarely experience large functional strains, for example, on the neutral axis of long bones and in the cranium.

We have previously suggested that in the appendicular skeleton low magnitude, high frequency strains may serve as an important regulatory component of functional strain. Using exogenously induced electric fields to modulate bone remodeling activity we have demonstrated bone adaptation to be a process strongly dependent on the frequency of the physical stimulus. Stimuli in the 15 to 30 Hz regime are far more effective in preventing bone loss and initiating new bone formation than lower frequencies. Indeed, the field intensities required to maintain bone mass are consistent with those induced endogenously by strains as small as 1 microstrain.

That low magnitude, high frequency strains may regulate bone remodeling also has direct applicability to the issue of morphologic adaptation in the axial skeleton. The exquisite architecture of certain bones (e.g. crania, bulla) is difficult to explain in terms of functional adaptation as these bones rarely, if ever, experience large loads. Alternatively, sufficient high frequency strain energy may be imposed on these structures to maintain their large bone mass in the absence of large, low frequency strains.

METHODOLOGY

We have investigated the spectra of induced strain energy in the axial skeleton through analysis of accelerometer recordings obtained from the cranium during functional activity. An accelerometer (Entran Devices, Inc., Fairfield, NJ), was firmly attached to the skin overlying the supra-orbital ridge of the cranium of human volunteers (3 male, 1 female). This site was chosen for its accessibility and minimal amount of overlying soft tissue. The subject was seated while recordings of 1 second duration were made with the subject at rest, engaged in chewing soft and hard edible substances, and while vocalizing sounds composed of single and multiple frequencies. The accelerometer signal was amplified (Vishay Measurements Group, Inc., Raleigh, NC), low pass filtered at 200 Hz, and digitized (DASH-16, Metrabyte Corp., Taunton, MA) at a sampling rate of 1024 Hz.

Accelerometer signal spectra were obtained by fast Fourier transform, and the spectra visually analyzed for the location of acceleration peaks. Cranial displacements at the peak frequencies were calculated based on a thin, uniform thickness spherical shell model, with an applied moment at the axis. An analytic solution for the displacements and strains developed at any location on the spherical shell has been used (1). To evaluate the accuracy of the conversion of acceleration to induced strain, the calculated data from the human was compared to strain data obtained (courtesy of Dr. William Hylander) from the supra-orbital ridge of the Macaque monkey.

RESULTS

Specific functional activities produce distinct acceleration spectra in the cranium. Increasing activity results in the appearance of higher frequency components in the spectra, with little alteration of the lower frequency components. A function such as chewing of a hard food creates easily recorded accelerations at frequencies up to 100 Hz (Fig. 1). Conversion of the recorded accelerations to strain suggests that peak strains occuring above 10 Hz rarely exceed a few microstrain. Comparison of human accelerometer and Macaque strain gage data shows a close correspondence between both the spectral patterns generated during a specific activity and the magnitude of the strains imposed (Table 1). This comparison is limited, however, to frequencies below 20 Hz due to filtering of the strain gage data.

DISCUSSION

These results demonstrate that peak strains of 0.1 to 10 microstrain occur in the cranium over a spectrum extending to several hundred hertz. Whether these strain components are important to the process of functional adaptation is not clear. Indeed, in comparison to the large static or quasi-static strains which can be demonstrated in bone, these high frequency strains appear to be extremely small. However, the activities with which these strains are associated extend over long durations and exposure time may be important in the process of functional adaptation. In addition, the frequency sensitivity of the bone cell population is undoubtedly critical in understanding the role of these strain components. For example, the mechanoreceptors in the skin are 1000 times more receptive to stimuli delivered at 200 Hz than at 2 Hz. Until the full dynamic range of bone's sensitivity to mechanical stimuli is elucidated it will not be possible to determine whether the small funcitonal strains occuring in the cranium affect the bone morphology.

(1) Seide, P. (1975) Small Elastic Deformations of Thin Shells, Noordhoff Int., Leyden, The Netherlands, pp. 374-386.

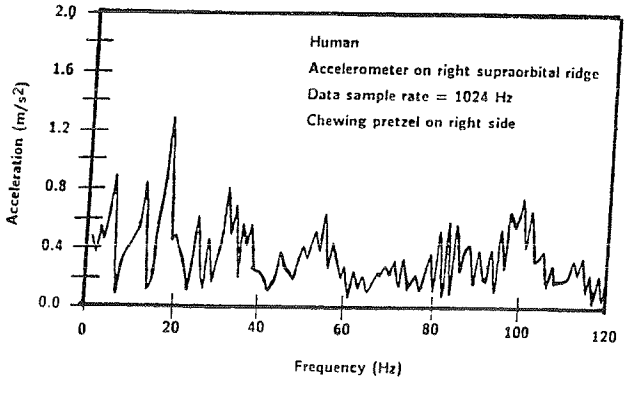

Figure 1

ACTIVITY	FREQUENCY (Hz)	MACAQUE MICROSTRAIN	HUMAN MICROSTRAIN
Rest	10	1.0	1.6
Chewing (Soft)	9 21 30 45	1.6 0.6 0.2 0.2	1.4 1.2 0.3 0.08
Chewing (Hard)	10 24 37 54		6.0 0.6 0.3 0.1
Humming	128 256		0.03 0.01

Table 1. A comparison of strains, as recorded in the Macaque and calculated in the human, crania.

Table 1

SESSION 8

SPINE #1

LUMBAR MOTION AS A FUNCTION OF TORSO ANGLE

Herbert M. Reynolds, Ph.D. and Raymond R. Brodeur, M.S., D.C.
Department of Biomechanics, Michigan State University, East Lansing, MI 48824

INTRODUCTION

Motions in the lumbar spine have been studied extensively in vitro (1) and in vivo (2). However, the ability to predict the angular position of vertebra in the lumbar spine from measurement of relative thorax to pelvis positions is useful for evaluating lumbar function. A linear model for each lumbar motion segment has been investigated based upon stereoradiographic measurements of eight, adult male, unembalmed cadavers. The average range of torso motion was 55.6°. The regression of vertebral on torso angles has slopes for each lumbar motion segment ranging from .07 to .43 with correlations between actual and predicted angles typically above .9.

REVIEW AND THEORY

Local vertebral motion segments of the lumbar spine are linked axially through soft tissue (i.e. disk, ligaments, and muscle) yet transversely their motion is constrained by the hard tissue geometry of the facets. In addition, the motion of the lumbar spine is constrained inferiorly by the pelvis and superiorly by the thorax. Given the above mechanical constraints, it is logical to propose that the sagittal motion of the lumbar spine is linearly dependent on the relative thorax-pelvis positions. To date, the vast majority of information on the lumbar spine has been obtained from excised spines. In the current investigation, the in situ behavior of the lumbar spine was investigated in 15 different seated positions.

METHODOLOGY

A stereoradiographic system (3) was used to measure the three-dimensional coordinates of implanted targets in C7, T1, T4, T8, T12, L1-L5, sacrum, and both innominate bones of eight unembalmed, fresh, cadavers (mean age at death 56.4 ±20.5 years). The measured postures began in maximum lumbar extension produced by a plexiglass bar which extended 4.9 cm from the seat back at approximately the level of L3. The body was sequentially repositioned by incrementally moving the plexiglass bar toward the seat back. For the flexion series, the pelvis was moved incrementally forward in the seat pan until the ischium had translated an average of 9.7 cm anteriorly. A hard, wooden seat with a seat back angle of 115° and a seat pan angle of 15° from horizontal was used to position the cadaver, held in place by straps restraining the pelvis, chest and head, as appropriate. The 3-D coordinates of each target were determined relative to a right-handed, coordinate system defined with +X in the anterior direction; +Y in the left lateral direction; and +Z in the superior direction.

RESULTS

The motion of each vertebrae was found to lie almost exclusively in the sagittal (X-Z) plane. All angles are measured as positive about the Y-axis, using the right-hand rule. The relative vertebral angles were

calculated for each subject; the initial (full extension) angle was called θ_o. Torso angle was calculated as the angle between the base of the sacrum and the average of the superior and inferior surfaces of T1 (T4 was used for one subject). Alternative means of determining torso angle were investigated and no significant differences were found. Sacroiliac joint motion was minimal, typically less than 2°. The initial (full extension) torso angle was called α_o. The average range of torso angle was 55.6° ±11.7. The change in vertebral angle relative to θ_o was plotted against the change in torso angle relative to α_o. Regression lines describing this relationship are shown for subject 21 in Figure 1. All regressions were calculated with a forced 0 intercept. Table 1 gives the correlation coefficients and the slopes of the regression lines for all subjects.

DISCUSSION

From Figure 1 and Table 1 it can be seen that there is a high linear correlation between the change in torso angle and vertebral angle. This suggests that the sagittal plane motion of each lumbar motor unit can be described relative to torso angle using a linear model ($d\theta/d\alpha = A$) where $d\theta$ is the change in the angle of the lumbar motion segment, $d\alpha$ is the change in the torso angle and A is a constant. The relationship between torso angle and lumbar motion in lateral flexion is currently being investigated. If the above relationships can be shown to exist in vivo, a useful model of the lumbar spine can be developed describing local vertebral motion as a function of torso motion.

REFERENCES

1. Goel, V. K., S. Goyal, C. Clark, K. Nishiyama, and T. Nye (1985) Kinematics of the whole lumbar spine. Effect of Discectomy. Spine 10(6):543-554.
2. Pearcy, M. J. (1985) Stereo radiography of lumbar spine motion. Acta Orthop Scand Suppl 212, vol 56.
3. Reynolds, H. M. (1989) Systems Anthropometry of the Shoulder/Vertebral Column/Hip Linkage System: Maximum extension to maximum flexion in the seated position. Final Report, USAAFMRL, Wright-Patterson AFB, Ohio.

TABLE 1. Regression slopes of relative lumbar angle compared to relative torso angle.

ID	L1-L2	L2-L3	L3-L4	L4-L5	L5-S1
21	.14(.92)*	.20(.95)	.15(.98)	.24(.94)	.26(.94)
22	.15(.95)	.14(.96)	.16(.98)	.14(.97)	.15(.95)
23	.23(.93)	.20(.99)	.16(.97)	.21(.98)	.07(.91)
24	.13(.90)	.14(.95)	.16(.93)	.11(.85)	.13(.95)
25	.43(.87)	.22(.95)	.07(.55)	.10(-.25)	.08(.85)
27	.16(.97)	.12(.93)	.13(.94)	.23(.95)	.34(.94)
28	.18(.91)	.17(.98)	.12(.92)	.17(.89)	.11(.71)
29	.22(.94)	.20(.96)	.28(.98)	**	**

* numbers in brackets are correlation coefficients.

** subject 29 had a spondylolisthesis of L5.

FIGURE 1 Simple Regression of Lumbar Motion Segments Versus Torso Angle For Subject 21

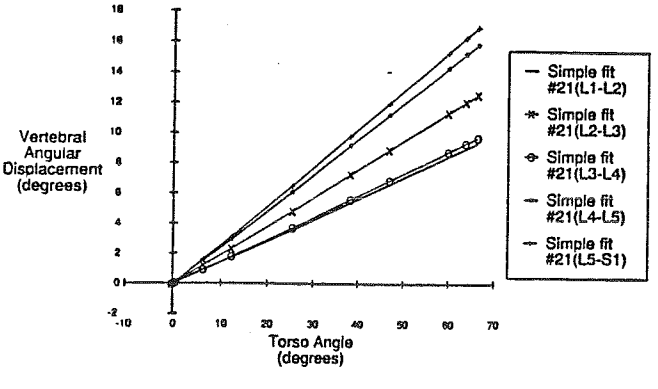

ACKNOWLEDGEMENTS. This research was supported in part by AAFAMRL Contract #F33615-85-C-0530. Educational support for Dr. Brodeur has come from Palmer College of Chiropractic and FCER.

MECHANISMS OF LATERAL DEVIATION AND AXIAL ROTATION IN SCOLIOSIS

Ian AF Stokes and Mack Gardner-Morse
Department of Orthopaedics and Rehabilitation
University of Vermont, Burlington, VT 05405, USA

INTRODUCTION

There is a lack of clear biomechanical analyses to support theories of the interaction of the lateral and axial deformity of the spine in scoliosis. Three variations on a finite element model were used to investigate two different hypotheses about the etiology of scoliosis and to define the forces required to produce a scoliosis deformity. The first hypothesis is that coupling within a motion segment produces the interaction between lateral deviation and axial rotation. The second hypothesis is that posterior tethering by soft tissues as the spine grows produces the observed interaction. The models consist of an isolated ligamentous spine with realistic elastic properties and with an idealized geometry. Modeling of both hypotheses failed to produce the clinically observed pattern of interaction. Therefore, to find which biomechanical forces were required to produce an idealized scoliosis, prescribed displacements were applied to the model. The prescribed displacements required large axial moments corresponding to anterior shear forces. Also, the pattern of lateral shear force and axial moment were not symmetric in the kyphotic and lordotic regions of the spine despite symmetric geometry. In vivo, these forces may result from asymmetric muscles which cross several vertebral levels, asymmetric rib growth, or asymmetric vertebrae development.

REVIEW AND THEORY

The clinically observed correlation of axial rotation and lateral deviation in idiopathic scoliosis is reported by Stokes, et al.[4]. Veldhuizen, et al.[5] showed qualitatively that the coupling of lateral deviation and axial rotation was due to the saggital profile of the isolated spine. However, the model did not include the coupling terms measured by Panjabi, et al. [3]. Jarvis, et al.[1] experimented with a posterior tether applied to excised calf and human spines. In one case of each species, compression of this construct caused both a lateral deviation and some rotation.

METHODOLOGY

The analysis was performed using a finite element model of an isolated ligamentous spine with an idealized geometry. The initial shape was straight in the frontal plane and in the form of a sine wave in the saggital plane. The Cobb angle of the complementary lordosis and kyphosis was 42.4° (see Figure 1). The idealized geometry defines 17 nodes representing the vertebral body centers of T1-L5. Three beam elements representing vertebral processes were attached to these nodes. The intervertebral motion segments are represented by stiffness matrices derived from those published by Panjabi, et al.[3]. The incorporation of experimental flexibility data into finite element models is described by Gardner-Morse, et al.[2].

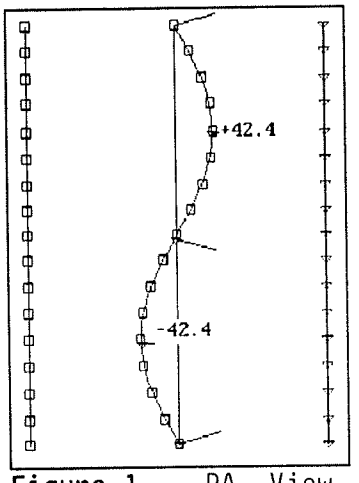

Figure 1 PA View, Lateral View, and Axial Rotation of Initial Geometry

A coupling model was used to investigate vertebral axial rotation accompanying lateral deviation in the model. Moments were applied to the ends of the spine to produce either single or double curvature deformities. An asymmetric posterior tether consisting of spring elements connecting the vertebral processes on one side of the spine was added to the tether model. Initial strains were applied to the spring elements to produce deformed shapes. A prescribed displacement model used an idealized scoliotic shape of a double curve with Cobb angles of 11° each as the end point of a lateral force and an axial moment applied to each vertebra in the initially straight spine (see Figure 2).

RESULTS

The pattern of lateral deviation and axial rotation for each model is shown in Figure 2. The single curve coupling model produced minimal axial rotation with lateral deviation. The double curve coupling model produced 0.18° of axial rotation per mm of lateral deviation. However, neither of the coupling models produced the clinical pattern. The tether model produced only 0.07° of axial rotation per mm of lateral deviation. While the pattern was correct in the kyphotic region, it was not in the lumbar region. The tether also reduced the kyphosis and increased the lordosis.

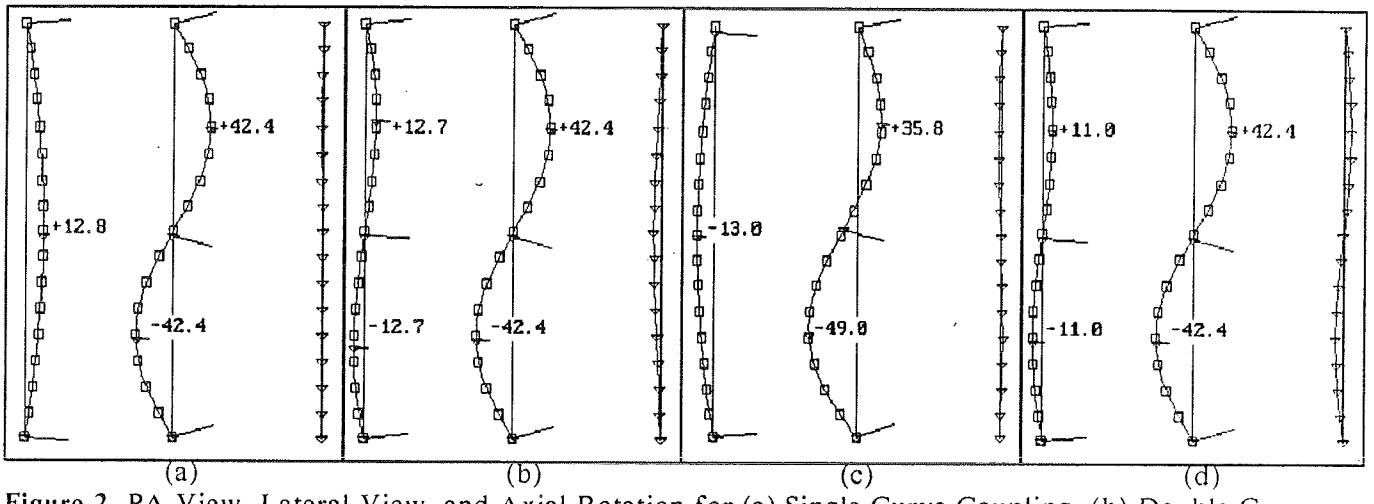

Figure 2 PA View, Lateral View, and Axial Rotation for (a) Single Curve Coupling, (b) Double Curve Coupling, (c) Tether Model, and (d) Idealized Scoliosis.

The required lateral forces and axial moments to produce the idealized scoliosis are shown in Figure 3. The lateral shear forces are on the order of 25N and the axial moments are on the order of 1000Nmm. This corresponds to the lateral shear forces being approximately 40mm anterior to the vertebral centers.

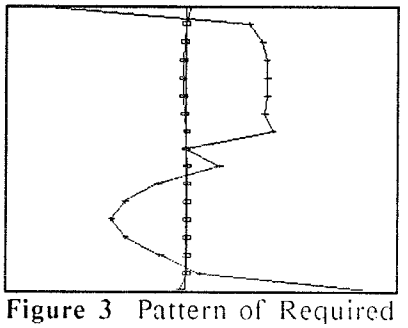

Figure 3 Pattern of Required Lateral Forces (▭) and Axial Moments (+) by Vertebral Level.

DISCUSSION

Coupling of lateral bending and axial rotation within motion segments failed to produce the clinically observed patterns of scoliosis. The asymmetric tether only produced a small amount of interaction between lateral deviation and axial rotation. The tether also failed to produce the correct pattern in the lordotic part of the spine. A symmetric tether or simple compressive forces only increased the kyphosis and lordosis and produced no lateral deviation. The lateral forces and moments required to produce the idealized scoliosis were not symmetric despite symmetric initial and final geometries. The main limitation of these models is that they represent only elastic behavior of the spine, and ignore adaptive changes and growth which are probably important in determining the eventual form of the scoliosis. by including only linear Another missing factor in the models was the effect of muscles which cross several vertebral levels.

REFERENCES

[1] Jarvis JG, et al., Clin Orthop 227:126-134, 1988
[2] Gardner-Morse, et al., J Biomech Eng, at press
[3] Panjabi MM, et al., J Biomech 9:185-192, 1976
[4] Stokes, et al., J Orthop Res 6:129-137, 1988
[5] Veldhuizen AG, et al., Spine 12:852-8, 1987

CORRECTED 3-D PARAMETRIC MODEL OF RECONSTRUCTED SCOLIOTIC SPINES

DANSEREAU, J., PAPILLON, B., LABELLE, H.,
Dept. of Mechanical Engineering, École Polytechnique,
P.O. Box 6079, Station A, Montreal, Canada, H3C 3A7.
Sainte-Justine Hospital, Montreal, Canada.

INTRODUCTION Several stereoradiographic or biplanar reconstruction techniques have been developed and used in order to obtain computed three-dimensional (3-D) representation of scoliotic spines. Such representations are hard to be evaluated visually by clinicians because of their inability to represent the real geometry of the anatomical structures and also because reconstruction errors on landmark coordinates (implicit to any stereoradiographic or biplanar reconstruction techniques) may generate a resulting distorted image. In order to obtain realistic 3-D representations of scoliotic spines, a corrected parametric model was developed from the stereoradiographic reconstruction technique routinely used at Sainte-Justine Hospital. This paper presents the method used to obtain such parametric model as well as some preliminary validation results.

MODELLING METHOD Three-dimensional reconstruction of anatomical landmarks on scoliotic spines is obtained by taking a conventional postero-anterior (P-A) view and a 20° angled down P-A view. Six anatomical landmarks per vertebra (center of the endplates and inferior and superior tips of both pedicles) are reconstructed using the DLT program [1]. The corrected parametric model was built from these reconstructed coordinates and from spinal anthropometric measurements reported from the literature [2,3] (interpedicular distance, pedicle length and diameters, pedicle - vertebral body distance, vertebral body P-A and transversal diameters, total vertebral P-A length, spinous process angulation). The computer methods used are the following:

1) A smoothed 3-D curve (least squares parametric Fourier series) is fitted through the pedicle midpoints of each vertebra (computed from the four pedicle landmarks) to compensate for the errors on reconstructed coordinates. New pedicle midpoint coordinates are then computed.
2) The frontal and lateral orientations of each vertebra are corrected by using the slope of the smoothed curve evaluated at the new pedicle midpoint coordinates. The axial rotation of each vertebra corresponds to the orientation of the line joining the middle points of right and left pedicles.
3) The centroid of vertebral bodies are corrected so as to be centered with respect to the line joining midpoints of both pedicles.
4) The vertebral body height corresponds to the projection of the endplate landmarks on a line (intersecting the vertebral body centroid) parallel to the line which defines the corrected orientation of the vertebra.
5) In order to consider variations in patient size and height, a generalized dimension coefficient for the whole spine is calculated by comparing, for each anatomical level, the projected frontal length between the center of both pedicles to the interpedicular distance reported from the literature.
6) Based on this dimension coefficient and on the anthropometric data (transversal and P-A diameters), the vertebral bodies are modelled as elliptical cylinders. Tips of both pedicles are corrected with respect to their midpoints and from the corrected vertebral orientation. Pedicles are modelled as straight lines. Spinous processes are extrapolated as triangles. Figure 1 shows P-A and lateral views of a corrected 3-D reconstruction model.

VALIDATION METHOD AND RESULTS Lateral projections of three corrected (modelled) spines were compared to their corresponding lateral radiographs on which the same anatomical landmarks were digitized. The lateral views were used for validation because they correspond to the plane on which the reconstruction error is greater. A least square algorithm was programmed to fit the different lateral views. The residual least square values were used as a validation index. Best fits were done on modelled lateral projections and on reconstructed lateral projections (on which no landmark correction has been done). The lateral angulation of each vertebra (line joining the center of the inferior and superior endplates) was also computed for the different representations. Results are summarized in Table 1. Student T-tests showed that there was a significant improvement in the resulting representation for the modelled spines compared to the reconstructed spines (α=0.05). Figure 2 shows the lateral radiographic projection as well as the reconstructed and corrected (modelled) lateral views for one of the three spines.

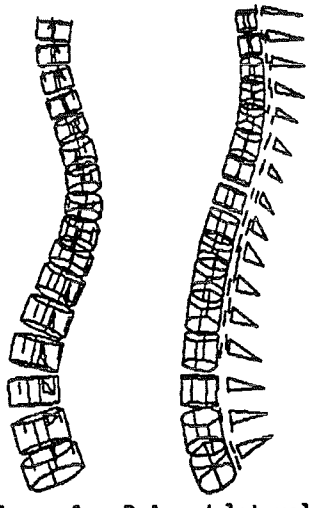

Figure 1 - P-A and lateral views of a modelled spine.

Table 1 - Means (and standard deviations) for lateral reconstructed and modelled spines compared to their lateral radiographic views.

		Spine 1	Spine 2	Spine 3
LEAST SQUARE METHOD (mm^2)	RECONSTRUCTION [no correction]	1.84 (1.05)	3.27 (1.05)	2.93 (1.27)
	MODEL [corrections]	1.75 (0.91)	1.42 (0.68)	1.72 (0.61)
VERTEBRAL LATERAL ANGULATION METHOD (degrees)	RECONSTRUCTION [no correction]	13.1 (7.9)	14.2 (11.9)	16.5 (13.3)
	MODEL [corrections]	4.2 (4.2)	5.4 (6.6)	7.4 (6.6)

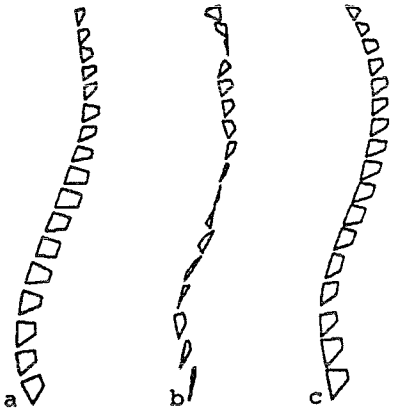

Figure 2 - Lateral views: a) X-ray, b) reconstructed, c) corrected.

CONCLUSION The above results indicate that corrections done by using the parametric model improve the quality of the 3-D graphical representation as well as the geometrical data describing the shape of scoliotic spines. However, it will be preferable to validate the model with more scoliotic spines in order to further support our conclusion. The parametric model presented in this paper is still a preliminary model. Improvement of it is presently on the way to obtain a more precise measure for the vertebral axial rotation and for verifying geometric incoherences. Finally, preliminary evaluation of the parametric model by clinicians reveals that this new tool is quite promising for clinical 3-D interpretation of scoliotic deformities.

REFERENCES

1. Marzan, GT, Ph.D.Thesis, University of Illinois at Urbana-Champaign, 1976.
2. Berry, J.L. et al., Spine, 12:362-367, 1987.
3. Scoles, P.V. et al., Spine, 13:1082-1086, 1988.

ACKNOWLEDGEMENTS This research was funded by NSERC and FCAR.

A COMPU ER MODEL OF SURGICAL CORRECTION OF SPINAL DEFORMITY.

Ian AF Stokes+, Mack Gardner-Morse+, Jeffrey P Laible*.
+Department of Orthopaedics and Rehabilitation
*Department of Civil and Mechanical Engineering
University of Vermont, Burlington, VT 05405, USA.

INTRODUCTION

Optimization of urgical management of spinal deformity and the development of new surgical techniques are l mpered by the difficulties of conducting scientific studies in humans. The purpose of this udy is to develop a biomechanical model for surgical planning. This paper presents compa ons between actual and simulated surgery in six cases, and some preliminary analyses of hyp hetical variations in surgical technique. The comparisons are in terms of 3-dimensional cor ction of deformity and intersegmental flexibility. Changes in compensating curves (as oppo d to instrumented curves) were sensitive to boundary conditions. Of all the components of e deformity, the models were least able to predict accurately the changes in vertebral and th racic axial rotation. Harrington rods slightly increased vertebral rotation at the apex, while -D rods slightly reduced it.

REVIEW AND THEORY

A 3-D model o he spine[5] later modified to include the rib cage[1] showed b mechanically how treatment might affect the shape of the pine with scoliosis[2]. In order to maintain the alignment o the head above the pelvis, and without axial rotation, reflex uscle contractions have to be recruited, to represent the 'r hting' forces[3] which maintain normal body alignment in th presence of external forces, or external stimulation of n scle. Individual characteristics of a patient can be incorpor ed into a model for individualized simulations. Sc ltz et al[5] used a mechanical model which was adjusted to it the spinal deformity of six different patients with sc iosis to investigate the extent to which Harrington rod nd other spinal instrumentations might alter the spinal defor ity in three dimensions. Patwardhan et al[4] and Viviani et a used a similar approach with a two-dimensional mo el. This paper describes an adaptation of a model originall designed to simulate initiation of scoliosis[6] to the new pur se of individualized simulations of surgery.

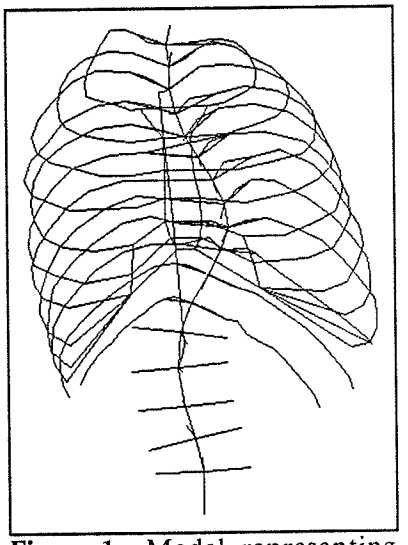

Figure 1 Model representing pre-operative geometry of patient JR, with Harrington rod installed. (PA view)

METHODOLOGY

Five adolescent atients operated with Harrington rods for idiopathic scoli is and one case with C-D instrumentation were studied. Stereo radiography was used to me ure the shape of the spine and rib cage before and after surgery. The measured pre-c erative shape was incorporated into a finite element model of the osseo-ligamentous co onents of the thorax and spine. Actual and simulated surgery were compared.

RESULTS AND DISCUSSION

Simulation of Harrington surgery: This was done by application of a rod to the vertebrae selected for the actual surgery, and displacing the rod ends until the true amount of correction of the Cobb angle was achieved. For the five patients, the required extensions of the rod had a mean of 24mm (range 16-29mm), with a mean force of 570N (range 354-887N). In patients with double curves, the simulations underestimated the reduction of the secondary lumbar curve Cobb angle in 2 patients, but overestimated it in one, with differences close to measurement accuracy. The directions of changes in the kyphosis or lordosis were correctly predicted by the model in most cases. Surgery produced increases of vertebral and rib cage rotations averaging 2.5° in 4 of the 5 patients. In general the models predicted minimal increase in vertebral rotation, and a similar increase in rib cage rotation. Inaccuracies of the models appear to be due to (1) possible contact between instrumentation and intermediate vertebrae, (2) accuracy of end constraints (boundary conditions), (3) passive muscle forces, or (4) alterations in thoracic and spinal shape resulting from braces worn at the time of post-operative x-rays.

Hypothetical variations on surgery: After using the model to simulate the actual surgery, hypothetical variations on surgical technique were modelled. Simulated costoplasty was associated with (1) reduction in the amount of elongation (2) a small reduction in the force in the Harrington rod to achieve the same curve correction, (c) no significant change in correction of the rotational deformities. Simulated tightening of a segmental wire at the apex level with shortening of a wire by 6mm (100N force) produced further reduction in Cobb angle by 3°, increase in apex vertebra rotation of 2°, and increase in rib cage rotation of less than 1°. Because the wire attaches to the posterior part of the vertebra, it was expected to increase the rotational deformity.

C-D Simulation: X-rays of 3 patients showed that C-D instrumentation converts scoliosis curvature into sagittal plane curvature, with some correction (average 31.6%) of the vertebral rotation. This contrasts with patients operated by Harrington rod where generally increased rotation was observed post-operatively. The surgical maneuver of rotating the C-D rod was simulated for one patient. A rotational moment was applied to the middle part of the rod in six incremental steps to allow for geometric non-linearity. The simulation was of the concave side rod only, and only of rod rotation; no distraction was applied. The best agreement between the simulation and measured pre-operative geometry was in the spinal curvatures (in both frontal and sagittal planes). The main difference between the simulation and measured pre-operative geometry was in the axial rotation components. Based on mechanical principles, we expected that the rotation maneuver with the hooks pulling on the posterior parts of the vertebrae would tend to increase the vertebral rotation, as did occur in the simulated surgery. Based on this simulation it appears that the convex side rod and interconnections (DTTs) between the rods have a crucial role in achieving rotational correction by applying additional forces to the posterior elements.

REFERENCES

1. Andriacchi T, et al.: J Biomech 7:497-507, 1974.
2. Andriacchi TP, et al.: J Bone Joint Surg 58A: 806-815,1976.
3. Haderspeck K, Schultz A: Spine 6:447-455, 1981.
4. Patwardhan AG, et al.: J Biomech 19:103-117, 1986.
5. Schultz AB, et al.: J Bone Joint Surg 55-A:983-992, 1973.
6. Stokes IAF, Laible JP: J Biomech in press.
7. Viviani GR, et al.: Automedica 6:159-173, 1985.

PARAMETRIC MODELING OF THE 20° POSTERO-ANTERIOR SPINAL RADIOGRAPH FOR THE STEREORADIOGRAPHIC RECONSTRUCTION OF THE SCOLIOTIC RIB CAGE

De Guise J., Dansereau J., Barbeau S., Labelle H*.
Biomedical Engineering Institute and Mechanical Eng. Dept.
Ecole Polytechnique, P.O. 6079, # A, Montréal, Canada, H3C 3A7
* Sainte-Justine Hospital, Montréal, Canada, H3T 1C4

INTRODUCTION: Stereoradiographic reconstruction technique is routinely used at Sainte-Justine Hospital to obtain three-dimensional (3D) representations of the spine and rib cage to evaluate deformities of idiopathic scoliosis patients. Conventional 0° postero anterior (PA) view and a 20° angled down PA view are used. Six anatomical landmarks per vertebra (centers of endplates, tips of both pedicles), rib midlines and calibration markers must be digitized in order to obtain their 3D reconstruction using the DLT program [2]. Since the stereoradiographic technique has been developed to evaluate clinically a large amount of scoliosis patients [1], it was necessary to design a computer vision-based system which allows fast and accurate identification and digitization of all anatomical and calibration landmarks needed for 3D reconstruction. This paper presents a parametric modeling method to approximate the 20° (PA) view of the midlines of each rib by using the rib shape information detected by the Wechsler and Sklansky algorithm (WSA) [3] applied on the image of the 0° PA radiograph.

METHODOLOGY: The image of each spinal stereoradiograph, illuminated by a high intensity light box, is registered by an IKEGAMI camera which transmits its output video signal to an ITT 80386 micro-computer by means of a MATROX PIP-1024b imaging card (512 x 480 pixels with 256 grey levels). The WSA consists in finding candidates for the dorsal and ventral portions of the rib contours of a 0° PA radiograph by matching straight, parabolic and elliptical curve segments to the result of a local edge detector, and subsequently, using these segments as plans for a heuristic search of the real rib contours. The WSA cannnot be used on the 20° view because the rib contours cannot be represented by simple parabolic and elliptical curve segments. Since the DLT method computes the exact geometry of the X-ray source it is possible to approximate the 20° view of the rib contours using this geometric information and parametric models of rib shapes. This information will be used in the heuristic search phase of the WSA.

A model of each rib contour from T1 to T11 on both sides was constructed on the transverse plane using a least square method which fit four coefficients of parametric spiral curve on 17 rib cage patient data previously reconstructed using a manual method [1]. The four parameters of the equation $r = a\theta^{\frac{1}{2}} + b\theta + c\theta^2 + d\theta^3$ are given in the Table 1 for each rib. Simulations of rib model projections from the location of the 20° angled down X-ray source are done to obtain the 20° view. Two projection geometries are considered, a parallel source geometry and a ponctual source geometry.

RESULTS AND CONCLUSION: For a population of 15 scoliotic patients, results (see Figure 1) show a very good estimation of the computed 20° PA view compared to the original one, for both the parallel source and the ponctual source geometries (mean difference of 2.8 mm and 3.2 mm, respectively).

From these approximate rib shape projections, on the 20° view, the "real" rib midlines can be easily detected and used for accurate 3D reconstruction.

		T1	T2	T3	T4	T5	T6	T7	T8	T9	T10	T11
R	a	0.1	0.1	-0.0	-0.1	0.1	0.2	0.2	0.1	-0.2	-0.3	-0.3
I	b	41.1	-2.2	10.0	3.7	21.3	42.0	40.3	27.7	45.3	60.6	73.5
G	c	-25.2	45.9	38.1	42.0	27.6	9.9	5.4	17.5	-4.2	-19.9	-48.6
H	d	7.6	-13.1	-10.5	-10.5	-7.3	-3.6	-1.4	-4.3	1.6	4.5	14.4
T												
L	a	0.1	0.1	0.1	0.1	0.0	-0.0	-0.0	-0.0	-0.1	-0.1	-0.3
E	b	45.5	25.0	19.6	19.8	26.4	24.7	13.2	-6.9	-13.5	-1.9	50.8
F	c	-24.5	20.0	26.3	28.6	22.4	26.3	33.7	56.0	67.4	52.1	-21.8
T	d	6.0	-7.3	-7.2	-7.2	-5.2	-6.0	-6.7	-12.5	-17.2	-13.4	9.2

Table 1 : Four parameters of the spiral model. The results are presented for the T1-T11 rib levels and for the right and left sides of the rib cage.

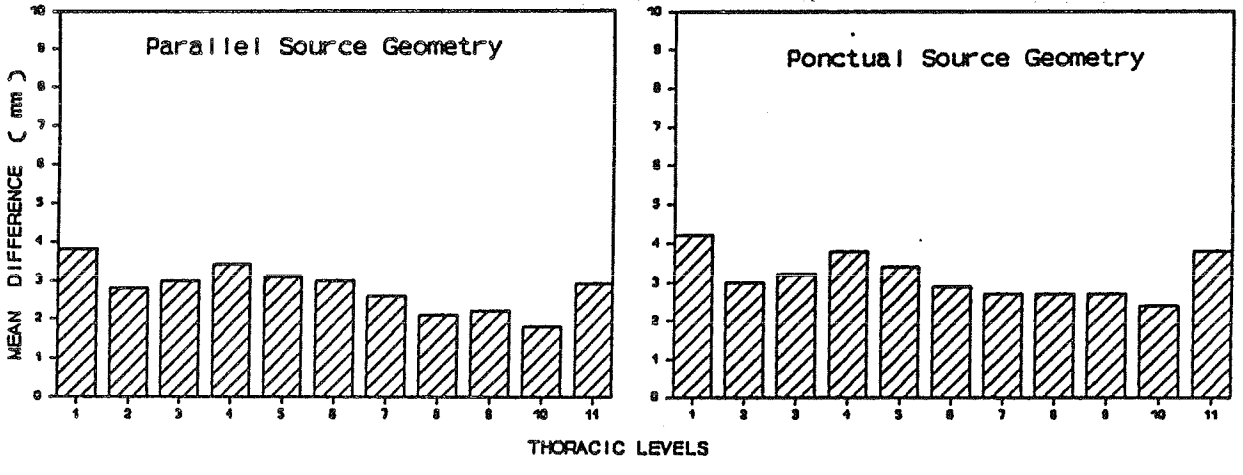

Figure 1 : Mean differences between estimated 20° view and the real one. The results are presented for the T1-T11 rib levels and for the two source geometries.

REFERENCES :

[1] Beauchamp A., Danserau J. et al., "Computer assisted digitization system for stereoradiograph of the scoliotic spinal column", 13th An. Met. Am. Soc. Biom., Vermont, U.S.A., pp. 206-207, 1989,

[2] Marzan, G.T., "Rational design for close-range photogrammetry", Ph.D. thesis, Dept. of Civil Eng. Univ. of Illinois at Urbana-Champaign, 1976.

[3] Wechsler H., Sklansky J., "Finding the rib cage in chest radiographs", Pat. Rec., Vol. 9, pp. 21-30, 1977.

SESSION 9

REHABILITATION

EFFECTS OF A STRENGTH-TRAINING PROGRAM ON THE DYNAMICS OF RISING FROM A CHAIR IN ELDERLY WOMEN

Melissa Hoy[1], Pamela Stevenson[1], Christine Snow-Harter[2], and Robert Marcus[2]

[1] Rehabilitation Research and Development Center, VA Medical Center, Palo Alto, CA 94304
[2] Geriatric Research, Education and Clinical Center, VA Medical Center, Palo Alto, CA 94304

INTRODUCTION

Falls are a serious problem in the elderly. Although many factors contribute to falls, decreased muscle strength with aging has been identified as one of the important risk factors for falling[1,2,3]. It is not known, however, how changes in muscle strength that occur with aging affect balance during movement, when most falls occur. To understand how muscles contribute to balance during movement requires knowledge of the musculoskeletal dynamics. Thus, we investigated the dynamics of rising from a chair in elderly women before and after a muscle strength-training program. Results showed that the dynamics of rising from a chair in elderly women are affected by changes in muscle strength subsequent to a strength-training program, as well as by movement speed. Since loss of balance during rising may be related to the ability to control the body mass not only at the initiation of the movement but also at the end, increased muscle strength may decrease the risk for falling even in healthy elderly women.

REVIEW AND THEORY

Previous studies have shown that dynamics are important in rising from a chair. Development of sufficient forward momentum is critical to maintaining balance during rising[4], and control of upper body momentum may be especially important when speed of rising from a chair increases. Upper body velocity (and therefore the upper body momentum) is altered as speed of rising changes[5], and the vertical momentum increases much more that the horizontal momentum[6]. However, little is yet known about the role of muscles in controlling the dynamics or in maintaining balance during the movement.

METHODOLOGY

Subjects in this study were healthy, active, and community-living elderly women (71 ± 6 yrs; n=17). Ten subjects participated in a muscle strength-training program, and seven subjects served as controls. The exercise group trained three times per week for 12 weeks under a well-controlled protocol that gradually increased the loads for hip adduction, abduction, flexion, and extension, knee flexion and extension, and ankle dorsiflexion, inversion, and eversion. Subjects were asked to rise from a standard height chair at both "normal" speed and "as fast as possible", without using their arms for assistance. Reaction forces were detected using a force plates under the subjects' feet and in the chair seat. Motion data were collected and digitized using a video-based system. Hip, knee, and ankle torques were calculated using the kinematic data and mass parameters estimated from regression equations[7].

RESULTS

Hip, knee, and ankle strength increased significantly in the exercise group. Hip and knee flexor strength and knee extensor strength increased by 101, 100, and 117%, respectively. Total movement time decreased from normal to fast speed trials (1.63 ± 0.15 s; 1.30 ± 0.12 s) for all subjects. The time from loss of chair contact to upright stance relative to total movement time also tended to decrease with movement time (normal 56 ± 11%; fast 49 ± 6%). Peak hip, knee, and ankle torques, and the change in peak torques with movement speed, were similar before and after strength-training.

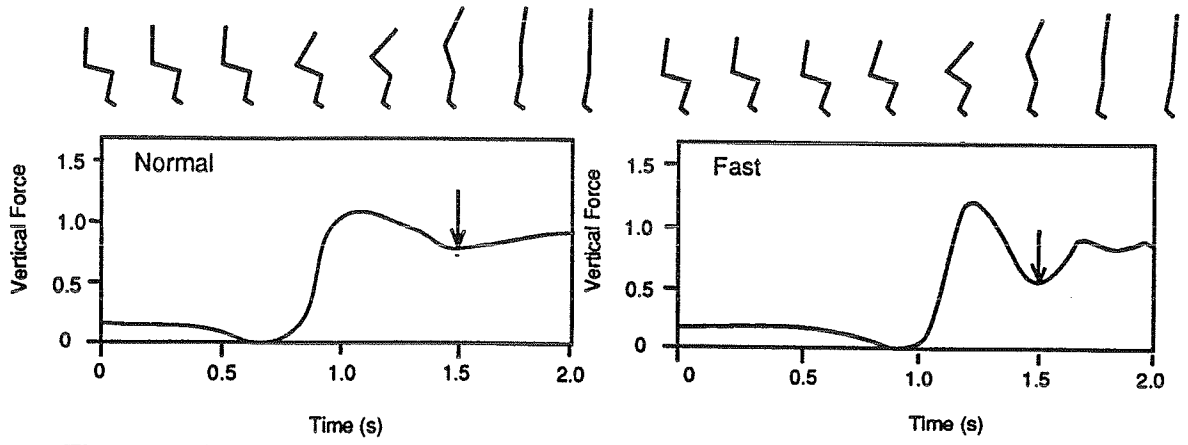

Fig. 1. Vertical ground reacton force during rising from a chair in an elderly woman. Vertical force is normalized by body weight. Stick figures show corresponding body positions. Arrows show differences in vertical force between normal (left) and fast (right) movements.

The vertical ground reaction force and the vertical component of the total body linear momentum changed with both movement speed and strength-training. In the fast trials, the body center of mass was accelerated downward at the end of the movement, primarily through forward angular acceleration of the trunk, resulting in a pronounced minimum in the vertical ground reaction force (see arrows in Fig. 1). The magnitude of this force minimum decreased following strength-training for both normal (pre-training 0.84 ± 0.07; post-training 0.78 ± 0.08) and fast speed trials (pre-training 0.66 ± 0.13; post-training 0.58 ± 0.26). The linear momentum of the body center of mass also changed with movement speed, as has been previously reported[7]. As movement time decreased, the magnitude of the vertical momentum increased substantially (normal 33 ± 6 kg·m·s^{-1}; fast 40 ± 4 kg·m·s^{-1}), while the horizontal momentum remained the same (normal 28 ± 6 kg·m·s^{-1}; fast 29 ± 1 kg·m·s^{-1}). The magnitude of the vertical component of the linear momentum also increased with strength-training (normal 36 ± 7 kg·m·s^{-1}; fast 49 ± 16 kg·m·s^{-1}).

DISCUSSION

The results of this study suggest that the dynamics of rising from a chair in elderly women are affected by changes in muscle strength subsequent to a strength-training program, as well as by movement speed. After strength-training, the elderly women were able to control the body mass and maintain balance during rising even though they generated more total body momentum. Since loss of balance may be related to the ability to control the body mass not only at the initiation of the movement but also at the end, increased muscle strength may decrease the risk for falling even in healthy, active elderly women.

This research was supported by the Department of Veterans Affairs.

REFERENCES

1. Campbell, A. J., *et al.* J. Gerontol. 44: M112-117, 1989.
2. Tinetti, M. E., *et al.* N. Engl. J. Med. 319: 1701-1707, 1988.
3. Whipple, R. H., *et al.* J. Amer. Geriatric Soc. 35: 13-20, 1987.
4. Alexander, N., et al. Proc. ASME Winter Ann. Mtg. 1989 San Francisco, CA.
5. Pai, Y.-C. J. Biomech. 22: 1105, 1989.
6. Schenkman, M. L., et al. Proc. 13th Ann. Mtg. ASB Burlington, VT, pp 162-163, 1989.
7. Winter, D.A. Biomechanics of Movement. John Wiley & Sons, 1979.

ASYMMETRIES IN BELOW-KNEE AMPUTEE RUNNING GAIT

François Prince [1-2], René Therrien [1] and Paul Allard [2].

[1] Faculté d'éducation physique et sportive, Université de Sherbrooke, Sherbrooke, Québec, Canada, J1K 2R1.

[2] Human Movement Study Laboratory, Pediatric Research Center, Sainte-Justine Hospital, 3175 Côte Ste-Catherine, Montreal, Quebec, Canada, H3T 1C5.

INTRODUCTION: An increase number of Below-Knee amputees (BK) express the desire to participate in recreational activities and running is required in most of these sports (Kegel et al., 1978). Seliktar et al., (1989) reported that the integration of the ground reaction forces (GRF) are the most informative data to quantify the pathological walking gait. In this study, we used this approach to analyse the asymmetries in BK amputee running gait. The results showed that maximum forces and impulses (integration of the force) are significantly greater ($p<0.05$) in the Sound limb (SL) compared to the Prosthetic limb (PL) for the anterior-posterior and the vertical components of the GRF. The ratio of braking and propulsive impulses PL/SL showed that the SL is more active during the support phase. The maximum impact during running is also greater for the SL of amputees.

REVIEW AND THEORY: Basic biomechanical variables have been used in previous studies in order to quantify the asymmetries in lower limb amputee walking gait (Skinner et al., 1985; Winter et al., 1988) and in running gait (Enoka et al., 1982; Miller, 1987). Seliktar et al., (1979, 1986, 1989) reported the use of GRF impulses for the identification of locomotion irregularities in normal and pathological gait. The intensity of braking and propulsive impulses gave us some clues in the change of the momentum acting at the center of mass of the subject during the support phase. The purpose of this study was to quantify the asymmetries in BK amputee running gait using the impulse-momentum theorem proposed by Seliktar et al., (1979).

METHODOLOGY: Seven unilateral BK amputees wore a patellar tendon bearing (PTB) socket with a solid ankle cushion heel (SACH) foot. They reported no other anomalies than amputation and were asked to run at a slow pace on a 20m runway. The orthogonal GRF were recorded with a Kistler force plate using an AST computer and the ARIEL CBS software package. Telemetric movement detectors at hip level were placed at 1.5m apart the force plate in order to estimate the speed of running gait. When the running speed was between 2.8 and 3.2 m/s, the trial was saved, in the other cases, was rejected. Two video cameras were placed parallel and perpendicular to the plane of movement in order to provide qualitative kinematics of running pattern. All subjects but one, wore a Bear Plus sport shoes and realized five good trials for the PL and the SL. The anterior-posterior GRF were analysed in term of maximum braking force and braking impulse; and the vertical GRF for the impact peak, maximum trust and vertical impulse. The following ratios were also calculated: braking impulse PL/SL, propulsive impulse PL/SL and the total impulse PL/SL for the stance phase. The data are normalysed in percentage of body weight (%BW) for the maxima and the impulse are expressed in ratio. See figure 1 for description of variables.

RESULTS AND DISCUSSION: The results (mean and standard deviation) of this research are shown in the table 1. The SL is more active than the PL during both braking and propulsive portions of the support phase. The braking ratio PL/SL = 0.779 mean that SL brake more than the PL and the propulsive ratio PL/SL = 0.506 confirm that the PL did not participate very much in the propulsion. The total impulse ratio PL/SL during the whole support phase (0.596) is also a proof of the lack of normal movement in the prosthetic equipement. The running patterns are very variable between amputees but they utilize considerably less their PL than their SL.

CONCLUSION: Research on sports prosthesis is in progress mostly in the area of ankle function restauration and the new developements in Dynamic Elastic Response (DER) prosthetic feet can supplied the lack of propulsion for the PL. The lack of mobility of the prosthesis lead to greater compensation of the locomotor system during running gait. There is also a need for complete bilateral analysis of BK amputee gait in order to record the strategies they used specially during running.

TABLE 1

	Prosthetic limb		Sound limb		
GRF COMPONENTS	X	sx	X	sx	p<0.05
Vertical Impact (%BW)	184.3	80.7	216.4	48.2	*
Vertical Trust (%BW)	213.3	49.2	274.7	47.0	*
Vertical Impulse	34.3	4.76	45.4	4.02	*
Braking Max (%BW)	32.8	10.1	40.7	9.82	*
Braking Impulse	1.90	0.55	2.84	0.96	*
Propulsive Max (%BW)	15.2	6.02	26.4	5.54	*
Propulsive Impulse	1.11	0.50	2.61	0.92	*

FIGURE 1
GROUND REACTION FORCES IN AMPUTEE RUNNING GAIT (3 m/s)
Typical curves for the Prosthetic Limb

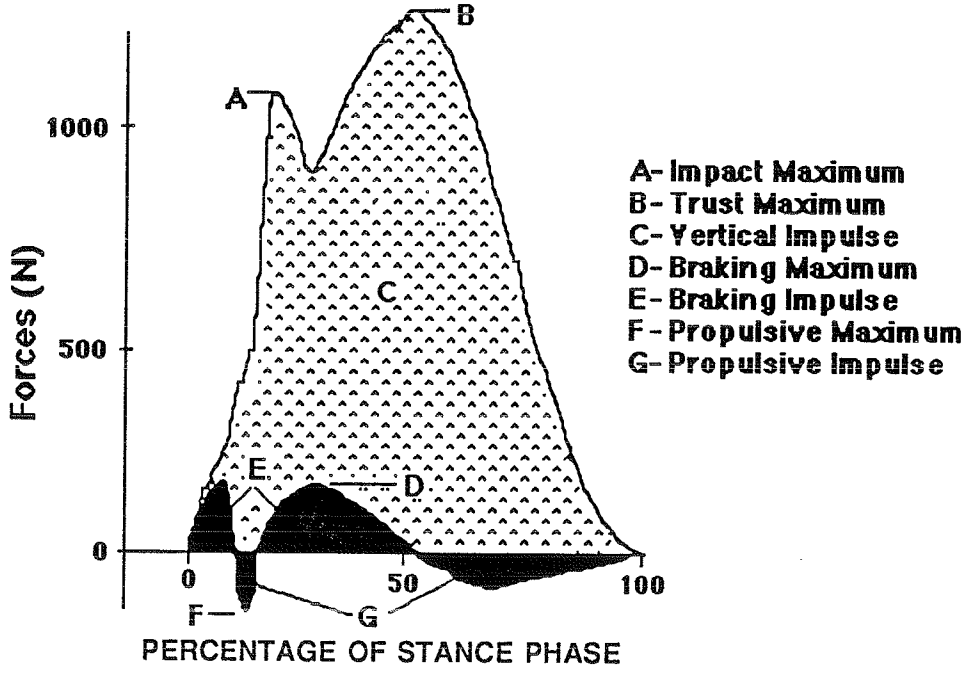

REFERENCES:

Enoka, R.M. et al., (1982). Am. J. Phys. Med., 61, 66-84.
Kegel, B. et al., (1978). Phys. Med. Rehab., 59, 109-120.
Miller, D.I. (1987). J. of Biom., 20, 529-541.
Seliktar, R. et al., (1979). Prosth. & Ort. Int., 3, 91-98.
Seliktar, R. et al., (1986). Eng. in Med., 15, 27-34.
Seliktar, R. et al., (1989). Automedica, 11, 145-162.
Skinner, H.B. et al., (1985). Am. J. Phys. Med., 64, 82-89.
Winter, D.A. et al., (1988). J. Biom., 21, 361-367.

A KINEMATIC COMPARISON OF HORIZONTAL COM LOCATIONS BETWEEN BELOW-KNEE-AMPUTEE AND NORMAL CHILDREN DURING WALKING

Jack R. Engsberg, Janice L. Patterson, Kathi G. Tedford+ and James A. Harder+

Human Performance Laboratory, Faculty of Physical Education, The University of Calgary, Calgary, Alberta, Canada, T2N 1N4. + Alberta Children's Hospital, 1820 Richmond Rd. S.W. Calgary, Alberta, T2T 5C7

INTRODUCTION The structural differences between the limbs of below-knee-amputee (BKA) and normal children have been shown through kinetic analyses to result in functional differences (1,3). This kinetic information, while vital to the understanding of etiologies and mechanisms for these gait differences, is difficult to translate into effective rehabilitation practices. In contrast, kinematic analyses may be used to compare existing gait patterns of the BKA child with respect to those of normal children. Results of such analyses may be utilized to define appropriate rehabilitation procedures such that the BKA child may have a more symmetrical gait or more closely emulate the gait patterns of normal children. This investigation compared the horizontal center of mass (COM) locations of BKA and normal children during walking.

METHODS Eleven normal children and three BKA children (mean age, 8 years) participated as subjects for this investigation. Each BKA child wore a SACH (solid ankle cushioned heel) foot on his/her prosthetic leg. Two locam cameras (frontal and lateral views) filmed (100 fps) typical walking strides (1.2 m/s $\pm$ 10%) during four experimental sessions held at six month intervals (3 strides/subject/session). Segmental endpoints (seven segment model) were digitized to obtain two-dimensional segmental location-time data for a complete stride. The direct linear transformation (DLT) method was utilized to obtain three-dimensional (3-D) location-time data for the segmental endpoints (2). The 3-D segment location-time data were then used to determine whole body COM locations for the entire stride with respect to the midpoint of the hip joint centers. Discrete values describing the horizontal locations of the COM at touchdown and takeoff were normalized by dividing by the height of the subject. The support limb was considered to be the limb that would remain on the ground during stance until takeoff. The contralateral limb was the limb that would experience a takeoff, swing and touchdown during stance. In the frontal plane a positive value indicated that the COM was positioned on the side of the support limb. A negative value indicated that the COM was positioned on the side of the contralateral limb. In the sagittal plane a positive value indicated that the COM was anterior to the midpoint of the hip joint centers. One way analysis of variance (ANOVA) was used to establish significant differences and a Tukey Post Hoc test defined which variables were significantly different ($p<0.05$).

RESULTS No significant differences existed between the values for touchdown and takeoff of the right and left legs of the normal children. The respective values were thus combined and mean values calculated. The results for the COM locations at touchdown and takeoff in the frontal plane for the normal children and the nonprosthetic (NP) and prosthetic (P) limbs of the BKA children are presented in Figure 1. For the normal children the COM of the body was located on the side of the support limb at touchdown, and at takeoff it was located on the side of the contralateral limb. In contrast, when the NP limb was the support limb for the BKA children the COM was

positioned on the side of the NP limb. However at takeoff, instead of crossing over to the contralateral limb like the normal children it maintained its position relative to the NP side. At touchdown of the P limb the COM was located on the side of the contralateral (NP) limb and it remained on that side at takeoff. Thus, where in normal children the COM oscilates relative to the support limb, in BKA children the COM appears to be consistently located over the NP limb.
The results for the locations of the COM at touchdown and takeoff in the sagittal plane are displayed in Figure 2. This figure indicated that the COM for both the NP and P limbs of the BKA children was significantly farther forward than the COM for the normal children for both touchdown and takeoff.

DISCUSSION If goals of the therapist are to help BKA children walk as symmetrically as possible and/or as close to normal as possible, then these results indicate that BKA children are not walking as the therapists desire. The BKA children have some segmental orientations that are causing their COM to be positioned 1) continuously on the NP side of the body in contrast to the oscilating position of normal children and 2) farther forward for the entire gait cycle when compared to the COM location of the normal children. In the frontal plane the trunk segment could be oriented towards the NP limb and/or the NP limb could maintain a greater than normal abducted position. In the sagittal plane the trunk could sustain a more flexed position when compared to that of normal children. Whether a therapist can modify these patterns to be more symmetrical or be closer to normal is not currently known. It is possible that these differences are mechanisms utilized by the BKA children to compensate for the atypical structure and function of the prosthesis.

ACKNOWLEDGMENT Funding provided by the Variety Club of Southern Alberta - Tent 61, through the Alberta Children's Hospital.

REFERENCES

1. Engsberg, JR, et al. Arch Phys Med Rehabil Submitted. 1990.
2. Engsberg, JR, et al. Med Sci Sprt Exerc 19(3):275-284, 1987.
3. Lewallen, R, et al. J Ped Orthop 6:291-298, 1986.

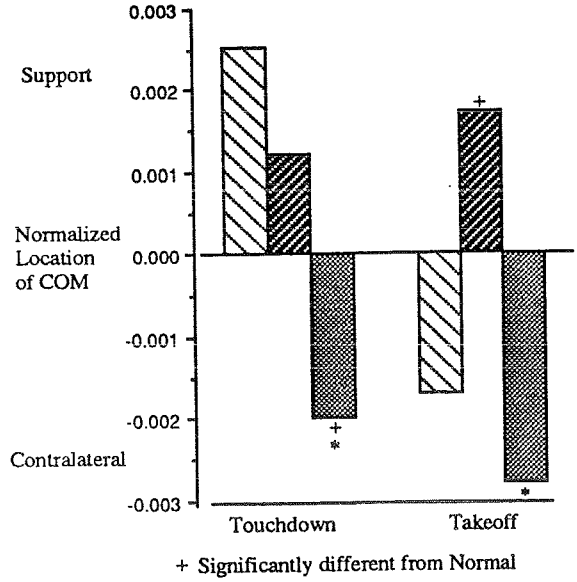

Figure 1 Frontal plane COM locations.

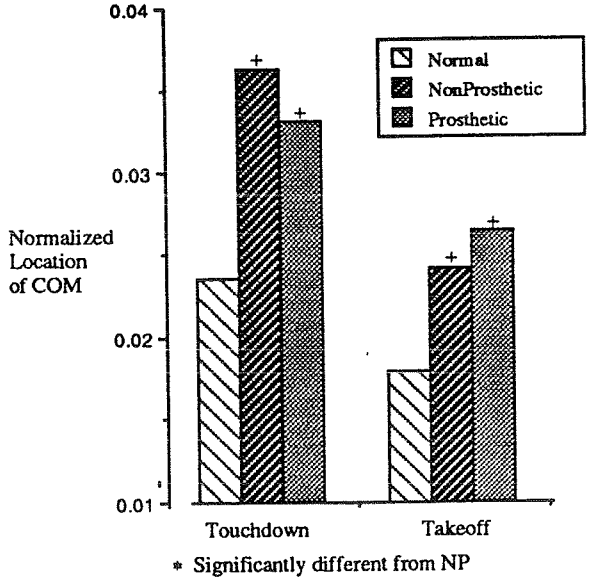

Figure 2 Sagittal plane COM locations.

HEAD FINITE SCREW AXIS PARAMETERS DURING VERTICAL, HORIZONTAL AND OBLIQUE TRACKING MOVEMENTS: NORMAL AND INJURED SUBJECTS

Jack M. Winters[1], Joseph D. Peles[1], Kathleen L. Derickson[1],

Paul J. Osterbauer[2], and Arlan W. Fuhr[2]

[1]Chemical, Bio & Materials Engineering, Arizona State University, Tempe, AZ 85287

[2]Fuhr Chiropractic Clinic, 3714 E. Indian School Rd., Phoenix, AZ, 85060

This study documents how finite screw axis parameters (*FSAP*) for head rotation change during voluntary horizontal, vertical, and oblique point-to-point head tracking movements. Both "normal" (control) subjects ($n=9$) and subjects with "whiplash" conditions ($n=10$) are considered, with each subject evaluated twice, separated by 6 weeks. The information collected here serves to document normal ranges, assess the effects of manipulation therapy, help validate *3-D* computer models, and assist optimization studies by providing reference data for a performance criterion. Here we emphasize the first two of these. The foundation behind the approach rests with the concept that the head is the most distal link of an open kinematic chain that includes the neck. Consequently, changes in neck kinematics, due to changes in passive neck tissue biomechanics and/or in neuromuscular function, should be reflected in changes in head kinematics (Chao et al., 1989). Traditional clinical measurements (e.g. ranges of motion; radiographs) appear limited in their information content. In this study changes in head orientation are essentially specified since the subject is asked to track targets with a laser pointer coupled to the head. By systematically varying target patterns, variation in helical screw axis parameters, and in particular the location and direction of the axis of rotation, can be documented for a wide variety of movements.

METHODS

The subject was seated facing a partial dome (radius *1.61 m*) which contained small lamps (*1 cm dia*) located at *10°* increments in the horizontal ($\pm$ *50°*) and vertical ($\pm$ *40°*) directions within a dark blue fabric background. A light-weight helmet was placed on the subject that included 5 reflective markers (*1.5 cm dia*) mounted to the left side of the helmet and a laser mounted to the top. These markers were viewed by two video cameras, each located *1.5 m* from the subject. The *3-D* Expert Vision system (Motion Analysis, Inc.) was utilized to obtain the *3-D* coordinates of the marker centroids.

Four target sequence patterns were used: *(i)* horizontal pattern, in *10°* increments (20 total movements); *(ii)* vertical pattern, in *10°* increments (16 total movements); *(iii)* oblique movements (along lines $\pm$ *45°* from horizontal), of magnitude $10\sqrt{2} = 14.1°$ (16 total); and *(iv)* a "box" target of off-center *20°* horizontal and vertical movements.

Given the marker centroids, an automated algorithm was used to determine screw axis parameters for rotations between targets. This algorithm: *(i)* lightly smoothed the marker trajectories; *(ii)* separated out parts of the movement based on marker kinematics; *(iii)* determined averaged marker postions for each target "hold" orientation; and *(iv)* calculated the *FSAP* using the Spoor-Veldpaus algorithm, as presented in Woltring et al. (1985). To facilitate gaining insight into trends for the entire population and for individual subjects, strategic *FSAP*'s were ranked for the 16-20 movements of each task. This allowed us to identify trends between subjects who invariably had different sized necks and heads.

RESULTS AND DISCUSSION

For vertical tracking movements in healthy normal subjects the axis of rotation vector was, with few exceptions, directed orthogonal to the mid-sagittal plane (e.g. Figure 1a). In general, the axis crossed the mid-sagittal plane at the highest level movements looking slightly upward (typically at *C2* for movements from $10 \rightarrow 20°$ and from $20 \rightarrow 10°$ and about *C3* for $0 \rightarrow 10°$ and $10 \rightarrow 0°$ movements). Interestingly, it lowered dramatically both for movements between *30°* and *40°* (looking upward) and for the four movements between *-20* and *-40°* (looking downward), with the lowest level typically being at *C7*. For most

subjects the entire front-back variation was only a few centimeters; the only consistent trend was that movements between *30* and *40°* crossed posteriorly by about *2 cm*. Subjects with pathological conditions due to "whiplash"-type injuries tended not to be able to make movements over the full *±40°* target range and were provided with a target sequence with which they felt comfortable. Results differed between these injured subjects. For instance, one (*P4*) had an axis of rotation at *C1-C2* for all movements; this suggests to us considerable stiffness in the lower- and mid-cervical spine. In contrast, others had a greater "spread" in values.

The axis vector for oblique movements was approximately at *45°*, halfway between the directions for vertical and horizontal movements. Interestingly, in terms of the ranking of the vertical and front-back coordinates crossing the mid-sagittal plane, these movements took on the characteristics of vertical movements, only with the movements with *+30-40°* vertical components not as low and more posterior than for pure vertical movements.

For horizontal tracking movements in healthy subjects, the axis direction vector was consistently close to vertical (e.g. Figure 1b). Some subjects would show consistent mild lateral tilt patterns that were often direction-specific; however, no consistent general trend in the vector direction was uncovered across the population except for movements from *40 → 50°*, where most subjects displayed a significant component in the direction causing the ear on the side of the movement to be higher than the opposite ear (e.g. movements 5 and 15 for subject in Figure 1b have the greatest tilt). A consistent finding across subjects was a lateral drift in the location of the axis crossing the neck to the side of the rotation, typically reaching *2-3 cm* in either direction.

REFERENCES

Chao, E.Y.S., Tanaka, S., Korinek, and Cahalan, T. (1989) Measurement of neck range and pattern of movement, Abstract 319, *XII Int. Congr. Biomech.*, UCLA, Los Angeles.

Woltring, H.J., Huiskes, R., De Lange, A. and Veldpaus, F.E. (1985) Finite centroid and helical axis estimation from noisy landmark measurements in the study of human joint kinematics. *J Biomech.*, 12: 911-920.

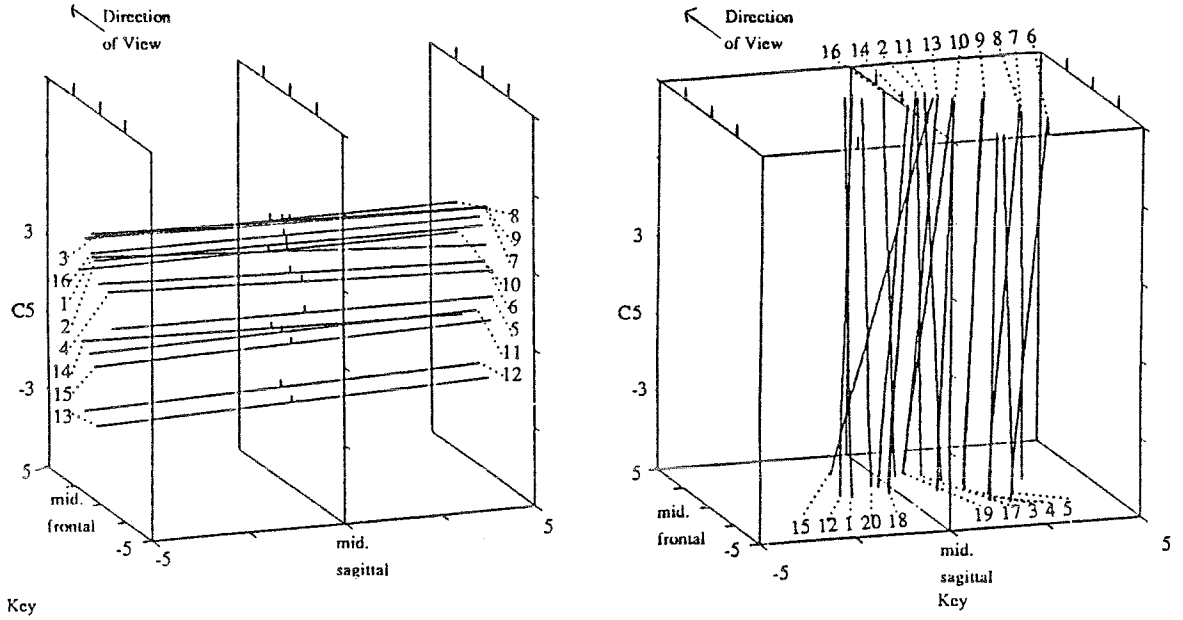

Key

1 = 0° to 10° 9 = 0° to -10°
2 = 10° to 20° 10 = -10° to -20°
3 = 20° to 30° 11 = -20° to -30°
4 = 30° to 40° 12 = -30° to -40°
5 = 40° to 30° 13 = -40° to -30°
6 = 30° to 20° 14 = -30° to -20°
7 = 20° to 10° 15 = -20° to -10°
8 = 10° to 0° 16 = -10° to 0°

Key

1 = 0° to 10° 11 = 0° to -10°
2 = 10° to 20° 12 = -10° to -20°
3 = 20° to 30° 13 = -20° to -30°
4 = 30° to 40° 14 = -30° to -40°
5 = 40° to 50° 15 = -40° to -50°
6 = 50° to 40° 16 = -50° to -40°
7 = 40° to 30° 17 = -40° to -30°
8 = 30° to 20° 18 = -30° to -20°
9 = 20° to 10° 19 = -20° to -10°
10 = 10° to 0° 20 = -10° to 0°

Figure 1: Finite axes of rotation passing through the neck region, in each case for a 10 *deg* rotation. The view shown is from the back, slightly to the left. Coordinate values (in *cm*) can be determined at "slice" locations. Data is for normal control subject N9.

a) Vertical tracking movements (key to left).

b) Horizontal tracking movements (key to right).

INFLUENCE OF LOADING HISTORY ON MUSCLE FIBER CROSS-SECTIONAL AREA

Robert Whalen
NASA/Ames Research Center, Moffett Field, CA 94035

Rapid metabolic, compositional, and microstructural adaptations occur in muscle fibers subjected to a change in their 'habitual activity level'. Although muscle fibers are known to functionally adapt to specific types of activity, little work has been done to model fiber properties as functions of the loading environment. The objective of this study is to formulate a mathematical model which relates muscle fiber cross-sectional area to the daily fiber stress history.

THEORY

The assumptions used in the derivation of this model are 1) remodeling of muscle tissue is regulated locally, at the fiber level, by the cyclic forces exerted by and on the fibers, 2) maximum force of contraction is proportional to fiber cross-sectional area, *i.e.*, peak specific tension is constant, 3) fiber cross-sectional area, or quantity of contractile protein, is regulated to maintain a constant level of daily fiber mechanical stimulus, and 4) the level of fiber stimulus at homeostasis is not site, or fiber, specific.

The forces and stresses imposed on the contractile elements of fibers are taken, as a first approximation, to act principally normal to the fiber cross-section. Figure 1a shows conceptually a portion of the history of the resultant force, f(t), exerted normal to the fiber cross-section of a muscle fiber selected from a whole muscle. The model also assumes that the peak fiber stress achieved during a fiber contraction cycle is the most important factor which influences fiber cross-sectional area. Other variables such as tissue strain rate, period of the contraction cycle, and work per cycle, which may also influence remodeling have not been considered. In this way the fiber loading history is reduced to a discrete set of peak cyclic forces. The peak cyclic normal component of the muscle fiber stress, σ_i, for the i th cycle is defined as the peak fiber force, f_i, divided by the fiber cross-sectional area, a_x (see Figure 1b).

The model postulates that each cycle of loading imparts a level of mechanical stimulus proportional to the magnitude of the fiber stress, or

$$s_i \propto \sigma_i^k$$

where the exponent, k, is an unknown model parameter which determines the relative importance of the magnitude of the peak cyclic stress. The cumulative stimulus over the course of a day can be expressed as a sum of the contributions from all the daily loading cycles, or

$$S = \Sigma s_i \propto \Sigma \sigma_i^{\,k} = \Sigma (f_i / a_x)^k.$$

The model derivation further assumes that as muscle tissue approaches homeostasis, the daily stimulus, S, approaches a constant tissue regulated level of stimulus. Re-arrangement of the above proportional relationship (with S constant) yields the following expression for fiber cross-sectional area

$$a_x \propto [\Sigma f_i^{\,k}]^{1/k}.$$

RESULTS

The influence of the value of the parameter, k, on the cyclic stimulus, s_i, can be seen in Figures 2a and 2b. In these figures the peak cyclic stress has been normalized by the peak (isometric) specific tension. High values of k imply that muscle is very sensitive to the level of mechanical stress. If k= 8, for example, a single fiber contraction at the peak specific tension provides the equivalent cumulative stimulus of 10 cycles at 75 % or 1000 cycles at 42% of the peak specific tension. Figures 3a and 3b show the predicted change in fiber area for two idealized loading states. In Figure 3a the peak cyclic force, f_i, is held constant and the number of daily loading cycles is allowed to vary. For high values of the exponent parameter, k, fiber area is relatively insensitive to the duration of cyclic loading *(i.e.*, number of loading cycles) until severe disuse is reached. On the other hand, if the number of loading cycles is held constant, the change in fiber area is independent of k and directly proportional to the peak cyclic fiber force (Figure 3b). Additional hypothetical activity levels can be created which superimpose either endurance or high-resistance activities on a baseline level of daily activity. The results indicate that, again for large

values of k, high cycle, low force (endurance) activity has a negligible effect on fiber area, whereas high-resistance loading significantly increases the fiber area, *i.e.*, increases fiber (muscle) mass.

DISCUSSION

The model postulates that muscle fibers maintain a tissue level stimulus by increasing fiber cross-sectional area and reducing the fiber stress when exposed to increased levels of cumulative stimuli. Conversely, a decrease in fiber area during disuse tends to maintain a tissue level stimulus by increasing the cyclic fiber stress. The value of k determines the characteristics of the model. Higher values of k are consistent with observations of muscle adaptation to various exercise regimens.

The modeling of musculoskeletal functional adaptation and the quantification of daily physical activity has particular relevance to longterm spaceflight since, in order to maintain muscle and bone mass, normal earthbound activity must be replaced with an equivalent form of activity in the weightless (or reduced gravitational) environment of space.

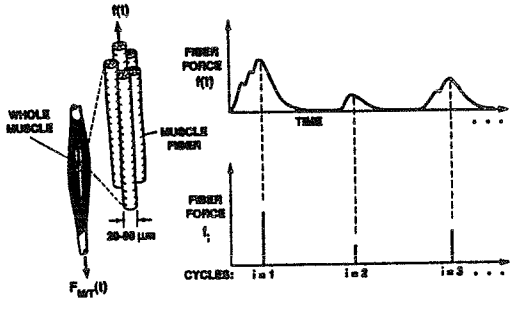

Figure 1a

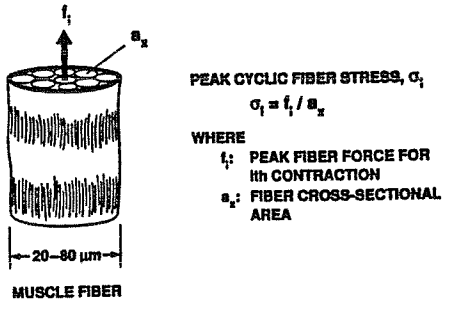

Figure 1b

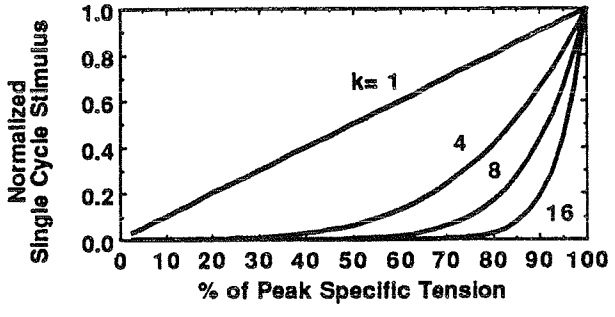

Figure 2a

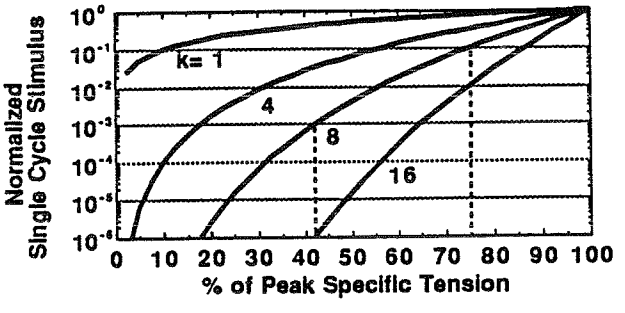

Figure 2b

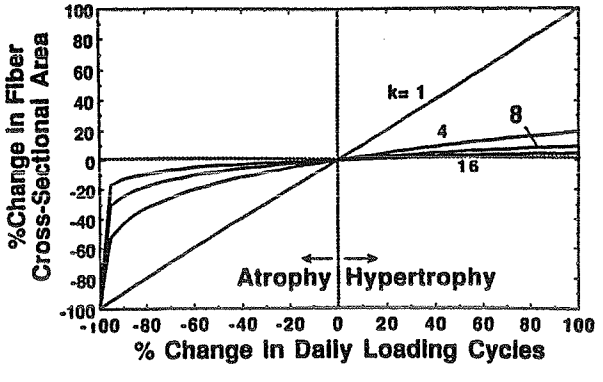

Figure 3a

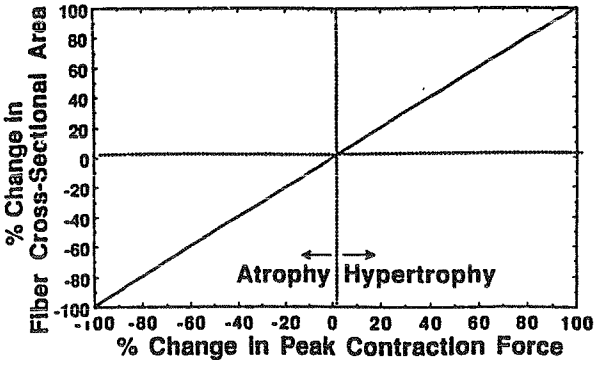

Figure 3b

LOW AND HIGH FREQUENCY ELECTRIC STIMULATION VERSUS ISOMETRIC EXERCISES FOR MUSCLE STRENGTHENING: COMPARISON OF EFFICACY

Elsayed M. Abdel-Moty, Tarek M. Khalil, Myron L. Goldberg, Shihab S. Asfour, Eugene Eckstein, and Hubert L. Rosomoff
Department of Industrial and Biomedical Engineering, and Neurological Surgery, University of Miami, Coral Gables, Florida, USA

INTRODUCTION: Forty chronic low back pain patients (CLBPP) received functional electrical stimulation (FES) or isometric exercises (IE) for strengthening the weak quadriceps muscle. Muscle weakness was attributed to pain and its effects on reduced physical activity and disuse. Results showed that FES and IE increased muscle strength significantly over two weeks. FES at 20 Hz was more effective in increasing muscle strength than at 50 Hz or isometric exercise. IE was more effective in increasing EMG of both the exercised and the contralateral muscles.

BACKGROUND: Unilateral weakness of the lower extremity is a common finding in CLBPP. Pain, inactivity, and prolonged muscle disuse create weakness, and in many cases atrophy. The purpose of this study was to compare the efficacy of administering the "passive" FES, in comparison to regular "active" isometric exercise, for the restoration of quadriceps muscle function in CLBPP.

METHODOLOGY: Fifty subjects (40 CLBPP and 10 healthy volunteers) participated in this study. Patients were from the University of Miami Comprehensive Pain and Rehabilitation Center (UMCPRC). The UMCPRC utilizes a multidisciplinary aggressive physical medicine approach to pain rehabilitation. Subjects Inclusion criteria were: pain of myofascial origin; intact neuromuscular system of the quadriceps muscle; and an initial difference of at least 15% between the maximum voluntary contraction (MVC) force of right and left knee extensors.

Patients were assigned to one of 4 groups: group S20 received FES at 20 Hz; group S50 received FES at 50 Hz; group ISOM performed knee extension isometric exercise; group CONT1 (first control group) did not receive the special knee extension exercises. A fifth group (CONT2) consisted of 10 healthy subjects who served as the second control group.

Pain level (scale 0 to 10), thigh circumference, MVC of knee extension, and EMG activity of rectus femoris corresponding to MVC were measured during the first session. Instructions to the subjects were to grasp hand grips mounted to the sides of the test chair, to hold their back firmly against the back support, to indicate the instant at which the MVC was reached, and to hold MVC until they were told to stop. As soon as the subject reached MVC, 4 seconds of surface EMG activity was amplified (x1000), filtered (3-1000 Hz), digitized (1000 per second), and stored in computer data files for processing. Evaluations were repeated after one week and at the end of the two weeks experimental period.

For groups S20 and S50, flexible conductive rubber stimulation electrodes (12.5x7.5 cm) were placed over the initially weak quadriceps muscle and secured with straps in a bipolar configuration. Damp sponges provided electric conductivity. The electric stimulus was applied in a total of 15 bursts (cycle: 15 sec ON and 35 sec OFF). The intensity of the stimulus was increased gradually to the tolerance of the individual. Subjects in the stimulation groups were instructed not to assist or resist the induced contraction. For group ISOM, subjects performed regular isometric exercise of knee extension of the weaker leg (15 sec contraction and 35 sec rest) for a total of 15 contractions in each session.

For data analysis of each dependent variable, a 5x3x2 Analysis of Variance (ANOVA) factorial design with one grouping factor, two within factors, and repeated observations on the within factor was adopted.

RESULTS AND DISCUSSION: Results of the ANOVA of MVC showed that there were significant (at the 0.05 level) differences between the initial MVC of group CONT2 and all patients groups (Table 1). All exercise groups showed significant improvement in MVC over the two weeks period. The change in MVC over the first week of treatment was not statistically significant. The final MVC of S20 was significantly higher than that of the ISOM, S50, and CONT1 groups. The final MVC of the group CONT2 was still statistically higher than that of group CONT1. For groups CONT1 and CONT2, the change in MVC was not significant. Results of analyzing EMG waveforms showed that, for S20 and ISOM groups, the increase in the integrated activity was statistically significant. For group ISOM, the overall change in integrated EMG was significant. For groups S20 and ISOM, thigh girth increased significantly. There was a reduction in pain level, However it was not significant over this short period of time.

Table 1
Means and (Standard Deviations) of the MVC (in Kg) at the Three Evaluation Periods for Both Quadriceps of all groups

	INITIALLY WEAK QUAD			INITIALLY STRONG QUAD		
GROUP	EVALUATION					
	1	2	3	1	2	3
S20	31(17)	40(18)	49(17)	40(17)	40(14)	45(14)
S50	25(14)	39(12)	38(13)	44(16)	42(14)	45(10)
ISOM	23(14)	34(13)	37(16)	31(17)	33(14)	39(18)
CONT1	27(13)	30(16)	35(17)	33(14)	34(18)	37(17)
CONT2	39(19)	42(21)	44(23)	43(21)	44(22)	44(24)

CONCLUSIONS: The findings of this study have indicated that FES is effective in increasing muscle strength of the weak quadriceps muscle. FES at 20 Hz was effective in increasing both muscle strength and the EMG of the stimulated muscle. Applying FES at 20 Hz was more effective in increasing strength and recruitment than at 50 Hz. FES at 50 Hz increased muscle strength; but not EMG activity. The "active" regular isometric exercises and the "passive" FES were effective in increasing voluntary force output over the same period of time. Isometric exercise was found to affect not only the exercised muscle but also the contralateral unexercised muscle. It was concluded from the analysis that FES is an effective and a viable muscle strengthening technique for subjects with CLBP and decreased muscular abilities due to pain and disuse.

SESSION 10

SPINE #2

ASSESSMENT OF PROGRESSIVE SURGICAL INJURY TO THE LOWER BACK

Frank A. Pintar, Ph.D., Joseph F. Cusick, M.D., Narayan Yoganandan, Ph.D.,
John Reinartz, M.S., Anthony Sances, Jr., Ph.D.
Department of Neurosurgery, Medical College of Wisconsin, Milwaukee, WI 53226
Marquette University, Milwaukee, WI 53233
Veterans Administration Medical Center, Milwaukee, WI 53295

INTRODUCTION

Routine lumbar surgical approaches involve structural alterations of the facets, lamina, and/or the posterior ligaments. It is well known that the intervertebral joints are the major determinants of the segmental motion of the spine. Therefore, it is prudent to expect that iatrogenic changes in the architecture of the facet articulation alter the mechanical characteristics of other components of the lumbar spine. This may have direct implications for spinal disorders such as low back pain, disc herniation, or degeneration. Although numerous *in vitro* biomechanical studies have been conducted in the past on functional units of the lumbar spine, they have primarily concentrated on static force applications under a given mode. Traditionally, low level static forces have been applied to lumbar spine specimens using a system of pulleys and dead weights. This technique must allow for the equilibrium or the creep of the preparation before any measurements are made. However, to understand the temporal biomechanical effects of many of the commonly performed surgical approaches such as facetectomy, unilateral or bilateral, medial or full, time dependent quasistatic force application is desired. Therefore, in this study we conducted a series of experiments to define the effects of partial and complete facet injury as well as selective alteration of the posterior ligaments and lamina by replicating common surgical procedures under increasing compression-flexion forces.

MATERIALS AND METHODS

Five fresh human male cadavers were used in the study. The L3-L5 specimens were prepared by transecting at the mid height of the L2-L3 and L5-S1 discs. The superior and inferior vertebrae were fixed in methyl-methacrylate. Spherical retroreflective targets, 1.5 to 3 mm in diameter, were inserted to the bony landmarks of the specimen. Four targets were fixed in the vertebral body with two each in the anterior and posterior aspects near the endplates bilaterally, two targets were fixed in the facet column (one target at the top portion of the superior facet and another target at the base of the inferior facet), and one target was fixed at the tip of the spinous process at each level from L3 to L5. A total of 25 targets were inserted into the specimen and radiographs were taken to document the relative position of the retroreflective targets. The specimen was positioned on an XY cross table fixed to the platform of a material testing device. Specimens were subjected to low level compressive forces (approximately 700 N) applied at an anterior eccentricity of 50 mm from the center of the intervertebral disc. The load was applied at a quasi-static rate of 60 N/sec. The specimen was reloaded to the same level and the process was repeated until the biomechanical responses were reproducible establishing the stabilization process. The specimens were tested under the following surgically altered conditions performed in a sequential manner: unilateral facetectomy, bilateral medial facetectomy, bilateral full facetectomy, and posterior ligament section. Standard surgical procedures were followed to induce iatrogenic changes. Briefly, unilateral and bilateral facetectomies were done using a high speed dental drill and/or a fine osteotome and currettes. A laminotomy was done. The initial facet removal was associated with interlaminar ligament removal and a small amount of transection of the lower parts of the superior lamina and the upper portions of the inferior lamina. Radiographs were taken to insure proper surgical procedures.

The applied load and deflection data were collected using a uniaxial force gauge and an LVDT attached in series with the piston of the testing device. The signals were recorded as a function of time using a digital data acquisition system. From the force time and deflection time signals the force-deflection biomechanical response was obtained. The biomechanical strength response was derived for the intact specimen as well as for specimens with surgically induced structural alterations. The overall deflection of the specimen at 200 N, 400 N and 600 N were calculated for each progressive run

and were statistically compared. Localized kinematic data was analyzed using a motion analyzer on a frame by frame basis. The motion analyzer traced the movement of the targets digitally as a function of time in a lateral plane. The test was photographed both in the left and the right lateral projections. A systematic computerized analysis was conducted to define the localized movements of the intervertebral disc, the facet joints and the interspinous process distance.

RESULTS AND DISCUSSION

For comparison, the piston deflection values at 200, 400 and 600 N of force with equivalent flexion moments of 10, 20 and 30 N.m were analyzed. Except for bilateral medial facetectomy at a compression-flexion force of 200 N (10 N.m of moment), statistically significant differences ($P < 0.08$) existed for all other runs compared to the intact specimen. In addition, bilateral medial facetectomy demonstrated significant increases ($P < 0.05$) at higher force levels (20 and 30 N.m). Complete facetectomy and facetectomy with ligament transection also demonstrated significant increases at all levels. A single ended pair T-test was conducted to determine the statistical significance of these surgical alterations. In contrast, a comparison of the various surgically altered preparations revealed no statistically significant changes in the overall displacement at all the load levels considered in the study. These findings are in general agreement with previous investigations that have reported significant increases in the overall range of motion for injured functional units compared to the intact specimen. It should be recognized that the previous functional unit studies consisted of one intervertebral joint in contrast to two intervertebral joints used in the present study. A plausible clinical implication of the finding that the sequential surgical alteration of the specimen results in significant differences in the deflections compared to the intact is that, at a higher physiologic load levels additional stabilization may be obtained by maintaining the integrity of the posterior ligament structure. Previous studies conducted in our laboratory have reported the failure strength of lumbar posterior interspinous and supraspinous ligament to be ranging from 300 to 800 N. The ability of these posterior ligaments to resist compression-flexion forces and their location central to the normal axis of rotation may contribute to the stabilization obtained.

The results presented from the kinematic analysis indicated statistically significant increases ($P < 0.05$) in the movement of the posterior spinal components (facet joint, and interspinous process distance) when comparing any of the surgical alteration runs with the intact run at the injured (L4-L5) joint. Furthermore, statistical comparisons of the motions of the individual spinal components in the present study reveal increasing posterior element distraction with progressive injury without significant changes in the anterior disc compression implying an anterior shift in the center of rotation for the spinal unit.

ACKNOWLEDGMENT

This research was supported in part by PHS CDC Grant R49CCR502508, DOT NHTSA Grant DTNH22-89-Z-07305, and Veterans Administration Medical Research Funds.

EXPERIMENTAL DETERMINATION OF SWITCHING CURVES OF LUMBAR MUSCLES

Kristin Neff and Zvi Ladin
NeuroMuscular Research Center and Biomedical Engineering Department, Boston University
44 Cummington Street, Boston, Massachusetts 02215 USA

INTRODUCTION

A biomechanical model of the lumbar musculature integrates postural and load information to determine the muscle force distribution at a given lumbar level. The model is based on the assumption that the lumbar muscles balance the externally applied moments, thereby defining three equilibrium constraint equations for the 22 unknown muscle forces [Shultz et al., 1983]. The muscle force distribution is assumed to minimize the spinal muscular compression force, while not exceeding upper bounds on the muscular stress levels. The muscle force distribution is therefor determined by the external moment loading. For a loading that does not involve torsion moments, the loading combination can be described as a point on a plane (called the 'loading plane'), whose axes are the two bending moments: flexion and lateral bending. Our previous work [Ladin et al., 1989] has suggested the existence of muscular switching curves. These curves, plotted on the loading plane, separate moment combinations that activate a given muscle, from those combinations that are not expected to activate the muscle. This study was aimed at experimentally measuring the switching curves of specific muscles on a small group of normal subjects.

METHODOLOGY

A simple task was designed which explores the switching region of various muscles. A subject holds a 4.5 kgf weight in the right hand with the arm externally rotated and laterally extended to form a 90° angle with the trunk. The subject then rotates the arm at a constant velocity by 90° to the front of the body. The bold curve in Figure 1 is the set of bending moment combinations resulting from the internal rotation task. Since the bold curve crosses over the switching curves of four different muscles, these muscles are expected to switch from one state to the other. The left rectus abdominus (R L) and the left medial external oblique (EOM L) muscles are expected to turn off (become inactive) when the internal rotation curves crosses their switching curves. The right erector spinae multifidus (EM R) and iliocostalis (EI R) are predicted to turn on (become active) when the internal rotation curves crosses their switching curves. To validate the model predictions, five subjects performed the internal rotation exercise with 3 different weights. The electromyographic signal was monitored using surface electrodes on the four muscles of interest.

RESULTS AND DISCUSSION

During the internal rotation task, the motion of the arm was monitored using the WATSMART optoelectronic system. Rigid segments instrumented with infrared light emitting diodes were attached to the right arm and the trunk. TRACK©software (developed at MIT) was used to process the WATSMART data and produce the arm and trunk position during the movement. EMG signals were collected from surface electrodes and processed using the Muscle Fatigue Monitor (MFM^{TM};a device developed at the NeuroMuscular Research Center). The point in time where the muscle switches on or off can be determined from the EMG signal. Using the motion data, the position of the arm and, thus, the moment combination at the instant in

time that the muscle switches can be calculated. This information was compiled from the five subjects and individual switching curves were determined for each of the four muscles.

Figure 2a displays the switching curves for the right medial external oblique abdominal for each subject along with the switching curve predicted by the biomechanical model. The results clearly show a consistency between the subjects in the position of the curve on the loading plane. For this particular muscle, the model has accurately predicted the moment combinations that will activate the left medial external oblique. A different situation is exhibited in Figure 2b which shows the switching curves for the right erector spinae iliocostalis and the switching curve predicted by the model. In this case, four out of the five experimental curves are in the same general location, whereas the fifth curve is separate. Also, the general trend of the five curves is not the same. Thus, the model predictions are a general guide to the location of the individual switching curves on the loading plane, but each subject must be analyzed individually.

In conclusion, the biomechanical model of the lumbar region is a valuable tool in the study of the muscle forces needed to perform certain tasks. Though the model is based on an average sized male, the experimental data shows that the model predictions are useful for providing a comparison for a range of subjects. Also, it is interesting to note that some muscles appear to be more consistent than other muscles when compared to the predicted data. Perhaps certain muscles vary greatly between subjects and other muscles are very similar. A larger data base would give more information and help isolate trends amongst particular muscle groups. Thus, the biomechanical model provides an important foundation for more detailed analyses which could consider corrections for individual anatomy and geometry.

REFERENCES

1. Ladin, Z., K.R. Murthy and C.J. De Luca. Mechanical recruitment of low-back muscles: theoretical predictions and experimental validation. Spine 14(9):927-938, 1989.
2. Shultz,A., K. Haderspeck, D. Warwick, and D. Portillo. Use of lumbar trunk muscles in isometric performance of mechanically complex standing tasks. J Orthop Res 1:77-91,1983.

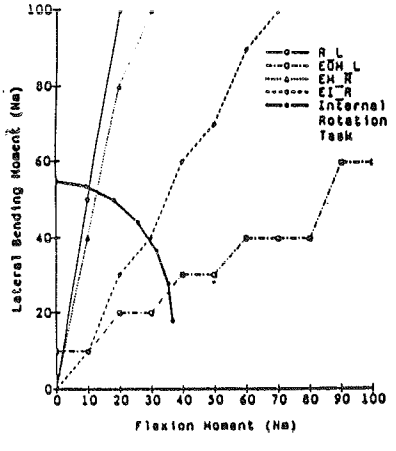

Figure 1. Theoretical Switching Curves and Internal Rotation Curve

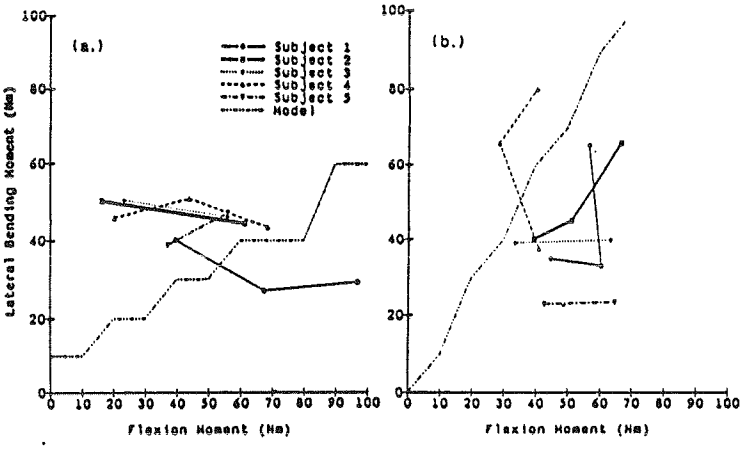

Figure 2. Actual Switching Curves
(a.) Left Medial External Oblique
(b.) Right Erector Spinae Iliocostalis

This work was supported by the Patricia Roberts Harris Fellowship.

EFFECTS OF ASYMMETRICAL LOAD CARRYING ON FRONTAL PLANE JOINT KINETICS

Paul DeVita, P.E. Dept., Southern Illinois Univ,. Carbondale, Il 62901
Der Ming Hong, Martial Arts Dept., Chinese Culture Univ., Taiwan, R.O.C.
Joseph Hamill, Dept. of Ex. Sci., U. of Massachusetts, Amherst, Ma 01003

INTRODUCTION

Effects of an asymmetrical sidepack carrying system on frontal plane lower limb and L5/S1 joint moments of force (JMF) were studied to evaluate this potentially injurious form of load transport. Ground reaction force (GRF) and film data were combined in an inverse dynamic analysis to produce the JMFs for left and right limbs and 3 load conditions, 0, 10 & 20% body weight (BW), during the stance phase in walking. Results showed that as frontal plane load asymmetry increased, JMFs in the unloaded side limb increased and the L5/S1 JMFs switched from alternating contralateral side dominance to unloaded side dominance for both left and right stance phases.

REVIEW AND THEORY

Symmetric lifting and load carrying activities have been analysed to identify various tissue loads and injury causing mechanisms of these movements (4,5). Frontal plane asymmetrical tasks however, have not received as much attention even though these activities may have more severe effects on the muscular and skeletal systems (1,3). The purpose of this study was to examine the effects of an asymmetrical, sidepack carrying system on frontal plane lower extremity JMFs and the L5/S1 spinal JMF during the stance phase of walking.

METHODOLOGY

The sidepack was carried on the left side with a vertical shoulder strap. Three load conditions, 0, 10 and 20% BW, along with load effects during left and right limb stance phases were examined in five healthy males (mean age: 25 years, mass: 67 kg). Experimental setup consisted of a force platform, timing system to monitor walking speed (1.34 m/s) and a 16 mm cine camera positioned 12 m in front of the force platform. Five trials per limb and load conditions were collected for each subject. Inverse dynamic analysis was used to calculate stance and swing phase JMFs for ankle, knee and hip joints. L5/S1 JMF was derived during single support only for both limbs using a mathematical model of the pelvis which incorporated the effects of both hip joint reaction forces and JMFs and L5/S1 joint reaction forces. Positive limb and L5/S1 JMFs represented abductor and left side trunk muscle dominance, respectively. A two-way ANOVA with repeated measures was used to identify ($p<.05$) significant load, limb and load by limb interaction effects for the parameter of total angular impulse for each JMF.

RESULTS AND DISCUSSION

Ankle JMFs were low and inconsistent, showing no effect due to loads and are not shown. Figs 1 and 2 show the mean JMFs for all subjects for both limbs and 0 & 20% loads. 10% load JMFs were intermediate to these curves.

Normal walking (0% load) was characterized by nearly identical frontal plane JMFs between limbs and a symmetrical JMF pattern around L5/S1 between left and right stance. Hip and knee JMFs had abductor dominance through most of stance and were similar to previously reported results (2). L5/S1 had contralateral side trunk muscle dominance during most of stance which provided support for the swing leg and swing leg side of the pelvis,

enabling the recovering limb to swing forward without touching the ground.

Statistical analysis identified significant load by limb interactions at all joints and significant simple main effects for limb at 10 and 20% loads and for load on the right limb. These results were evident in the 20% load curves. With increased load, hip and knee abductor JMFs increased on the unloaded side (right) by 52 and 67%. The asymmetrical load also caused unilateral and unbalanced use of the trunk muscles on the right side of the L5/S1 spinal joint for both limb stance phases. The primary function of the lateral trunk muscles changed to maintaining proper trunk orientation with asymmetrical shoulder loads. These results suggest that asymmetrical load carrying may lead to back injuries due to overworked lateral muscles and asymmetrical spinal compression and shear forces which would be associated with the observed L5/S1 JMF results.

REFERENCES

1 Andersson, G.B.J. Ergonomics, 28; 323-326, 1985.
2 Bocardi, S. et al. J. Biomech. 14; 35-45, 1981.
3 Drury, C.G. et al. Ergonomics, 32; 565-583, 1989.
4 Freivalds, A. et al. J. Biomech. 17; 251-262, 1984.
5 Martin, P.E. & Nelson, R.C. Ergonomics, 29; 1191-1202, 1986.

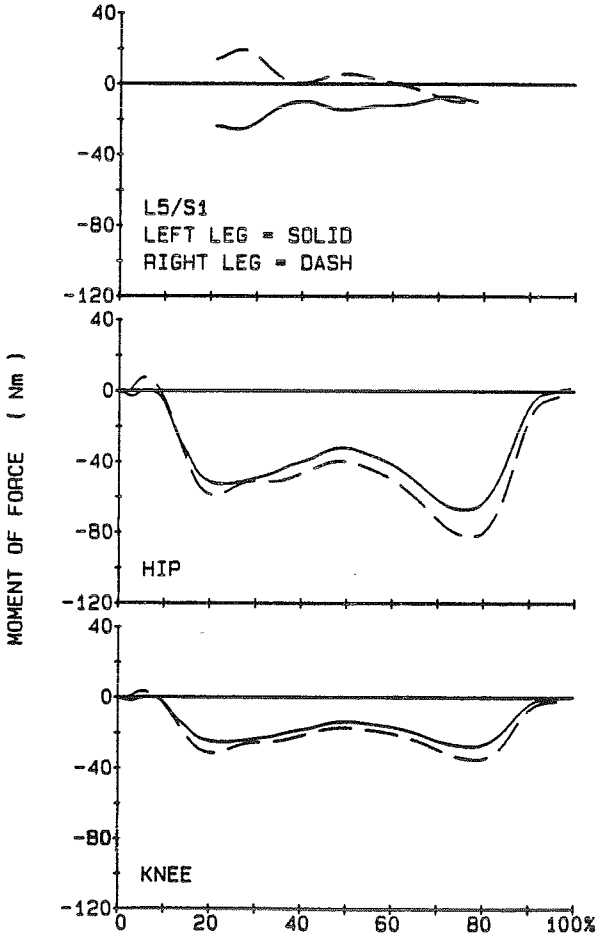

Fig 1. Frontal plane JMFs, 0% load. Positive values are abductor and left side trunk muscle dominance.

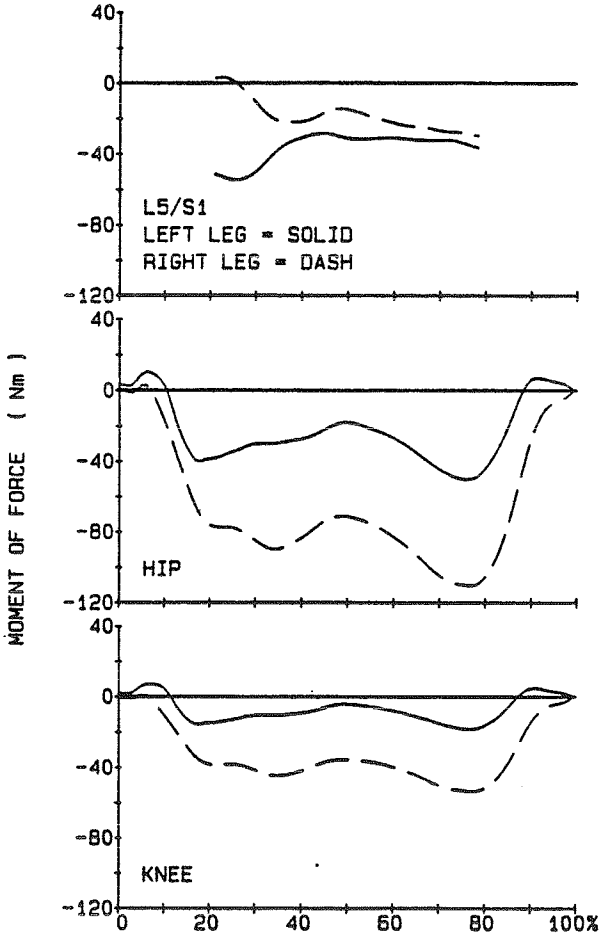

Fig 2. Frontal plane JMFs, 20% load Positive values are abductor and left side trunk muscle dominance.

LUMBOSACRAL COMPRESSION IN MAXIMAL LIFTING EFFORTS WITH VARYING MECHANICAL DISADVANTAGE IN ISOMETRIC AND ISOKINETIC MODES

SHRAWAN KUMAR
Department of Physical Therapy, University of Alberta
Edmonton, Alberta, T6G 2G4, Canada

INTRODUCTION

Frequently design of work tasks are based on the strength capability of the workforce. Since the tasks can vary significantly, the strength capability of a sample was tested under varying conditions and corresponding lumbosacral compression calculated using a biomechanical model of the back.

REVIEW AND THEORY

Kumar et al (1988) reported a progressive decline in strength capability with increase in the velocity of exertion while maintaining a standardized posture. However, the effect of mechanical disadvantage under same velocity conditions on strength capability and corresponding lumbosacral compression has not been reported. Lumbosacral compression has been accepted as a criterion for tasks design due to its load tolerance characteristics (NIOBH 1981). It will be important to know and understand the relationship between strength, mechanical disadvantage and the lumbosacral compressive force. The latter has been frequently used as a cost function in optimization biomechanical back models.

METHODOLOGY

Male subjects with no history of low-back pain or musculoskeletal disorders were recruited for the study. The sample had a mean age of 28.2 years, mean height of 177.4 cm, mean weight of 72.6 kg, and a mean reach of 64.3 cm. The subjects were attired in comfortable clothes and placed on Dynamic strength Tester (DST) as described by Kumar et al (1988). The platform of the DST was marked with a centimeter scale in the midsagiltal plane of the subject facing the load cell. The DST had a SM 1000 load cell. The DST could be used either in isometric mode or isokinetic mode at any preselected velocity. For isokinetic trials a fixed 50 cm. sec^{-1} velocity was chosen.

All subjects were required to perform twenty standardized maximal effort lifting tasks. They were asked to perform stoop and squat lifts at half, three-quarter, and full reaches in mid-sagiltal plane in isometric and isokinetic conditions. Both stoop and squat isokinetic lifts were started at the floor level and terminated at the individuals knuckle height. For the isometric exertions, two stoop (hip angle 60^{o} and 90^{o}) and two squat (knee angle 90^{o} and 135^{o}) postures were used. All subjects were also required to perform a standard isometric stoop and squat lift test as described by Chaffin et al (1978). While the subjects performed these activities, a continuous measurement of force, time, and linear displacement was made on an IBM XT with Data Translation board at 50 H_z. The entire activity was videotaped. Using a two dimensional biomechanical model (Chaffin and Andersson 1984) lumbosacral compression force was calculated for every activity of each subject.

RESULTS AND DISCUSSION

The mean peak strengths measured for the 20 different tasks, their corresponding external moments and lumbosacral compressions are presented in Table 1. The ANOVA revealed that the strength varied significantly between the conditions and between the reaches ($p<0.01$). When the maximal recorded strength (standard squat) was treated as

100% the variation ranged from 25% (isometric squat at full reach with knee at 135°) to 98% (isometric stoop at half reach with hip at 90°). The range of variation was reduced when one compared the external moments ranging between 43% and 101% respectively for these conditions. However, the least variation was found among the values of the lumbosacral compressions. This variable ranged between 64% to 96% for isometric squat at full reach with knee at 135° and isometric stoop at half reach with hip at 90°. The compressive load between the conditions (leaving aside standard stoop and squat) varied by 26% at half reach, 16% at three-quarter reach and 13% at full reach. However, looking across the reaches within the condition the differences were significantly reduced, generally within or around 10% except isometric stoop with hip at 90°. Based on these observations one can see that though the variation in strength exertion ranged up to 73%, the range of variation in the lumbosacral compression was only 15%. For all exertions studied the lumbosacral compression was maintained at high end. Such an integrated behaviour of the system is mediated through the characteristics of mechanical design of the human body and a physiological limitation of human capability. In any case, it also appears that the lumbosacral compression generated between the 18 conditions ranged between 51% to 76% of the ultimate compressive strength, the lower values associated with the activities of greater mechanical disadvantage. In a self-selected optimal posture the maximal compressive force generated was only 79% of the ultimate compressive strength indicating a 21% margin of safety. This as the conditions became more difficult the capability dropped such that it favoured the margin of safety.

Table 1. Strength, external moment and lumbosacral compression during

CONDITIONS	STRENGTH (N)			EXTERNAL MOMENT (Nm)			LUMBOSACRAL COMPRESSION (N)		
	2/4 R	3/4	4/4	2/4	3/4	4/4	2/4	3/4	4/4
Isokinetic stoop	580	300	240	174	150	153.6	6,186	5,996	6,229
Isometric stoop 60	680	354	205	231	166	131	6,796	6,496	5,912
Isometric stoop 90	700	380	209	280	190	133	7,813	6,608	5,292
Isokinetic squat	451	339	221	166	169	139	5,729	6,437	5,767
Isometric squat 90	391	286	201	175	160	140	6,539	6,031	5,711
Isometric squat 135	400	279	179	176	147	119	6,273	5,261	5,246
Standard stoop		668			267			7,604	
Standard squat		709			276			8,082	

CONCLUSIONS

1. The strength capability varied widely with the variation in tasks but the lumbosacral compression stayed high.

2. The mechanical design of the human body and the physiological limitations of exertion by lowering the lumbosacral compression favour system safety.

REFERENCES

Chaffin, D.B. and Andersson, G.B.J. (1984) Occupational biomechanics Pub. Wiley and Sons

Chaffin, D.B. et al (1978) J. Occup. Med., 20, 403-408

Hutton, W.C. et al (1982) Spine I, 386-590

Kumar, S. et al (1988) J. Biomech 21, 35-44

NIOSH (1981) Work Practice Guide

DETERMINATION OF OPTIMAL LIFTING POSTURE USING NON-LINEAR PROGRAMMING

I. M. Jomoah, S. M. Waly, and C. Ip
Industrial Engineering Department,
University of Miami,
Coral Gables, Florida 33124

Since the levers of the human system were adapted for ranges, speed, and precision of movements, rather than for weight lifting, the posture of the human body has a great effect on lifting because the person may injure himself while lifting with a poor posture. The incidence of back injuries attributed to manual lifting is extremely high among industrial workers. The main objective of this study is to develop a biomechanical model using non-linear programming to find the optimal posture for manual lifting.

A 2-dimensional static model in the sagital plane was utilized in this study. The objective function used in this model was to minimize the compressive forces on the back. A 5-link rigid system was used as shown in Figure (1). Table 1 shows the allowed range of joint motion used in developing the constraints of the model. The model was developed with the assumption that the box is located in front of the knee (i.e. the box can not fit between the legs). Also, it was assumed that the back muscle exerts its force 2" posterior to the center of rotation of the spine. The center of gravity of the combined external load and body weight falls within 2" from the ankle joint to ensure stability.

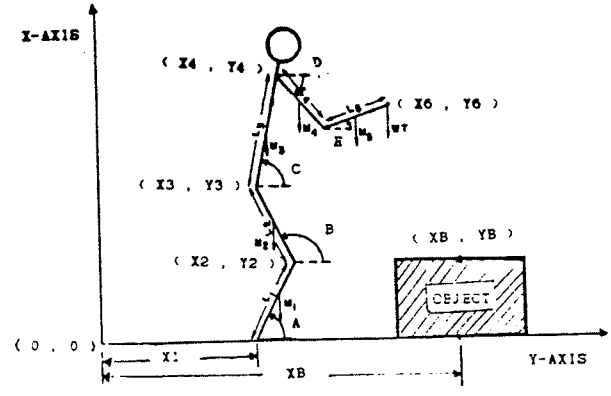

Figure 1: The 5-link system

Table 1: The relationship between the body angles.

Angles	Minimum	Maximum
A	55	90
B	90	A + 113
C	0	90
D	-151	98
E	D	D + 142

The model was solved using General INteractive Optimizer package (GINO). A sample of the results is shown in Figure 2. This posture was found to be an optimal solution when lifting a 70 lbs load. The corresponding compressive force was found to be 618.43 lbs. The compressive forces was found to increase with the load lifted as expected. It is worth noting that the amount of load lifted did not affect the optimal posture obtained as shown in Table (2). Also, increasing the distance between the external load and the ankle position resulted in a higher compressive force (Table 3).

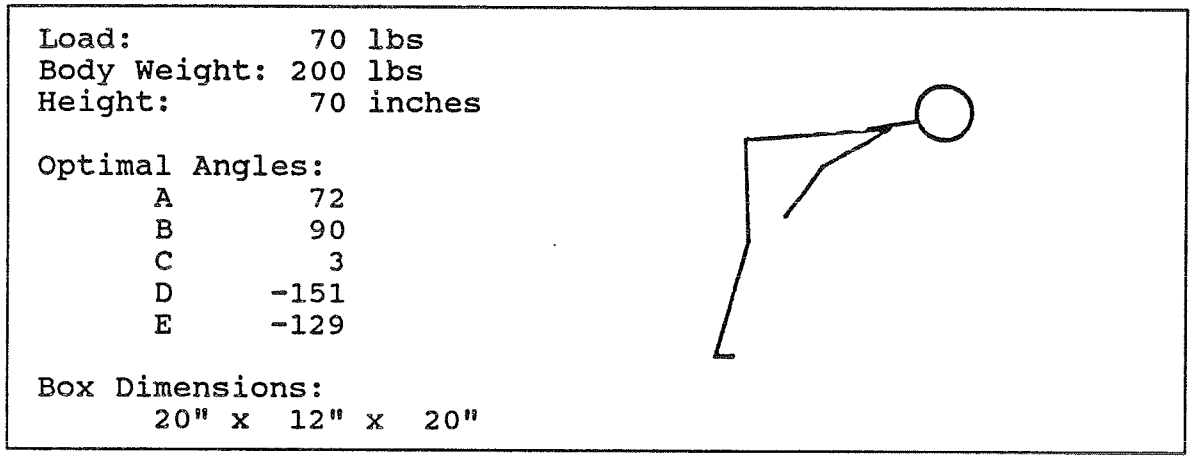

Figure 2: A sample of the an optimal solution

Table 2: Optimal solutions for different loads

Load	A	B	C	D	E	Comp. F.
10	72	90	3	-151	-129	615
70	72	90	3	-151	-129	618
100	72	90	3	-151	-129	620

Table 3: Optimal solutions for different load location

Location	A	B	C	D	E	Comp. F.
10	83	90	7	-151	-111	765
20	72	90	3	-151	-129	618
50	72	90	3	-151	-129	618

The results obtained show that utilizing non-linear programming techniques allows the determination of the optimal posture that should be assumed during manual lifting of heavy objects. Further investigations are needed to modify the biomechanical model used and verify the results obtained.

THE ROLE OF LUMBAR SPINE LIGAMENTS DURING WEIGHT-LIFTING

Nicholas M. Newman[1], Steeve Asselin[2] and Serge A. Gracovetsky[2,3]
1- Hotel-Dieu Hospital, Montreal, Canada
2- Diagnospine Research, Montreal, Canada
3- Department of Electrical Engineering, Concordia University, Montreal, Canada

INTRODUCTION

Recent anatomic data on the lumbar spine musculature revealed that the lumbar multifidus must contribute only to the rotatory component of extension of the lumbar spine, and little or not at all to its posterior translation.[8] Hence in the absence of external load, the back muscle may be sufficiently strong to raise the trunk from a forward bend position. However to lift an external load, the lumbar muscles must be assisted by an additional mechanism that also contributes a backward moment.[9] The possible role of the intra-abdominal pressure (IAP) was put at rest by recent data showing that for a lift of 100 kg, the IAP would have to raise up to 250 mmHg. If this was the case, the abdominal aorta would be occluded.[9] What, then, can contribute a the backward moment?

It was earlier suggested that the intervertebral ligaments, mechanically in parallel with the erector spinae m., were the structures most likely to sustain the external moment in lifts with straight knees (SK).[3] Unfortunately it was calculated from biomechanical model of the spine, that high compressive stress would be induced on motion segments hence rendering this lifting technique very dangerous. The straight-back, flexed-knee lifting technique (FK) than arose. Yet, it was later observed that when lifting heavy weights with the FK technique, initially the hips rose faster than the shoulders, the trunk inclining towards a more stooping posture.[1,10] This behavior of the spine / pelvis complex may offset the apparent advantages of this method of lifting. In view of these results, it is obvious that independent of the lifting technique used, the spine will always take an optimal position to lift an external load. We suggest that an important parameter of this lifting position is the degree of lumbar flexion. Two factors are at play in the choice of a flexed lumbar spine in lifts of external loads. First, following accurate mathematical modelling of the spine, it was suggested that transferring the load to the posterior ligamentous system (PLS) is advantageous since its leverage arm is greater thus decreasing the compression at the inter-vertebral joint.[4] Second, it was observed that when a lumbar joint is flexed, the stress distribution proved to be more favorable for sustaining higher compressive stress.[7] The action of the PLS depends on the amount of lumbar flexion, for it is necessary for the spine to elongate enough posteriorly, and remain essentially fully flexed, for tension to be stored in the ligaments. Since the degree of tension of the PLS is a result of passive stretching thus dependant on the spine geometry, it is advantageous to reduce lordosis to support the external load through ligamentous tension.[6]

This study was done to investigate the role of lumbar spine ligaments during weight-lifting by the use of an infrared spinal marker system (Spinoscope™) permitting precise analysis of motion, including lumbar spine flexion and posterior elongation (Schober test).

METHODOLOGY

Seven healthy amateur weight-lifters (no LBP history, age 20-35) were studied dynamically using and infrared spinal skin marker system (Spinoscope™) permitting precise analysis of motion, including lumbar spine flexion and posterior elongation (Schober test). Multifidus EMG (at level of L_5-S_1) was also recorded during lifting of weight of up to 100 kg. The subjects were unconstrained and hold the standard weight-lifting bar at arm's length, inferiorly, and beginning at a standing position, lowered the weight to the floor and return with weight to a standing position. The degree of knee bending, speed of lifting, spine and pelvic flexion were determined by the subject according to comfort. Power output was calculated from spinal geometry and velocity of lifting.

RESULTS AND DISCUSSION

The multifidus muscle relaxation phenomenon (Floyd & Silver 1955, Örtengren et al. 1981) was observed in maximum flexion without weights but not with weights over 25 kg. Flexion / extension patterns of our subjects (see Fig. 1) reproduced the results of others[2] in that they were similar for lifting with no external load and weight of up to 100 kg although subjects tended to preflex the lumbar spine via pelvic rotation as they prepared to lift heavier weights. The presence or absence of knee flexion did not alter the pelvic-spine contours ie the degree of lordosis and

hence posterior ligamentous elongation during lifting was always initiated with the lumbar spine in close to maximum flexion (minimal lumbar lordosis). The calculated maximum power was developed with the lumbar spine in maximum flexion and thus with maximum posterior ligamentous elongation (see Fig. 2). This maximum elongation of posterior structures corresponds to suboptimal length and geometry for maximal muscle contraction but maximizes the muscle and ligamentous elastic tension.[9] Increasing speed of lifting permits development of greater tension in the viscoelastic posterior ligaments, without greater elongation, thus permitting lifting of heavier weights. Greater acceleration requires greater power transmission via posterior ligaments but rapidity of motion is essential to prevent overstretching of passive viscoelastic ligaments. This would not be necessary if weight-lifting were done by active muscle contraction which would imply less acceleration and lower speeds for heavier weights lifted. In fact, EMG activity increased to a plateau as weight lifted increased (see Fig. 3).

CONCLUSION

These data support the contention that the power for lifting heavy loads in trunk flexion is not primarily developed by spinal muscles but is rather transmitted by the viscoelastic posterior ligamentous structures.

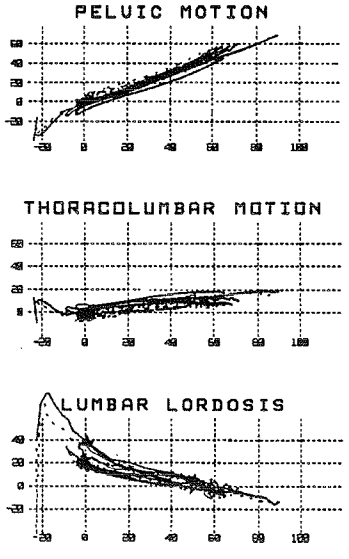

Fig. 1 The data from several lifts of increasing loads is overlayed. Notice the similarity of the responses. The data suggests that the coordination chosen by the volunteer is independent of the load to be lifted.

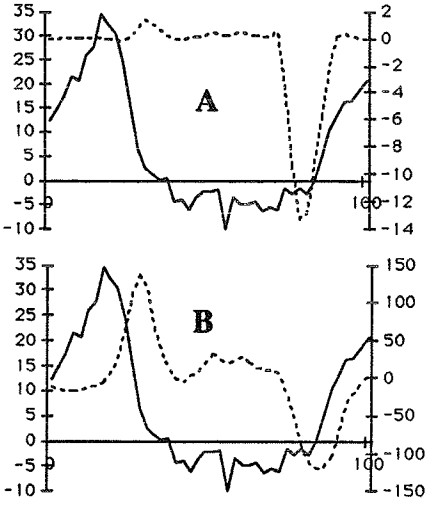

Fig. 2A-B This figure illustrate the variation of lordosis (left axis, plain line) versus power variation (A-right axis, dotted line) and versus trunk velocity variation (B-right axis, dotted line) for subject MB as a weight of 100 kg is lifted (see methodology). Minus signs indicate a backward motion of the trunk and positive sign indicate a forward motion of the trunk. It can be seen that maximal power up is developed while the posterior elongation is near maximum.

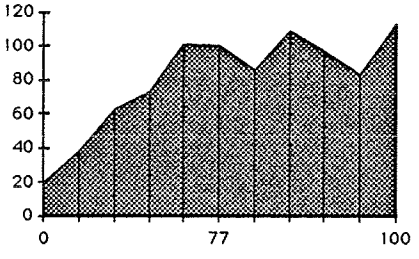

Fig. 3 This figure illustrate the EMG amplitude of the multifidus as the load to be lifted increased. The X-axis is in percent of the load lifted. Th Y-axis is the activity level in arbitrary units.

REFERENCES

1-Davis et al. J Anat Lond 99 (1), 13-26, 1965.
2-Ekholm et al. Ergonomics 25 (2), 145-161, 1982.
3-Floyd et al. J Physiol 129, 184-203, 1955.
4-Gracovetsky et al. Spine 6 (3), 249-262, 1981.
5-Gracovetsky et al. Spine 10 (4), 317-324, 1985.
6-Gracovetsky et al. Spine 14 (4), 412-416, 1989.
7-Hutton et al. Spine 7 (6), 586-590, 1982.
8-McIntosh et al. Spine, 1-18, 1986.
9-McIntosh et al. Clin.Biom. 2, 78-83, 1987.
10-Németh et al. Scan J Rehab Med 16, 103-111, 1984.
11-Örtengren et al. Spine 6 (1), 98-103, 1981.

SESSION 11

MODELING

A FINITE ELEMENT FORMULATION FOR THE INCISED HUMAN CORNEA BASED ON A MICROSTRUCTURAL MODEL

Peter M. Pinsky, Associate Professor, Dept. of Civil Engineering
Deepak V. Datye, Doctoral Student, Dept. of Civil Engineering
Tara Tabesh, Medical Student, Stanford Medical School
Stanford University, Stanford, CA 94305-4020

INTRODUCTION

Although radial keratotomy (RK) has been accepted as a surgical procedure by many ophthalmologists, the predictability of its outcome on a case by case basis is still in doubt. In fact, only in half the cases does this surgery lead to correction within $\pm$ 1.0 diopters of emmetropia [1] and this has not changed much even during the late eighties. Although a number of commercial software packages are being advertised for RK, their scientific basis and veracity are often questionable [2]. In this paper we present a new finite element formulation for modeling the effects of surgical incisions on the human cornea. This is based on a rational microstructural model of the physiology of the incised cornea, and incorporates the effects of anisotropy and nonhomogeniety induced by the incisions. It is found that the anisotropy of an incised cornea plays a critical role in its response and its accurate modeling is essential for simulating any keratotomy procedures.

REVIEW AND THEORY

The physiology and structure of the cornea is described at length in Ref. 3. It is known that the stroma accounts for 90% of the corneal thickness and due to its large stiffness it virtually dictates the corneal structural behavior. In the absence of intraocular pressure, the cornea offers very little resistance to bending but great resistance to stretching and hence, to a first approximation, can be effectively modeled as a membrane shell structure. Like a balloon, the cornea supports transverse loads mainly through the effects of a "geometric" stiffness resulting from the tension induced by the intraocular pressure. The present work is based on a nonlinear finite element formulation for generally curved membranes that consistently incorporates the geometric stiffness induced by the intraocular pressure.

The stroma consists of about 300-500 randomly oriented lamellae, each made up of parallel collagen fibrils with high Young's modulus embedded in a jelly-like soft ground substance. These lamellae run continuous from limbus to limbus. When a fibril is cut during keratotomy, its load carrying capacity is assumed to be lost. The remaining uncut fibrils in the intact lamellae are then assumed to carry all the internal forces. Thus the membrane stiffness at a point in an incised cornea depends on the number of uncut lamellae at that point as well as the distribution of the angular orientation of these uncut lamellae [4]. As shown below, these characteristics of the incised cornea change dramatically from point to point and give rise to the induced anisotropy and nonhomogeniety of the cut cornea. In the present work, this microstructural view of the corneal physiology has been rationally modeled as described below, and introduced into the nonlinear finite element membrane formulation.

METHODOLOGY

The equivalent modulus of elasticity E' of a lamella in the fibril direction depends on the modulus of elasticity of the collagen fibrils E_f and their area fraction (A_f / A). It is premised here that the ground substance being very soft has negligible Young's modulus. Accordingly, we define:

$$E' = E_f A_f / A$$

Assuming no shear transfer between adjacent lamellae, the equivalent corneal membrane rigidity at a point depends on the magnitude and angular orientation of uncut lamellar sectors at that point (Fig.1). This assumes that the distribution of the angular orientation of the lamellae and the fibrils is uniform throughout the thickness. The cornea is also assumed to be incompressible with an inplane Poisson's ratio of zero and the incompressibility constraint controlling the corneal thickness.

If an incision is made to a depth of αt where t is the corneal thickness, which may vary from point to point, the stress-strain relationship between the second Piola Kirchhoff stress S and the Green-Lagrange strain e [5] defined for plane stress relative to a curvilinear lamina coordinate system for the membrane can be expressed by $S_{ij} = Q_{ijkl} : e_{kl}$ with i,j,k,l = 1,2 where:

$$Q = \left[\sum_{i=1}^{n} \tilde{Q}_i\right] \alpha t + (1-\alpha) Q_0 t; \quad \tilde{Q}_i = \int_{\theta_a^i}^{\theta_b^i} \begin{bmatrix} c^4 & c^2s^2 & c^3s \\ c^2s^2 & s^4 & s^3c \\ c^3s & s^3c & c^2s^2 \end{bmatrix} E' \, d\theta; \quad Q_0 = \int_0^{\pi} \begin{bmatrix} c^4 & c^2s^2 & c^3s \\ c^2s^2 & s^4 & s^3c \\ c^3s & s^3c & c^2s^2 \end{bmatrix} E' \, d\theta$$

and θ_a^i, θ_b^i are the angles defining the limits of the i^{th}uncut sector relative to the lamina coordinate system; $c = \cos\theta$ $s = \sin\theta$; n is the number of uncut sectors lying in the region $(0,\pi)$.

Fig. 2 shows typical spatial variation of the tangential component of rigidity Q. This Q is consistently incorporated into the finite element model by calculating it at every Gauss point and using it in turn to calculate the elastic-geometric kernel matrix. A full Newton technique with a consistently linearized tangent stiffness is used to solve the nonlinear equations [7].

RESULTS AND DISCUSSION

As published data on the material properties of the collagen fibrils vary, a precise value for E' was not available. Fig. 3 shows a plot of the decrease in corneal power for a typical incision pattern as a function of E'. The value of E' = 100 MPa was found to be appropriate and moreover corresponds quite well with the published values of E_f (1 GPa) (Ref. 6) and the area ratio (A_f/A) 0.1 (Ref. 3). Effect of incision depth is shown in fig.4. A drastic reduction in corneal power is obtained as the depth of incisions are increased beyond 90%. A small error in incision depth when the design depth is more than 90% results in very large inaccuracies and this partly explains the lower success rate obtained in patients with substantial preoperative myopia. The results obtained are quite similar to those found in practice [1].

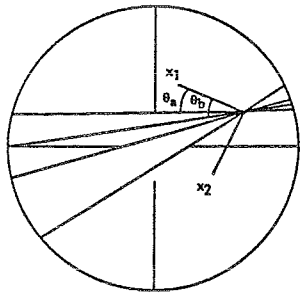

Fig. 1. Diagram showing uncut lamellar sectors at a typical point and angles θ_a, θ_b. Number of incisions = 4, x_1,x_2 are lamina coordinate axes.

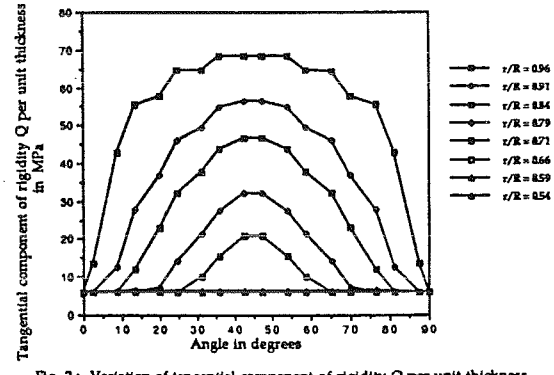

Fig. 2: Variation of tangential component of rigidity Q per unit thickness. 4 incisions, 95% deep, optical zone size = 3.0 mm, outer radius R = 5.75 mm.

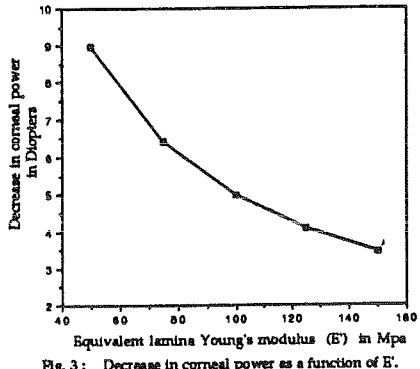

Fig. 3: Decrease in corneal power as a function of E'. 8 incisions, 95% deep, optic zone size = 3.0 mm

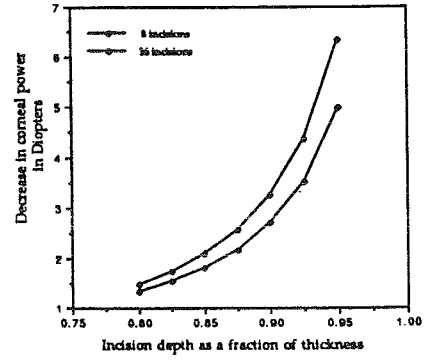

Fig. 4 : Effect of incision depth E' = 100.0 Mpa; Optic zone size = 3.0 mm

REFERENCES

1) Sanders D. et. al., Radial Keratotomy, SLACK, 1984.
2) Swinger C.A., "Variables in R.K," in Cornea, Refractive Surgeries and Contact Lenses, Raven ,1987.
3) Maurice D.M., "The Cornea and Sclera," in The Eye, ed. Davson H., 1984
4) Schachar R.A. et.al., "A Physicist's view of R.K.," in Keratorefraction, Lal, 1980.
5) Marsden J.E. et.al., Mathematical Foundations of Elasticity, Prentice Hall, 1983.
6) Fung Y.C., Biomechanics,, Springer-Verlag, 1981.
7) Pinsky, P.M. and Datye, D.V., "A Microstructurally Based Model of the Human Cornea," in preparation.

CONTACT FORCES DURING THE "STANDARD TEST" FOR MEDIO-LATERAL STABILITY OF THE KNEE

Gerard J. Gouw
Department of Mechanical Engineering
Concordia University
1455 de Maisonneuve Blvd. West
Montreal, QC, Canada H3G 1M8

Henk W. Wevers
Clinical Mechanics Group
Department of Mechanical Engineering
Queen's University
Kingston, ON, Canada K7L 3N6

INTRODUCTION: Several researchers have developed computer models of the knee which can be used to investigate medio-lateral (ML) motion [1-3,5-7,11]. Few report contact forces. This paper describes a 3D kinematic model of the knee which was used to determine contact forces during passive ML motion.

MODEL DESCRIPTION AND VALIDATION: A 3D kinematic model of the knee was developed. Shape of articular surfaces and location of ligament attachments were obtained from a cadaveric knee. The ligaments are modeled as non-linear elastic springs [8,10]. Friction is neglected and femur and tibia are assumed to be rigid. The model was validated by comparing the calculated moment-rotation curves (moment about the knee due to a force at the ankle vs. varus/valgus rotation) with those obtained clinically on a "Knee Analyzer" [9] for normal knees and knees with known complete cruciate ligament tears. Good correlation was found between calculated and measured curves. A second validation was performed by comparing model results with those obtained from a mechanical knee, where the femur consisted of two cylinders, the tibia of a flat plate with or without an eminence, and the ligaments of linear springs. The calculated model results were identical to those obtained from the mechanical knee.

METHODOLOGY: Since femur and tibia are assumed rigid, there will be point contact. The geometry of the condylar surfaces then prescribes the possible contact conditions: one point contact on the medial side, two point contact on the medial side (one at the eminence, the other more centrally), two point contact (one medially, the other laterally), and one point contact laterally. When the knee is put in a varus or valgus position, a force is applied at the ankle. The tibia will be in equilibrium, whereby forces and moments due to ligament forces, contact forces and force at the ankle are balanced. This study reports the type of contact, the contact forces and the effect on these of complete tears in one or both cruciate ligaments.

RESULTS AND DISCUSSION: Figure 1a shows the contact forces when all ligaments are intact. In valgus there is always only one contact point, laterally. In moderate varus, 0 - -3.3 deg, there is one point contact on the central part of the medial condyle. Between -3.3 and -4.2 deg there is the possibility of one or two point contact medially. Beyond -4.2 deg there is two point contact medially, with the larger contact forces centrally and the smaller on the eminence. Furthermore, the knee is stiffer in valgus than in varus. Figure 1b assumes that there is no PCL. There is a small decrease in varus stiffness and a significant decrease in valgus stiffness, and corresponding decreases in the contact forces. When the ACL is torn (Figure 1c) there is only a small decrease in the valgus stiffness and lateral contact force. However, in varus there is a remarkable shift in the contact conditions, i.e. most of the load is taken by the eminence and the varus stiffness is decreased considerably. Figure 1d shows the contact forces and conditions when both ACL and PCL are

torn. Again, the eminence bears most of the load medially. The decreases in stiffness and contact forces are the result of the combined effect of an ACL tear and a PCL tear.

CONCLUSIONS: In extreme varus there is two point contact in the medial compartment, in valgus there is always one point contact laterally. There is a decrease in stiffness and contact forces when one or both cruciate ligaments are torn. When the ACL is torn the tibial eminence bears most of the load in varus.

ACKNOWLEDGEMENTS: The research was supported by the National Research Council of Canada, the Natural Sciences and Engineering Research Council of Canada and the Medical Research Council of Canada. The first author was supported by a Government of Canada Scholarship for Foreign Nationals.

REFERENCES

1. Andriacchi, T.P., et al. ASME Biomechanics Symposium, AMD 23: 227, 1977
2. Andriacchi, T.P., et al. J. Biomech. 16: 23, 1983
3. Crowninshield, R.D., Pope, M.H. J. Biomech. 9: 397, 1976
4. Gouw, G.J., Wevers, H.W. ASME Biomechanics Symposium, AMD 43: 197, 1981
5. Grood, E.S., Hefzy, M.S. In L. Thibault (Ed.): 1982 Advances in Bioengineering: 3, 1982a
6. Grood, E.S., Hefzy, M.S. J. Biomech. Eng. 104, 331, 1982b
7. Hefzy, M.S., Grood, E.S. J. Biomech. Eng. 105: 145, 1983
8. Kennedy, J.C., et al. J. Bone Joint Surg. 58A: 350, 1976
9. Lowe, P.J., Saunders, G.A.B. Med. & Biol. Engr. & Comp. 15: 548, 1977
10. Noyes, F.R., Grood, E.S. J. Bone Joint Surg. 58A: 1074, 1976
11. Wismans, J., et al. J. Biomech. 13: 677, 1980

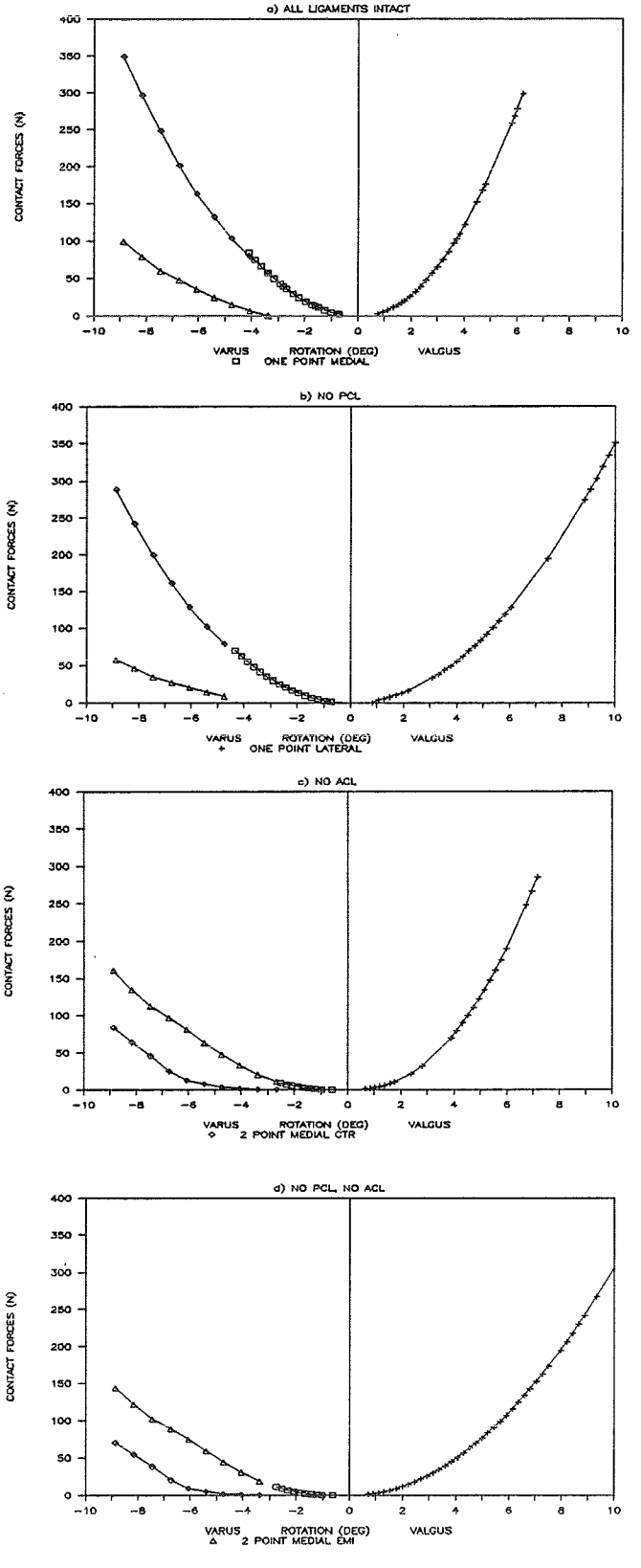

Fig. 1 Contact Forces vs. Rotation

A GEOMETRIC MODEL OF THE HUMAN TORSO

Maury Nussbaum and Don B. Chaffin
Center for Ergonomics, University of Michigan, Ann Arbor, MI 48109-2117

INTRODUCTION

Biomechanical modeling of the human torso often requires the estimation of several anatomic parameters which are usually difficult to determine in vivo. These parameters include vertebral positions and orientations and muscle lengths and moment arms. A model of the torso developed by Andriacchi, *et al.* (1974) and Takashima, *et al.* (1979) is extended to include anthropometric scaling, muscle orientations based on serial CT scans, predictions of torso passive restorative moments, and muscle passive stiffness and length-tension relationships. The model geometry is validated via comparisons with experimental motion data from several subjects. A method for translating motion to an input set for the model is described.

REVIEW AND THEORY

The new model is based on a three-dimensional mathematical model developed by Andriacchi, *et al.* (1974) to study the mechanics of the human skeleton. Their model idealized the vertebrae, ribs, sternum, and pelvis as rigid bodies, while the discs, ligaments, and cartilage were modeled using linear springs. Input to the model consists of a constraint set and an equilibrium state for the model is found using the direct-stiffness method of structural analysis. To study the mechanical effects of muscle contraction, Takashima, *et al.* (1979) incorporated the torso musculature into the previously described model. The muscle centroids and lines of action were derived from scaled cross-sectional anatomy drawings. The muscles were 'operated' by applying a constant force along the line of action.

METHODOLOGY

Two methods are developed for improving the geometry of the existing model. The first is the use of 'scaling factors' derived from anthropometric data taken from a subject. These factors are used to modify the linear dimensions of the rigid bodies, and several factors are employed for each orthogonal axis. The second method modifies the location of the muscle centroids using data taken from a set of horizontal CT scans. Operating the model, via an input set of constraints, requires the development of a marker system. The markers, placed on the skin surface, together with estimates of the position of a surface marker relative to vertebral interspaces allows the model to be constrained using digitized video or photographic data. Through the complex interaction of length and moment arm, the force generating potentials as well as the passive stiffnesses of the torso muscles are not constant over a range of body orientations. A mathematical representation of the length-tension relationship and stiffness properties is included and used in combination with muscle lengths calculated using the model. The original model idealized the tendons, ligaments, discs, and cartilage of the spine using a set of linear springs. Using the results of ongoing research into the passive properties of the spinal column, the new model predicts the passive stiffnesses of the motion segments. Moments and forces are generated following a calculation of displacements and rotations for a given posture.

RESULTS

The present geometric model was designed specifically to provide input for an optimization model for predicting torso muscle forces in asymmetric lifting. As such, it provides those values required by the optimization model: muscle moment arms and lines of action, passive restorative moments generated by the motion segments and muscle tissues, and maximum potential muscle forces. Calculations of muscle lines of action and moment arms is highly dependent on achieving a correspondance between the geometry of the model and that of the subject. Early results show that a fairly close match can be attained using a minimum, well

defined set of anthropometric measurements (Figure 1). Predictions of muscle geometry in other than a neutral upright posture requires a match between movement of the model and the subject. Using a set of approximately 10 markers on the torso and pelvis, a constraint set is computed for the model. The computation involves translating marker positions over time into rigid body displacements and rotations. In our experiments this was done for the pelvis, L1, and T4. Using constraints at only these three locations, the model was able to reasonably 'move' in parallel to the subject. Maximum potential muscle forces and passive stiffnesses as well as restorative forces and moments in the spinal column, while also dependent on geometry, require estimates of length-tension relationships and stiffness properties. The index of architecture and resting length of torso muscle, for example, is not well documented. Further, values such as the torsional stiffness of the lumbar vertebrae are difficult to determine for an individual. In these cases, the most reasonable value taken from the existing literature was used, and the results are largely dependent on them.

DISCUSSION

The Takashima, *et al.* (1979) implementation of the Andriacchi, *et al.* (1974) model is useful for modeling the mechanics of the torso in a neutral posture for an 'average' size subject. The additions described enable the model to be used in lifting studies where the postures will often involve motion and asymmetry and where subject anthropometry will vary considerably. Statistical comparisons will be presented. Many existing models either control anthropometry by restriction of subjects to near 50th-percentile males (McGill, *et al.*, 1986), or use a simpler method for scaling, such as at a single vertebral level (Schultz, *et al.* 1985).

REFERENCES

1. Andriacchi, T., *et al.*, (1974) J. Biomechanics, 7: 497-507.
2. McGill, S.M., *et al.*, (1986) Spine, **11**: 666-678.
3. Schultz, A. B., *et al.*, (1985) J. Orth. Res., **3**: 189-197.
4. Takashima, S. T., *et al.*, (1979) J. Biomechanics, **12**: 929-939.

Acknowledgements: This work was supported by NIH Grant-1R01-AR39599, in cooperation with Rush Institute, Chicago, Ill.

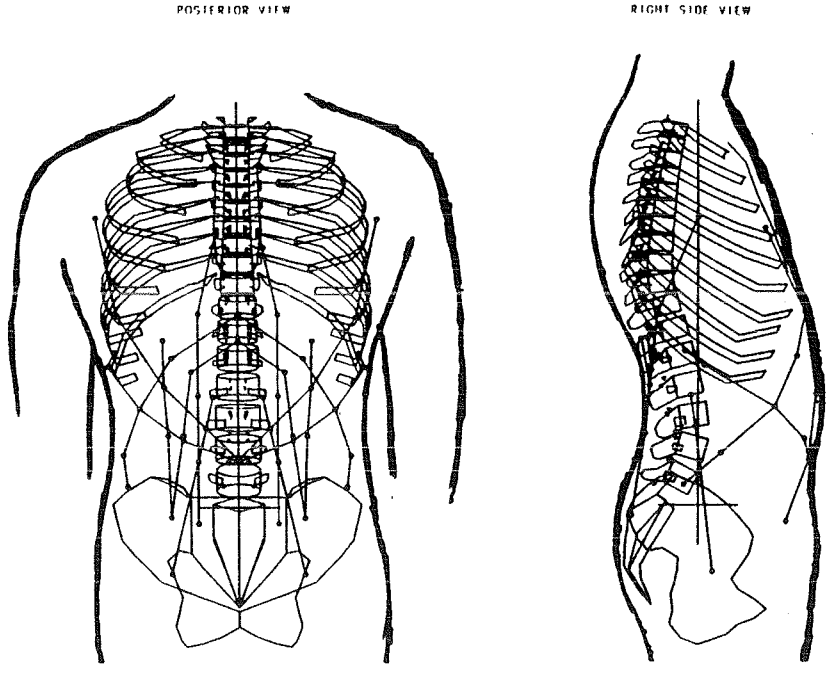

Figure 1. Torso Model of Takashima, et al.(1979) scaled to specific subject anthropometry.

LUMBAR SPINE BONE LIGAMENT MODELING BY MEANS OF COMPUTER TOMOGRAPHY AND THREE-DIMENSIONAL DIGITIZATION

BELLEFLEUR, C., DANSEREAU, J., de GUISE, J.,
Dept. of Mech. Eng., Ecole Polytechnique, P.O. Box 6079,
Station A, Montreal, Quebec, Canada, H3C 3A7

INTRODUCTION: Recently, computer tomography (CT) has been used to obtain a precise tridimensional (3-D) bone reconstruction of cadaveric lumbar spine specimens [1]. Meanwhile, studies of Dumas et al. [2] have determined various spinal ligament and muscular insertion sites in the lumbar region by 3-D digitization. Thus, the main purpose of this paper is to reconstruct bone and ligamentous lumbar spine (L1-L5) by means of CT scans and 3-D digitization according to the studies of de Guise et al. [1] and Dumas et al. [2]. This paper presents geometric characteristics of 3-D reconstructed ligament insertion sites obtained on a complete cadaveric lumbar spine (L1-S1) specimen.

METHODS: The lumbar spine was placed in a rigid acrylic frame to prevent any relative displacement of the vertebrae. Then, 178 sequential CT sections (1mm thick) were taken and the 3-D bone model was made by superimposing bone structures isolated on each slice. Visibility of the following ligaments were evaluated: ligamentum flavum (LF), supraspinous (SSL), interspinous (ISL), anterior longitudinal (ALL), posterior longitudinal (PLL), and intertransverse ligaments (ITL). Ligaments that show very good or excellent visibility were reconstructed as well as the bone structure. Following reconstruction, coordinates of ligamentous insertion sites were measured with the RES-TECH digitizer [2]. The digitization was made in two steps. First, the following ligaments were digitized: ALL, ITL, ISL, SSL. Then, the laminae and the vertebral bodies were separated in order to give access to the LF and PLL. Afterward, the digitized coordinates of the insertion sites were transfered to the 3-D bone model by using a least square algorithm in order to express the reconstructed and digitized data in the same coordinate reference system [3]. The transformation procedure allows to complete the 3-D bone model and to compare the digitized coordinates of the sites with the reconstructed sites. This comparison was expressed by the length differences and by the 3-D distances between the digitized and reconstructed sites.

RESULTS AND DISCUSSION: The visibility study shows that ISL, LF and SSL have a very good visibility as well as the PLL and ALL (but only at vertebral body levels). Table 1 presents the vertebral level on which the ligaments insertion sites were reconstructed and digitized. Mean 3-D distance between digitized and reconstructed coordinates of insertion sites is 2.2 mm with standard deviation of 0.7. This result has an order of magnitude similar to the accuracy of the 3-D techniques described in this paper (CT reconstruction: 1.2 mm; digitization: 0.7 mm; mean error from transfer: 0.2 mm, and identification error of anatomical structures: 0.4 mm). Figure 1 shows the length of digitized and reconstructed insertion sites of several ligaments at vertebral level L3. Differences in length of insertion sites can be explained by the difficulty of identification of both ends of the insertion sites on CT slices and on the lumbar specimen. For example, the begining and the end of the insertion sites of ISL are not easily recognizable on CT slices and on the lumbar specimen because this ligament is the continuity of LF and SSL [4]. This difficulty of identification results in different

position measurements of the ends of the insertion sites between the two 3-D techniques.

Table 1 - Vertebral level of reconstructed and digitized ligaments

	Vertebral and Intervertebral Level										
Ligament	L1	L1 L2	L2	L2 L3	L3	L3 L4	L4	L4 L5	L5	L5 S1	S1
ALL	D	D	D	D	RD	D	RD	D	D	D	
PLL	D	D	RD	D	RD	D	D	D	D		R
LF		RD		RD		RD		D		R	
ITL left		D		D		D		D			
ITL right		D		D		D		D			
ISL				RD		RD		D		RD	
SSL	D	RD	RD	RD	RD	RD	RD	RD	RD		

R: reconstructed
D: digitized

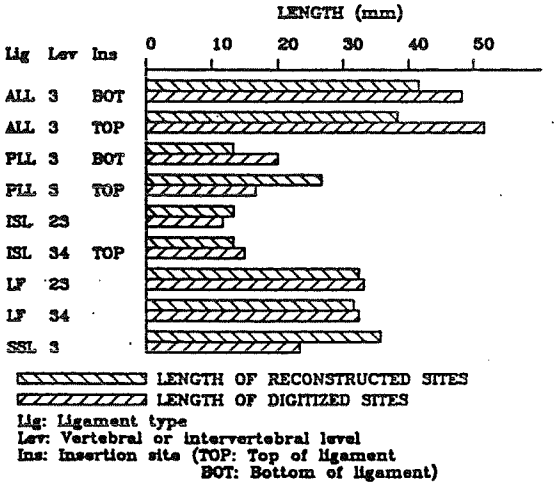

Fig. 1 - Length of digitized and reconstructed insertion sites (L3)

CONCLUSION: The 3-D reconstruction of ligament insertion sites by CT scans was possible for five ligaments (ALL, PLL, ISL, SSL and LF). Thus, the digitization of the insertion sites was necessary to complete the 3-D bone model of the spine. The differences or errors of identification were generated implicitly by the two methods described in this paper. However, such numerical and computing techniques are adequately accurate for 3-D reconstruction because the errors found are quite small (between 2 or 3 mm). The addition of ligamentous insertion sites to the 3-D bone model of the lumbar spine increases the realism of this model for future finite element modeling in order to study low back pain or lumbar injuries.

REFERENCES

1. de Guise, J., and Martel, Y., 10th annual IEEE engineering in medicine & biology Society, New Orleans, La, 426-427, 1988.
2. Dumas, G.A. et al., Spine, 13:532-541, 1988.
3. Wolf, P.R., Elements of photogrammetry, 549-596, McGraw-Hill, New-York, 1983.
4. Aspden, R.M. et al., Journal of Anatomy, 155:141-151, 1987.

AKNOWLEGMENTS: This research was founded by IRSST and NSERC.

DEFORMATION IN HEALTHY DISK AND UNHEALTHY DISK: A COMPARATIVE STUDY USING FINITE ELEMENT TECHNIQUE

Mohamed W. Fahmy and Shihab S. Asfour
Department of Industrial Engineering
University of Miami, Coral Gables, Fl, 33124

One of the most powerful methods to represent the intervertebral disk is the finite element technique. Belytschko et al.(1974) reported the first detailed finite element model to study the response of the disk under compression force. This was a three dimensional model that was rotationaly symmetrical with respect to the vertical line. The nucleus was modeled as incompressible fluid that had an unknown pressure. Both the vetrebral body and the intervertebral disk were assumed to be of an elastic and isotropic material. However, the intervertebral disk was considered non-homogeneous material. The vertical load was applied as a vertical displacement. Kulak et al. (1976) utilized the same model but treated the intervertebral disk as a viscoelastic material. Spilker(1980) constructed his model to study the impact of the geometry and the materials properties on the behavior of the disk. He used the four-nodes axisymmetric ring element to model the vertebral body and the annulus fibrosis. Furlong and Palazotto (1983) used a three parameter Kelvin solid to study the infleunce of surgical herniation on the viscoelastic properties of the intervertebral disk. Shirazi-Adl et al.(1984) considered the disk as a composite material that consists of the annulus fibrosis and the ground substances. The annulus fibrosis was modeled as a nonlinear tension element while the haxahederal element was used to represent the vertebral body as well as the ground substances. The nucleus was incorporated as an incompressible fluid that has an unknown pressure.

In the current study a finite element model was constructed to represent a superior vertebra, an inferior vertebra, and their associated disk using ANSYS software pakage. The 8-node element was selected to represent the vertebral body while the plate element and the shell element were chosen to represent the end plate, and the outer thin shell respectively. The nuclues was modeled using the 8-node fluid element. This element has the ability to represent the condition of the nucleus whether it is compressioin or in suction. Besides, it can simulate the degree of degeneration of the nucleus by changing the bulk modolus of elasticity. The disk was divided into two parts; the annulus fibrosis modeled by the tension-only spar element, and the ground substances represented by the 8-node element. This model could be modefied to handle dynamic loading with slight changes in the program.

Loading

The load was applied as a uniformly distributed pressure on the upper surface of the superior element. The pressure on the shell elements was assumed to be five times that on the vertebral body since it has a higher Young's Modulus. The normal load on the superior vertebral body was varied from 0 to 3000 N in steps of

500 N, in the case of a healthy disk (with nucleus) while it was varied from 0 to 1750 N in steps of 250 N in the case of a herniated disk (without nucleus).

Boundary Conditions

Due to the symmetry arround the sagittal plane, half of the structure was studied. The nodes that lie on the sagittal plane, i.e. Y = o, were prevented from deforming in the y direction. The nodes that lie on the upper plane of the superior vertebra were coupled to have the same vertical deformation. They were restrained from deforming in X direction as well as in the Y direction. The lower plane of the inferior vertbra was assumed to be fixed , i.e, DX = DY = DZ = 0.

Results

It was found that the nucleus plays a very important role in the vertical deflection. The vertical deformaion is larger when the nucleus is absent. It was also found that the largest horizontal displacement took place in the posterior part in the healthy disk while in case of the unhealthy disk the largest horizontal displacement was at the interior part. The nucleus was also found to affect the deformed shape of the disk. The outer surface of the intervertebral disk always bulges outwards. The inner surface bulges outward in the healthy disk while it bulges inwards in case of the degenerated disk. The medical implications of these findings are discussed.

JOINT FORCE ESTIMATION USING AN INTEGRATED KINEMATIC SENSOR

Zvi Ladin and Ge Wu
Biomedical Engineering Department and NeuroMuscular Research Center
Boston University, Boston, MA 02215, USA

Introduction

In non-invasive study of joint loading two approaches have been used for the assessment of the kinematic variables necessary to calculate the joint loads: direct measurement of acceleration or direct measurement of position. The limits of the accelerometry approach are the sensitivity of the accelerometers to the field of gravity and the difficulty in monitoring the segmental center of mass. Some researchers have tried to overcome the above difficulties by using multiple accelerometers [1]. On the other hand, the major difficulty with position measurement arises from the need to calculate second time derivatives of position data and the use of low pass filters that can distort some of the original signal contents [2]. This paper describes a new approach that integrates the position information *measured* by an accurate optoelectronic system, a six degree of freedom rigid body analysis and the acceleration information *measured* by a single triaxial accelerometer to provide an accurate and reliable estimate of joint forces. A compound two degree of freedom pendulum instrumented with an array of strain gauges was used to conduct a three-way comparison: joint forces measured by the strain gauges were compared to the estimates of the integrated segment, and to estimates based on position measurements alone.

The Experimental System and Data Processing

The experimental set-up shown in Fig. 1 consisted of a two degree of freedom pendulum mounted on two vertical supports. Two sets of bearings provided the two degrees of freedom of rotation. The vertical support beams were instrumented with an array of strain-gauges that directly measured the joint forces in the inertial reference system (**I**).
The *integrated kinematic sensor*, bolted to the center of mass of the pendulum for the synchronous kinematic measurements, includes infra-red light emitting diodes (LEDs) for position measurements and a triaxial accelerometer(model EGA3-f-10 by Entran Devices) for linear acceleration measurements. The WATSMART optoelectronic system (Northern Digital) with two infra-red sensitive cameras was used for the three-dimensional reconstruction of each LED. The analog data from the accelerometer and the strain gauges was synchronized with the position measurements of the WATSMART system using the WATSCOPE A/D unit and was sampled at $100Hz$.
The momentary spatial orientation of the pendulum in system **I** was calculated using the MIT-developed software package TRACK and was used to derive the transformation information between system **I** which is attached to the vertical supports and the body-fixed coordinate system **B** moving with the pendulum. The gravity acceleration vector **g** was transformed first from **I** to **B** to extract the acceleration at center of mass $\mathbf{a}_{cm}$ from the accelerometer output $\mathbf{a}_{acc}$ according to equation (1):

$$\mathbf{a}_{cm} = \mathbf{a}_{acc} - T_{BI}\mathbf{g} \tag{1}$$

and then the acceleration $\mathbf{a}_{cm}$ (measured originally in **B**) was transformed into **I** and substituted into equation (2) with the joint forces **F** as the only unknown.

$$\mathbf{F} + m\mathbf{g} = mT_{IB}\mathbf{a}_{cm} \tag{2}$$

A second estimation of joint force was conducted by estimating the linear accelerations based on the position measurements alone as calculated by TRACK. The kinematic variables were low pass filtered with different cut off frequencies in order to improve the signal to noise ratio. The estimated accelerations were then substituted into eq. (2), resulting in estimates of the joint forces that are based *exclusively* on the position measurements.

Results and discussions

The estimated and measured X, Y and Z components of the joint force are compared and shown in Fig. 2. The estimated forces based on the integrated measurements are practically on top of the measured force trajectories. The estimated forces based only on the position measurement and the derived acceleration estimates show a clear dependence on the cutoff frequency of the filter: the $5Hz$ low pass filter generates much better estimates of the joint forces, especially close to the beginning and the end of the trajectory.
A closer examination of the frequency spectrum of the measured joint forces revealed the existence of a high frequency component at about $12Hz$. The application of filters with cut off frequencies smaller than that value will clearly result in the elimination of this component. The close correspondence between the estimated forces by the integrated kinematic sensor and the measured ones suggests that by integrating the three elements that comprise such an estimation, namely accurate position measurements, a six degree of freedom rigid body kinematic analysis, and the use of this information to dynamically calibrate the linear accelerometer's output one can obtain high-quality 'non-invasive' estimates of joint forces. It appears that such an approach is more accurate than the position measurement approach and is computationally simpler than the multiple-accelerometer system.

References:
[1] Hayes, W.C.,et al., J. Biomech. Eng., 105:283-289, 1983
[2] Ladin, Z. et al., J. of Biomech., 22(4):295-308, 1989

Acknowledgement: This work was supported by a National Science Foundation Grant No. EET-8809060 and by a grant from the Whitaker Foundation.

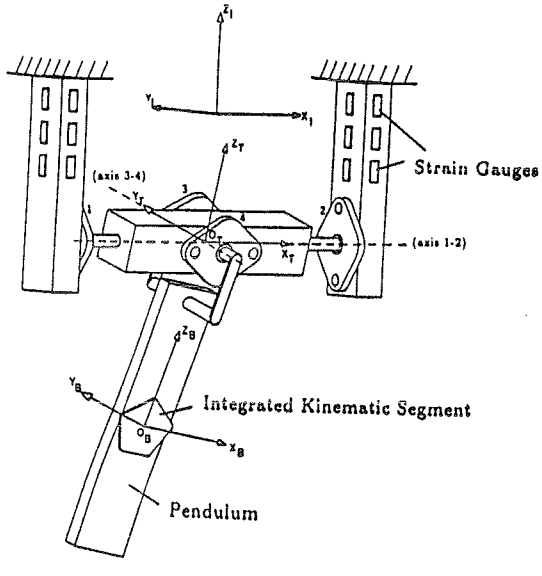

Fig.1 Experimental Setup

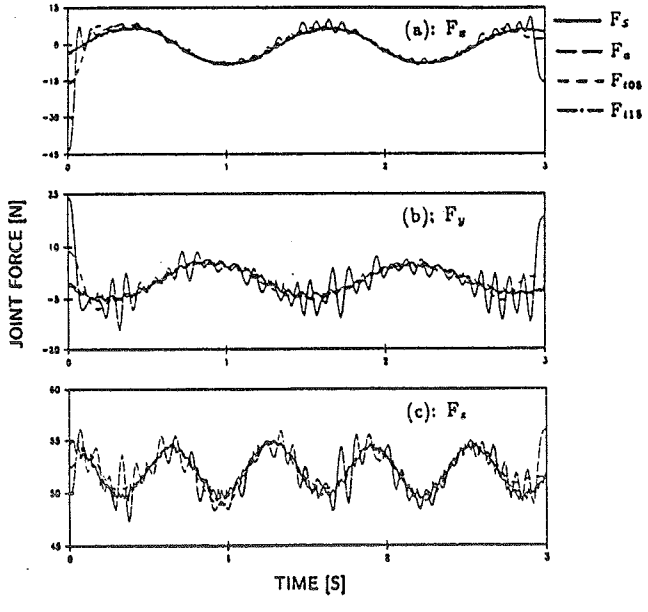

Fig.2 Measured and Estimated Joint Forces

EFFECT OF BONE BLOCK REMOVAL ON PATELLAR STRESSES: A FINITE ELEMENT ANALYSIS

E.A. Friis*, F.W. Cooke*, D.L. Hahn*, D.A. McQueen*+, C.E. Henning+
*Orthopaedic Research Institute, Inc. Wichita, KS
+Dept. of Orthopaedic Surgery SFRMC, Wichita, KS

INTRODUCTION

A popular form of autogeneous graft anterior cruciate ligament reconstruction involves harvest of the central third of the patellar tendon with bone blocks from the patella and tibial tubercle. Recent concern about the effect of bone block removal on the mechanical integrity of the patella has been raised.(1) Some transverse patellar fractures under normal loading conditions have been observed following removal of large bone blocks. A three-dimensional finite element model of the patella was created to evaluate the stress and strain distributions produced by removal of a typical square shaped bone block.

REVIEW AND THEORY

Because of the irregular shape and complex bending of the patella, the magnitude and distribution of this stress increase is unknown. Since a large bone block allows better fixation of the graft, it would be beneficial to the surgeon to have guidelines for the optimum bone block size. A previous experimental study using thermographic stress analysis (the SPATE method) was performed to analyze the stress raising effect of a square bone block removal from the patella. This study showed that resection of the bone block increased the maximum tensile stress in the patella by an average of 50 percent. A finite element model of the patella was constructed to: (1) verify that the maximum stress in the patella is located on the anterior surface, (2) theoretically confirm the patellar stress distribution pattern seen in the thermographic analysis, and (3) build a realistic patella model which can be subjected to a variety of mock surgeries and reconstructions for future testing.

METHODOLOGY

Patellar geometry was obtained by digitizing transverse sections of a normal male human cadaveric right patella. From this geometry, a finite element model of the patella was formed utilizing 3114 8-node isoparametric solid elements. Four regions of bone were defined and material properties assigned according to elastic modulus estimates based on dry relative density measurements.(2) These moduli values correlated with reported values of patellar and tibial cancellous bone properties.(3,4) The COSMOS-M finite element analysis program was used. The patella was modelled in 60 degrees of knee flexion with the quadriceps tendon forces applied at angles of 25 degrees AP/-15 degrees ML and 30 degrees AP respectively across 150 nodes at the appropriate corresponding sites of anatomical tendon insertion. The loading condition modelled the Q-angle and quadriceps liftoff from the femoral axis. The boundary conditions were defined by constraints in the medial-lateral (ML) and anterior-posterior (AP) directions at the nodal points corresponding to an average region of retropatellar surface contact, as shown by previous investigators.(5) Load magnitudes applied were 2400 Newtons quadriceps tendon force and 1600 Newtons patellar tendon force. Figure 1 illustrates the model geometry and individual load components. The 1.5:1 ratio of F_Q:F_{PT} corresponds to previously reported experimentally measured ratios of F_Q:F_{PT} at 60 degrees knee flexion. The load magnitudes correspond to maximum normal conditions in vivo.(6) The models tested were: (1) an intact patella and (2) a patella with a central 10 mm square cross section bone block excised.

RESULTS

Figures 2 and 3 show the Von Mises stress distribution pattern in the intact and bone block compromised patella, respectively. The amount of bending in the patella was increased by removal of the bone block and the maximum tensile stress on the anterior surface was increased by about 105 percent (57 vs 117 MPa) . The stresses experienced by the patella on the anterior surface were comparable to the stresses measured thermographically (when linear correlation between applied load and resulting stress is assumed) and the stress distribution (pattern) followed the same trend. Figure 4 illustrates the superior-inferior stress in the bone block comprimised patella. This stress is perhaps a more suitable comparison of the first stress invariant measured by thermographic techniques. The trend of zero to compressive stresses at the medial superior edge of the cut was seen in both the FEM and the thermographic analysis.

DISCUSSION

These results show that removal of even an average sized square bone block may seriously compromise the patella under maximal loading conditions. The maximum anterior surface stress seen was near the fracture stress of cortical bone. If a larger bone block with sharper corners or nicks at the corners were modelled, the stress raising effect would undoubtedly be even greater. The intact patella yielded reasonable results with a factor of safety of around 2 under maximal loading conditions. Although maximal loading is not likely for individuals who have just undergone ACL reconstruction, it must be considered that complete remodelling of the patellar defect may not occur and that the patella may remain in an at least partially comprised state after return to the patient's normal level of physical activity.

REFERENCES: (1) McCarroll, J.R., Am J Sports Med, 11(1):26-27, 1983. (2) Cellular Solids: Structure and Properties, L.J. Gibson and M.F. Ashby, Pergamon Press, pp. 316-331. (3) Goldstein, S.A., et al, J Biomech, 11/12:1055-1061, 1987. (4) Ashman, R.B., et al, J Biomech, 8/9:895-900. (5) Ahmed, A.M., et al, Trans of the ASME, 105:226-236, Aug 1983. (6) Ahmed, A.M., et al, J Orthop Res, 5:69-85, 1987.

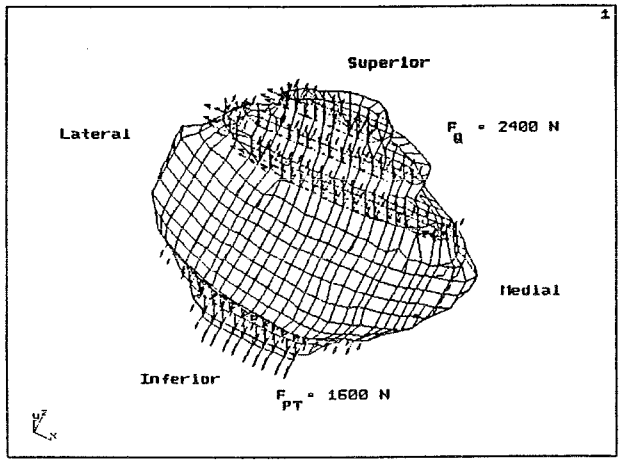

Fig. 1. Patella Model Geometry

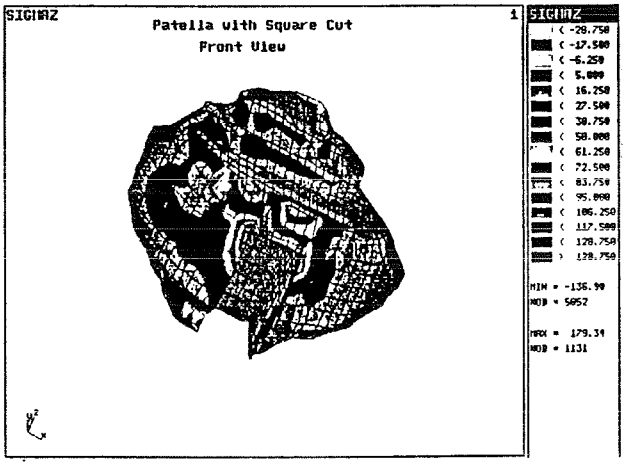

Fig. 4. Superior-inferior stress distribution in patella with square bone block excised.

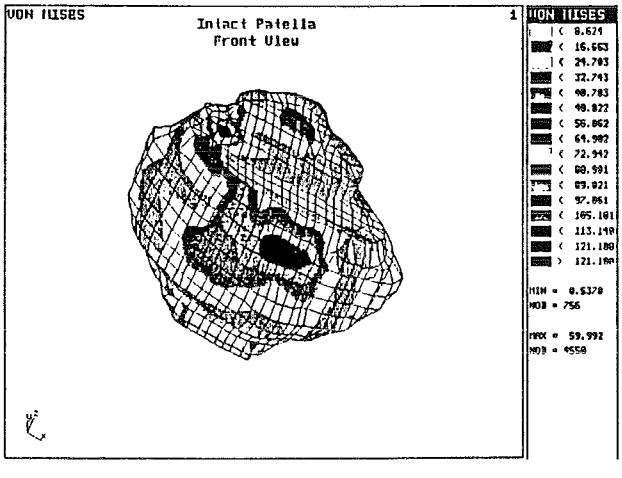

Fig. 2. Von Mises Stress in intact patella.

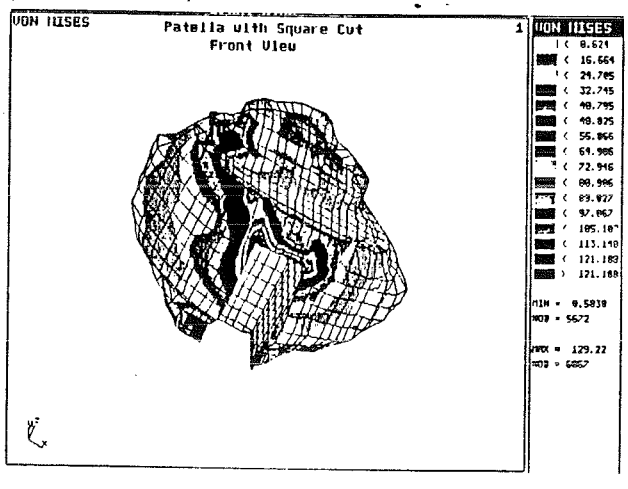

Fig. 3. Von Mises stress in patella with square bone block excised.

THE INFLUENCE OF FIXED ROTATIONAL DEFORMITIES OF THE FEMUR ON THE PATELLOFEMORAL JOINT: IN-VITRO AND IN-VIVO ASSESSMENT

Thay Q Lee
STAMP Program - Long Beach VA Medical Center (117S)
5901 East 7th. Street, Long Beach, California 90822, USA
Division of Orthopaedic Surgery - University of California, Irvine

INTRODUCTION

The patellofemoral force system is complex and considered to have a strong correlation with patellar disorders such as chondromalacia and subsequent arthrosis (1). The biomechanics of patellofemoral joint disorders that result from the problems associated with soft tissue or the tibia have been well documented. However, the biomechanics of the patellofemoral disorders resulting from angular and torsional deformities of the femur have not been determined. The objectives of this study were: 1. To determine the quantitative effects of fixed rotational deformities of the femur on patellofemoral contact pressures and the tension in quadriceps tendon in human cadaver knees; 2. To determine the long term response of the articular cartilage on the retropatellar surface to 30 degrees of fixed rotational deformities of the femur in a canine model.

METHODOLOGY

For the in-vitro study, seven fresh frozen human cadaver knees were used. The specimens had no previous surgery, with macroscopically intact cartilage, radiographically normal bone structure and intact joint capsule. The ages were unknown, but they appear to have been between 60 to 80 years old. The specimens were carefully dissected leaving only the femur, tibia, joint capsule and quadriceps tendon. The femur and the tibia were then cut 25 cm. away from the tibial plateau, and the fibula was eliminated. The specimen was clamped rigidly into steel cylinders and mounted onto a custom jig specifically built to be used in conjunction with an Instron machine. This system simulates fixed rotational deformities of the femur at various knee flexion angles and permits simultaneous measurement of the patellofemoral contact pressures and the tension in the quadriceps tendon. Once the specimen was securely mounted and positioned at a desired knee flexion, the neutral position of the patellofemoral joint was determined, and then the patellofemoral contact pressures were measured under 200 N of tension in the quadriceps tendon using Fuji pressure sensitive film (Range: 0.2 to 2.0 MPa). For the patellofemoral contact pressures in rotated state, a new film was inserted and the tension in the quadriceps tendon was maintained at 200 N for 45 minutes in neutral position before rotating the specimen. The internal and external rotation of 20 and 30 degrees was accomplished at 2 RPM using a motorized assembly built into the jig while continuously monitoring the tension in the quadriceps tendon. The entire procedure was performed at knee flexion angles of 30, 60, 90 and 120 degrees. The contact pressures from Fuji film were quantified by using a calibrated scale from the manufacturer which was also verified in the laboratory by compressing cylindrical rubber discs with Instron machine. For the In-vivo study, fifteen skeletally mature mongrel dogs were used. Thirty degrees of fixed rotational deformities of the femur were surgically imposed using six hole Dynamic Compression Plates on twelve experimental animals. Three remaining animals were used as controls. Twelve experimental animals were divided into four groups with three dogs in each group (Internal rotation (3 and 6 months); external rotation(3 and 6 months)). All the procedures were performed bilaterally to insure even weight bearing. At the end of the experimental period, the dogs were euthanized and the hind legs were disarticulated at the hip and the ankle joint. Then all the musculature, ligaments and menisci were carefully dissected away to expose the articular surface of the patellofemoral joint for indentation test. The unrelaxed (0.1 sec.) and relaxed (2000 sec.) shear modulus were determined for each quadrant of the retropatellar articular cartilage using a custom built indenting apparatus (force of indentation = 0.98 N, diameter of the cylindrical ram indenter = 1.0 mm.). The mathematical analysis was based on theoretical indentation mechanics of an infinite elastic layer bonded to a rigid half space. The elastic layer corresponds to the articular cartilage and the rigid half space to the underlying bone. For this model, the analysis by Hayes (2) provides an exact

elastic solution for indentation by a plane end cylindrical ram, assuming the shear traction between ram and the layer is negligible for small strains.

RESULTS AND DISCUSSION

The in-vitro study revealed that the increase in the degree of fixed rotation of the distal femur in human cadaver knees resulted in a nonlinear increase in patellofemoral contact pressures on the contra-lateral facets of the patella (i.e. external rotation resulted in a contact pressure increase on the medial facet and internal rotation resulted in a contact pressure increase on the lateral facet of the patella). With the initial isometric tension of 200 N in the quadriceps tendon for 30, 60, 90 and 120 degrees of knee flexion, the peak contact pressure showed no significant differences between the medial and lateral facets of the patella in neutral position ($P>0.5$). Upon 20 degrees of femur rotation, only a slight increase was noted for the tension in the quadriceps tendon and the contact pressures in the contra-lateral facets of the patella. However, upon 30 degrees rotation, both the external and internal rotations of the distal femur resulted in significant increase in the tension of the quadriceps tendon and the contact pressures on contra-lateral facets of the patella. In addition, the external rotation for knee flexion angles of 30, 60 and 90 degrees showed significantly higher peak contact pressure increases on the medial facet of the patella as compared to the internal rotation of the femur ($P<0.05$) (Figure 1). For the in-vivo canine study, the morphological examination revealed early signs of arthrosis (redness of the articular cartilage) on the retropatellar surfaces at 6 months for both the internal and external femur rotations. The indentation tests showed no difference between each quadrant of the patella for all experimental groups regardless of the direction of the femur rotation ($p>0.5$). However, a statistically significant decrease was observed for both the unrelaxed (Figure 2) and relaxed shear modulus at 6 months for both direction of the femur rotation ($P<0.05$). This was further supported by histological findings where the disorganization of the collagen fibers in the tangential layer was observed. These findings indicates that the cartilage softening occurred on patellar facets with both the increased and decreased contact pressures. This study provides baseline information regarding changes in patellofemoral contact pressures that may be significant for the development of chondromalacia patella and subsequent arthrosis due to fixed rotational deformities of the femur. Further, surgical procedures involving osteotomies of the distal femur should only be performed after an accurate assessment of the femur rotation and angulation.

Figure 1

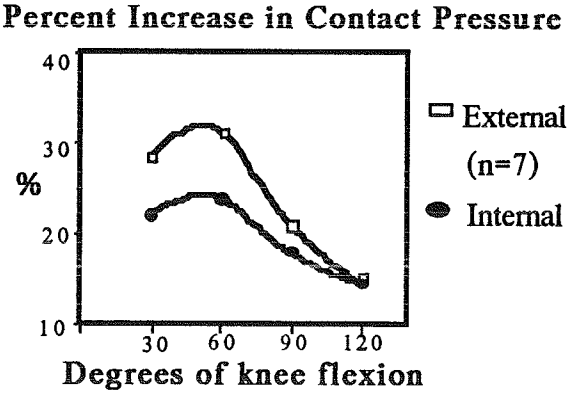

Figure 2

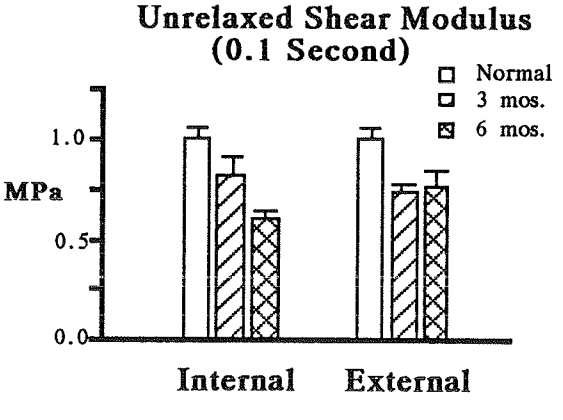

REFERENCES

1. Ficat, R.P., Hungerford, D.S.: Disorders of the Patellofemoral Joint. William &Wilkins, 1977.
2. Hayes, W.C., Keer, L.M., Herrmann, G., Mockros, L.F.: A Mathematical Analysis for Indentation Tests of Articular Cartilage. J. Biomechanics, 5:541-551, 1972.

AKNOWLEDGEMENT

RR&D Grant # A474R of the Veterans Affairs and California Orthopaedic Research Institute.

SESSION 12

ERGONOMICS

PRELIMINARY EVALUATION OF A COMPREHENSIVE BIOMECHANICAL MODEL USING STRENGTH, STABILITY, AND COEFFICIENT OF FRICTION CONSTRAINTS TO PREDICT HAND FORCE EXERTION CAPABILITY DURING SAGITTALLY SYMMETRIC STATIC EXERTIONS

Carter J. Kerk[1], Don B. Chaffin[1], and George B. Page[2]

[1] Center for Ergonomics, University of Michigan, Ann Arbor, MI 48109-2117
[2] Research and Test Dept., Association of American Railroads, Washington, DC 20001

INTRODUCTION

Separate models related to strength, stability and static coefficient of friction (COF) currently exist that predict hand force exertion capability during sagittally symmetric static exertions. A mathematical, biomechanical model has been developed which comprehensively and simultaneously predicts feasible reaction forces at the hands based on these same factors. This preliminary study is an attempt to evaluate the theoretical hand force predictions with observed data from the laboratory. The preliminary findings are aiding in evaluating parameters used by the model and in testing hypotheses about the model.

REVIEW AND THEORY

Previous models are useful for iterative evaluation of the factors (strength, stability, and COF). A two-dimensional static strength prediction model by Chaffin *et al.* (1970), predicts percentile strength capability for a given hand force vector using methods described in Chaffin *et al.* (1984). It also calculates the required COF and stability status, i.e. static equilibrium. A graphical model called Postural Stability Diagram (PSD) has been developed by Grieve (1979a, 1979b). Equations for stability and COF are plotted on a graph, with axes as vertical and horizontal hand forces for specific locations of the feet and hands. These equations provide limits for the feasible hand force capability envelope. In the new comprehensive model, a set of fifteen linear constraint equations (of the form $\mathbf{Ax} \leq \mathbf{b}$) in three classes (COF, stability, and strength) have been developed to map out a feasible hand force solution space for a given posture, anthropometric profile, strength profile, COF, and type of footwear. The COF constraint class requires that the absolute value of the horizontal component of the hand force is less than or equal to the product of the COF and the normal force at the foot. The stability constraint class requires that moments to maintain stability at extreme points of the foot are greater than or equal to moments that disrupt stability. The strength constraint class requires that the muscle-produced strength moment at a given joint for a given function, e.g. flexion be greater than or equal to the moment acting at the joint due to external forces at the hands and body segment weights. The resulting graphical, feasible hand force solution space, with axes of horizontal and vertical hand force, provides interesting hypotheses for testing. The model can also predict the hand force generating capability for a any hand force vector direction without specifying the vector direction beforehand. The model also predicts a combination of vertical and horizontal hand force vector components which maximizes force magnitude for a task of interest, e.g. pushing.

METHODOLOGY

Anthropometric and strength profiles were collected on the pilot subject. These profiles were used as inputs to the new comprehensive model where postures of interest from the hypotheses were simulated. The subject then stood on force platforms, assumed a specific posture and was asked to exert a maximum hand force in a specific direction for 6 seconds. The precise posture was recorded and digitized. Forces and moments at the hands and feet were recorded. The precise posture was used as an input to the model, which in turn yielded a predicted feasible hand force solution space. This feasible solution space could then be compared to the observed hand force magnitude.

RESULTS

Figure 1 shows the results of the pilot subject exerting maximal forces in sixteen directions for the specific posture. Only the five limiting constraints are shown to preserve some simplicity.

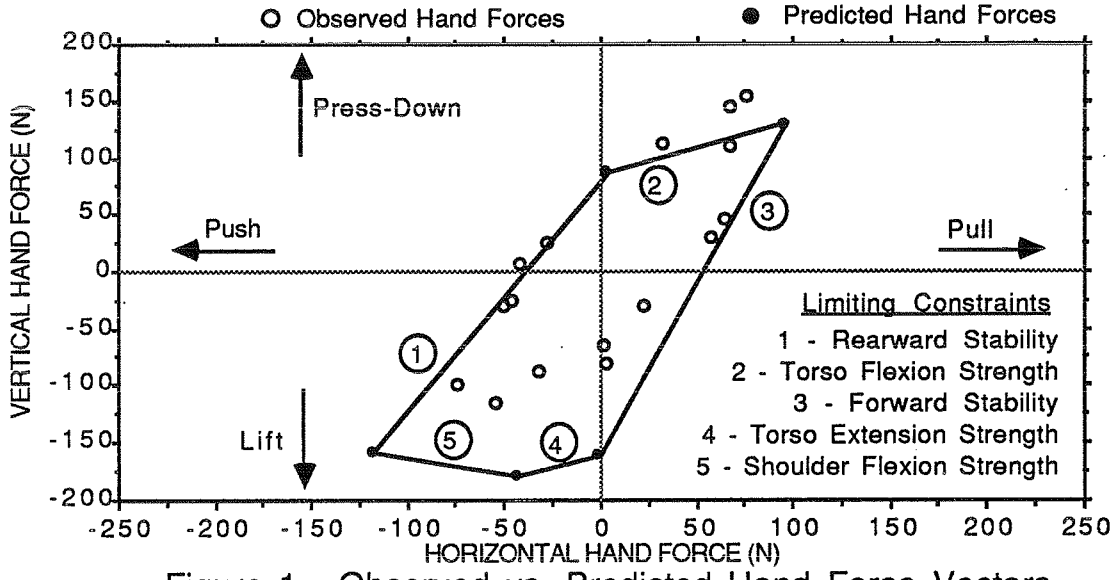

Figure 1. Observed vs. Predicted Hand Force Vectors

DISCUSSION

The results in Figure 1 showed graphically that the predicted feasible solution space exhibited a reasonable ability to predict hand forces and there appeared to be similar trends between the observed and predicted patterns. The stability constraints (1 and 3) appeared to be the most reasonable and parameter estimation studies are in progress to test and improve the model assumptions concerning these factors. The limiting strength constraints (2,4, and 5) showed less agreement with the observed values. This was expected, as the development and underlying assumptions with the strength constraints are based on more complex scientific foundation. The COF constraints were not among the limiting constraints. This was also expected, as the COF level in this pilot study was controlled at a high level so only the strength and stability constraints were tested in this case.

CONCLUSIONS

This preliminary study appears to support the need for further efforts with this research. There are many hypotheses of interest which are currently being studied. These results will be reported. These include the isolated and comprehensive testing of the specific factors in the model (stability, COF, strength), the effects of varying anthropometry, strength, COF, posture, and footwear. The most promising aspect of this model appears to be its ability to comprehensively combine multiple factors that can affect hand force exertion capability.

REFERENCES

1. Chaffin, D.B. and Baker, W.H. (1970) *AIIE Transactions* **2**: 16.
2. Chaffin, D.B. and Andersson, G.B.J. (1984) *Occupational Biomechanics*, Wiley.
3. Grieve, D.W. (1979a) *Ergonomics* **22**: 1155.
4. Grieve, D.W. (1979b) *Ergonomics* **22**: 1165.

This work was supported by a grant from the Association of American Railroads.

NORMAL WRIST POSITION DURING MAXIMAL GRIP

Shawn W. O'Driscoll*+, Richard Ness+, Tom D. Cahalan+
Robin R. Richards*, E.Y. Chao+, Kai-Nan An+

+ Orthopaedic Biomechanics Laboratory, Mayo Clinic/Mayo Foundation, Rochester, Minnesota
* Upper Extremity Reconstructive Service, Division of Orthopaedic Surgery, St. Michael's Hospital, University of Toronto, Canada

INTRODUCTION: Arthrodesis of the wrist is an operation that provides excellent pain relief, but is not as successful at restoring grip strength. One possible explanation is that the patients have been fused in positions that are suboptimal for grip strength. The purpose of the present investigation was to answer the question what is the position of the normal wrist assumed during maximal unconstrained grip?

MATERIALS AND METHODS: Twenty healthy young adults (ten males, ten females) with no past or current history suggestive of neuromuscular or orthopaedic dysfunction potentially affecting the upper extremity were used in this study.

Grip Strength Testing: Grip strength was measured with a Jamar dynamometer in a standard fashion with the patient sitting, the shoulder in the neutral anatomic position, the elbow flexed to 90°, and the forearm in neutral rotation. Unconstrained motion of the wrist in the sagittal and transverse planes was allowed, but they were instructed not to rotate the forearm.

Wrist Position Measurement: Wrist position was measured using bi-axial electrogoniometers. The neutral alignment of the wrist was defined as alignment of the long axis of the third metacarpal and the radius in the sagittal and coronal planes. To accomplish this marks were placed on the skin over the midpoints of the distal and proximal ends of the third metacarpal, as well as over Lister's tubercle and the radial head. The centers of rotation of the electrogoniometers were aligned with the center of the head of the capitate for radioulnar deviation and the midpoint between the ulnar styloid and triquetrum for flexion and extension. Thus both accuracy and reproducibility were estimated to be approximately ±3°.

Grip Strength Measurements in Different Positions: The optimum setting on the Jamar was determined by testing the left nondominant hand. All testing was performed in a standardized fashion. Grip strength was tested twice at each wrist position and the average value obtained. The patient was instructed to exert maximal grip effort in any position that the wrist felt most comfortable. This comfortable position was referred to as the self-selected position. The patient's wrist was then positioned into approximately 10° of deviation in either flexion, extension, radial deviation, or ulnar deviation away from this self-selected position. The order of testing the positions of deviation from the self-selected position were selected from a random table. Finally, the subject was instructed to once again attempt maximal grip in the position that felt most comfortable as with the first testing. This position was referred to as the final self-selected position.

RESULTS: There was no significant difference between males and females with respect to the self-selected position of the dominant wrist. Therefore, male and female data were grouped and analyzed collectively.

The natural or self-selected position chosen by the patients when performing maximum grip effort was consistent (Table I). Not only was the self-selected position consistent, but it was also highly reproducible and not influenced by fatigue effect after testing multiple other positions. The corresponding grip strengths were significantly reduced in each of the deviated positions compared to that in the self-selected position.

DISCUSSION: Based on the experimental data in the present report, it would be predicted that patients whose wrists are fused in neutral radio-ulnar deviation would have two-thirds (59%-78%) of normal strength. Those fused in 15° of extension and 5° of ulnar deviation would have three-quarters (66%-83%) of normal strength. These figures agree closely with those reported for grip strength following wrist arthrodesis.

TABLE I

Wrist Position	Extension (Degrees)	Ulnar Deviation (Degrees)	Strength (kg)
Self Selected:			
Dominant: Initial	35±2	7±2	41±3
Dominant: Final	33±3	5±2	38±3
Nondominant	40±2	2±3	37±3
Flexion	15±2	5±5	30±2
Extension	47±1	5±2	33±3
Radial Deviation	32±2	-1±2	28±3
Ulnar Deviation	29±2	17±2	30±3

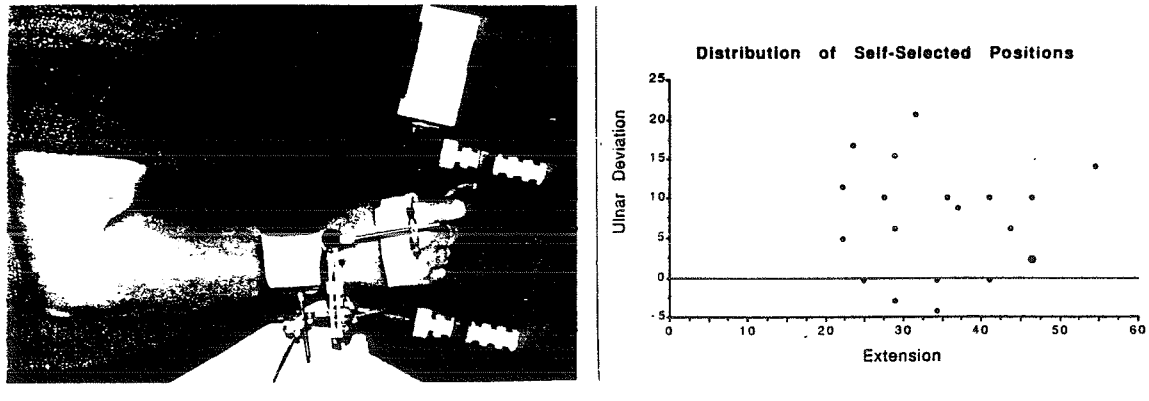

Fig. 1 Test arrangement with electrogoniometer and Jamar, showing patient and limb position.

HAND POSTURE PREDICTON FOR POWER GRASP OF CIRCULAR CYLINDERS

Bryan Buchholz and Thomas J. Armstrong
Center for Ergonomics, The University of Michigan, Ann Arbor, MI 48109, U.S.A.

INTRODUCTION

A kinematic model has been developed to predict and simulate the prehensile posture of the human hand. This model is formulated from kinematic considerations and uses ellipsoids to approximate the geometry of the hand segments. The model predicts the hand posture needed for power grasp of ellipsoidal objects of various sizes. Hand posture is quantified via the joint angles. Contact points and vectors along the hand-object interface are calculated, also. The model will be used to evaluate tool designs so they may be used efficiently without mechanical trauma.

REVIEW AND THEORY

The kinematic skeleton of the hand is characterized by ideal joints connected by simple segments. For each segment, a local coordinate system is defined so that finger-joint angulation can be characterized by yaw (abduction-adduction), pitch (flexion-extension) and roll (axial rotation) angles. The neutral angular position of the thumb CMC joint is defined from the data of Cooney (1981), i.e. the reference axes of the trapezium are flexed 48°, abducted 38° and pronated 80° with respect to the third metacarpal.

The three-dimensional geometry of the surface of the hand is approximated by ellipsoids attached to each hand segment, which are used for determining contact points and therefore are called segment contact bodies. Objects are also described using ellipsoids, with cylinders established as ellipsoids with an infinite long axis that is truncated. Contact is determined mathematically based on the geometrical relationship between two ellipsoids that just touch in a single point, i.e. the outward normal vectors from the two ellipsoids are parallel but in opposite directions. The ellipsoids are expanded or contracted until a single point of contact is determined. If contraction was necessary, then the ellipsoids are in contact and soft tissue deformation may be estimated from the amount of contraction. This contact algorithm was developed by Fleck and Butler (1981).

The model functions by reducing the posture prediction problem to a sequence of one degree of freedom problems, i.e. all joint angles are initially set and only the flexion-extension angle for a specified joint is varied until a specified hand segment contacts the object and the soft tissue deformation criterion is met. The model begins by flexing the proximal joints and then proceeds distally, "wrapping" the hand around the object.

This algorithm for power grasp of ellipsoidal objects is implemented on a microcomputer using Pascal. Coefficients for determining segment lengths, breadths and depths from hand length and breadth measurements are incorporated in the model, so that the prehensile capabilities of any size hand may be analyzed by the model. Ellipsoidal semi-axes lengths for describing the object and object orientation angles are needed as model input. Graphics procedures are included for visual display of the model. Examples of the graphical display of the model are shown in Figure 1.

METHODOLOGY

The goal of this study was validation of the predictive capabilities of the hand model. Validation was broken into three steps. These were: 1) collection of angular measurements from six living subjects with hand lengths ranging between 15.4 and 21.9 cm, 2) determination of the model's sensitivity to the various input parameters and 3) evaluation of the model's ability to predict flexion-extension joint angles. Circular cylinders were chosen because they are readily available. Six cylinders, with diameters from 1.6 to 7.6 cm, were employed. Two different power grasps were examined (Figure 1): 1) a transverse grasp with the thumb abducted for added power and 2) a diagonal grasp with the thumb adducted for an element of precision.

RESULTS AND DISCUSSION

Angular measurements collected from living subjects were well correlated with hand length and cylinder diameter using linear regression equations. These regressions explained between 41 and 94% of the variation in measured flexion angle for the four fingers. The effect of cylinder diameter was much larger than that of hand length. Flexion angle decreased between 3.19 and 10.0 degrees per centimeter increase in cylinder diameter. An increase in hand length usually led to an increase in flexion angle, except for MCP-II and MCP-III. The effect on flexion angle varied from a decrease of 4.12 to an increase of 3.86 degrees per centimeter increase in hand length.

Regression analysis was used to examine the sensitivity of the joint angles predicted by the model to variations in hand length, cylinder diameter, cylinder angle, ellipsoid penetration and X-location. These regressions explained

between 78 and 93% of the variation in the predicted joint angle for MCP and PIP in this analysis, but only between 9 and 34% for DIP. The DIP joint showed the most variance in the predicted joint angles due to a "zig-zag" effect, which caused errors to increase for the distal joints because of their dependence on the prediction of the proximal joint angles. It was found that the joint angles predicted by the model showed a similar sensitivity to hand length and cylinder diameter as was seen in the measured data. The sensitivity of the model to cylinder angle was relatively small. The effect was largest for MCP-II and MCP-V. For digit II, predicted MCP flexion decreased an average of 1.42 degrees per degree increase in cylinder angle and for digit V, MCP flexion increased an average of 0.88 degrees per degree increase in cylinder angle. The effect of ellipsoid penetration was also relatively small, flexion increased between 0.43 and 0.73 degrees for a one percent increase in strain for PIP, the most sensitive joint to penetration. The model is very sensitive to the X-location of the object center, with the "zig-zag" effect obvious. For MCP, moving the object center distally decreased the joint flexion between 12.7 and 21.1 degrees per half centimeter of movement. The opposite was seen at PIP, flexion increased from 9.88 to 15.1 degrees per half centimeter distal move in object location. At DIP, smaller decreases in flexion were seen. These decreases ranged between 2.60 and 9.24 degrees per half centimeter.

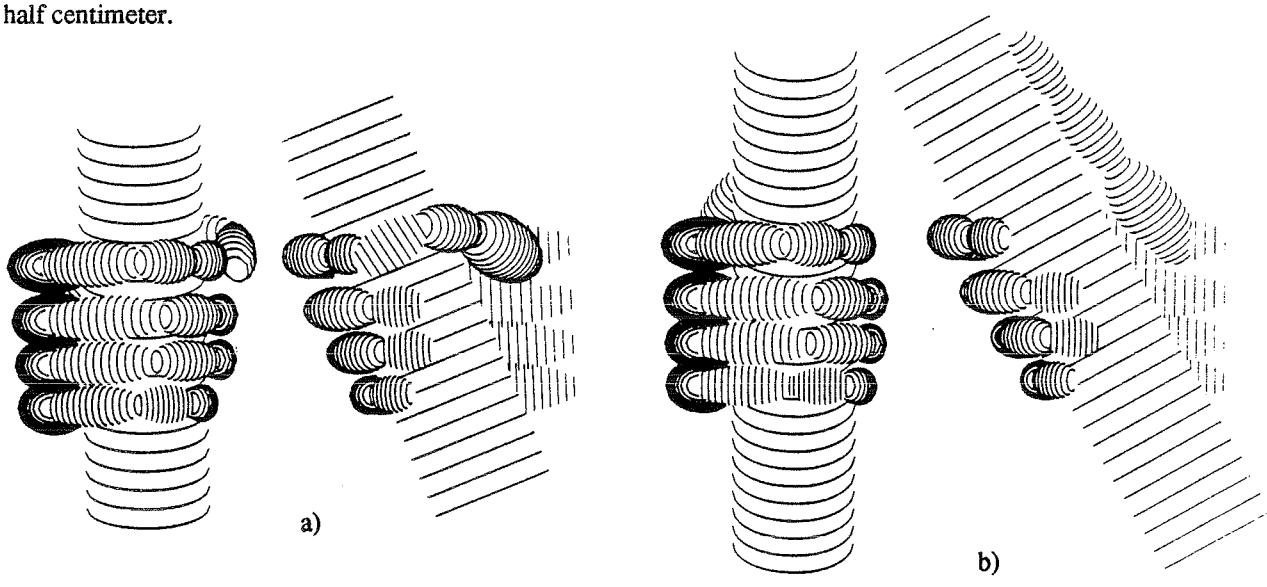

Figure 1. Graphical depiction of the hand posture predicted by the model for power grasp of a circular cylinder: a) transverse volar grasp and b) diagonal volar grasp.

The final step of the validation was actual comparisons of the measured and predicted joint angles. These comparisons indicated that the model is capable of predicting the hand posture used in the power grasp of circular cylinders, although slight overpredictions of joint flexion were found in these comparisons. For the transverse volar grasp, the mean difference beteen predicted and measured flexion angles was -3.7 ± 10.0 degrees and for the diagonal volar grasp, the mean difference was -1.8 ± 14.0 degrees. For MCP and PIP, these predictions were consistent for the hands and cylinders examined. Standard deviations for these joints ranged from 4.3 to 13.9 degrees. Predictions for DIP were more variable because of this joint's dependence on the angles predicted for the proximal joints. Standard deviations for the differences at DIP ranged from 9.8 to 31.7 degrees. Differences between predicted and measured angles were most variable for the DIP joint of digit V. For this joint, the model underpredicted flexion on small cylinders and overpredicted flexion on the larger ones.

CONCLUSIONS

This biomechanical hand model provides an accurate description of power grip function and will aid in the design of hand tools for both performance and safety. Algorithms for more complex-shaped objects are currently being developed. Grip force prediction is another goal of this research.

REFERENCES

Cooney *et al., J. Bone and Joint Surgery*, **63A**, 1371-1381, 1981.
Fleck and Butler, *Validation of the Crash Victim Simulator*, Vol. 1, NTIS, Springfield, VA, 1981.

This work was supported by NASA Training Grant NGT-23-005-802, NIOSH and gifts from private industry.

THE RELATIONSHIP OF ISOMETRIC STRENGTH TO PEAK DYNAMIC HAND FORCES DURING SUBMAXIMAL WEIGHT LIFTING

Deborah D. Thompson and Don B. Chaffin
Center for Ergonomics, University of Michigan, Ann Arbor, MI 48109-2117

INTRODUCTION. It has been well documented that back and overexertion injuries are a major problem (in terms of injury and economic costs) in industry today. Therefore, the issue is no longer whether or not the problem exists, but rather how these types of injuries can be prevented. It is generally accepted that the assessment of isometric strength assists in predicting whether a worker is capable of performing a lifting task without incurring injury or strain. However, manual material handling activities are generally dynamic in nature, and thus the isometric values may be limited (Garg *et al.*, 1980). So, it was of interest to determine if peak hand forces under submaximal loads were at all related to maximal isometric strength values.

REVIEW AND THEORY. Studies of others have indicated that workers who were placed in jobs where the strength requirements exceeded their isometric strength capabilities had incidents of strains and sprains that were three times higher than those whose isometric strength exceeded the job strength requirements (Chaffin and Park, 1973). However, given the dynamics of work activities, dynamic strength testing has been proposed to be more predictive of job strength performance, but such dynamic testing is more complex, due to the number of parameters which must be controlled.

The validity of dynamic strength testing has been based on a psychophysical method, wherein the subjects are allowed to adjust the load lifted until they obtain, in their judgement, the maximum amount of weight that can be lifted safely (Snook, 1978). This is then compared to the strength test results (Aghazadeh and Ayoub, 1985). In reality, a worker normally does not adjust the weight of a load. Usually, constant loads are presented, and the worker is required to lift the load, by whatever means necessary, in order to perform the task. Therefore, the exertion is conducted over the range of motion with a constant mass (isoinertial method).

In this study, the authors attempted to simulate submaximal weight lifting tasks, which are common to industry, while carefully measuring the dynamic hand forces and postures displayed by the subjects (whose isometric lifting strengths were known).

METHODOLOGY. The subjects were required to exert a lifting force on a strength testing fixture. The test fixture allowed for the two handed, sagittal plane lifting assessment of isometric and isoinertial lifting strength. It also allowed for an unrestricted lifting posture. The isometric strength testing was performed according to procedures and methods recommended by Caldwell et al (1974) and Chaffin (1975).

For each subject, dynamic and static strength measurements were in terms of peak hand forces. The static strength values were measured at three different heights (i.e., 26, 33.7 and 41.3 cm.). The submaximal loads lifted were varied from 6.8 kg. to 48 kg., which ranged from 5% to 76% of the subjects' maximum static lifting strengths.

RESULTS AND DISCUSSION. In comparing the peak hand forces for isometric and isoinertial lifting, a regression analysis determined that peak submaximal hand forces were not related to the static lifting strength values (Figure 1). Given these results, it was necessary to analyze the acceleration effects with the lifting of submaximal loads, in order to understand the inertia affect.

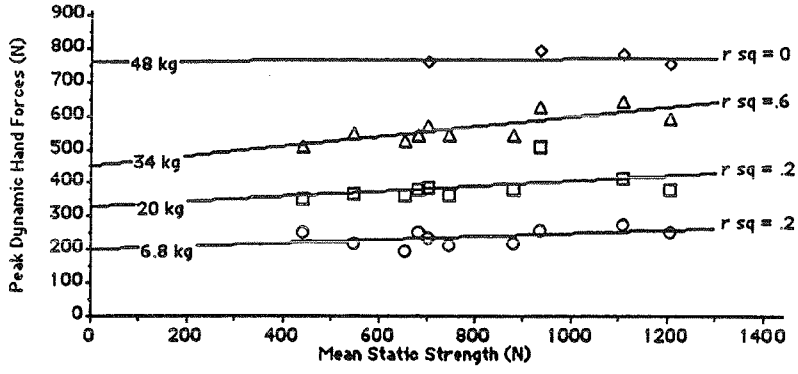

Figure 1 - Regressions of peak hand forces for the four submaximal loads lifted on each subject's static lift strength.

For each subject tested, the results indicated that there was an inertial effect that increased as the mass lifted was increased, though the acceleration decreased with increasing loads (Figure 2). Research by Carlsoo (1980) indicates that the increased inertial effect is due to an increase in the mass, which more than offsets the decreased acceleration with larger masses. The results here are consistent with Carlsoo's research. In fact, in the moderate load range from 46% MVC to 76% MVC, the subjects demonstrated a relatively constant peak acceleration of the different masses. Further discussion of motor behavior will be presented to explain this phenomena.

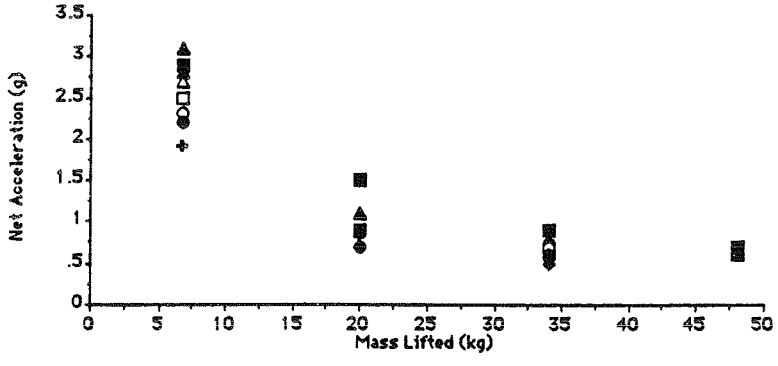

Figure 2 - Peak accelerations demonstrated by each subject lifting the four different loads.

REFERENCES

1. Aghazadeh, F. *et al.*; *Ergonomics*; **28**; 1409-1417; 1985.
2. Caldwell, L *et al.*; *AIHA Journal*; **35**; 201-206; 1974.
3. Carlsoo, S.; *Applied Ergonomics* **11**; 66-72; 1980.
4. Chaffin *et al*; *AIHA Journal* ; **34**; 513-525; 1973.
5. Chaffin, D.; *AIHA Journal* ; **36**; 505-519; 1975.
6. Garg, A. *et al.*; *Ergonomics*; **23**; 13-27; 1980.
7. Snook, S.; *Ergonomics* ; **21**; 963-985; 1978.

The authors wish to acknowledge the support of both The Association of American Railroads (contract SFR-87-024) and the National Institute of Arthritis and Musculoskeletal and Skin Disorders (R01-AR39599).

ANALYSIS OF LIFTING BY MEANS OF SIMULATED GROUND REACTIONS

Lars Lindbeck
Division of Technical Work Physiology,
National Institute of Occupational Health
S-171 84 SOLNA, Sweden

INTRODUCTION

This paper deals with the possibility to compensate for dynamic effects by using mathematical functions for the ground reactions during different lifting situations. The primary purpose was to determine the loads on the lower back with the facility of static models but with the accuracy of dynamic models. In order to find usable functions, complete dynamic analyses of joint loads during sagittal lifting were performed. It was found that the contributions of single body segments to the dynamic effects of the whole body were rather small. The results also indicated that reasonably accurate values of the net moments at the L5/S1 could be calculated by means of polynomials representing the ground reactions, normalized with respect to body weight and lifted load.

REVIEW AND THEORY

In recent years a number of models to simulate the body movements during lifting activities have been reported. The models usually assume that the movements of single body segments can be described by mathematical functions, e.g. Slote & Stone's (1963) space-time relationship, together with certain constraints to compute angular displacement, velocity, and acceleration of the body links during the lift. In the present study the inertial effects of single body segments were neglected compared to reactive forces and moments from adjacent segments. It was assumed that the dynamic effects were characterized by the linear accelerations of the whole body as measured by force plate ground reactions.

METHODOLOGY

Ten male subjects were instructed to lift a 12.8 kg box with handles, standing on a Kistler force plate. Ground reaction force vectors and body movements were measured simultaneously by means of the force plate and an optoelectronic system (Selspot II) and transferred to a Compaq Deskpro 386 computer. The task included two different methods, leg lift (flexed knees) and back lift (straight knees), and two speeds, viz. a fast lift of about 1 s and a slow lift of 2 s.

A 2-D, 6 segment model was used, consisting of feet, lower legs, thighs, head-neck-trunk, upper arms and lower arms-hands. Joint reaction forces and net moments were calculated by applying Newton's laws of motion on free body diagrams of the segments one at a time, starting with the foot segment. Necessary body segment parameters were taken from Pheasant (1986) and assumptions about the position of the L5/S1 joint relative to the hip and shoulder from Freivalds et al.(1984).

For the analysis of the movement a sampling frequency of 100 Hz was considered to be sufficient. Coordinate data were digitally filtered using a fourth order Butterworth filter, as described in Winter (1974). Velocities and accelerations were calculated using Lanczos' forms, described by Lees (1980).

The components of the measured ground reaction forces were normalized by division of the weight of the subject and the box. For each of the lifting tasks averages of centers of pressure and the normalized ground reactions at corresponding points in time were calculated. Least-square polynomials of the 9:th degree were fitted to the averaged curves.

Net moments at L5/S1 were determined in three ways: 1) a complete dynamic analysis considering linear and angular accelerations of each segment as well as measured ground reaction forces, 2) a "simulated" dynamic analysis where linear and angular accelerations of each segment were zeroed and the measured ground reactions replaced by the least-square polynomials, and 3) a static analysis.

RESULTS AND DISCUSSION

The simulated analysis produced peak values of the net moments at L5/S1 that were close to the values from the dynamic analysis. It was found that the results could be improved by multiplying the normalized ground force components by a factor 1.2 - 1.3. Figure 1 presents two examples of moment curves calculated by the three methods. The simulated analysis accounts for dynamic effects using a predetermined feature of the ground reactions for different lifts and gives more accurate results than common static models. The method can be used by e.g. occupational health services or the labor inspectors in analyzing lift situations. On the other hand, there is still a lack of data on acceptable limits for loads under dynamic conditions which makes it difficult to relate dynamically calculated forces and moments to risks involved with the lifting task. The results from dynamic analyses may not be applicable to e.g. the guidelines from NIOSH (1981) which are based on a static model and cadaver studies.

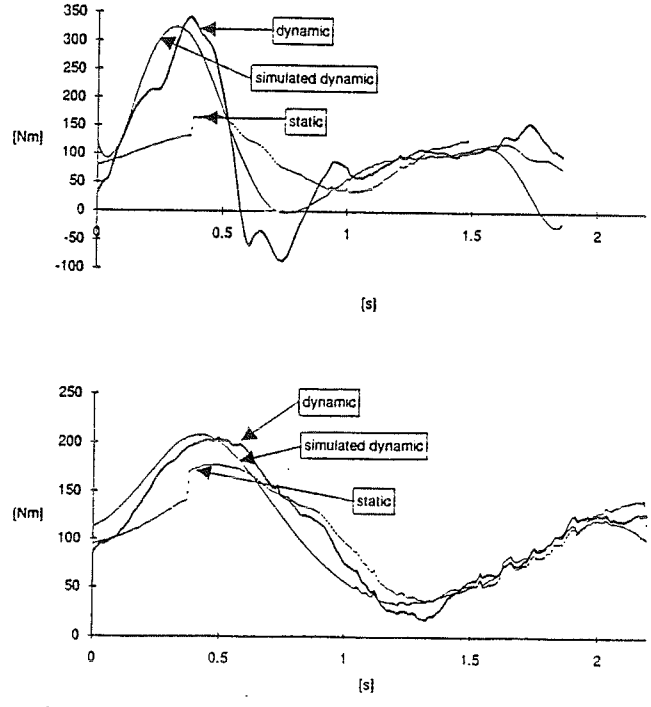

Fig 1. Examples of dynamic, simulated dynamic, and static calculations of moments at L5/S1 for fast leg lift (upper curves) and slow back lift.

CONCLUSION

Accurate values of the peak loads on L5/S1 can be estimated by means of predetermined ground reaction functions for different lift types. Existing limits for safe lifting may not, though, be applied to the results of dynamic analyses.

REFERENCES

Freivalds et al. J Biomech, 17, 251-262, 1984.

Lees, A. A. J Hum Mov Studies, 6, 165-180, 1980.

NIOSH. Work Practices Guide for Manual Lifting, DHSS (NIOSH) Publication No. 81-122, Cincinatti, OH, 1981.

Pheasant, S. Bodyspace - Anthropometry, Ergonomics and Design. Taylor & Francis, London and Philadelphia, 1986.

Slote, L. & Stone, G. Hum Factors, 5, 443-452, 1963.

Winter, D.A. Biomechanics of Human Movement, John Wiley & Sons, New York, 1979.

A Biomechanical Analysis of Switch Stand Operation Using a Two Dimensional Dynamic Model

Maury Nussbaum, Don B. Chaffin, George Page*, James Foulke, and Charles Woolley
Center for Ergonomics, University of Michigan, Ann Arbor, MI 48109-2117
*Research and Test Dept., Association of American Railroads, Washington, D.C. 20001

INTRODUCTION

Epidemiologic studies suggest a significant injury incidence rate for railroad employees. Within this group yardworkers account for a more than proportional amount of injuries, claims, and lawsuits. Among their various responsibilities, yardworkers point to operating difficult switch stands as being one of the more strenuous manual tasks, a perception which is supported by injury statistics.

The operation of the very common High-Star horizontal throw type switch stand was investigated. A two-dimensional dynamic biomechanical model developed by the University of Michigan Center for Ergonomics was used to compute the kinetics occurring during operation using input gathered from field studies of existing switches. Data was collected at five switches using three typical throwing techniques.

In a previous study of the dynamics of lifting, Freivalds, et al. (1984) found that the forces in a dynamic lift could be 30% greater versus an equivalent static task. McGill and Norman (1985) found that, on average, peak moments determined with a fully dynamic model were 20% greater than peak moments determined using a static model.

METHODOLOGY

A measurement system based on standard video equipment was developed and employed to track joint positions simultaneously with hand forces. Markers were affixed to the subject overlying the joint centers of rotations at the ankle, knee, hip, shoulder, elbow, and wrist. Hand forces were monitored using a strain gauged handle and an electronic system which converted the gauge output to a video signal. This video signal was superimposed on the camera motion images which allowed the simultaneous monitoring of joint positions and two-axis hand forces on a single portable field system. The dynamic biomechanical model generated: forces and moments at the body joints calculated using a dynamic and sequentially static model; positions, velocities, and accelerations of the joints; static strength capabilities; and required coefficients of friction between the feet and the ground.

RESULTS

The L5/S1 joint was the focus for a specific comparison between the dynamically and statically computed moments (Table 1). The peak dynamic moments were on average 3.5 times or 474 Nm greater than the static estimates. A significant linear relationship existed between these two moments, but the correlation was low. The five switches were subjectively ranked based on a perceived difficulty of operation. The moments at L5/S1 were generally larger in magnitude at switches ranked more difficult. Furthermore, the ratio of dynamic to static moments also increased with switch difficulty.

Examination of the trials in which the largest dynamic moments occurred, showed that large upper limb and torso accelerations were present. The accelerations resulted from the subject jerking or bouncing during the switch throw and were a major source of the dynamic component of the total moment. Shoulder accelerations reached peaks of 0.8-0.9 g. Assessment of the trials in which small dynamic moments occurred showed that the operation was consistently smooth throughout with no rapid changes in motion.

Several metrics for comparison between the switches and techniques were derived: peak static and dynamic L5/S1 moments, peak hand forces, peak required coefficients of friction, and percentages of joints where computed moments exceeded static strength capability.

An analysis of variance of the derived metrics showed consistent significant relationships between the metrics and the switches. In addition, groupings of the metrics using significant pairwise comparisons generally matched the pattern of subjective grouping of the switches based on difficulty. More difficult switches corresponded to higher moments, hand forces, required coefficients of friction, and percentages of moments exceeding static capability. No consistent differences were found between the three throwing techniques employed.

DISCUSSION

The differences, in terms of the large ratio of dynamic to static moments, in the results of previous work and the present study are probably due to the high degree of rapid trunk accelerations employed in operating a switch stand. This is in contrast to the Freivalds, et al. (1984) study which involved lifting boxes from the floor to a table and the McGill and Norman (1985) study which involved lifting a load from the rear of a pallet. With the goal of minimizing dynamic moments, and possibly the injury incidence among railroad yardworkers, the sources of these moments are of interest. Two sources of dynamic moments were realized. The first was a switch that is subjectively difficult to operate; an 'easier' switch results in decreased dynamic moments. The second was the smoothness of switch operation; by minimizing the amount of jerking or bouncing when throwing a switch, dynamic moments can also be decreased. Implications for worker training and switch maintenance are suggested.

REFERENCES

1. Freivalds, A., et al., (1984) J. Biomechanics, **17**: 251-262.
2. McGill, S.M. and Norman, R.W., (1985) J. Biomechanics, **18**: 877-855.

Table 1. Means of peak L5/S1 moments by switch.

Switch	Dynamic (Nm)	Static (Nm)	Dynamic/Static (%)
1	429	174	223
2	748	221	336
3	1433	199	754
4	237	145	165
5	408	150	274

ACKNOWLEDGEMENT

This work was supported by the Association of American Railroads.

A REALISTIC MODEL OF THE HUMAN HAND-ARM EXPOSED TO SINUSOIDAL EXCITATION

R. Gaertner, F. Bermond and J. Dimnet
Groupe de Biomécanique
Université Claude Bernard - LYON I
43, boulevard du 11 Novembre 1918
69622 Villeurbanne Cédex - France

INTRODUCTION

In occupational health, several pathologies are observed amongst workers using vibrating hand-held tools. However, their vibration-induced origin is not always evident, particulary when tendinous and osteo-articular injuries arise. Indeed, such ones are very similar to those due to heavy manual work [1]. When non-invasive investigation techniques don't exist explaining the degenerative process, a model is required for doing so. Thus, the authors propose a methodology to analyze the internal force state into the limb under ergonomic contidions including both static and dynamic effects. The present paper deals only with the dynamic model. It is grounded on the structural mechanics techniques. It provides the response to a sinusoidal excitation. Then, the dynamic internal forces in joints and tendons as well as the stresses in muscles and bones are available. The strain energy and the dissipated power versus frequency curves can be also obtained.

REVIEW AND THEORY

Many authors [2-3] proposed lumped parameter models with few degrees of freedom. Such models allow to get the same transfert function as the limb but don't describe its internal behaviour. So, they are not able providing assistance and allowing the understanding of relations between vibration and occupational disorders.

The present purpose is to carry out a realistic model of the limb. Main assumptions are: a) The displacement field is not continuous from a muscle to an other. Connections exist between muscles and bones only at the tendinous insertions; b) The elastic and dissipative properties of the orthotropic materials are described by complex moduli allowing for structural damping; c) The elastic moduli of muscles depend on their static strength according to the posture and the task; d) The dynamic behaviour of the limb is assumed to be linear in the vicinity of a static configuration. So, it doesn't depend on the intensity of the excitation force.

Each muscle and bone being considered as an independant substructure, its mass, stiffness and structural damping matrices are calculated by means of a finite element discretisation. Such matrices are meaningful of the shape and constitution of the substructure. They are relative to the nodal displacements and, due to the great number of nodes, their size is excessive. In order to save a lot of computing time during the analysis phase, it must be reduced using Guyan condensation and truncated modal analysis techniques.

Owing to the complexity and variable angulation of the joints, their stiffness and damping matrices can not be calculated. Then, they must be determined experimentally on cadaveric parts.

After that, characteristic matrices of the whole structure are obtained through assembling the substructures according to the chosen posture. The response to a sinusoidal force transmitted to the hand is then calculated by solving the equation of motion.

METHODOLOGY

Shapes and sizes of anatomical constituents are obtained from scannerized slices of the limb. Then, the mesh of each bone and muscle is performed in order to define the finite elements.

The mechanical constants of the materials are sought in the litterature. Unfortunately, the values of the reported elastic moduli are very dissimilar from an author to an other, depending on the measurement technique and on the physiological conditions of measurement. This is particularly important for muscular material. So, three levels of elastic modulus have been used, depending on the activity level (low, medium, high) of each muscle according to its participation in the task. Moreover, the damping characteristics being not available have been estimated.

The hand has not been discretized by finite elements. Due to its confined disposition around a rigid handle transmiting the excitation, it is assimilated to a mass and its elasticity and damping are transferred onto the wrist matrices.

After assembling the characteristic matrices of constituents and solving equations of the steady-state motion, the estimated parameters have been adjusted in order to obtain the best fit between calculated and measured dynamic mass and phase in the 20 -200 Hz frequency range.

RESULTS AND DISCUSSION

The model has been used to calculate the response of the hand-arm system to an excitation force of 20 Newtons. This value corresponds to that imposed to a simulator device. The posture is that of an operator working with a chipping hammer, the direction of excitation corresponding that of the tool.

The dynamic mass and phase have been measured on the simulator (fig. 1) in the same conditions. Figures 2 and 3 show the comparison between calculated and measured results.

Fig. 1

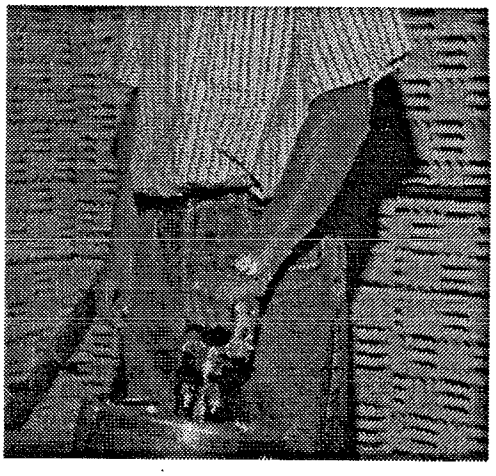

Fig. 2

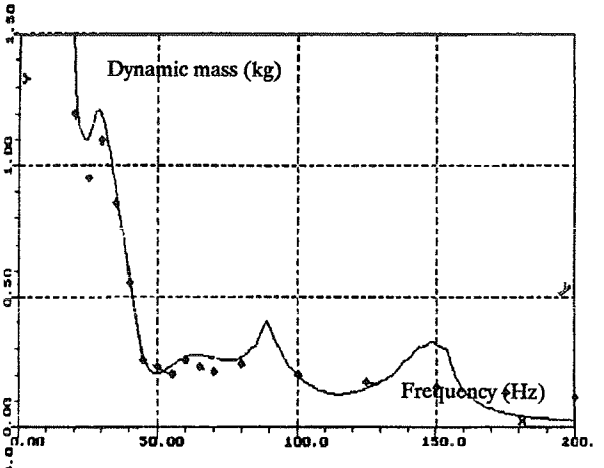

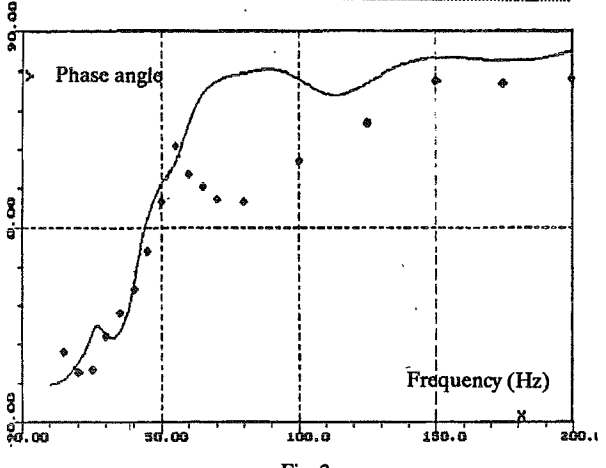

Fig. 3

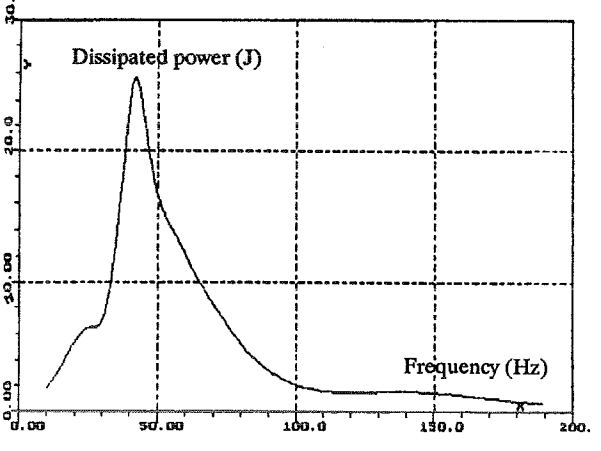

Fig. 4

Figure 4 shows the global power dissipated in the limb in function of the excitation frequency. It could be possible to show the way in which this dissipation is distributed in the anatomic constituents. The dynamic internal forces in joints and tendons as well as stresses in muscles and bones can be calculated too, but these results are not reported here.

REFERENCES

1 - Gemne G. et al., Scand J Work Environ Health, 13, 290-300, 1987.

2 - Wood L.A. et al., J Sound Vib, 57, 157-169,1978.

3 - Reynolds D.D. et al., J Sound Vib, 95, 499-514, 1984.

EVALUATION OF THE STRAIN IN THE SCAPHOID WAIST DURING WRIST MOTION

Romdhane, L., PhD
Chidgey, L., MD
Miller, G., PhD
Dell, P., MD

Department of Orthopaedics
College of Medicine
Box J-246 JHMHC
University of Florida
Gainesville, FL 32610

INTRODUCTION

While the biomechanics literature does contain descriptions of the measurement of strain in several long, easily accessible bones such as the femur, tibia, radius and ulna (Finlay et al. 1982, Carter et al. 1980), only one previous study of carpal bones has measured the strain in the lunate during static loading (Trumble et al. 1986). The literature lacks any study documenting the strain imparted to the scaphoid during normal wrist motion. This experiment was undertaken to measure the strain in the scaphoid during wrist motion using a newly developed strain gage method, which allows monitoring strain at the intramedullary cortex without damage to ligamentous or articulating structure.

MATERIALS AND METHODS

Strain Gages

Stacked 45 ° strain gage rosettes (Micro-Measurements 120 Ohms WA-13-030-WR-120) approximately 5x5 mm, were mounted within the body of the scaphoid. Due to the small size of the scaphoid and the limited accessibility to a surface site for gage application, a special mount or "carrier" for the rosette was designed.

Implantation

Ten fresh cadaver upper extremities were used for strain rosettes. The scaphoid was exposed through the palmar longitudinal approach recommended by Herbert et al. (1984) for fixing scaphoid fractures with the Herbert screw. A cylindrically shaped hole measuring 8 mm in diameter was made through the palmar cortex and continued through the waist of the scaphoid up to but not penetrating the dorsal cortex. The wrist was pre-loaded by suspending free weights from braided wire connections to the tendons of the primary wrist movers. Once mounting was complete, each hand was placed through a range of motion incorporating all combinations of flexion/extension (F/E), radial/ulnar deviation (R/U) and supination/pronation (S/P). To verify the validity, as to the outer cortex strain, of the collected data, the instrumented scaphoid was carefully dissected from the hand after completion of ROM data acquisition. A strain gage rosette, identical to the one applied to the intramedullary cortex, was applied to the outside surface of the scaphoid overlying as close as possible to the internal gage position.

Data Analysis

The principal strains were determined using the following formula (Perry 1989)

$$\epsilon_{p,q} = \frac{\epsilon_1 + \epsilon_3}{2} \pm \sqrt{\frac{(\epsilon_1 - \epsilon_2)^2 + (\epsilon_2 - \epsilon_3)^2}{2}} \qquad (1)$$

The strains ϵ_1 , ϵ_2 , and ϵ_3 represent the strains measured in the three active gages of the implanted rosette. Burstein et al. (1981) noted that shear failure was the predominant initiating factor in bone

failure. Hence, shear strain was chosen as a criterion to evaluate the strain in the scaphoid *waist*. The shear strain was calculated as follows:

$$\epsilon_{eq} = \frac{\epsilon_p - \epsilon_q}{2} \qquad (2)$$

RESULTS

The S/P was isolated from the F/E and R/U motions. Little scaphoid shear strain variation was seen with this isolated motion. Biostatistical evaluation, using the SAS statistical package, was used to analyze the strain vs the ROM data. A full quadratic regression was Found to be the best fit to the data of each specimen. For each specimen a contour map, shown in Figure 1, was generated.

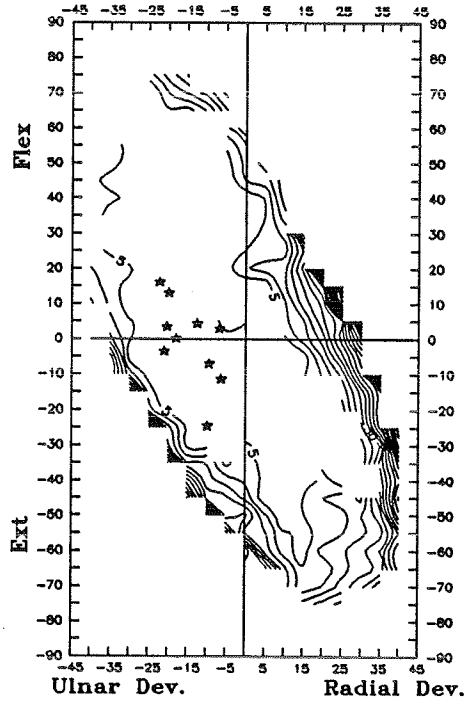

Figure 1: Contour map representing strain at the waist of the scaphoid, along with the locations of minimum strain for the 10 specimens.

From the contour map a central valley of low strain values can clearly be seen. This central valley is bordered on all sides by higher strain values. The data was further analyzed to determine the relative hand position for the minimum strain at the gage site for each specimen. Figure 1 shows the location of the minimum strain for different specimens, overlaid on the contour map. The mean location for all the specimens is at neutral F/E (approximately 1 degree of extension) and approximately 15 degrees of ulnar deviation.

DISCUSSION

A qualitative evaluation of the strain in the dorsal waist area of the scaphoid is presented. Clinically this is a very important area as most scaphoid fractures occur through the waist (Taleisnik, 1985). Results show that near the neutral F/E position of the hand with approximately 15 degrees of ulnar deviation the minimum strain was observed. The contour plot of the scaphoid strain versus the range of motion shows a valley where the strain is low. The differences seen between specimens is due to the flatness of the surface near the minimum. However, figure 1 shows that these points lay within the valley of low strain. Thus, using the strain at the inner dorsal surface of the waist of the scaphoid as an indicator, it appears that scaphoid strain can be minimized by placing the hand in neutral F/E and slight ulnar deviated (15 degrees) position.

BIBLIOGRAPHY

Burstein, A.H. *et al.* Perspectives in Biomed. Eng., 131-134, 1981.

Carter, D. R., *et al.* J. Biomech. **13**, 27-38, 1980.

Finlay, J. B., *et al.* J. Biomech. **15**, 723-739, 1982.

Herbert, T. J., *et al.* J. Bone Joint Surg. **66B**, 114-123, 1984.

Taleisnik, J. The Wrist. Churchill Livingstone, New York, 1985.

Trumble, T., *et al.* J. Hand Surg. **11A**, 88-93, 1986.

POSTERS

NONLINEAR CONSTRAINED OPTIMIZATION MODEL FOR BIOMECHANICAL SIMULATION OF A GENERALIZED PLANAR MANUAL MATERIAL HANDLING TASK

M. Parnianpour, H. Dastmalchian, D. Martin.
Occupational Industrial Orthopaedic Center, Hospital for Joint Diseases
Orthopaedic Institute, New York University, N.Y., N.Y. 10003.

INTRODUCTION: In pursuit of purposeful activities of life, one applies forces to the environment, which consequently loads various joints. NIOSH (1981) stated over-exertion injuries associated with manual material handling accounted for 12 million lost work days. Three approaches have been suggested for prevention of low back pain: training, screening/selection, and workplace (job) design. The validity and utility of the recommended "safe" lifting technique (straight back/bent knee) has been questioned (Parnianpour et al 1987). Avoidance of the excessive loads on the joints is a rational objective that should be encouraged in the workers education and the workplace design. The following biomechanical model is to provide us such a tool. The purposes of this study are: a) to present the implementation of a static planar model of the generalized manual material handling task, b) to compare the optimum configuration at different locations of the hand and different magnitude of external forces, and c) to compare the predicted joint angles using different objective functions.

METHOD: A planar static model, composed of five bar-links, is developed to mathematically simulate a generalized material handling task. The inputs of the model are the anthropometric data of the subject, the horizontal (H) and the vertical (V) coordinates of the hands (position of the end effector), and the external force vector, F. Upon specifications of the hand location the system looses two degrees of freedom (DOF). The remaining three degrees of freedom make the set of the joint angles indeterminate. A nonlinear optimization method based on generalized reduced gradient algorithm (Lasdon et al 1978) is used to find the optimal joint angles which minimizes the cost (objective) function. Different cost functions are used: a) the sum of the square of the external moments of all the joints, which is called the global cost, and b) the square of the external moment about each joint, called the local cost. The minimization of the local cost is implemented to simulate the situation of the individuals with an injured joint undergoing a rehabilitation program, i.e. patients after shoulder, knee or back surgery. The optimal joint angles, the corresponding moments at the optimal joint angles and the values of the minimum cost functions are the outputs of the model. The equality constraints are geometrically derived in addition to the moments calculated about each joint (satisfying the equilibrium conditions). The inequality constraints are the physiological range of motion, the upper bounds of the torque generation capability of each joint, and the requirement for insuring the stability of the body (linkage system). The population based isometric static strength models include the torque-angle relationship.

RESULTS: The graphical display of the results of the optimization is shown in figure 1. The maximization and the minimization of the global cost show the best and the worst possible configurations. For this particular hand position (H=.3 m, V=.3 m), bending of the knee is recommended, but for slightly different location (H=.1 m, V=.3 m) a bent back is recommended. The optimum joint angles and the corresponding external moments at a given hand location (H=.3 m, V=.3 m) with different vertical forces (i.e loads with different weights) are compared in figures 2 and 3. The moments are highly affected by vertical forces but the joint angles are not. The location of the hand (H=.3m; V=.3, .8, 1.2 m) affects the

global cost significantly (Fig 4). The effects of minimizing the local or global cost depend on the location of the load. The global cost is increased when the external moments of the knee or the shoulder are being minimized. A subject with knee or shoulder pain may minimize the load on these joints, however the price is paid by stressing the other joints disproportionally.

CONCLUSION: This model may aid the workplace evaluation and redesign by identifying the infeasible "tasks" and the limiting factors, such as the excessive muscular torque and/or range of motion requirements at particular joints. The model may also be used in illustrating the proper lifting techniques. The results point to the importance of the proper work place design as oppose to proper lifting techniques.

REFERENCES

Lasdon et al. (1978), Design and testing of a generalized reduced gradient code for nonlinear programming, ACM Transactions on Mathematical Software, 4, 34-50.

NIOSH (1981), A work practices guide for manual lifting. Tech. Report No. 81-122.

Parnianpour et al. (1987), Workers training: the fallacy of a single, correct lifting technique. Ergonomics, 30, 331-334.

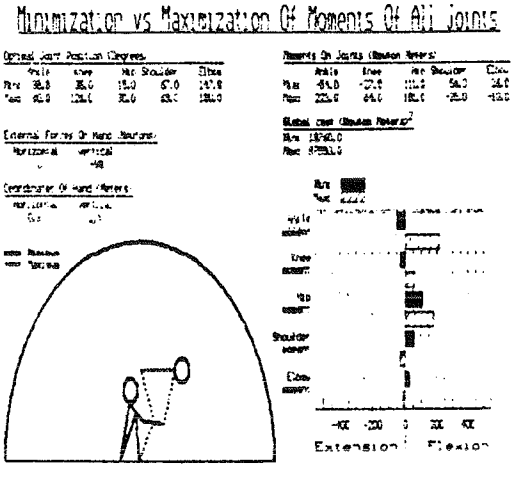

Figure 1. Graphic display of the results of an optimization run (H=.3 m, V=.3 m; Fy=-98 N).

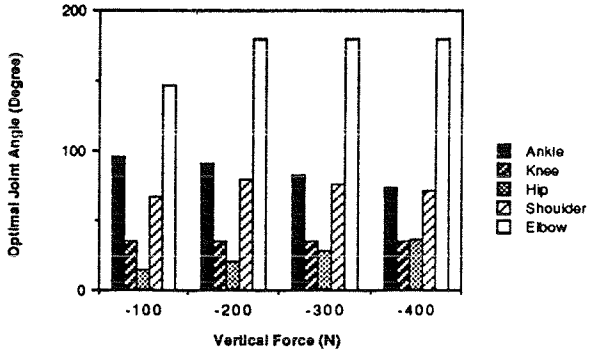

Figure 2. The effect of the magnitude of the vertical force on the predicted optimum angular position of joints (H=.3 m, V=.3 m).

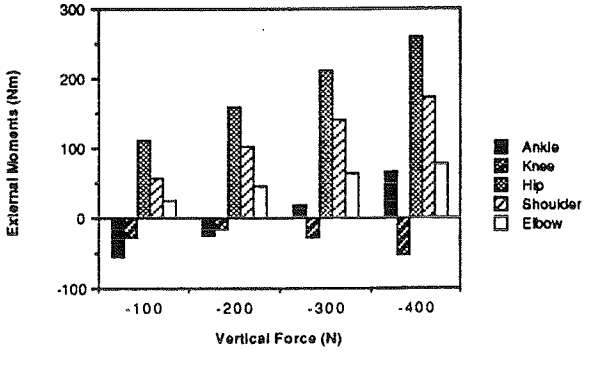

Figure 3. The effect of the magnitude of the vertical force on the external moments about each joint at the optimum posture (H=.3 m, V=.3 m).

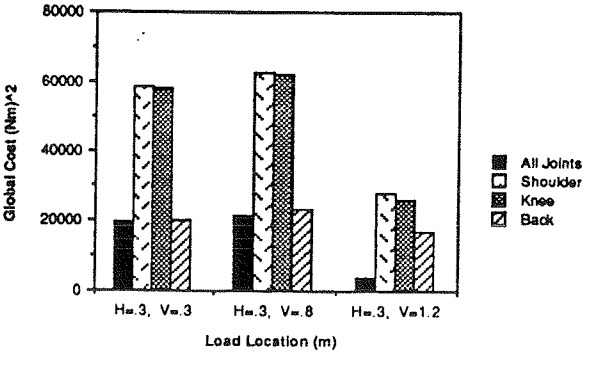

Figure 4. Comparison of the global costs for the predicted optimal posture minimizing different cost functions at three load locations.

A NONLINEAR OPTIMIZATION MODEL OF TRUNK MUSCLES RECRUITMENT DURING PURE AND COUPLED ISOMETRIC EXERTIONS

Mohamad Parnianpour, Ph.D.
Occupational Industrial Orthopaedic Center, Hospital for Joint Diseases Orthopaedic Institute
New York University, New York, N.Y. 10003.

INTRODUCTION: The internal loading of the spinal structure not only depends on the external load but also on the trunk muscle recruitment patterns. Given the mechanical disadvantage of the trunk muscles (their short lever arm), the tensions needed to balance the external moments will be very high. Therefore, spine experiences high levels of load during streneous activities such as manual material handling tasks. Unable to measure the muscle tensions directly, we investigate muscular tensions either with EMG studies (mapping the muscle activity to muscle tension) and/or optimization studies. Both techniques have their advantages and disadvantages (McGill 1990). The problem of load distribution amongst trunk muscles during isometric exertions has been modeled. This overcomplete system can be written in a matrix form as: $Ax = b$, with $x_i \geq 0$ for $i = 1, \ldots, 10$. Matrix A contains the geometric and anatomical organization of the muscles, vector x is the tension vector of the ten muscles and the resultant shear $(S_x,\ S_y)$ and compression forces(C), and b is the load vector which contains the external forces $(F_x,\ F_y,\ F_Z)$ and moments $(M_x,\ M_y,\ M_z)$. The abdominal pressure has been excluded from the model since its exact role and contribution to extensor moment is not clear. Despite the fact that the system is underdetermined, the whole system is not often utilized. The most widely used optimization based model is that of Schultz *et al* (1983). Few limitations exist: (1) there is no consideration about the resultant shear forces, although a modified version of the model (Hughes and Chaffin, 1987), minimum shear model uses "hard constraints" on the shear forces; (2) due to the linear programming limitation the synergies and cocontraction are not well predicted; (3) the implicit assumptions that trunk muscles produce pure moments is not valid (Parnianpour *et al*, 1988). Purposes of this study were (a) to develop and validate a nonlinear optimization model of torso recruitment, (b) to delineate the effect of competing cost functions on the internal loading of spine, (c) to illustrate the need for triaxial measurement of the torques in attempts to accurately model torso muscle recruitment.

METHOD: A nonlinear constrained optimization program based on modified generalized reduced gradient method is used to model recruitment of ten torso muscles at the level of L3 (Schultz *et al*, 1983). It is clear that the contributions of passive elements, facets, the disc and the ligaments are most significant in the extreme ranges of motion. Therefore, limitation of the shear forces is enforced by soft constraints (penalizing the shear forces in the cost function). The hard constraint is simulated by either increasing the cost of the shear force at a certain limit or introducing additional inequality constraint. The nonlinear programming allows us to choose nonlinear cost functions which shall predict higher degree of synergy and cocontraction. At this time, it is not clear whether the inaccuracy of the existing models' prediction during complex tasks, is due to selection of an inappropriate cost function or incomplete characterization of the external load vector b. To illustrate these points we have solved the problem by minimizing six different cost functions: (1) $(Stress/10000)^2 + {S_x}^2 + {S_y}^2$, (2) $(Stress)^2$ (3) $Stress$, (4) ${S_x}^2$, (5) ${S_y}^2$, and (6) ${S_x}^2 + {S_y}^2$; where $Stress$ is the maximum muscular stress. Various pure and coupled exretions have been simulated and the predicted muscle tensions and the resultant forces for the six the cost functions have been compared.

RESULTS: The results show the sensitivity of the solutions to the choice of the cost function (Figure 1). In fact due to nonnegativity constraints, identical results are obtained from minimization of both $Stress$ and $(Stress)^2$. The important distinction in addition to the higher compression and stress levels for some of the cost functions, is the higher

number of muscles that are recruited. A weak feature of linear programming models which limit the number of muscles taking the non-limit values, is thus alleviated. Results also indicate that the minimization of compression (C) and shear forces (S_x and S_y) are two competing costs (Figure 2). The results clearly illustrate that the solutions are extremely sensitive to the characterization of the load vector, b. If an uniaxial dynamometer is used during the validation of the optimization models, the simulated pure and coupled exertions would be erroneously identified as identical (Figure 3). Therefore, for a rigorous modeling of torso muscle recruitment, we propose using the triaxial dynamometer. The nonlinear optimization is promising since it allows higher synergies and cocontraction. The validation of the cost function with EMG is an important ongoing stage of this research.

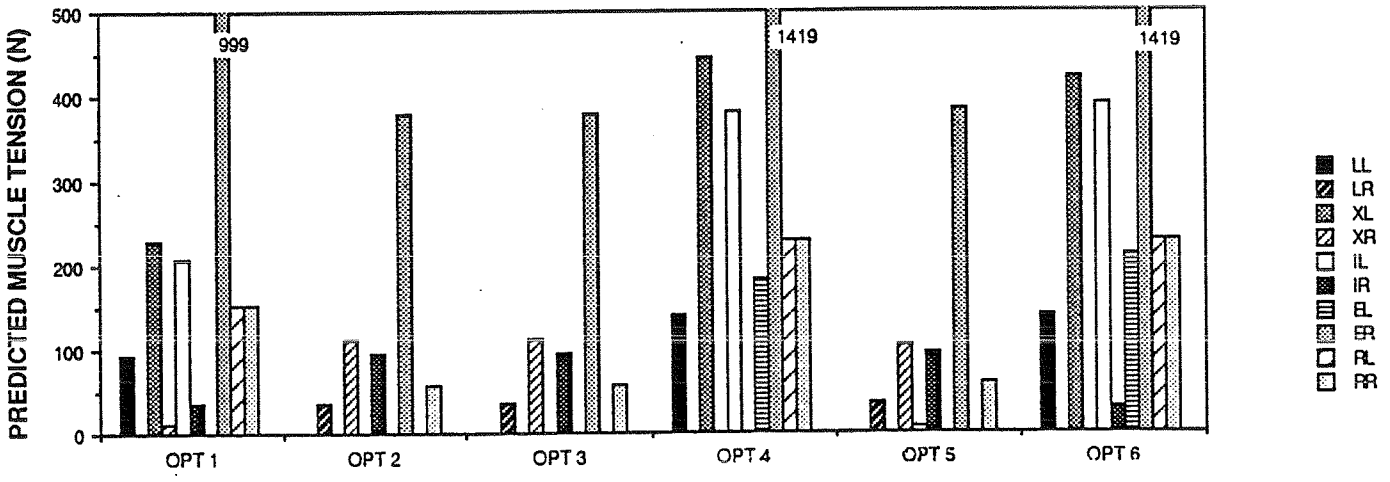

Fig 1. The predicted tension in the ten muscles of the trunk during an attempted right lateral bending (Fx=-100 N, My=-30 Nm).

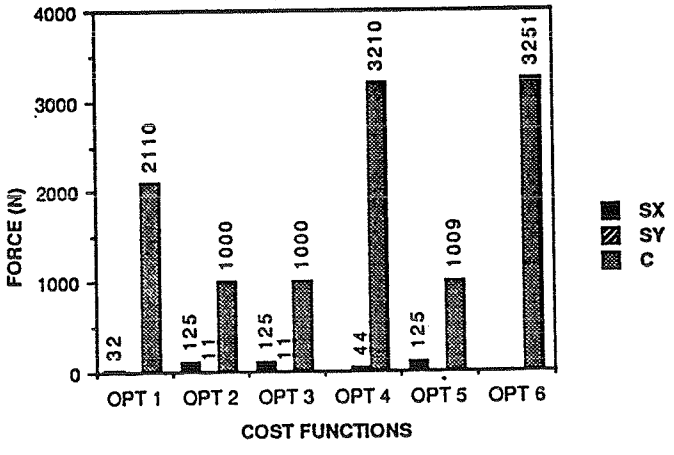

Fig 2. The prediced shear and compressive forces for the six different cost functions during an attempted right lateral bending (Fx=-100 N, My=-30 Nm).

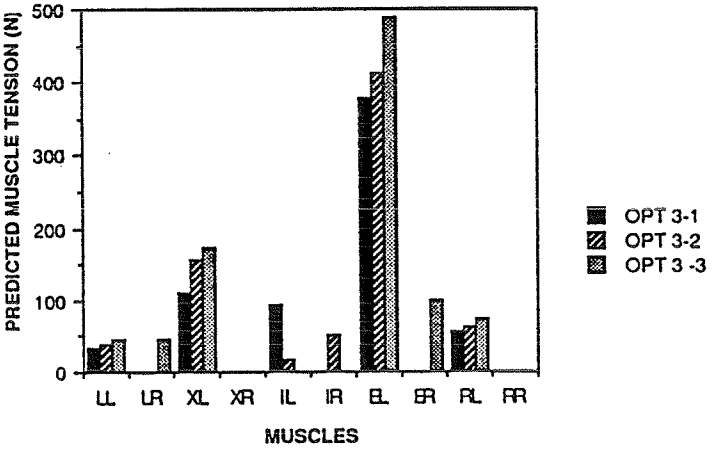

Fig 3. The predicted muscle tension for the minimum stress cost function under three different loading cases:
Case 1: Fx=-100 N, My=-30Nm;
Case 2: Fx= -100N, My=-30 Nm, Mz=15 Nm;
Case 3: Fx=-100 N, My=-30 Nm, Mz=15 Nm,
Fy=50 N, My= -15 Nm;

ANALYSIS OF PELVIC TILT IN ANATOMICAL NEUTRAL POSITION

R.H. Deusinger, P.T., Ph.D.
Box 8083/660 S. Euclid Ave.
Wash. Univ. Med. School
St. Louis, MO 63110

INTRODUCTION

Three dimensional coordinate values representing anterior superior iliac spines (ASIS) and posterior superior iliac spines (PSIS) directly taken on 13 human cadaver pelves in an oblique plane served as criterion measures whereas values obtained by application of the oblique plane caliper trigonometric technique (CTT)[3] represented a clinical method for deriving pelvic tilt measurements. Oblique plane pelvic angle measurements derived from the criterion coordinate values were correlated (multiple R) to oblique plane pelvic angles determined from the CTT coordinate values followed by a regression analysis to determine validity of the CTT. Validity was established by multiple R values of 0.83-0.99 and Bartko Intraclass Correlation Coefficient (ICC) values of 0.96-0.99. ICC values for reliability were 0.86-0.99. Also, an inherent bony tilt of the pelvis was found to exist (as much as 9 degrees posterior tilt to 12 degrees anterior tilt).

REVIEW AND THEORY

Lumbar spinal posture during sitting and lifting has been implicated in the etiology of low back pain.[2] Several authors have indicated that pelvic orientation (i.e., angle of pelvic tilt) may be related to lumbar spine postural defects present in many types of patients.[1,2,5,6] However, it is necessary that angle of pelvic tilt measures be established as valid before such relationships can be thoroughly studied. The CTT and other clinical techniques of measuring pelvic tilt are based on a "neutral position" of zero degrees pelvic tilt wherein the ASIS's and symphysis pubis are aligned along the same vertical plane in anatomical position of the upright posture.[4] The purposes of this study were to determine the validity of the CTT technique and whether there exists a bony tilt intrinsic to the pelvis in anatomical neutral position using this technique.

METHOD

Two sets of measurements were taken in an X, Y, Z coordinate system defined by a mutually perpendicular straight-edge, L-square, and combination square configuration. Thirteen human pelves were removed from cadaver specimens and dissected to clearly expose the ASIS, PSIS, and symphysis pubis and placed on plexiglass in simulated anatomical neutral pelvic position. One set was obtained using the clinical values (CTT oblique plane) whereas direct measurements, obtained by using only the configuration of a ruled straight-edge, L-square, and combination square, served as criterion values (true oblique plane). The Bartko Intraclass Correlation Coefficient (ICC) was used to determine reliability; and the ICC, multiple R correlation, and multiple linear regression analysis were used to establish validity.

RESULTS

All subject data, angle of pelvic tilt values, and correlation coefficients were grouped into categories of anterior tilt and posterior tilt. Of the thirteen pelvic specimens nine exhibited anterior tilt on the right side and eight demonstrated anterior tilt on the left side. Only two of the thirteen specimens that exhibited anterior tilt on one side of the pelvis (left or right) exhibited posterior tilt on the opposite side of the pelvis. For both right and left pelves of both planes the mean range of anterior pelvic tilt was 0.4-12.4 degrees whereas the mean range of posterior pelvic tilt was 0.2-9.3 degrees. All specimens exhibited some degree of pelvic tilt either anterior or posterior. ICC values of reliability for pelvic tilt measurements obtained on two different days ranged from 0.86 to 0.99. Verification of the CTT oblique plane pelvic tilt angles as valid predictors of true oblique plane pelvic tilt angles is provided by Bartko ICC values of 0.96 to 0.99 and multiple R values of 0.83 to 0.99. Multiple linear regression further substantiated the validity of CTT oblique plane pelvic tilt angles. Standard errors of estimate indicated only small quantitative differences between predicted and criterion values.

DISCUSSION

Since all specimens demonstrated either an anterior or posterior tilt for both the right and left sides while in neutral position, it is evident an intrinsic bony tilt is present. In current clinical practice the neutral position serves as a baseline for measurement of angles of pelvic tilt. It is likely most clinical measurements of pelvic tilt do not account for intrinsic bony tilt of the pelvis. Thus, the role of the pelvis in sitting, standing, walking, and lifting postures and movements of patients who experience low back pain may be seriously misjudged. Therefore, validity and reliability of the CTT and similar techniques need to be determined on human subjects. Determining a clinical method or correction factor for intrinsic bony pelvic tilt would be valuable as well. This would contribute to a more sound mechanical basis for accurately determining the role of hip-pelvis-lumbar spine complex in the manifestation of low back pain during a variety of movements and postures.

CONCLUSION

Differences exist between right and left side angles of pelvic tilt in cadaver specimens, the CTT is highly valid on cadaver specimens and an intrinsic bony tilt exists within the pelvis which suggests that the clinical concept of pelvic tilt be re-examined.

1. Gracovetsky S, et al: Spine 14:412-416, 1989
2. McKenzie RA: The Lumbar Spine: Mechanical Diagnosis and Therapy, 1981
3. Sanders G, et al: Physical Therapy, 1981
4. Steindler A: Kinesiology of the Human Body, 1970
5. Wickstrom G: Scand J Work Environ Health (Supp 1) 4:1-12, 1978
6. Wood PHN, et al: The Lumbar Spine and Back Pain (chapter 1), 1987

INTERACTIVE BIOMECHANICS INSTRUCTION FOR ORTHOPAEDIC RESIDENTS

Tamara Harder, MS, Chris Peters, Ed D, Christopher Vaughan*, PhD, Jonathan Black, PhD
Clemson University, Clemson, SC 29634
*University of Virginia, Charlottesville, VA 22908

INTRODUCTION

The goal of fracture treatment is to maintain position, facilitate union and to restore function. The use of internal fixation methods to treat femoral shaft fractures has become standard orthopaedic practice. A computerized instructional program on the biomechanics of internal femoral fracture fixation was developed to assist in training orthopaedic residents. This program applies engineering principles, including material and structural properties, directly to orthopaedic devices and practices.

REVIEW AND THEORY

Several studies in the medical field have concluded that Computer-Assisted Instruction (CAI) is at least as effective as the traditional lecture method when comparing post-test performance (1, 2, 3, 4). Aronberg [5] compared the lecture method to CAI in the instruction of radiology to second year medical students. A written post-test given two weeks later to both groups showed a 24% increase in scores for the CAI group, compared to an 11% improvement for the lecture group. Garrett et al. [6] compared hematology and oncology lecture and CAI instruction. Each of the two groups were exposed to the two methods. The results on a written post-test indicate that the CAI method was as least as effective as the lectures. Calhoun et al. [7] showed that Orthopaedic in Training Examination (OITE) scores were as much as 60% higher for those residents who had used the CAI course. Their program covers five major areas: (1) stress-strain, (2) statics, and material characteristics of (3) bone, (4) implants, and (5) cartilage and ligaments.

METHODOLOGY

These promising results motivated the development of an instructional course in orthopaedic biomechanics. A schematic of the course developed in this study is shown in Figure 1. A five question pre-test on biomechanical principles is given and eleven demographic questions are asked before the user starts the course.

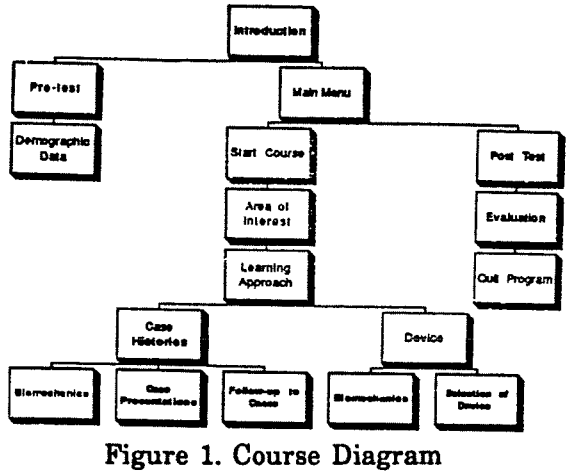

Figure 1. Course Diagram

The user then advances to the main menu where the instructional course, the post-test, the evaluation and quit options are available. The structure of the course mandates that the course be explored in the order above so as to insure maximum student participation. Accessory functions that are available to the student are: (1) an explanation of the post-test answers, (2) a dictionary of selected terms that includes related formulas and concepts, (3) a help section to decipher icons associated with each section, (4) a summary of the scoring of the pre- and post-tests, (5) a restart option to begin the instructional process, (6) suggested references for each surgical procedure and for answers to the post-test. The program was developed using Hypercard® on a Macintosh SE/30® computer. All data collection routines are

on-line in order to facilitate collection and organization. A tracking system records the course chosen by the user and the time spent in each section. In anticipation of the user being called away from the computer, the system automatically resets after an idle time of five minutes, storing all data in a separate file.

RESULTS AND DISCUSSION

Preliminary reviews by in-house staff have confirmed relevance of content, acceptance of CAI as a medium, user-friendliness and visual appeal. The title screen is shown as Figure 2.

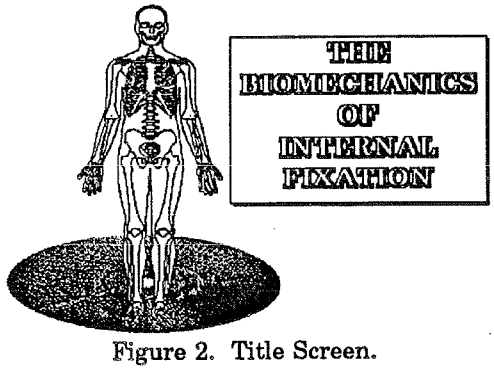

Figure 2. Title Screen.

Their comments and recommendations were incorporated into revisions of the design and content of the program. The two-dimensional mechanics of each of four femoral regions (subcapital, intertrochanteric, subtrochanteric and shaft) are available. The course discusses the effect of body weight and the muscle forces on each of these regions. Shear and compressive forces and stresses; as well as bending moments associated with the anatomical geometry of the femur are detailed. This program has seven major instructional modules: multiple pins and nails; sliding compression hip screw and side plate; fixed angle nail plate; multiple intramedullary flexible pins ; intramedullary rods; plates; and screws. Other fixation methods, such as skeletal traction, casting and arthroplasty, are options in the program. The biomechanics of these treatment methods have not been detailed: rather, a brief clinical application is provided. Material properties, presented by stress-strain and stress-cycles curves, and the significance of these concepts in the implantation of orthopaedic devices is discussed is many of the modules. Area and polar moments of inertia, open versus closed sections and anatomical loading forces are explored in the intramedullary rod section. Stress protection, stress concentration and the tension band principle are explored in the plate section. A photoelastic motion sequence demonstrates the videodisc technology and lag screw effect.

An evaluation of the course is currently being conducted by two separate orthopaedic training programs, with thirty residents total participating. The results of these findings will be discussed. We believe that an exciting learning environment will elicit a positive response to the medium, as well as an appreciation for and application of engineering knowledge in orthopaedic practice.

This study was supported by the State of South Carolina and the Department of Bioengineering, Clemson University.

REFERENCES

1. Holley, H.S. et al.: Microcomputers for CAI in Anesthesiology. J Med. Ed., 59:521-522, 1984

2. Fincher, R.E. et al.: A Comparison of CAI and Seminar Learning of Electrocardiogram Interpretation. J Med. Ed., 62:693-695, 1987.

3. Day, R.: CMI: An Alternative Teaching Strategy. J Nursing Ed., 26(4):30-36, 1987.

4. Neil, R.M.: Effects of CAI on Nursing Student Learning and Attitude. J Nursing Ed., 24(2):72-75, 1985.

5. Aronberg, D.J. et al.: CAI in Radiology. Radiology, 154:345-346, 1987.

6. Garrett, T.J. et al.: A comparison of CAI and Tutorials in Hematology and Oncology. J Medical Ed., 62:918-922, 1987.

7. Calhoun, J.H. et al.: Computer-Assisted Instruction in Orthopaedic Biomechanics. Orthop. Clinics, 17(4):599-604, 1987.

DIRECTIONAL AND SPATIAL SENSITIVITY OF NECK MUSCLE ACTIVITY DURING COMFORTABLY-PACED 3-D HEAD TRACKING MOVEMENTS

Joseph D. Peles, Jack M. Winters and Todd R. Hurley

Chemical, Bio & Materials Engineering,
Arizona State University, Tempe, AZ 85287

INTRODUCTION

Head movements are the end product of a complex biomechanical process involving relative motion between cervical vertebral bodies. Such motion differs with the spinal level and with the type of movement, and additionally motions may be kinematically coupled. Thus, head rotations require proper interactions between all the cervical joints. This is accomplished by the 36 or so relevant muscles of the neck, which include the long superficial muscles connecting the skull to the vertebral column and the short deep muscles inter-linking vertebrae. In the past, the long superficial muscles have been considered the prime movers while the short deep muscles have been regarded as stabilizers. This, however, may not be the case for all situations and the question of what neck muscles do what is still a relevant one. To answer this question more thoroughly, both dynamic and quasi-static movements are considered, and to maximize insight three approaches have been employed: human experiments, anthro-robotic head neck modeling and computer simulation. This talk concentrates on the human experiment subset, and more specifically, self-paced tracking with the head of various target patterns. By correlating the activity of four pairs of EMG electrodes placed over strategic neck regions to the head finite screw axis parameters (FSAP) between target locations, two questions are addressed: (i) Does the exact location approached from two different directions exhibit the same level of steady state neck muscle activity?; (ii) Do muscle recruitment strategies change while doing horizontal and vertical movements at various spatial orientations?

METHODS

Nine healthy subjects were utilized in this study. EMG electrodes (Motion Control, Inc.) were placed over four paired locations: (i) the sternocleidomastoids (SCM); (ii) the splenius capitis (SPL); (iii) the upper cervical spine, orientated vertically and about 1 cm lateral of the mid-sagittal line (measuring semispinales capitis and Occiput-C1-C2 deep paraspinal musculature), (UC); and (iv) the lower cervical spine, orientated vertically and about 1 cm laterally (including superficial and deep paraspinal muscles crossing this region) (LC). A light weight helmet with five reflective markers on the left side and a laser pointer on top was worn by the subject. Located 1.61 meters in front of the subject, on a partial dome, was a grid of 59 computer controlled light-emitting diodes. The subjects were instructed to track various target sequences via laser feedback. Tasks included vertical and horizontal movements starting at the center of the grid, moving out to an extreme and then coming back. This protocol was used to address question (i) cited in the introduction. To address question (ii), horizontal movements were also made while following targets at the top and bottom of the grid while vertical movements were made while at the left and right of the grid. Two video cameras recorded the positions of the five reflective markers, and the coordinates of the marker centroids were obtained using the 3-D Expert Vision System (Motion Analysis Inc.). The averaged marker positions at target "hold" locations were used to calculate the FSAP's by means of the Spoor-Veldpaus algorithm, as presented in Woltring et al. (1985).

RESULTS

For vertical movements made along the grid mid-line from the center (0°) to the upper extreme (40°) and back, the SPL and the UC were the primary agonists with the SPL showing an increase in steady-state EMG level from 0° to 40° and a corresponding fall from 40° to 0°. The UC showed large movement pulses from 0° to 40° but had very little

activity while moving back to the center. The LC exhibited increased activity at the movement extreme (40°); this may correlate with the lowering of the head FSAP as extreme upward orientations (> 30°) are reached. Direction sensitivity was observed in the SCM. Both the right and left SCM had a slight rise in steady-state EMG level while tracking from 20° to 40°. The EMG levels, however, were significantly higher for some subjects during "holding" aspects while going from 40° to 20°, during which the SCM's were prime movers for the initial movement phase. Spatial sensitivity was then tested by making vertical movements while 40° to the left and right of the grid mid-line. The greatest distinction between these off-center movements and the mid-line movements described above were in the SCM. The SCM ipsilateral to the off-center direction showed the same or greater behavior as for mid-line movements while the contralateral SCM showed no significant EMG activity (Figure 1). This observation demonstrates spatial asymmetry between muscles that have traditionally been regarded as synergists for vertical movements.

Mid-line horizontal movements started at the grid center, moved out to the extremes (+50° or -50°), and then back to the center. The SPL on the side of the movement direction and the contralateral SCM were observed to be the primary agonists. There was no significant direction sensitivity observed for the horizontal movements. Spatial sensitivity involving the two agonists (SPL and SCM), however, was detected. For horizontal movements made at the top of the grid, the SCM were the prime movers and the SPL muscles showed almost no activity. The exact opposite was true for movements made at the bottom of the grid.

In summary, two fundamental effects were documented. The first is related to muscle redundancy: postural muscle "holding" activity can depend on the prior direction of approach. The second is related to initial position sensitivity: use of different muscles at various spatial orientations to produce the same direction of head movement.

REFERENCES

Woltring, H.J., Huiskes, R., De Lange A. and Veldpaus,F.E. (1985) Finite centroid and helical axis estimation from noisy landmark measurements in the study of human joint kinematics. **J Biomech.**,12:911-920.

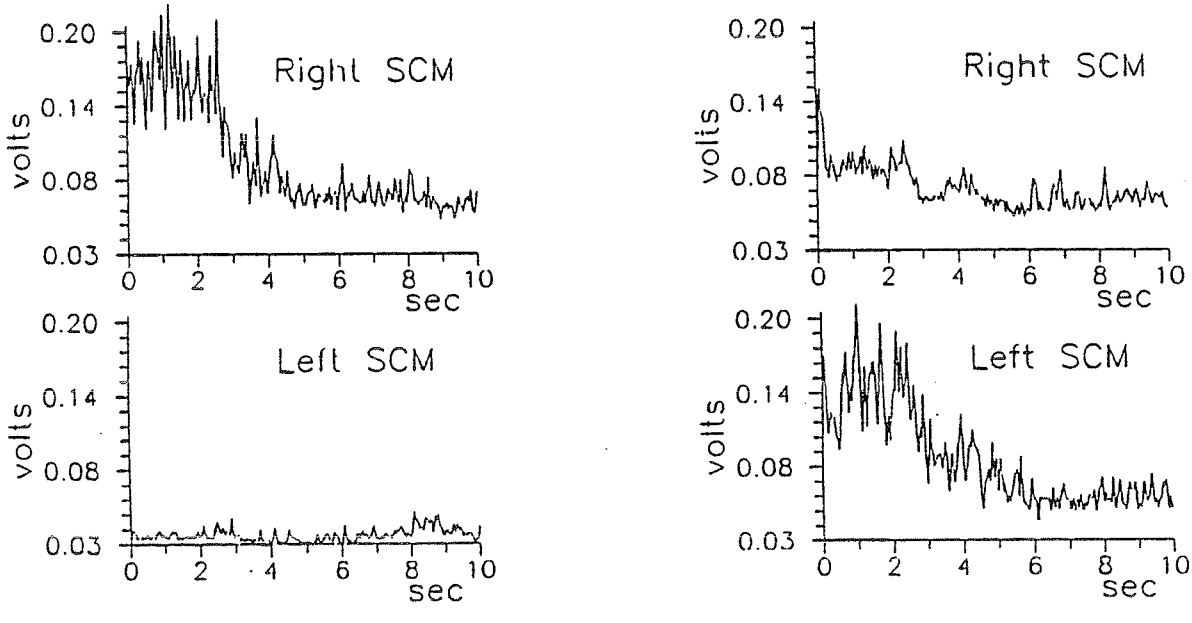

Figure 1: Sternocleidomastoid muscle activity during downward vertical tracking movements starting with a vertical coordinate of +40° and making -20° movements every 2 sec until -40° is reached. In the traces on the left, the horizontal tracking coordinate is off-center to the left by 40 deg, while for the right traces, it is off-center by 40° to the right. Note asymmetric activity for both cases.

Cervical Spine Manipulation: Applied Loads, Motions and Myoelectric Responses

John J. Triano, M.A., D.C. and Albert B. Schultz, Ph.D.
The National College of Chiropractic &
Department of Mechanical Engineering and
Applied Mechanics, University of Michigan

INTRODUCTION

Loads are applied dynamically to the head and neck during manipulation (SMT) of the cervical spine. A large number of cervical complaints are treated by SMT each year. No quantitative information is available about the biomechanics of these procedures. This study was designed to estimate the applied loads and to monitor the kinematic and muscular responses to them.

METHODS

Sets of SMTs were carried out on 11 healthy volunteer male subjects at the level of the C2 vertebra from both the right and left sides. The intent of these procedures is to apply forces transverse to the body from right-to-left or from left-to-right. Altogether, 42 manipulations, 36 right and 6 left, were studied. A table surface was rigidly connected to a force plate sensitive to all 6 components of applied loads. Infrared light emitting diodes (LEDs) were placed on the torso and head and monitored optoelectronically to observe body segment kinematics. Motion of LEDs on the head were compared to bite-bar motions and found to agree within 16%. The inertial loads created by these motions were calculated. Myoelectric action of eight muscle areas around the perimeter of the neck were monitored. A series of maximum voluntary exertions (MVE) were used to calibrate neck muscle activities.

RESULTS

Loads applied to the head and neck from both right and left manipulation procedures were similar (Tables 1 & 2). Forces were transmitted primarily in the mid-frontal plane of the body defined by the longitudinal axis (Y) and one right-directed X-axis. The largest variation in force direction was along the antero-posterior axis. Variation of load magnitudes was larger for procedures applied from right-to-left, but the number of left directed procedures was small. All six load components reached their peak values within 150 to 240 ms of initial load application. Load application ceased within 200 to 300 milliseconds.

Myoelectric response to SMT showed wide variations between muscles and subjects. Table 3 presents typical myoelectric activities during the SMT application and those immediately before and after. The mean amplitude of muscular activity during maximal voluntary exertions (MVE) is given to the right and the percentage MVE for the activity during the SMT is listed. Muscle activities ranged from 18% to 54% MVE values.

Movement artifact may explain the particularly high response observed for electrodes overlying the right semi-spinalis capitis muscle since they were often in direct contact with the manipulator's hand.

CONCLUSION

Manipulation loads applied to the head and neck from either the right or the left appeared to be consistent in magnitude and nearly bilaterally symmetric in orientation. In addition to the intended transverse (X) axial component, a large longitudinal (Y) axial tension was observed in all of the manipulations. Their influence on the loads transmitted to the neck vertebra needs to be considered. From the type of descriptive information supplied in this report, biomechanical estimates of the effects of neck manipulation on the motions of and internal loads on the spine and its component tissues can be made.

ACKNOWLEDGEMENT: Supported by a restricted grant from the Foundation for Chiropractic Education and Research, made possible by the Foundation for the Advancement of Chiropractic Education.

Table 1: **Peak Manipulation Loads**

	Right SMT	Left SMT
Number	36	6
Magnitudes:		
Force	123.1 (28.3)	110.9 (7.1) N
Moment	25.9 (20.4)	26.9 (10.2) Nm

Table 2: **Peak Load Vector Orientations**
(Angles to axes, degrees)

	Right	Left
Forces:		
X axis:	+41.2 (4.4)	-43.3 (5.0)
Y axis:	36.4 (4.3)	32.7 (6.3)
Z axis:	-3.3 (14.6)	+1.1 (16.6)
Moments:		
X axis:	-19.3 (16.7)	-22.2 (4.0)
Y axis:	18.5 (5.2)	-17.1 (1.1)
Z axis:	-47.4 (4.0)	+49.7 (1.8)

Table 3: **Typical Myoelectric Activities**
(RMS,uV)

Muscle	PreSMT	SMT	PostSMT	MVE	%MVE
R L Col	5.6 (4.2)	22.9 (13.4)	6.4 (3.5)	103.8	22.0
R SCM	14.9 (22.7)	71.4 (76.3)	17.1 (14.1)	287.5	25.0
R SSP CAP	4.9 (3.0)	67.8 (85.7)	7.7 (5.0)	124.0	54.0
R TRAP	18.7 (15.2)	31.8 (17.1)	20.4 (16.9)	94.7	34.0
L TRAP	4.6 (2.0)	14.6 (12.4)	4.8 (1.8)	68.1	23.0
L SSP CAP	6.4 (4.2)	33.9 (19.0)	7.3 (4.4)	121.4	28.0
L SCM	12.5 (8.8)	46.7 (32.4)	13.8 (8.8)	259.3	18.0
L L COL	6.1 (3.3)	19.9 (16.5)	8.0 (5.4)	91.2	22.0

Upper-limb Kinematics for the propulsion of a tilt seat wheelchair

Mario Lamontagne*, Benoît Giroux*, Hugh Barclay**, Guy Martel*** and Thomas John***
* School of Human Kinetics, University of Ottawa, Ottawa, On., Canada K1N 6N5
** Advanced Mobility System Corp., Kingston, On., Canada K7M 4H5
*** The Rehabilitation Centre, Ottawa, On., Canada K1H 8M2

Introduction

In the recent past, wheelchair seating has become a concern for clinicians, researchers, and industrialists. As a result of experimentation into this area a tilt seat wheelchair design has been developed to deal with pressure problems, spinal curvature (Andersson and Ortengren, 1974), postural control, mechanical propulsion efficiency (Rudwick, 1979; Spooren, 1981), and seating comfort. This type of wheelchair design can be the solution of these problems.

Various studies have examined the effects of different seated positions in terms of biomechanics, physiology, and ergonomics; however, few of these studies have dealt with a tilt seat wheelchair design or with amputee subjects. The research that does exist supports the benefits of tilt seat designs on pressure problems and seating comfort, however the benefits on mechanical propulsion efficiency have not yet been shown.

The purpose of this investigation is to analyze the upper-limb kinematics involved in the propulsion of a tilt seat wheelchair at two different seat angles and at two different wheelbase lengths for ten above-knee amputees.

Methods

Ten bilateral above-knee amputee subjects (high amputation) were selected on a voluntary basis for this experiment. All subjects were tested on an adjustable tilt seat wheelchair designed and built by Advance Mobility System Corporation. The wheelbase length (horizontal distance between the rear wheel axle and the front wheel axle) and the seat angle were the two possible adjustments on this wheelchair. The subjects were tested for four experimental conditions consisting for two horizontal positions of the rear wheel (wheelbase length of 16 and 19 inches) at a 90 degree seat angle, one position at a maximal back tilt seat angle (wheelbase length 16 inches) and one using their own wheelchair.

In order to perform the four experimental conditions in this study for a controlled environment, the subjects were asked to propelled the wheelchair on a set of stationary rollers equipped to compensated for the subject-wheelchair Inertia. A tachometer was attached to the rollers to determine the wheeling speed. Adhesive Markers were placed on the shoulder, elbow, wrist, hand, hip, and right limb appropriate joint centre locations to facilitate the kinematic data reduction of the body segments.

The subjects were asked to propel the wheelchair at 50% of their maximum speed while a cinecamera was used to film the upper-segment motions at 50 frames/seconds. Three trials were recorded for each condition. Kinematics parameters of the upper-segments were obtained for a complete wheelchair cycle by processing the digitized cinefilm coordinates (BIOMECH, U. of Ottawa). All kinematic data obtained for a cycle were time normalized (100%) and ensembled averaged across subjects.

Results and Discussion

Differences were observed in the pushing style across subjects. Hand movement analysis from the stick figures showed that five subjects were characterised as using circular arm motion (CAM) while the remaining five subjects were described as using pump arm motion (PAM). In order to decrease inter-subject variability, two distinct groups were formed for the CAM and PAM subjects.

No significant differences were found between conditions in the degree of contact ($F(3,34) = 0.35$, $p > 0.05$). Some differences in the peak angular velocities and accelerations of shoulder and elbow were observed among the experimental conditions. It was observed that the back tilt condition had higher peak angular velocities and accelerations for the shoulder and the elbow in both pushing styles than the other conditions. For the PAM group, the lowest peak angular velocity of the elbow was found when the subjects propelled their own wheelchair. For the CAM group, the highest peak shoulder angular velocity and elbow angular acceleration were obtained when propelling their own wheelchair. Consequently, the pushing styles and the type of wheelchair used affect the angular kinematics of the upper-segments.

Increasing angular velocity to the pushrims can be assisted by trunk motions (Sanderson & Sommer, 1985). From our results, the angular momentum of the trunk was found to highly fluctuate for the PAM group at all experimental conditions. The same observations were found for the CAM group except for the back tilt condition, the trunk angular momentum had less fluctuation.

From the results of this study, none of the experimental conditions showed strong advantageous from the kinematic parameters except for the CAM group in the back tilt seat position. This can be explained by the selection of subjects (bilateral above-knee amputee) and the low skilled subject to propel wheelchairs.

References

Andersonn, B.J.G. and Ortengren, R. (1974). *Scandinavian Journal of Rehabilitation Medicine*, 6, 122-127.

Rudwick, L. (1979). *Sports 'n Spokes*, 5(4), 10-12.

Sanderson, D.J. and Sommer, H.J. (1985). *Journal of Biomechanics*, 18(6), 423-429.

Spooren, P. (1981). *Sports 'n Spokes*, 7(6), 19-20.

Acknowledgements

This research project has been funded by the University Research Incentive Fund (OT12-001) of the Ministry of Colleges and Universities of Ontario, Canada.

LOWER BODY SEGMENT FORCES AND THE PERCENT CYCLE WHERE THEY OCCUR DURING LEVEL WALKING, STAIR ASCENT, & STAIR DESCENT

Gregory S. Rash, Robert Shapiro*, and Charles F. Knapp*
United States Sports Academy, Daphne, AL 36526 and
*Biodynamics Group, Wenner Gren Laboratory, University of Kentucky, Lexington, KY 40506

INTRODUCTION: There have been numerous investigators which calculated forces in the lower body during different types of gait. Most of these investigators reported both compressive and shear forces. Typically, these investigators also reported where the peak force occured in the stance phase. No study could be found which calculated the segment forces [Forces parallel (compressive) and normal (shear) to the long axis of the segment]. All of the studies found calculated joint forces. This study investigated where in the gait cycle the compressive and shear segment forces occurred.

METHODS: Eighteen normal males served as subjects in this study. Their average age, height, and weight were 27.3 years, 177.6 cm, and 756.6 N respectively. The subjects were analyzed while performing three tasks. The tasks were: Level walking, stair ascent, and stair descent. A Kistler force plate collected the ground reaction forces (GRF) and center of pressure while three 200 Hz Nac cammeras attached to a Motion Analysis VP310 video processor recorded the tasks. The 3D joint centers were obtained using the information from the three cammeras via the Motion Analysis software package EV3D.

Utilyzing the synchronized force plate data and the joint center locations a Fortran 77 program written by the investigator on a Sun 3/260 mini computer calculated the compressive and shear segment forces (Addition of the proximal and distal segment forces with respect to segment angle). The lower body segment compressive and shear forces were calculated for one cycle of gait (i.e. for walking, a cycle was from right foot contact on the force plate until the right foot contacted the ground again). All forces were standardized to body weight (BW) and the percent of the gait cycle where the peak force occurred was calculated.

RESULTS AND DISCUSSION: Table 1 shows the average of all subject's peak compressive and shear forces on the force plate and in the foot, shank, and thigh for level walking, stair ascent, and stair descent. Table 2 shows the average for all subject's percent cycle where the peak force occurred on the force plate and in the foot, shank, and thigh for level walking, stair ascent, and stair descent.

The lower body forces did not dissipate as they transferred from distal to proximal segments in all situations. For compressive and resultant forces, the force was greatest in the shank, followed by the thigh and foot respectively. Shear forces did follow a dissipation from distal to proximal. The

Table 1. Average of all subjects GRF & segment forces for each task performed (All force in BW).

	Fz	Fy	C1	S1	C2	S2	C3	S3
WALK	1.13	Ø.13	-Ø.43	Ø.45	-2.12	-1.4Ø	-1.9Ø	-1.Ø2
UP	1.2Ø	-Ø.21	-Ø.99	1.2Ø	-2.34	-Ø.84	-1.96	-1.19
DWN	1.59	Ø.22	-1.39	2.2Ø	-2.95	-1.59	-2.79	-Ø.35

Fz=Vert GRF, Fy=Ant-Post GRF, C1=Foot Comp, S1=Foot Shear, C2=Shank Comp, S2=Shank Shear, C3=Thigh Comp, S3=Thigh Shear

Table 2. Average of all subjects percent cycle where the peak force occurred for each task performed.

	Fz	Fy	C1	S1	C2	S2	C3	S3
WALK	33.8	45.8	16.6	37.6	15.4	51.Ø	39.9	13.7
UP	24.8	13.2	15.4	29.3	16.Ø	51.6	35.5	14.Ø
DWN	57.1	87.8	57.1	57.3	57.1	87.3	57.7	75.9

Fz=Vert GRF, Fy=Ant-Post GRF, C1=Foot Comp, S1=Foot Shear, C2=Shank Comp, S2=Shank Shear, C3=Thigh Comp, S3=Thigh Shear

force plate yielded the smallest amount of force for compressive, shear, and resultant forces. Only the interaction between the foot compressive and vertical GRF during walking and stair ascent were not significantly different at the Ø.Ø5 alpha level. MANOVA's with A priori Bonferonni adjusted paired t test were utilized for testing within each task. An overall MANOVA for testing between task could not be performed due to the number of subjects.

The percent cycle where the peak force occurred was not the same with respect to compressive or shear forces during walking or stair ascent. The peak force generally occurred as the center of gravity passed over the base of support or during the late support phase in these activities. Stair descent had the majority of peak forces occur during the initial part of the support phase for compressive while the majority of peak shear forces occurred during the late stance phase.

REFERENCES:

1. Bresler, B., & Frankel, J. (1950). Trans. Amer. Soc. Mech. Engrs. 72, 27.
2. Frankel, V., & Nordin, M. (1980). Basic Biomechanics of the Skeletal System Philadelphia: Lea & Febiger.
3. Morrison, J. B. (1969). Bioengineering analysis of force actions transmitted by the knee joint. Biomed. Engng., 3, 164-170.
4. Rohrle, H., Scholton, R., Sigolotto, C., & Sollbach, W. (1984). Joint forces in the pelvis-leg skeleton during walking. J. Biomechanics, 17, 409-424.
5. Stauffer, R., Chao, E., & Brewster, R. (1977). Force and motion analysis of the normal, diseased and prosthetic ankle joint. Clinical Orthopaedics and Related Research, 189-196.
6. Winter, D. A. (1979). Biomechanics of Human Movement (pp. 29-46). New York: John Wiley & Sons.

THE EFFECTS OF MUSCULAR FATIGUE INDUCED BY A SUB-MAXIMAL EXERCISE TEST ON SELECTIVE KINEMATIC PARAMETERS OF GAIT

Spiros G. Prassas
Exercise and Sport Science Department, Colorado State University
Fort Collins, CO 80523, USA

There is an abundance of scientific literature on human movement patterns, especially on walking and running. The biomechanics of the two activities have been studied extensively, including electromyographic, kinematic, and to a lesser degree, kinetic studies. The effect of muscular fatigue on human performance has also been investigated in length, with emphasis given to physiological parameters such as oxygen consumption, blood lactate, and heart activity responses. However, research on the relationship between muscular fatigue and the mechanics of human locomotion is limited to a few studies involving the running/sprinting patterns of highly skilled (young) subjects (Sprague and Mann, 1983; Bates and Haven, 1974). In light of existing evidence that performance deteriorates with aging and in the absence of published data relating muscular fatigue to gait patterns, this study was undertaken to investigate the relationship between muscular fatigue and gait in healthy individuals of two age groups.

Methods

Twenty individuals divided by age into two equally numbered groups participated in the study. Group I included subjects aged 25 years and younger (average age: 22 yrs), group II included subjects aged 60 years and older (average age: 65.2 yrs). For each subject, a full walking cycle was videotaped with a Panasonic PV-330 video camera prior to and following a sub-maximal bicycle ergometer exercise test. The exercise test was administered according to the guidlines of the American College of Sport Medicine (ASCM). Both pre- and post-fatigue walking cycles were digitized and the extracted raw data was digitally filtered before being submitted to further analysis.

Results and Conclussion

Table one presents means (M) and standard deviations (SD) of selective temporal and spatial kinematic parameters. Swing time (ST) was defined as the time of the (swinging) limb from toe-off to heel strike, stance time (STT) was the time of the supporting limb from heel strike to toe-off (including double and single support), stride length (SL) was the distance from toe-off to toe-off expressed as a percentage of height, and AJ/KJ/HJROM was the difference in ankle, knee and hip minimum and maximum joint angles of the swinging (SW) and support (SU) extremities during the swing and stance time respectively as defined above. Independent paired t-tests revealed that muscular fatigue induced by the ASCM sub-maximal bicycle ergometer test does not influence significantly ($p \leq .05$) the gait patterns of healthy individuals. However, before conclusive remarks regarding the effects of muscular fatigue on gait can be made, it is recommended that a maximal exercise test should be utilized to induce fatigue. In the present study, personal interviews with the majority of the subjects indicated that the ASCM submaximal bicycle ergometer test is not of sufficient intensity to induce substantial muscular fatigue which in turn, might significantly effect gait characteristics.

Table 1

Variable		Measurement			
		Group I (N=10)		Group II (N = 9)	
		Pre-Fat.	Post-Fat.	Pre-Fat.	Post-Fat.
Swing time (ST)	M	0.350	0.350	0.375	0.367
	SD	0.047	0.032	0.044	0.048
Stance time (STT)	M	0.736	0.713	0.851	0.814
	SD	0.041	0.039	0.150	0.151
Ratio of ST/STT	M	0.475	0.493	0.445	0.455
	SD	0.062	0.062	0.051	0.044
Stride Length (SL)	M	59.2	60.000	64.222	64.000
	SD	5.712	5.598	8.333	7.280
% change in SL	M	-0.200		-0.222	
	SD	3.765		3.563	
AJROMSW	M	19.600	20.100	21.222	21.333
	SD	13.134	5.087	9.431	7.000
KJROMSW	M	47.100	47.000	53.222	53.667
	SD	4.977	4.320	4.969	3.873
HJROMSW	M	13.100	13.600	14.000	13.000
	SD	4.332	4.300	5.568	5.657
AJROMSU	M	34.900	31.300	23.778	24.889
	SD	5.744	4.218	3.833	6.112
KJROMSU	M	41.300	38.500	41.889	43.889
	SD	5.056	4.720	8.100	5.798
HJROMSU	M	27.300	27.400	28.889	29.667
	SD	2.751	3.471	6.864	6.305

Note: *Times are listed in seconds. Joint angles are listed in degrees.*

References

Bates, B.T. & Haven, B.H. Effects of fatigue on the mechanical characteristics of highly skilled female runners. In Nelson, R.C. & Morehouse, C.A. (Eds.) *Biomechanics IV*. Baltimore: University Parks Press, 1974.

Sprague, P. & Mann, R. The effects of muscular fatigue on the kinetics of sprint running. *Research Quarterly for Exercise and Sport,* 54(1): 60-66, 1983.

AUTOMATED COMPUTER SYNTHESIS AND SIMULATION OF HUMAN GAIT

TaChung Yih; Gautam Ray and Bernardo Donoso
Mechanical Engineering Department
Florida International University, Miami, Fl 33199, USA

INTRODUCTION

A computer-aided synthesis approach is presented to simulate the normal human gait automatically. The lower limbs are characterized as a multi-link redundant linkage system. For the gait within a complete cycle, the lower extremity forms a 7-link open-chain system during the swinging phase, whereas an 8-link closed-chain mechanism is formed during the period from heel-strike to toe-off. Based on the characteristics of open-chain and closed-chain linkage systems along with the dimensional and motion constraints, the automated gait simulation is made possible through the inverse kinematic synthesis. The dimensional constraints are specified by the limb lengths and stride distance, which can be measured directly from the subject or calculated numerically based on the average anthropometric data as percentage of the body height. The motion constraints are described by the range of motion of each physiological joint and the time period in completion of the motion. The open- and closed-chain systems are synthesized separately to acquire the joint positions and orientations. The gait is simulated, according to the stored kinematic dada, by the stick diagrams on the Tektronix graphic terminal.

REVIEW AND THEORY

Marey(1895) investigated human gait by the interrupted light method using photographic techniques to measure the motions directly. Cinematographic techniques are widely used in collecting data for the analysis of locomotive movements of human body(Cappozzo et al., 1975; Murray et al., 1967; Sutherland et al., 1972). In addition to the experimental techniques, computer based analysis became popular in simulating human motions nowadays (Zarrugh et al., 1981; McGhee, 1981; Chen et al., 1986).

Research to date toward the understanding of human gait has been primarily experimental and analytical. However, human musculo-skeletal system can be modeled as a multi-loop linkage system and then synthesized to obtain the joint flexions and positions for a variety of motions. Gait is one of the most primary motions in our daily activities, thus; emphasized in this paper.

METHODOLOGY

Elftman(1967) presented a kinematic model of the human skeleton consisting of seven articulated segments. The body is divided into right and left lower limb linked together by the composite head-arm-trunk (HAT) segment, and each lower limb includes thigh, shank and foot. The same structure is used for automated gait synthesis and simulation.

One cycle of the normal gait viewed, and recorded experimentally, on sagittal plane is shown in Fig. 1 by the stick diagram. Joints 1, 2 and 3 represent the head of the first metatarsal, the ankle joint and the knee joint of the right limb, respectively. The joints of the left limb, indicated by 5, 6 and 7, are defined in a similar manner. The right and left hip joints are assumed to be coincident at point 4 while observed on sagittal plane.

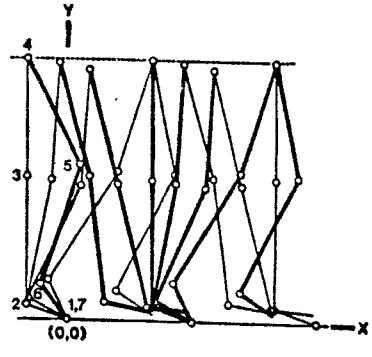

Fig. 1 Stick diagram of gait recorded on sagittal plane

Referring to Fig. 2 for the kinematic skeleton diagrams that disintegrated from Fig. 1, at least five phases are needed to simulate one complete cycle of gait. Each phase is defined according to the motion characteristics of the lower limbs to be open-chain or closed-chain linkage system in nature. For example, phase one of the gait starts from one's initial standing position followed by the swing of left

lower limbs and end at the instant of heel-strike (stage 1 through 4). The motions in phase one fit into the characteristics of an open-chain linkage system, thus; characterized by the open-chain system. Similarly, phase two starts from the instant of heel-strike to toe-off of the left foot (stage 4 through 5) which complies with the motion characteristics of a closed-chain linkage system.

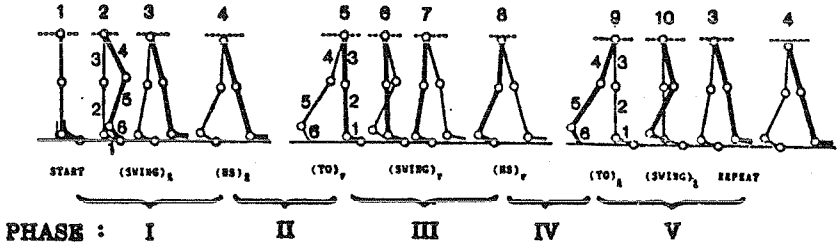

Fig. 2 Phase analysis of normal gait

Analogy is applied to the right lower limbs until the motion is repeated. Consequently, the gait can be further defined as the motion transmission between open-chain and closed-chain linkage systems.

Once the gait is characterized, the transitional joint flexions and positions within each stage can be calculated by the inverse kinematic synthesis of open- and closed-chain systems. The dimensional and motion constraints are introduced to obtain the numerical results iteratively. The numerical schemes utilized in the computer iteration include least-squares regression, point relaxation and separation of variable in matrix.

RESULTS AND DISCUSSION

Simulation of normal gait obtained by the iterative kinematic synthesis of lower limbs are displayed on Tektronix graphic terminal, Fig. 3. In comparison with the experimental results, Fig. 1, individual joint motions for both cases are illustrated in Fig. 4. It is noticed that the synthesized numerical results are sufficiently close to that of the experimental results.

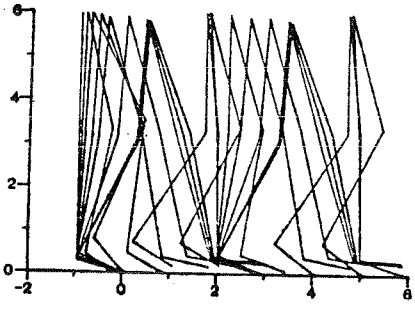

Fig. 3 Synthesis of gait

CONCLUSION

In addition to the conventional experimental and analytical approaches, inverse kinematic synthesis for the motion transmission between open-chain and closed-chain linkage systems is applied successfully to simulate the normal gait. An algorithm is developed to complete the synthesis and simulation automatically with single input of body height. However, this algorithm is applicable to simulate other human or animal movements with similar motion characteristics, such as running and stair-climbing, by modifying the build-in dimensional and motion constraints.

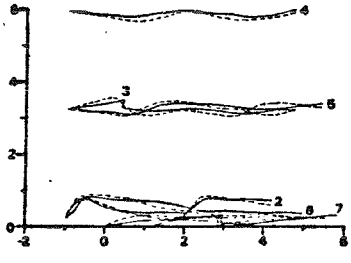

Fig. 4 Joint motions of gait

REFERENCES

Cappozzo A, Leo T and Pedotti A(1975) "A general computing method for the analysis of human locomotion", J. Biomechanics 8, pp.307-320.

Chen BR,Hines MJ and Hemami H(1986) "Dynamic modelling for implementation of a right turn in bipedal walking", J. Biomech. 19, pp. 195-206.

Elftman H(1967)"Basic function of the lower limb", Biomed. Engr 2, pp. 342-345.

Marey EJ, Movement(1895), Appleton, New York.

McGhee RB(1981) "Mathematical models for dynamics and control of posture and gait", Biomechanics VII-A, Univ. Park Press, pp. 183-193.

Murray MP(1967) "Gait as a total pattern of movement", Am. J. Phys. Med. 46, pp. 290-333.

Sutherland DH and Hagy JL(1972) "Measurement of gait movements from motion picture film", J. Bone Jt Surg.(A)54, pp. 787-797.

Zarrugh MY(1981) "Power requirements and mechanical efficiency of treadmill walking", J. Biomechanics 14, pp. 157-165.

A PRELIMINARY COMPARISION BETWEEN CUTANEOUS AND OSSEOUS MARKERS USED TO ESTIMATE BONE DISPLACEMENT AT THE ANKLE AND SUBTALAR JOINT

Norman Murphy [1, 3], Paul Allard [1, 3],
Hubert Labelle [1, 2], Morris Duhaime [1, 2], and Michel Leroux [1, 3]
1) Pediatric Research Center, Sainte-Justine Hospital, Montreal, Que., Can., H3T 1C5.
2) Department of Orthopaedics, University of Montreal, Montreal, Que., Can., H3C 3J7.
3) Faculty of Physical Education, University of Montreal, Montreal, Que., Can., H3C 3J7.

INTRODUCTION

This paper reports preliminary findings between estimated three-dimensional (3-D) bone displacements using cutaneous markers and true bone displacements using osseous markers at the ankle and subtalar joint. The purpose of this study was to determine if cutaneous marker displacements are good estimates of true bone displacements to warrant normal and pathological *in vivo* biomechanical investigations of the ankle and subtalar joint. The preliminary findings tend to support that range and pattern of motion displacement repeatability are obtained with the use of cutaneous or osseous markers. On the otherhand, the comparisions between cutaneous and osseous markers tend to support that bone displacement estimates using cutaneous markers are attached with errors.

REVIEW AND THEORY

Cinematography, clinical observations, dissections and radiographs are primary methods used to investigate normal and pathological biomechanical functions of the ankle and subtalar joint. Unfortunately, most of these methods lack accurate quantitative 3-D data (Manter, 1941; Hicks, 1953 and Isman et al., 1969) while others are restricted to *in vitro* conditions (Van Langelaan, 1883; Engsberg, 1987 and Ottevenger et al., 1989). Presently, a stereophotogrammetric system combined with the Direct Linear Transformation (DLT) technique is available to collect accurate 3-D marker displacement data (Allard et al.; 1987). Unfortunately, this procedure is limited to *in vitro* investigations of the ankle and subtalar joint since the correlation between cutaneous (estimated bone) and osseous (true bone) marker displacements at these two articulations is not well documented. Consequently, the comprehension and understanding of normal and pathological biomechanical function of these two articulations is confined to *in vitro* conditions. The use of cutaneous markers to estimate bone displacement represents an alternative which should be used to collect data to analyze and comprehend the normal and pathological *in vivo* biomechanical function of the ankle and subtalar joint. More importantly, the pathomechanics of injuries such as the lateral sprain could be understood and clarified.

METHODOLOGY

The experimental set-up consisted essentially of four motorized still cameras, one mounted at each corner of a rectangular baseboard. At the center of the baseboard, a calibration object having 36 fiducial marks was used to calibrate and determine the 3-D reconstruction accuracy and precision. Afterwards, the device was removed and an amputated lower leg was fixed into position. Cutaneous markers were then placed on the skin over the bones of the ankle and subtalar joint on the medial and lateral sides. Stereophotographs of the markers were taken for five consecutive static positions during five repeated movements of dorsiflexion and plantar flexion at the ankle as well as eversion and inversion at the subtalar joint. The movements were induced by a pulley and weight system attached to the primary muscle tendons. Windows were then dissected to expose the bones and osseous markers were embedded directly into the bones. Stereophotographs of the markers were taken as described above. The planar coordinates of the cutaneous and osseous marker displacements were obtained by manual hand digitization. The 3-D coordinates of the markers were then reconstructed. With the availability of one more specimen, the

procedure was then repeated. Cutaneous markers were not used with this specimens since the skin over the bones was partially removed during amputation. Finally, the range and pattern of motion observed at each articulation with the cutaneous and osseous markers were compared.

RESULTS

The overall 3-D reconstruction accuracy and precision was calculated to be 0.07mm and 0.36mm respectively. The accuracy and precision of the technique was not influenced when either the number of calibration marks (20, 25 and 30) and the number of parameters (11, 12, 14 and 16) were entered in the DLT algorithm. For the movements of dorsiflexion and plantar flexion at the ankle, the range of motion for the cutaneous markers was similar for all movements. The regression correlations for the pattern of motion varied from 0.75 to 0.97. For the osseous markers, the range of motion was also similar. The regression correlations for the pattern of motion varied from 0.74 to 0.96. For the movements of eversion and inversion at the subtalar joint, the range of motion for the cutaneous markers was similar for all movements while the regression correlations for the pattern of motion varied from 0.40 to 0.96. For the osseous markers, the range of motion was also similar while the regression correlations for the pattern of motion varied from 0.33 to 0.99. For the comparision between the cutaneous and osseous markers, the range of motion at the ankle for the movements of dorsiflexion and plantar flexion for the cutaneous markers was 10 to 75% greater than with the osseous markers. The regression correlations, on the otherhand, varied from 0.61 to 0.85. For the movements of eversion and inversion at the subtalar joint, the range of motion for the cutaneous markers varied from 25% smaller to 50% greater than with osseous markers. The regression correlations, on the otherhand, varied from 0.39 to 0.99.

DISCUSSION

The preliminary findings tend to support that range and pattern of motion displacement repeatability are obtained with the use of cutaneous or osseous markers. On the otherhand, the comparisions between cutaneous and osseous markers tend to support that bone displacement estimates using cutaneous markers are attached with errors. This finding has also been reported by other investigators (Weeren, 1988 and Van Den Bogert, 1990). More specifically, the findings show that ankle cutaneous and osseous markers show better range and pattern of motion repeatability than the subtalar joint markers. Additionally, the correlations between the cutaneous and osseous markers at the ankle tend too vary less than those at the subtalar joint. Support for these observations may be partially due to skin wrinkling that was observed during the movements at the subtalar joint. Although that two specimen were investigated, the preliminary findings tend to support that range and pattern of motion displacement repeatability are obtained with the use of cutaneous or osseous markers and that cutaneous marker displacements are attached with errors. This investigation is currently being conducted with a greater number of fresh amputated human specimens.

REFERENCES

ALLARD P et al.: Eng Med & Bio Sept: 31-36, l987.
ENGSBERG JR: J. Biomech 20:429-442, 1987.
HICKS JH: J. Anat 87:345-357, 1953.
ISMAN RE et al.: Bull Pros Res 10-11:97-129, 1969.
MANTER JT: Anat Rec 80:397-410, 1941.
Ottevenger EJC: J. Biomech 22:957-962, 1989.
Van Den Bogart AJ: J.Biomech 23: 97-101, 1990.
Van Langelaan EJ: Acta Ortho Scand 204: 1-169, 1983.
Weeren PR: J. Biomech 19:879-883, 1988.

COMPARISON OF MECHANICAL POWER AND AEROBIC DEMAND DURING WALKING

Philip E. Martin[1], Gary D. Heise[2], and Don W. Morgan[3]
[1]Exercise and Sport Research Institute, Arizona State University, Tempe, AZ 85287; [2]Biomechanics Laboratory, Penn State University, University Park, PA 16802; and [3]Department of Physical Education, University of North Carolina, Greensboro, NC 27412

INTRODUCTION

Total body mechanical power output (PO) was quantified for 14 subjects during 1.69 $m \cdot s^{-1}$ walking using center of mass-(CM), segment-(SEG), and kinetic-based (KIN) computational models to determine if PO accounts for a substantial portion of observed interindividual differences in aerobic demand ($\dot{V}O_2$). Expressions for PO varied considerably from one computational method to another as expected. Correlations between PO and $\dot{V}O_2$ were generally low and not statistically significant. In addition, no computational method was clearly superior to others in the ability to account for $\dot{V}O_2$ differences. It appears that either the PO modeling schemes were inadequate or simply that PO does not satisfactorily explain interindividual differences in steady state aerobic demand.

REVIEW AND THEORY

Previous research has indicated that differences between individuals in movement economy (i.e., steady-state $\dot{V}O_2$ normalized to body mass) can be considerable (Conley & Krahenbuhl, 1980; Daniels, 1985). It has been suggested that mechanical descriptors of the gait cycle may help to explain interindividual differences in economy (Frederick, 1985). Because mechanical PO is often considered to reflect muscular output of the body during a movement, it is reasonable to hypothesize that PO may explain a substantial portion of sample variability in economy. PO was found to correlate highly with metabolic demand for both walking and running when multiple speeds were studied (Shorten et al., 1981; Burdett et al., 1983). The strength of the $\dot{V}O_2$-PO relationship is less clear, however, for a given speed of locomotion.

METHODS

Fourteen healthy, young adult males ($\bar{X}_{age}$=26.7±4.8 yrs, $\bar{X}_{mass}$=75.0±8.3 kg, $\bar{X}_{ht}$=176.5±7.8 cm) served as subjects. Each subject performed treadmill walking for 6 min at 1.69 $m \cdot s^{-1}$ (0% grade) for $\dot{V}O_2$ determination. Overground walking at the same speed (±3%) was subsequently performed on a 10 m walkway containing a force platform. PO and total body angular impulse (AI), which provides an additional kinetic descriptor of muscular output, were computed using data from a sagittal plane cine record of the gait pattern recorded at 50 fps and ground reaction force data synchronized with the cine record. Two trials were analyzed for each subject. CMPO (e.g., Fukanaga et al., 1980) was computed with and without exchange between kinetic and potential energy components ($\dot{W}_{CMex}$ and $\dot{W}_{CMnex}$, respectively). Similarly, SEGPO (e.g., Pierrynowski et al., 1980; Williams & Cavanagh, 1983) was computed using assumptions of no energy transfers ($\dot{W}_{SEGn}$), within segment transfers ($\dot{W}_{SEGw}$), within and between adjacent segment transfers ($\dot{W}_{SEGwba}$), and within and between any segment transfers ($\dot{W}_{SEGwb}$). KINPO quantification (e.g., Elftman, 1940; Robertson & Winter, 1980) focused on the average PO attributed to the actions of the net joint

moments ($\dot{W}_{JM}$). AI was computed by first integrating the net joint moments with respect to time and then summing across joints (Burdett et al., 1983).

RESULTS

Table 1. Correlations between $\dot{V}O_2$ and PO.

Variable	Mean±SD	$r_{\dot{V}O2}$
$\dot{V}O_2$ (ml·kg^{-1}·min^{-1})	15.5±0.8	----
$\dot{W}_{CMnex}$ (W·kg^{-1})	3.08±0.35	0.57*
$\dot{W}_{CMex}$ (W·kg^{-1})	0.85±0.26	0.30
$\dot{W}_{SEGn}$ (W·kg^{-1})	6.88±0.41	0.18
$\dot{W}_{SEGw}$ (W·kg^{-1})	4.20±0.35	-0.20
$\dot{W}_{SEGwba}$ (W·kg^{-1})	3.43±0.32	-0.18
$\dot{W}_{SEGwb}$ (W·kg^{-1})	1.69±0.42	0.14
$\dot{W}_{JM}$ (W·kg^{-1})	6.24±0.43	-0.07
AI (N·m·s·kg^{-1})	2.07±0.17	0.32

DISCUSSION

$\dot{V}O_2$ for the sample ranged from 14.3 to 17.0 ml·kg^{-1}·min^{-1}, displaying somewhat less variability than has been observed previously in other samples. Results demonstrated that only one correlation ($\dot{W}_{CMnex}$ vs $\dot{V}O_2$) was statistically significant ($p<0.05$). The strength of this relationship was exaggerated, however, by the somewhat extreme responses of two subjects. With this in mind, none of the PO expressions accounted for a significant portion of the variability in $\dot{V}O_2$. In addition, there was no indication that one computational approach produced a PO estimate more closely related to $\dot{V}O_2$. These results were contrary to the expected trend of stronger relationships between kinetic-based estimates of muscular output ($\dot{W}_{JM}$ and AI) and $\dot{V}O_2$. In summary, no PO expression from the present study satisfactorily explained the somewhat limited variability observed in $\dot{V}O_2$ during walking. It appears that either the PO modeling schemes used in this analysis were inadequate or that explanations for interindividual differences in steady state aerobic demand lie elsewhere.

REFERENCES

Burdett, R.G. et al. Comparison of mechanical work and metabolic energy consumption during normal gait. J Orthop Res 1: 63-72, 1983.

Conley, D.L. & Krahenbuhl, G.S. Running economy and distance running performance of highly trained athletes. Med Sci Sports Exerc 12: 357-360, 1980.

Daniels, J.T. A physiologist's view of economy. Med Sci Sports Exerc 17: 332-338, 1985.

Elftman, H.J. The work done by muscles in running. Am J Physiol 129: 672-684, 1940.

Frederick, E.C. Synthesis, experimentation, and the biomechanics of economical movement. Med Sci Sports Exerc 17: 44-47, 1985.

Fukanaga, T. et al. Effect of running velocity on external mechanical power output. Ergonomics 23: 123-136, 1980.

Pierrynowski, M.R. et al. Transfers of mechanical energy within the total body and mechanical efficiency during treadmill walking. Ergonomics 23: 147-156, 1980.

Robertson, D.G.E. & Winter, D.A. Mechanical energy generation, absorbtion, and transfer amongst segments during walking. J Biomech 13: 845-854, 1980.

Shorten, M.R. et al. Mechanical energy changes and the oxygen cost of running. Engin in Med 10: 213-217, 1981.

Williams, K.R. & Cavanagh, P.R. A model for the calculation of mechanical power during distance running. J Biomech 16: 115-128, 1983.

A DYNAMIC CONSTRAINT ON UPRIGHT STANDING

Yi-Chung Pai
Programs in Physical Therapy, Northwestern University Medical School
Chicago, IL 60611

Introduction

Falling in the elderly frequently occurs during different forms of dynamic weight transfer[2,3,5]. A basic question may be raised as to what the constraints are imposed on a person who is trying to maintain upright standing upon the completion of a dynamic weight transfer.

One of the constraints often used in mathematical modelling for the control of standing is that the vertical projection of the body center of mass (CM) has to be confined within the base of support[1]. During the termination of a dynamic weight transfer, there seems to be another crucial constraint, that is, the maximum horizontal linear momentum of the CM that a person can brake to bring the body to a stop.

A previous study[4] revealed that among healthy young adults there was an apparent limit on the amount that one could increase the maximum horizontal linear momentum of the CM during the performance of the sit-to-stand (STS). The purpose of this study was to examine the hypothesis that this limit was related to the need to maintain upright standing at the termination of the STS.

Methods

Nine healthy adults (27-39 year-old) participated in the experiment. Each person performed five trials of the STS task at slow, natural and fast speeds. In addition, each person also performed the STS at fast speeds, and continued to fall-forward upon the completion of the STS until the movement was stopped by a railing placed 0.5m in the front.

A WATSMART motion analysis system was employed to determine the location and orientation of the body segments during the performance. The linear momentum of the CM was computed from the motion analysis. A two-way ANOVA with repeated measures was applied to evaluate the differences in the maximum linear momentum of the CM in different directions and under different test conditions. A multiple paired t-test was used to determine the source of significance.

Results

The results from the two-way ANOVA indicated significant differences ($p<0.01$) in the maximum linear momentum of the CM for the horizontal and vertical directions and for different speed (test) conditions. Fig. 1 shows the mean and standard deviation of the maximum horizontal and vertical linear momentum of the CM derived from different test conditions. Horizontal bars show the pairs of means which are **not** significantly different from each other ($p<0.01$).

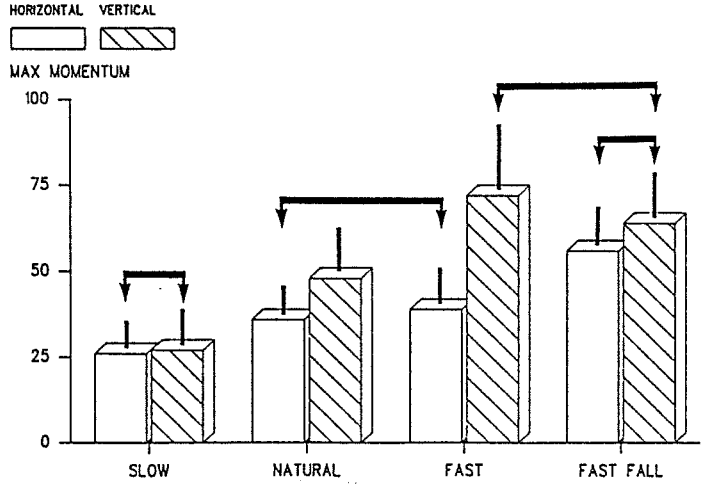

Fig. 1 The group (n=9) mean and one standard deviation of the maximum linear momentum of the body center of mass in the horizontal and vertical directions during sit-to-stand at slow, natural, fast speeds and fast sit-to-stand followed by fall-forward. Any two means NOT connected by double-arrow-headed line are significantly different ($p<0.01$).

Discussion

The results of the present study confirmed the previous observation[4] that there was an apparent limit on the maximum linear momentum of the CM in the horizontal direction during the STS from natural to fast speeds, whereby the increase in the speed of ascent was primarily achieved through the increase in the maximum vertical linear momentum of the CM. However, when these subject were allowed to fall-forward at the termination of the STS, they were able to generate greater maximum horizontal linear momentum than in the regular fast STS movement. These results indicated that the limitation in the maximum horizontal linear momentum was one of the constraints imposed on a standing person at the termination of the STS. These subjects were able to exceed this limit only when they did not have to stand upright. It remains to be identified, however, that such a limit exists in the termination of other types of dynamic weight transfer.

The results also indicated that the subjects were able to produce greater propulsive impulses with greater maximum horizontal linear momentum of the CM once the motion could be stopped by the additional contact force received through arm support during the fast STS-fall-forward movement. Thus, the limitation on the maximum horizontal linear momentum during the fast STS appeared to be related to a person's ability to generate sufficient braking impulses. The ability to brake the linear momentum to bring the body to a stop within the region of stability may be further limited among individuals with neurological or musculoskeletal disorders.

Acknowledgement: The author wish to thank Dr. Jack L. Lewis for his valuable comments. This project was supported by Northwestern University Medical School BRSG RR-05370, USPHS, NIH.

References

1. Gordon, M.E. The biomechanics and muscular synergies of human upright posture. Internal report, Stanford University, 1986.
2. Naynov, R and Rosin A. J. Falling as a cause of admission to a geriatric unit. *Practitioner* 205:327-330, 1970.
3. Overstall, P.W., Exton-Smith, A.N., Imms, F. J., Johnson, A. L. Falls in the elderly related to postural imbalance. *Br. Med. J.* 29:261-262, 1977.
4. Pai, Y.C. and Rogers, M.W. Control of body mass transfer as a function of speed of ascent in sit-to-stand. *Med. Sci. Sports Exer.* In press, 1990.
5. Sheldon, J. H. On the natural history of falls in old age. *Br. Med. J.* 2:1685-1690, 1960.

ACCURACY AND PRECISION OF THE DIRECT LINEAR TRANSFORMATION TECHNIQUE (DLT) IN VERY CLOSE RANGE PHOTOGRAMMETRY WITH VIDEO CAMERAS

Michel Leroux, Paul Allard and Norman Murphy

Pediatric Research Center, Sainte-Justine Hospital, Montreal, CANADA, H3C 3J7.
Departement of Physical Education, University of Montreal, CANADA, H3T 1C5.

INTRODUCTION:

Several researchers have reported acceptable accuracies afforded by the DLT but few have analysed 3-D reconstruction errors arising from very close range photogrammetry. The object of this study is to determine how sensitive the DLT technique is in three-dimensional (3-D) very close range reconstruction using video cameras. The factors studied were the number and the distribution of control points, as well as extrapolations outside the calibration device. The results show that the DLT is an accurate technique when used in very close range using video cameras. The number of control points dont have to be numerous, especially if they are not well distributed. The calibration device must deliminated the space occupied by the experimental set-up since extrapolation and reconstruction gives poor accuracy and precision. Optimal control point distribution permit that the calibration device be seen throughout the experimental procedures.

REVIEW AND THEORY:

The methods of analytical photogrammetry are used because of the high measurement precision required in the context of 3-D kinematic and kinetic studies of the movements of a few or of small body segments, for instance the foot movement or for the geometrical modelling of body joints like the ankle (Allard et al., 1987; de Lang et al., 1990; fioretti et al., 1985). Several researchers (Shapiro, 1978; Wood and Marshall, 1986) have reported acceptable accuracies afforded by the DLT technique (Marzan and Karara, 1975) but few have analysed 3-D reconstruction errors arising from very close range photogrammetry. The reconstruction accuracy of present photogrammetric studies of the ankle (Allard et al., 1987) is limited by the digitizing tablet (± .4 mm). The utilisation of video cameras with direct X, Y position measurement (pixels) should provided less limitations. The object of this work is to determine how sensitive the DLT technique is in very close range using video cameras as opposed to photographs. More specifically, the effect of the number and the distribution of control points, as well as extrapolations outside the calibration device were verified. An other important consideration lies in the possibility to have control points visible on each image providing the opportunity to move cameras during experimental session.

METHOD:

The experimental set-up consisted of two CCD (NEC TI-23A) video cameras fixed at 58 cm from the calibration device. The distance between cameras was 42 cm, each camera making an angle of 21 degrees with this base line. The calibration device 300 mm high, 245 mm long and 185 wide consisted of nine vertical rods (3 rows and 3 columns). Nine flat reflective markers, 3mm diameters, were located on each rod at approximatively 20 mm intervals. A vertical height vernier, accurate to .02 mm was used to measure the real 3-D coordinates of the reference markers. The centroids of each marker on the video stereopairs were reconstructed using the 11 parameters DLT. The sensitivity of the DLT using 8, 15 and 21 control points was verified with 16 points located in the calibration space were used to measure reconstruction accuracy. Additionnally, control points distribution was evaluated in two ways. Firstly, 15 points were randomly selected to define an asymetric large space. Reconstruction results were then compared to the previous 15 control point recontruction. Secondly, non-uniform control point distribution (eight control points, one

at each corner of the device) and 7 other points located at the front, the right or the bottom of the calibration device was verified. Finally, extrapolation in each dimension was made using only an half device for calibration. The accuracy of outside point reconstruction was compared with inner point reconstruction.

RESULTS AND DISCUSSION:

The reconstruction accuracy (absolute error) and precision (variable error) were calculated for length (X), height (Y) and depth (Z) for each condition. When video cameras were chosen, digitizing time was shorter. Pixel fluctuations in different images were also observed but this phenomenon dit not alter the results.The number of control points slightly influenced the results. More specifically, the accuracy and precision are slightly better with 15 and 21 points (0.15 ± 0.13 mm, 0.13 ± 0.10 mm and 0.27 ± 0.19 mm for X, Y, Z respectively) then for 8 points (0.22 ± 0.16 mm, 0.17 ± 0.10 mm, 0.30, ± 0.25 mm). Due to these results, 15 control points were used for all other conditions. The results for an asymetric distribution of control points are not as good (0.18 ± 0.13 mm, 0.19 ± 0.17 and 0.30 ± 0.22 mm). While non-uniform distribution conditions (Table 1) show even worse results, with the major differences occuring in the reconstructed (Z) dimention. The accuracy and the precision for every extrapolation (Table 2) showed the worst results. The major differences also occured in the z dimension with errors around 1mm.

In conclusion, the DLT technique provided accurate and precise 3-D coordinates when used in very close range photogrammetry with video cameras. Good results can be obtain with a few number of control points. Results are only slightly better if several control points are used and if they are well distributed. but they must deliminated the space used with the experimental set-up because extrapolation and reconstruction produced erroneus coordinates. Optimal control point distribution permit that the calibration device be seen throughout the experimental procedures.

Table 1. Non-uniform distribution

	X (mm)	Y (mm)	Z (mm)
High			
AE	0.23	0.18	0.46
VE	0.19	0.18	0.36
Right			
AE	0.22	0.23	0.48
VE	0.17	0.22	0.36
Front			
AE	0.23	0.23	0.47
VE	0.19	0.22	0.40

Table 2. Extrapolation

		X (mm)	Y (mm)	Z (mm)
back				
intra	AE	0.16	0.17	0.31
	VE	0.13	0.15	0.20
extra	AE	0.21	0.33	0.46
	VE	0.24	0.26	0.31
left				
intra	AE	0.17	0.21	0.48
	VE	0.10	0.17	0.24
extra	AE	0.47	0.39	1.37
	VE	0.23	0.26	0.96
up				
intra	AE	0.14	0.26	0.44
	VE	0.08	0.17	0.19
extra	AE	0.54	0.39	0.43
	VE	0.27	0.26	0.29

REFERENCES:

Allard et al. (1987) IEEE, sept., 31-36.

de Lang et al. (1990) J. Biomech., 25, 259-270.

Fioretti et al. (1985) J. Biomech., 18, 831-842.

Marzan and Karara (1975) Symposium on Close Range Photogram. Systems, 420-473.

Wood and Marshall (1985) J. Biomech., 19, 781-785.

THE RELATIONSHIP BETWEEN MAXIMUM GROUND REACTION FORCES AND LOWER EXTREMITY EXTENSOR JOINT MOMENTS DURING LANDING

J.S. Dufek and B.T. Bates
Biomechanics / Sports Medicine Laboratory
University of Oregon
Eugene, Oregon 97403, USA.

INTRODUCTION

The forces acting on a performer during landing have been documented by several investigators (1, 2, 3). More recent research attention has focused on joint moments of force (JMF). This latter emphasis may have emanated from comments by Winter (4) suggesting that the joint moment patterns may be representative of the desired motor program. Both ground reaction forces (GRFs) and extensor moments (EMs) have implications to injury, therefore, a better understanding of the relationships between these performance characteristics is essential for injury prevention. The purpose of the study was to examine the relationships between the maximum vertical ground reaction forces and the peak lower extremity extensor joint moments of force during landings. More specifically, the timing, magnitude and variability of the first and second maximum vertical ground reaction force and peak lower extremity extensor moment values were evaluated during landings while manipulating height, distance and technique (knee joint flexion).

METHODS

Three volunteer male subjects performed landings (total n=156) onto a force platform (500 Hz) from three heights (40, 60, 100 cm) and three distances (40, 70, 100 cm) using three landing techniques (slight = SF, moderate = MOD, full flexion = FF) while being filmed (100 Hz) from a right sagittal view. The first (F1) and second (F2) maximum vertical GRF and the times to these events (T1 and T2, respectively) were identified for each trial. Anthropometric measures were obtained and ankle (A), knee (K) and hip (HP) JMFs calculated using a Newtonian model. The peak EMs and corresponding times were identified for all joints during the landing phase (150 ms post-contact).

RESULTS AND DISCUSSION

The average temporal occurrences of the peak EMs (369, 271, 432 ms for A, K and HP, respectively) were more closely associated with F2 (420 ms) than F1 (126 ms). The specific sequencing of F2 and the peak EMs was variable across the levels of H and D with a general temporal pattern of K-A or A-K followed by HP-F2 or F2-HP. The main effect of T exhibited the only consistent sequencing pattern (K-A-F2-HP). Overall temporal variabilities as expressed by the coefficient of variation (CV) were 23.8, 25.3, 25.9, 48.0 and 97.8 for T2, T1 and the HP, A and K joint peak EM occurrences, respectively.

Group mean GRF and peak EM values are given in Table 1. Although a distinct temporal patterning was observed for F1 and F2, both events occurred within the first 50 ms of contact and therefore can be classified as passive impact forces. For this reason, it may be more appropriate to evaluate these two events collectively. The combined values (F1 + F2) for the conditions of greatest task demand (H100, D100, SF) were on the average 1.35 times greater than for the comparable least demanding tasks (H40, D40, FF). These values compare with 1.18 and 1.43 times for F1 and F2, individually. The corresponding CVs for these events were 75.9 (F1) and

36.4 (F2). Increased task demand produced inconsistent results for the peak EMs. An increasing EM magnitude pattern was observed for the K joint across H and D (2.36 and 1.11 times, respectively) while both the A and HP joints exhibited varying orders of magnitude relative to the task demands. The greatest single difference for the A joint EM was observed across T (2.10 times) and across H (1.55 times) for the HP moment. The EM data results illustrate the dominance of the proximal joints with the overall magnitude of the HP EMs being 2.67 and 1.52 times those of the A and K joints, respectively. Conversely, EM variability values increased from proximal to distal with mean CV values for the HP, K and A of 61.2, 90.2 and 174.5, respectively. This pattern of joint variability is opposite that reported by Winter (4) for normal gait. A possible explanation for these differences may be the reverse contact pattern (toe-heel vs heel-toe) associated with the two activities. A toe-heel contact could result in a more active role on the part of the HP joint in decelerating the trunk mass and securing and maintaining balance during the landing.

In summary, the GRFs increased in magnitude and variability with task demands imposed by landing H, D and T. This pattern was not observed for the peak EMs which exhibited differential responses across landing conditions. EM joint variability was observed to increase from proximal to distal in contrast to the patterns reported for normal gait.

REFERENCES

1. Lees, A. Engineering Med., 1981.
2. Panzer, et al. Biomech. XI, 1988.
3. Valiant, et al. Biomech. IX-B, 1985.
4. Winter, D.A. Human Movement Science, 1984.

Table 1. Mean Ground Reaction Force and Lower Extremity Joint Extensor Moment Values

Source	(trials)	Forces (N/kg) F1	Forces (N/kg) F2	Extensor Moments (N.m/kg) Ankle	Extensor Moments (N.m/kg) Knee	Extensor Moments (N.m/kg) Hip
Overall		11.40	37.31	3.93	6.92	10.50
		(8.65)	(13.58)	(6.86)	(6.24)	(7.28)
H40	(n=44)	11.49	26.82	3.34	3.91	8.02
		(12.77)	(10.43)	(2.65)	(1.14)	(4.62)
H60	(n=45)	6.54	36.31	4.43	6.39	10.03
		(3.41)	(11.55)	(12.13)	(10.03)	(11.67)
H100	(n=67)	14.61	44.87	3.97	9.25	12.44
		(5.92)	(11.87)	(2.74)	(2.72)	(3.43)
D40	(n=52)	9.62	36.05	3.12	6.55	9.32
		(5.49)	(11.09)	(1.35)	(3.59)	(3.64)
D70	(n=62)	11.87	36.06	4.87	7.00	11.36
		(9.45)	(15.62)	(10.36)	(8.99)	(10.48)
D100	(n=42)	12.92	40.72	3.54	7.26	10.70
		(10.27)	(12.83)	(3.71)	(3.30)	(4.22)
FF	(n=47)	12.89	32.10	3.65	6.88	10.29
		(10.23)	(9.86)	(2.40)	(2.92)	(5.41)
MOD	(n=61)	9.79	33.19	3.13	5.99	9.34
		(7.29)	(12.29)	(3.14)	(3.42)	(3.63)
SF	(n=48)	12.00	47.65	5.23	8.16	12.23
		(8.39)	(12.71)	(11.72)	(10.23)	(11.25)

Note: See text for abbreviations.
Values in parentheses are standard deviations.

EFFECT OF AXIAL LOAD AND ANKLE POSITION ON ANKLE STABILITY

*D.A. Skrade, †R.L. Needleman, *J.B. Stiehl, and *K.B. Scheidt
*Dept. of Orth. Surg., Med. Coll. of Wis., Milw., 53226, USA
†15 Lowell St., Portland, Maine, 04102, USA

Introduction

Cadaveric ankle stability was evaluated in 4 different modes of testing, and with varying axial loads and ankle positions. The purpose of these experiments was to acquire basic knowledge of ankle mechanics, and to provide a basis for further study. Results show that load and ankle flexion significantly effect ankle stability, and that the ankle is not necessarily most stable in dorsiflexion.

Review and Theory

Previous studies have shown that torsional stability of the ankle increases with loading, but the effects of flexion angle were not entirely clear[1,2]. Ankle stability has also been evaluated in the unloaded condition for torsion, inversion/eversion, and anterior/posterior drawer[3]. It was stated that in the majority of the tests, the dorsiflexed ankle tended to show the least amount of laxity. This corroborates the well-accepted belief that the dorsiflexed ankle is more stable because of a tighter fit of the talus in the ankle mortise[4].

Methodology

10 cadaveric ankle specimens were tested according to methods reported previously[5]. Briefly, this involved testing on an MTS system in 4 modes: 1) flexion; 2) torsion; 3) version; and 4) drawer. The latter 3 modes were carried out in dorsiflexion, neutral, and plantar flexion. All 4 modes were done with 15kg and 70kg axial loads. A repeated measures ANOVA statistical method was used.

Results and Discussion

The effect of load on ankle flexion (Figure 1) was significant ($p<.0005$). This effect was much greater for plantar flexion than for dorsiflexion. Clinical measurement of this range of motion is often taken in the unloaded state[6].

The effects of load and ankle position on torsion (Figure 2) were significant ($p<.005$), as was the interaction between load and flexion for external rotation ($p=.006$). These results conflict with those of McCullough and Burge, who stated that flexion angle had no effect on internal/external rotation. Results for external rotation show that the ankle is not necessarily more stable in dorsiflexion.

The effect of load and flexion on ankle version (Figure 3) was significant ($p<.005$), as was the interaction between load and flexion ($p=.05$). Stability was greatest in dorsiflexion and least in plantar flexion, but this effect was much less pronounced for eversion, and inversion at 70kg.

Figure 1. Effect of Load on Ankle Flexion

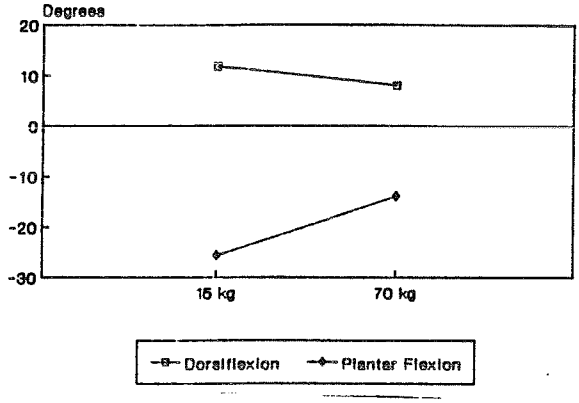

Figure 3. Effect of Load and Ankle Position on Ankle Version

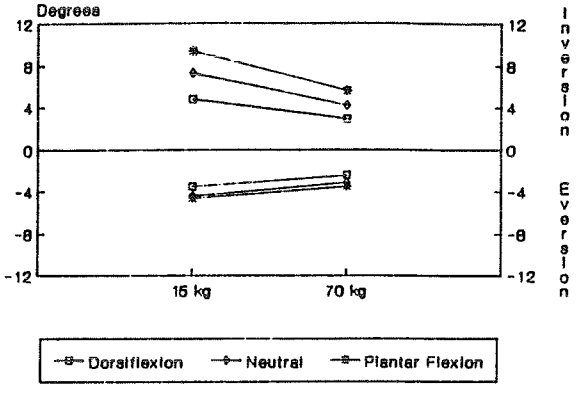

Figure 2. Effect of Load and Ankle Position on Ankle Torsion

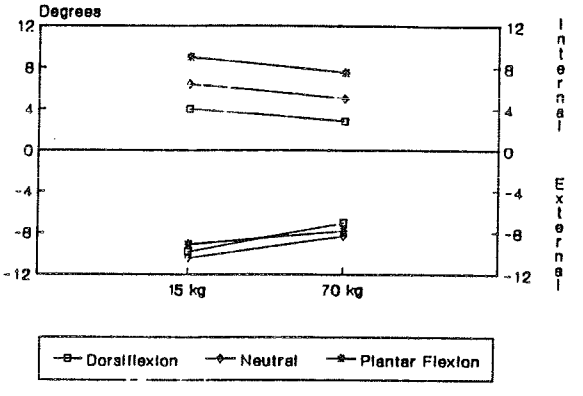

Figure 4. Effect of Load and ANkle Position on Ankle Drawer

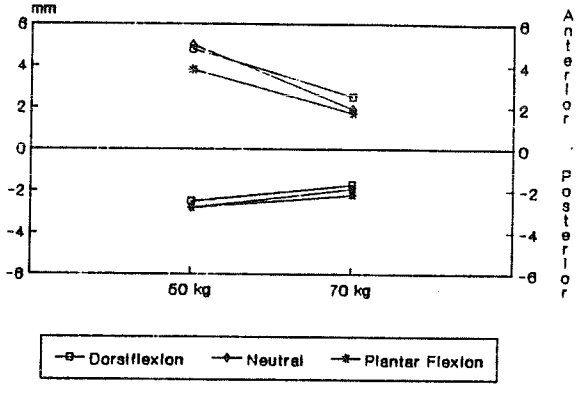

The effect of load was significant for ankle drawer ($p<.005$; Figure 4). Flexion angle had a significant effect on anterior drawer ($p=.017$), but not on posterior drawer. There was not a significant interaction between load and flexion. For anterior drawer, plantar flexion was the most stable position. Factors other than mortise geometry may be much more critical in anterior/posterior translation than in other modes of testing. A/P stability is critical because of the shear forces at the ankle joint during gait[7].

Further studies will aim at delineating the mechanisms for the effects found in this study, focusing especially on the effects of load and ankle position on ligament tension. Preliminary data indicates that strain in the syndesmotic ligaments is affected by these factors, thereby providing a means for stabilization of the ankle joint.

References: 1. Fraser & Ahmed, Orthop Trans 7:248, 1983. 2. McCullough & Burge, JBJS 62-B:460-464, 1980. 3. Johnson & Markolf, JBJS 65A:81-88, 1983. 4. Frankel & Nordin, Basic Biom. of the Skel. System, 2nd Ed., 1989. 5. Needleman et al., Foot and Ankle 10:17-24, 1989. 6. Lindsjo et al., CORR 199:68-71, 1985. 7. Stauffer et al., CORR 127:189-196, 1977.

A THRESHOLD TO DETERMINE OPTIMUM CUTOFF FREQUENCY IN AUTOMATIC DATA SMOOTHING USING DIGITAL FILTER

Takashi Yokoi* and Jill L. McNitt-Gray**
*Industrial Products Research Institute,Tsukuba,Ibaraki 305,JAPAN
**Dept. of Exer. Sci., Univ. of South. California,Los Angeles, CA

INTRODUCTION

Digital filter is often used in the data smoothing for kinematic and kinetic analysis of human movement. It is indispensable for automatic smoothing using the filter to make automatic selection of the optimum cutoff frequency(OCF).

Several ideas were proposed for the automatic determination of OCF[1,2,6,8]. Welles and Winter[6] introduced a method using root mean square deviation(RMS) and the threshold for automatic specification of a cutoff frequency. Jackson[2] and Hinricks[1] proposed an idea to determine optimum cutoff frequency using the 2nd derivative of RMS deviation (2DRMS). Since the 2nd derivative settles down to a small value as soon as a certain value is passed and the 2DRMS curve is nearly linear, the 2DRMS method may enable clear selection of OCF. However, suitable threshold to choose OCF was not proposed in the 2DRMS method. The purposes of this study were to present a modified technique for determining OCF using 2DRMS method and to propose the threshold to select OCF for smoothing data of various human movement.

METHOD

To create a test data set, Pezzack's data[3] was modified by adding normal random noises with the standard deviations of 0.02, 0.03, 0.04 and 0.05 rad[5]. Several human movement was also analyzed to create test data sets.

Second order Butterworth type digital filter proposed by Saito and Yokoi[4] was used in the smoothing. The RMS residuals between raw and the smoothed data were computed for the cutoff frequencies ranging from 0.5 to 15.0 Hz. For normalizing the RMS, standard deviation of each raw data was computed and the RMS residual at each cutoff frequency was expressed as the percentage of 3*(standard deviation). The 2DRMS was obtained based on the normalized RMS data.

RESULTS AND DISCUSSION

The examples of 2DRMS curves for modified Pezzack's data set(MPD) were shown in Figure 1. The 2DRMS curve shifted to the left with increase in the amount of noise. Also, rapid change due to the noise was shown in 2DRMS curves of MPD. These results may indicate the OCF for MPD depends on the amount of noise included in the data. Based on the previous investigations[5,7], the optimum cutoff frequency for Pezzack's data is around 4Hz. In order to satisfy this value, the suitable threshold in the present method was assumed to be 0.1[%/Hz^2]. Figure 2 shows representative acceleration curves of the smoothed MPD using OCF selected based on the above threshold. The patterns and peak

values of these curves were similar to those obtained in previous reports[5,7].

The present threshold was also applied to the data smoothing for several human movement. For example, the OCFs for the vertical coordinate of the toe were around 9Hz in sprint running and around 6Hz in walking. Based on the previous investigations, the cutoff frequencies selected by using present threshold were thought to be appropriate for the data smoothing in human movement analysis.

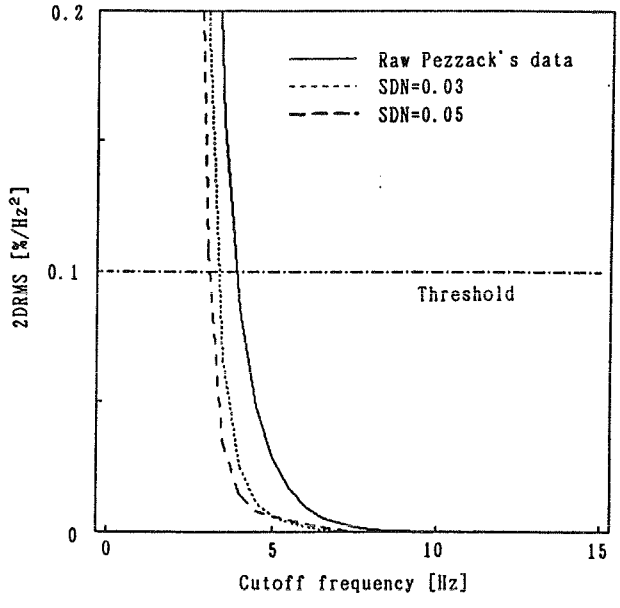

Figure 1 2DRMS vs cutoff frequency for modified Pezzack's data(Sampling frequency=49.8Hz).
SDN:Standard deviation of normal random noise[rad]

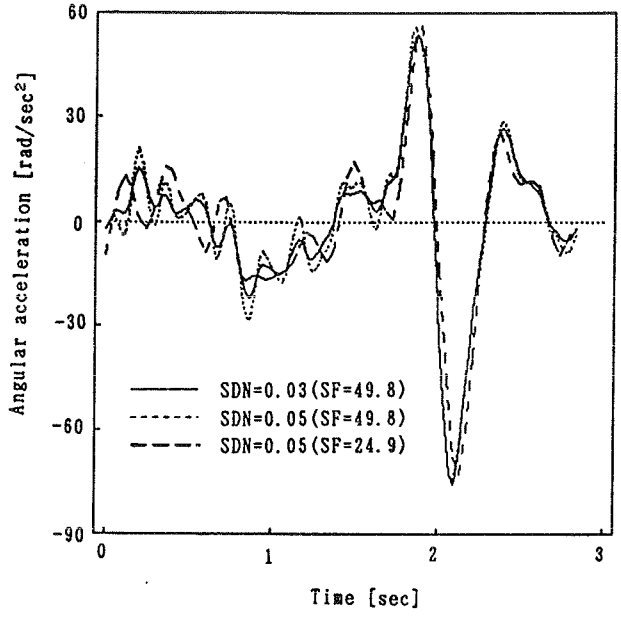

Figure 2 Angular acceleration of modified Pezzack's data.
SDN:Standard deviation of normal random noise[rad]
SF:Sampling frequency[Hz]

REFERENCES

[1]Hinrichs,R.N., Ph.D. dissertation, Pennsylvania State University, 1982.
[2]Jackson,K.M., IEEE transactions on biomedical engineering BME-26, 122-124. 1979.
[3]Pezzack,J.C., J. Biomechanics 10:377-382. 1977.
[4]Saito,S. and Yokoi,T., Health & Sport Science, The University of Tsukuba 5:201-206. 1982.
[5]Smith,G, J. Biomechanics 22:967-971. 1989.
[6]Welles,R.P. and Winter,D.A., Human Locomotion I:92-93. 1980.
[7]Wood,G.A., Exercise and Sport Science Reviews Vol.10,pp.308-362. 1982.
[8]Yu,B., Proceedings of the XII International Congress of Biomechanics, pp.113-114. 1989.

A NEW AUGMENTED FEEDBACK SYSTEM FOR IMPROVEMENT OF CYCLING EFFICIENCY

Everett Harman, Richard Rosenstein and Peter Frykman
Exercise Physiology Division
U.S. Army Research Institute of Environmental Medicine
Natick MA 01760-5007

INTRODUCTION

A new hardware/software system was developed to provide instantaneous, animated feedback of motor performance as a tool for teaching cycling efficiency. The system was effective in rapidly bringing about the desired changes in motor technique. A controlled experiment, using the feedback training system, is currently under way to determine if the motor changes improve efficiency, and if learned motor patterns are retained. The methodology shows considerable potential for application to sport training and rehabilitation.

REVIEW AND THEORY

Augmented feedback training is a well established clinical tool for neuro-muscular re-education and establishing control over autonomic functions (7). More recently, attempts have been made to employ feedback to facilitate learning of motor skills (1), but few of the experimental results have been reported in refereed journals or textbooks.

Feedback that is continuous and instantaneous has been shown to facilitate skill acquisition most effectively (6). Yet, the motor activity feedback experimentation reported on to date has provided only delayed feedback, due to technology-based limitations in the speed at which data could be input, processed and displayed.

In responding to an apparent need, our goal was to develop a new motor learning system in which feedback would be virtually instantaneous, allowing immediate technique modification by the subject. Ergometer cycling was selected as the activity to which the methodology would initially be applied, because of its relatively simple, repetitive, localized nature. Efficiency was chosen as the parameter to be improved because of its relationship to effective performance of a wide range of human activities.

Force exerted on a cycle pedal can be resolved into 1) a tangential component which serves to rotate the crank, and 2) a radial component which unsuccessfully acts to stretch or compress the crank arm. The latter force is of significant magnitude but has no motive effect (2). Because generation of even ineffective muscle force requires metabolic energy expenditure, it has been hypothesized that minimization of the radial forces would improve cycling efficiency (5).

METHODOLOGY

Transducers mounted on a cycle ergometer (3,4) produced voltages proportional to 1) forces applied perpendicular and parallel to the surface of each pedal, 2) the angle of each pedal relative to its crank-arm and 3) the angle of the crank-arm relative to the cycle frame. These signals were digitized by a Microstar DAP 1200 data acquisition/ signal processing board and passed to a Zenith 248 PC-compatible computer with 12.5 Mhz Intel 80286 CPU. Using a method previously described (3), the radial components of

the transduced left and right pedal forces were rapidly calculated directly on the board, allowing computer processing time to be dedicated to displaying the feedback. Figure 1 is a black-and-white rendition of the feedback-providing color-display on the computer monitor. The left and right vertical bars were proportional to the radial forces exerted by each foot. The rapid signal processing enabled update of the bar heights 30 times per second, making the information appear animated and instantaneous. Subjects were instructed to try to minimize the bar heights while cycling.

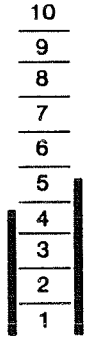

Figure 1. Appearance of the feedback-providing computer screen. Animated vertical bars reflected instantaneous left and right radial forces on an arbitrary scale.

RESULTS

Preliminary testing of the feedback system showed that, almost immediately, it enabled subjects to make readily observable reductions in radial forces while cycling at a constant power level.

DISCUSSION

A controlled study is presently underway to determine 1) the specific changes in pedalling technique brought about by the feedback training, 2) whether the technique changes are accompanied by greater cycling efficiency as measured by rate of oxygen consumption at a given power output, and 3) if and at what rate the feedback-acquired skills degrade.

Augmented feedback training for improvement of motor skills is a nascent area of biomechanics, but one that has considerable potential for application to sports training and rehabilitation. Using different types of transducers, the methodology described herein can be adapted for modifying motor activities other than cycling, such as walking and running. The faster signal processing required by more complex physical activities could readily be implemented with higher-speed computers, signal processing boards, and graphics boards. Current PC-compatible computers based on the Intel 80386 and 80486 CPUs, used in conjunction with faster signal processing boards from Microstar and other companies, as well as 16-bit VGA boards can increase system processing speed many times over.

CONCLUSIONS

The new system for improvement of cycling efficiency represents an advance in the area of feedback training because it provides feedback that is both continuous and virtually instantaneous, allowing a trainee to make immediate adjustments in technique. This type of system has applicability to the training of many human motor activities.

REFERENCES

1. Broker, J. et al. J Biomech. 22(10):991, 1989.
2. Davis, R. et al. J Biomech. 14(12):857-872, 1981.
3. Harman, E. et al. J Appl Physiol. 62(2)831-836, 1987.
4. Knuttgen, H. et al. J Appl Physiol. 53(3):784-788, 1982.
5. Kunstlinger, U. et al. Eur J Appl Physiol. 54:58-61, 1985.
6. Newell, K. et al. Appl Cog Psych. 1:273-283, 1987.
7. Wolf, S. in **Biofeedback**, J. Basmajian (Ed), Williams and Wilkins, 1979, pp. 5-30.

A NEW TECHNIQUE OF THREE-DIMENSIONAL CINEMATOGRAPHY

John W. Chow
Department of Exercise Science
The University of Iowa, Iowa City, IA 52246

Cinematography has been an essential tool for studying the external mechanics of human motion in the last few decades. Several methods of cinematography have been developed to obtain three-dimensional (3-D) spatial coordinates. However, there are disadvantages and limitations associated with the implementation of these methods. It is the purpose of this study to develop a new technique which incorporates procedures that are much simpler than those associated with existing methods.

Theoretical Consideration of the New Technique

Consider two views of a rectangular box obtained from two cameras (Figures 1a and 1b). The x and y coordinates of a target T inside the box can be determined by projecting T in the negative z direction onto the x,y plane. By simple geometry, the projection of T on the x,y plane must lie on both line *ab* and line *ef*. Thus, the intersection of these two lines in the x,y plane will yield the x and y coordinates of T (Figure 1c). Using the same algorithm, the z coordinates of T can be determined by projecting T in the negative y direction onto the x,z plane (Figure 1d).

Data Collection

A 2-m cube object field was defined by placing a reference pole at the vertical edges of the cube. The object field was videotaped using two super-VHS video cameras located approximately 10 m from the center of the object field. The cameras were placed with their optical axes approximately 1.1 m above the floor level, at right angles to each other, and in line with the diagonals of the base of the cube.

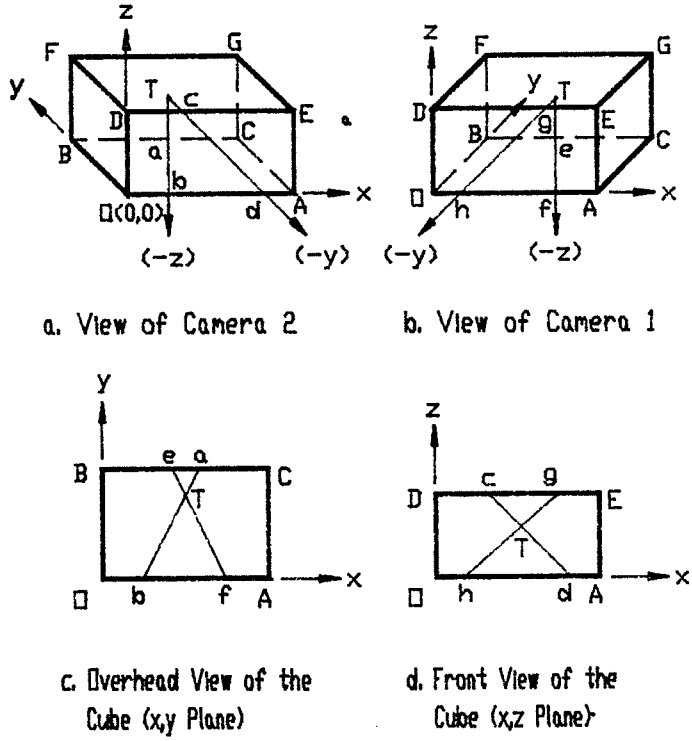

Figure 1. Reconstruction of Spatial Coordinates

A 2-m long reference pole was videotaped when it was placed at the four corners of the base of the cube (i.e., points O, A, B, and C in Figure 1). Two spirit-levels were attached to the pole for the adjustment of the vertical alignment of the pole. 85 targets, evenly distributed inside the cube, and 40 targets, located within 0.5 m outside the boundary of the cube, were also videotaped. The Peak Performance Technologies System for motion analysis was used to obtain coordinate data from the videotapes.

Computation of 3-D Coordinates

The actual images of the cube recorded by the cameras were slightly different from the ones shown in Figure 1 due to lens distortion and the property of linear perspective (i.e., an object appears to be smaller when it is farther away). The negative z projection was obtained by taking the average of the slopes of the four vertical edges -- lines OD, AE, BF, and CG -- of the cube. The negative y projection was obtained by connecting the target to the convergent point of lines OB, DF, AC, and EG. A computer program was written to perform the computations.

Results and Discussion

The computed spatial coordinates of the targets were compared with known actual coordinates and the absolute error was defined as the distance between the computed and actual locations. The results are summarized as follows (S.D. under average value):

	Average Absolute Error (mm)			Resultant
	X	Y	Z	$(X^2+Y^2+Z^2)^{1/2}$
Inside targets (N=85)	6.2	27.4	7.1	30.9
	(4.4)	(20.3)	(9.0)	(20.0)
Outside targets (N=40)	8.2	66.0	4.7	69.1
	(7.8)	(61.2)	(3.1)	(58.9)
Overall (N=125)	6.8	39.8	6.3	43.1
	(5.8)	(42.2)	(7.7)	(41.0)

Further experiments on computational procedures showed that additional procedures such as using polynomial regression equations for scaling image size and dividing the object field into several sub-units could reduce the overall resultant error to less than 15 mm. However, these studies required that the reference pole be videotaped at a few more locations to provide information required for the additional procedures.

Further Studies

Although the measurement errors using this technique are greater than those reported by some users of existing 3-D methods [i.e., Direct Linear Transformation technique (Kennedy, et al., 1989)], the results confirm the feasibility of the new technique and the merit of further study. Further studies have been planned to examine the effect of different camera locations on the accuracy of measurement, and to explore the possibility of extending the new technique to panned cinematography.

Acknowledgement

The author wishes to thank Professors James Andrews and James Hay for their supervision and support of this study.

Reference

Kennedy, P.W., et al., Intl J Sport Biomech, 5:457-460, 1989.

COMPARISON BETWEEN CLINICAL AND COMPUTERIZED EVALUATION OF RESIDUAL CAPACITY IN DISABLED WORKERS

F.J. Bejjani, V.M. Titiloye, J. Jocelevitz, N. Xu
Human Performance Analysis Lab. , New York University
35 West Fourth Street, New York , NY 10003

INTRODUCTION

The incidence of severe disability has increased by more than 70% over the 13 year period from 1966 to 1979, rising from 213 to 365 Americans per 10,000 population (1). An increased number of workers have primary musculoskeletal impairments which may respond to mechanical solutions for resuming activity. In 1977, disability- related expenditures of 63.5 billion were made on behalf of working-age people. These data indicate the gigantic cost of disability and the need to objectively assess residual functional capacity and develop job retraining techniques for disabled workers. The purpose of this study are :1) to establish computerized and clinical evaluations of residual capacity and 2) to determine the reliability of computerized evaluation in disabled workers.

REVIEW AND THEORY

Parish and James (2) illustrated that accurate measurement of disability is an essential component of rehabilitation. Whiting et al.(3) emphasized the clinical value of exercise testing in handicapped patients, using arm crank, bicycle and wheelchair exercises, in order to determine their work capacity and safety of exercise. In his Physical Capacity Evaluation , Austrew (4) discarded standard disability evaluation tests such as neurological screening, localized range of motion, and manual muscle testing as being redundant and not easily applicable to needs mentioned by referrants. He utilized instead gait and posture screening, body mechanics evaluation, and biomechanical analysis. North and Rohmert (5) demonstrated the usefulness of job analysis data in solving a wide range of rehabilitation and ergonomic problems of the disabled at work. Mittelstein-Scheid (6) emphasized the need for matching functional capacity and job requirements, as a tool to facilitate reintegration of disabled people into the workforce. While the former authors used cluster analysis procedure, and the latter used questionnaire data, Ranu (7) adopted an engineering approach to functional assessments of the moderate-to-severely physically handicapped. Thus, the authors of this paper propose to demonstrate and validate a new objective and reproducible method to measure primarily musculoskeletal disability. This method will focus on dynamic quantification of residual functional capacity for work performance - specifically determining both the kinetic and kinematic job requirements.

METHODS

Forty-seven disabled SSDI recipients with musculoskeletal problems of 4 to 10 years duration participated in the study. Subjects' main diagnoses were osteoarthritis (20%), lower extremity injury (18%), and low back injury (18%). Most subjects had jobs involving machine and equipment; requiring a lot of walking, standing, reaching and bending. Clinical Disability and Residual Functional Capacity questionnaires were administered to the subjects. Multifunction Computerized Exercise System (CES) was used to measure global right, left and bilateral upper extremity residual function as follows: with the Multifunction CES, in a sitting press position - maximum velocity was measured in isotonic mode, strength and endurance were recorded in isokinetic mode (60 degrees/ second). The arm/leg/back CES was used to measure maximum velocity, and isokinetic strength (120 degrees/ second) of the knees and ankles. For low back patients a lifting simulation, triceps curls, and low back endurance tests were performed on the CES in both isotonic isokinetic modes. Range of motion data from the clinical questionnaires were normalized, using AOA standards and DDS range of motion charts. Range of motion data measured with the CES were also normalized for lifting simulated test, triceps curls and the sitting press.

RESULTS

Comparison of both data obtained on CES with that from the clinical questionnaires yielded the following results:
-significant correlation for upper extremity range of motion ($r = 0.53$, $p = 0.03$).

- significant correlation of CES global upper extremity strength with clinically measured grip strength (r = 0.24, p = 0.04)
- significantly different upper extremity maximum upward velocity and upward strength (Figures 1 & 2).
- significant correlation of CES maximum knee and maximum ankle velocity with clinical timed gait speed respectively(r = .67, p = .0004; r = .87, p = .0001).

DISCUSSION

CES knee and ankle velocity data show the highest correlation with the clinical data followed by upper extremity range of motion. However, the reliability of CES global upper extremity strength should be interpreted cautiously. The small r coefficient may be due to subjects' individual differences that cannot be controlled. In general the results in this study are corroborated by findings in other studies. The positive effects of training with CES, on physical fitness was demonstrated by Jacobs et al.(1985). Thesame authors (1988) used the CES to compare lifting tests predicting lifting capacity, in Canadian military personnel. Palma et al. (1988) demonstrated that the CES can advantageously replace the traditional treadmill for improving the cardiovascular response of disabled cardiac patients. Our study further validates the use of CES in assessing residual function in workers with musculoskeletal impairments. Its dynamic state, variable speed and potential for exercise training makes it a useful tool for disability determination and occupational rehabilitation.

REFERENCES

1. Dejong, G. & Lifchez, R. (1983). Physical Disability and Public Policy. Scientific American, 248(6) , 40-49.
2. Parish, J.G.,and James, D.W. (1982). A Method fir evaluating the level of independence during the rehabilitation of the disabled. Rheumatology and Rehabilitation, 21, 107-114.
3. Whiting, R.B, Dreisinger,T.E., & Abbort, C. (1983). Clinical Value of Exercise Testing in Handicapped Subjects. Southern Med. J. 76(10), 1225-1227.
4. Austrew, R. (1984). Physical Capacities Evaluation: The application of Corrective Therapy evaluation techniques to assist in determining physical abilities after disability. Amer. Corr. Ther. J., 38(3), 67-68.
5. North, K. & Rohmert, W. (1981). Job analysis applied to the special needs of the disabled. Ergonomics, 24(11), 889-898.
6. Mittelstein-Scheid, E.E. (1985). Abilities and requirements profiles: a tool to facilitate reintegration of people with disabilities into employment, Int. Rehabil.Med., 7, 82-84.
7. Ranu, H.S.(1986). Engineering aspects of rehabilitation for the handicapped. J. Med. Eng. Technol., 10(1), 16-20.
8. Jacobs, I., Bell,D.G.,& Pope, J. (1988). Comparison of isokinetic and isoinertial lifting tests as predictors of maximal lifting capacity. Eur. J. Appl. Physiol., 57, 146-150.
9. Palma, T.A., Maier, T.J. (1986). Cardiovascular response of a cardiac population to isokinetic testing. Amer. Assoc. Cardiovascular Pulmonary Rehabil., Ist Annual National Convention. Westpoint: New York.

QUESTIONNAIRE Vs EXERCISE DATA

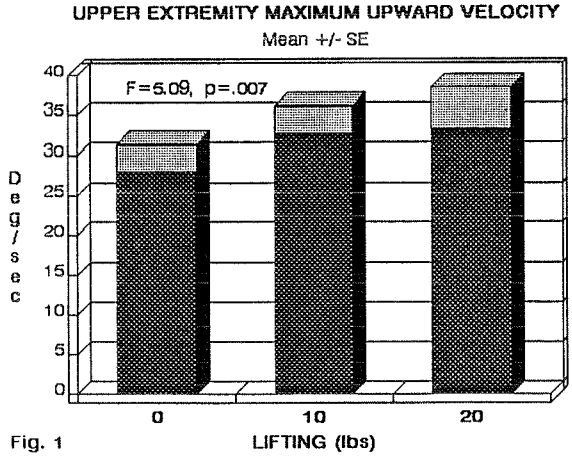

Fig. 1

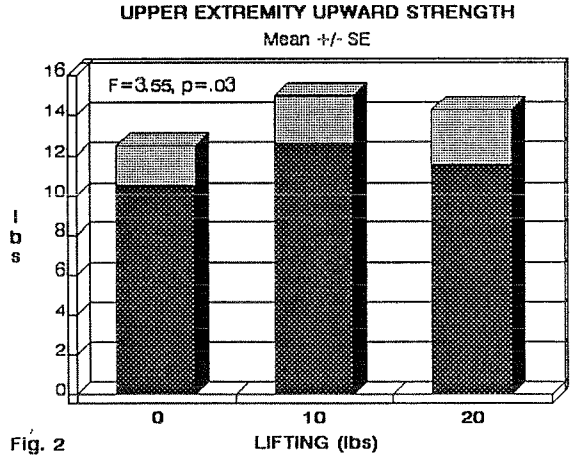

Fig. 2

COMPARISON OF WEIGHED AND PREDICTED ARM MASS IN TRAINED AND UNTRAINED MEN

Tibor Hortobágyi and Frank I. Katch†
Department of Sport Science, University of Denver, Denver, CO 80208 and
†Dept. of Exercise Science, University of Massachusetts, Amherst, MA 01003

INTRODUCTION

We have compared the mass of the dominant arm in strength-trained and untrained young men using a method of arm weighing and prediction of segmental arm mass based on Dempster's segmental mass to body mass ratio. The data suggest that arm mass may not be a fixed proportion of body mass in strength-trained athletes. It is recommended that segmental mass of strength-trained subjects should be assessed with a direct method and not with prediction based on cadaver data that are non-representative of athletes.

REVIEW AND THEORY

Kinetic analyses in biomechanics require information on segmental dimensions of the involved extremity or body part. Conventionally, such data have been derived from ratios of segmental mass to total body mass of cadavers. However, cadavers in prior studies have not been representative of the average adult or highly trained athlete with respect to age, gender, stature, body mass, and training status. For example, in the widely used study of Dempster (1955) the mean (±SD) age, stature, and body mass of the 8 cadavers was 68.5 y (10.99), 1.694 m (0.112), and 59.8 kg (8.35). It is apparent that athletes may have fundamentally different physical characteristics compared to cadavers. In deriving segmental mass data, a fixed relationship is assumed to exist between the mass of the segments and total body mass (Miller and Nelson, 1973). It is unclear whether the assumed fixed relationship is tenable between segmental limb mass and body mass in trained athletes. The purpose was to compare weighed and predicted arm mass in strength-trained and untrained subjects.

METHODOLOGY

Subjects for the present study were 40 young men. Twenty were varsity athletes who had been weight-lifting for 2 to 8 years (TR, 23.1 y) and 20 were untrained students (UT, 22.6 y). For TR and UT, mean (±SD) body mass was 90.9 kg (16.73) and 76.6 kg (11.50) ($p < .05$), and mean stature was 1.788 m (0.0707) and 1.775 m (0.0905) ($p > .05$).

Arm mass was weighed for 6 min in the supine position on a large table. The dominant arm was placed on a board attached to a sling that was suspended from a Chatillon autopsy scale. The scale was hung by a chain from the ceiling. The position of the arm at all times was perpendicular with reference to the hanging scale. On the board, the arm was supported at the center of mass corresponding to 43.1% of arm length measured from the acromion to the styloid process. Subjects were instructed to close their eyes, to breath normally, to relax their body, and to let their arm become "heavy" to facilitate relaxation. In the dark room, a flashlight was used to read the scale at a right angle. Readings were taken at the end of every min for 6 min. The criterion score was the average of the final three readings. To obtain reliability, the 6 min procedure was repeated 2 to 3 days later in 20 of 40 subjects. Arm mass was predicted from body mass using the constant of 4.925% based on the average arm mass to body mass ratio for Dempster's 8 cadavers.

RESULTS AND DISCUSSION

Intraclass reliability was R = 0.971 for the 6-min weighing procedure over 2 days. Figure 1 summarizes the data. Weighed, arm mass was 4.157 kg (0.699) for TR and 3.793 kg (0.521) for UT ($p < .05$). Predicted, arm mass was 4.477 kg (0.622, TR) and 3.773 kg (0.501, UT; $p < .05$). Analysis of variance revealed a significant interaction ($F_{1,38} = 6.5$, $p < .05$) between the methods of obtaining arm mass and training groups.

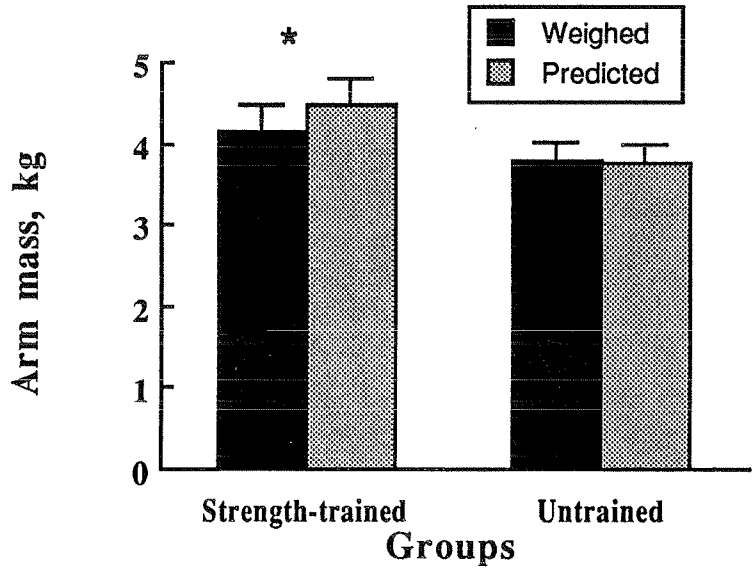

Figure 1. Comparison of weighed and predicted arm mass in strength-trained (N = 20) and untrained (N = 20) men. Bars are ±SE. * $p < .05$ within strength-trained and between groups.

The data of the present study suggest that the segmental arm mass of TR was overpredicted by 8% ($p < .05$). However, the difference between weighed and predicted arm mass was only 0.5% in UT ($p > .05$). These data suggest that for biomechanical analyses that require segmental mass data of strength-trained athletes, such data should be obtained by direct weighing and not by prediction.

REFERENCES

Dempster, W.T. *Space requirements of the seated operator*. WADC Technical Report #55-159, Wright-Patterson Air Force Base, Ohio, 1955.

Miller, D.I. and Nelson, R.C. *Biomechanics of Sport*. Philadelphia: Lea and Febiger, 1973.

Precise Description of a Scoliotic Spine

C. N. DeSilva and King H. Yang
William Beaumont Hospital, Royal Oak, Michigan
Dept. of Mechanical Engineering, Wayne State University, Detroit, Michigan

Introduction

A normal spine is assumed to lie entirely in the sagittal plane. This assumption implies that there exists a plane curve which is representative of the spine. We develop in this paper a model of the spine which, as a three-dimensional body, is described by a space curve and transverse sections through the centroid of each vertebra. In the scoliotic spine, this space curve (or neutral axis curve) is no longer plane but has associated with it curvature and torsion. The curve itself is chosen as connecting the centroids of the transverse vertebral sections. Each of these sections has an area, two principal axes of inertia and the corresponding moments of inertia.

This curved beam-column model yields three measures for the severity of scoliosis. One measure $K_1^{(0)}$ gives the curvature of the spine in the sagittal plane, a second measure $K_2^{(0)}$ is the curvature in the frontal plane. The third measure, $K_3^{(0)}$, which we term the tortuosity, describes precisely what in the literature is noted as a "rotational asymmetry about the vertical axis, with axial rotation of the vertebrae, of the plane of maximum curvature of the spine" (1, 2, 3, 4, 5, 6). For the non-scoliotic spine, $K_2^{(0)} = K_3^{(0)} = 0$ and the curvature is entirely in the sagittal plane. We are proposing that $K_2^{(0)}$ and $K_3^{(0)}$ replace Cobb's angle in a description of scoliosis.

Geometry of the Scoliotic Spine

Let us consider a transverse section through an arbitrary vertebra. This section will have an area, a centroid, principal axes of inertia and principal moments of inertia. We may define a regular curve which passes through the centroids of each such vertebral section. This curve is uniquely determined by its curvature K_n and its torsion T. Let D_3 be the unit tangent vector to the curve at the centroid of an arbitrary vertebral section; let D_1, D_2 be the principal axes of this vertebral section. Then D_1, D_2, D_3 are an orthonormal basis attached at each vertebral level. Each D_i is function of S, the distance along the curve.

The geometrical measures which describe the three-dimensional spine are $d/dS\ (D_i) = F_{ip}\ D_p$, where F is a skew tensor and a computation shows: $F_{23} = K_1^{(0)}$, $F_{31} = K_2^{(0)}$, $F_{12} = K_3^{(0)}$, where $K_1^{(0)}$ may be interpreted as the curvature of the spine in the sagittal plane. $K_2^{(0)}$ is the curvature in the frontal plane. $K_3^{(0)}$ which we call the "tortuosity" after Love (7) is a measure of the rotating and twisting of the vertebrae about the vertical axis (1). If we define a curvature vector $K = K_n b$ where b is the binormal of the axis curve, $K_1^{(0)} = K \bullet D_1$; $K_2^{(0)} = K \bullet D_2$; and $K_3^{(0)}$ is approximately equal to T.

Methods

Transverse MRI scans were performed to obtain the area, centroid, principal moment of inertia, and principal axes at the mid-section of each vertebral body. A computer program was written to calculate the area and the first moment of inertia of each section. Figure 1 shows the kth vertebral section with all the corresponding vectors. For kth section, the centroid C can be obtained by dividing the first moment of area by the area. The global position vector of C is denoted as r_k.

An arbitrary point Q is selected from this section. A unit vector e_1 along the C-Q can be obtained. Define another point not co-linear with C-Q and denoted as P, then

a line C-P is formed. Then the cross product e_1 X C-P yields $|e_1$ X C-P$|$ e_t with e_t the perpendicular unit vector to the section and denoted as D_3.

To obtain the principal axes D_1 and D_2, we first compute D_3 X e_1 to find e_2. The moments of inertia I_{11}, I_{22} and I_{12} with respect to e_1 and e_2 were calculated. Then the I matrix was diagonalized, the angle theta obtained, and the principal axes D_1 and D_2 determined by rotating e_1 and e_2 by the angle theta. Finally, we computed the first and second derivatives $e_t'(S)$ and $e_t''(s)$. The curvature of the curve K_n can be obtained from the inner product of $e_t' \cdot e_t'$. The torsion T is calculated using $T = 1/k_n^2$ [$(e_t$ X $e_t')$ $\cdot e_t''$]. After the binormal b is obtained, all the components of K can be obtained as described above.

Concluding Remark

The measures proposed as indicators of the severity of scoliosis arise from a rigorous engineering model of the spine. The curvature in the frontal plane, $K_2^{(0)}$, is a more meaningful measure than Cobb's angle. The tortuosity $K_3^{(0)}$ describes precisely the phenomenon observed by surgeons in which there is asymmetric rotation of the vertebrae along the spine. The physician may now design a treatment which will result in the vanishing of $K_2^{(0)}$ and $K_3^{(0)}$.

References

(1) I.A.F. Stokes: Axial rotation component of thoracic scoliosis. J. Orthopaedic Research 7:702-708, 1989

(2) G.W.D. Armstrong, N.D. Livermore, N. Suzuki, J.G. Armstrong: The mechanism of rotation in combination with lateral deviation in the normal spine. Spine 7:50-54, 1982

(3) D.R. Benson, R.L. DeWald, A.B. Schultz: Harrington rod distraction instrumentation. Its effect on vertebral rotation and thoracic compensation. Clin. Orthop. 125:40-44, 1977

(4) G. Deane, R.B. Duthie: A new projectional look at articulated scoliotic spines. Acta. Orthop. Scand. 44:351-365, 1973

(5) R. Perdriolle, J. Vidal: Etude de la courbure scoliotique. L'importance de l'extension et de la rotation vertebrale Rev. Chir. Orthop. 67:25-34, 1981

(6) A.A. White: Kinematics of the normal spine as related to scoliosis. J. Biomech. 4:405-411, 1971

(7) A.E.H. Love: Mathematical theory of elasticity. Dover NY 1927

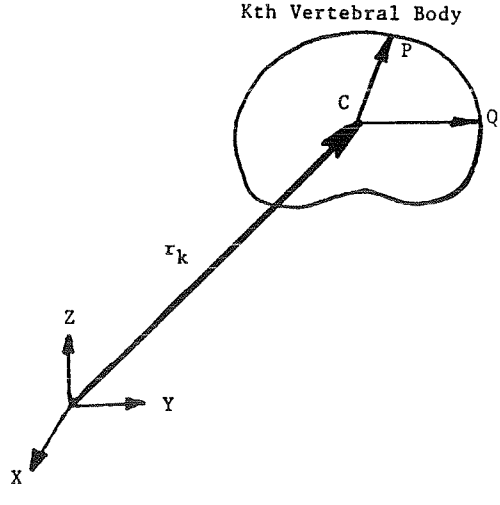

Figure 1: Global coordinate system of the kth vertebral body.

THE ROLE OF SERIES ELASTICITY IN A COUNTER MOVEMENT JUMP

Scott Selbie and Marc van Leemputte
Institute of Physical Education, Katholieke Universiteit Leuven, Tervuursevest 101, 3030 Heverlee, Belgium

INTRODUCTION

The greater maximum height achieved using a counter movement versus a squat jump has often been ascribed to the storage of potential energy in elastic tissue. The purpose of this research was the development of a dynamic simulation of jumping used for the assessment of the role of the series elasticity.

METHODOLOGY

The model of the human body consisted of four linked rigid segments connected by holonomic constraints. The equations of motion were derived using Lagrange dynamics. The contribution of the musculature is represented by seven muscle groups acting across three joints: Rectus Femoris, Vasti, Hamstrings, Biceps Femoris (Short Head), Gastrocnemius, Soleus and Dorsi Flexors. The muscle model is based on the morphology of human muscle. The parameters of the model (Peak Muscle Force, Moment Arms, Optimal muscle fibre length) have been partially derived from the literature (Hoy, Zajak and Gordon, 1990) and partially from experimental determination (force-length, force-velocity). The experiment consisted of a modified standing jumping in which the subject was constrained in a vertical swing. Jumping conditions were controlled by varying the inertia of the swing. The inclusion of the hip constraint minimized the problem of balance in the simulation.

The inputs to the system of equations are the initial kinematic state of the system and the activation of the individual muscle groups. Integration is performed using an extrapolated mid point method with variable step size and variable order. The simulation program has been implemented in Object Oriented Pascal on an IBM 386 personal computer. The user interactively controls the model parameters, initial kinematic state, activation levels and external forces acting on the system.

To determine an initial set of reasonable activation profiles a series of boundary value problems were specified and solved resulting in the reproduction of kinematics derived from a recorded human jump. The system is over determined since seven activation values must be calculated from only four equations of motion. The remaining three equations are derived by specification of constraint relationships between synergistic muscle groups using the EMG quantification technique of Van Leemputte (1987).

The benefits derived from the counter movement can be partially explained by the attainment of maximum muscular activation at the start of the concentric portion of the jump. This was accounted for in the simulation by careful choice of the time of onset of activation so that maximum activation occurred at the start of the concentric phase independent of the spring constant.

RESULTS

The effects of series elasticity have been addressed by comparing the results of simulations using inelastic tendons with simulations using series elastic elements.

The results show that:

a: there is a direct relationship between the stiffness of the elasticity and the onset of muscle activity;

b: the benefits derived from the counter movement can be adequately explained without the concept of storage of elastic potential energy if the timing of the muscle activities is appropriate;

c: the EMG recordings from the experiment reveal that the activation of the individual muscles is organized in the same manner as in the simulations without series elasticity.

DISCUSSION

In summary, the simulation results suggest that the benefits derived from the counter movement could be adequately explained without the inclusion of the elasticity. The addition of the elasticity did not result in an increase in the maximum height but only in differences in the timing of the activation.

REFERENCES

Hoy G.H., Zajak F.E., Gordon M.E. (1990), A Muscluloskeletal Model of the Human Lower Extremity: The Effect of Muscle, Tendon and Moment Arm on the Moment-Angle Relationship of Musculotendon Actuators at the Hip, Knee and Ankle, J. Biom 23, pp 157-169

Van Leemputte M. (1987), EMG Quantification and its Application to the Analysis of Human Movement, Medicine and Sport Science Vol 25, pp 177-194

ERGONOMETRIC ACCOMMODATIONS FOR A WHEELCHAIR PROPULSION-SPECIFIC ARM-CRANK ERGOMETER

Manssour H. Moeinzadeh*, José Colucci, Jr.*, and Brad N. Hedrick+
University of Illinois at Urbana-Champaign

Department of General Engineering*
117 Transportation Building
104 S. Mathews Avenue
Urbana, IL 61801

Division of Rehabilitation Services+
1207 S. Oak Street
Champaign, IL 61820

INTRODUCTION

A wheelchair locomotion specific ergometer was designed to provide a close simulation of the wheelchair handrims movement pattern, without the potentially injurious high impact associated to wheelchair propulsion. The device permits the simulation of a wide range of wheelchair models through the adjustment of several important geometric and physical parameters, thus allowing power measurements to be taken with arm-crank exercise that is biomechanically proximal to the subject's own propulsion technique. The ergometer was dynamically calibrated by means of a specially designed torque calibrator using a direct current motor. The system was connected to a microcomputer for data acquisition. A commercial I/O board was used for that purpose and a program was written in FORTRAN that sets the pace for the test according to established protocols, acquires, processes, and displays the data in real time.

REVIEW AND THEORY

With the growing interest in both competition and performance evaluation for the wheelchair disabled, several studies on physiological measurements and responses to training for wheelchair athletes have been published. The treadmill and the cycle ergometer are commonly used in the laboratory to assess the physiological response of able-bodied subjects to exercise. For measuring the work of wheelchair-bound subjects, however, instrumentation has been a major problem. Many different designs have been tried but none of them has acquired the status of a standard for the test. Among the devices for wheelchair ergometry described in the literature we can recognize five basic types: cycle ergometer adapted to arm-cranking (Morse et al., 1988), wheelchair adapted to a cycle ergometer (Forchheimer et al, 1986), wheelchair on treadmill (Van der Woulde et al., 1989), wheelchair on rollers (Eriksson et al., 1988), and specialized wheelchair ergometers (Burkett et al, 1987). Ideally, the evaluation of wheelchair propulsion should be performed using the same movement pattern to which the individual has become accustomed in competition or normal ambulation, but most of the commonly used devices lack this specificity with regard to actual wheelchair locomotion. Thus, to overcome the deficiencies of previous designs as far as specificity is concerned, and to provide athletes as well as researchers with a biomechanically adequate training and research equipment, a *wheelchair-locomotion specific arm-crank ergometer* was developed.

METHODOLOGY

The wheelchair-locomotion specific arm-crank ergometer was designed to

provide a close simulation of the wheelchair handrims movement pattern, without the potentially injurious high impact (Curtis and Dillon, 1985) associated to wheelchair propulsion. The device permits the adjustment of several important geometric and physical parameters, and thus allows the simulation of a wide range of wheelchair models. The load-generating system makes use of two automotive alternators, one for each side, connected to the arms of the ergometer through a mechanism using pulleys, a belt, and a D-shaped cam. The cam controls the starting and releasing points of the propulsion cycle. The load is adjusted by a circuit that controls the input current for the alternators. The system was dynamically calibrated by means of a specially designed torque calibrator employing a direct current motor. The calibrator drives all the system through the alternators shaft and, this way, internal losses including frictional resistance of all the elements of the transmission from the pedal shaft are taken into account.

As a way to automatize the tests and thus greatly reduce the time for their application, the equipment was connected to a microcomputer for data acquisition. A commercial I/O board (Data Translation, Inc.) was used to interface the ergometer with an IBM-compatible computer. The board contains 16 analog channels and two I/O digital ports. From those 16 analog channels, 4 were used for speed (rpm) from the left and right hand sides, field current, and start and stop functions. In order to match the voltage levels of the various signals from the ergometer with the level required for the analog inputs, signal conditioners were built. A FORTRAN program was written so as to provide a user friendly (menu driven) interface. In its basic version, the program sets the pace for the test, according to the WINGATE protocol, acquires, processes and displays the data in a useful form.

RESULTS AND DISCUSSION

As it is, the system has shown to be a practical and reliable means for application of the WINGATE test of anaerobic power. Displaying of data analysis and graphics in real time by linking the program to compatible application software packages is under development. The remaining channels in the I/O board will be used in the future for acquisition of physiological data, like heart rate, blood pressure, temperature, etc. The potential for further refinement is virtually limitless due to the flexibility of both hardware and software.

REFERENCES

Burkett, Lee N. et al, *Adapted Physical Activity Quarterly*, 4: 60-71, 1987.
Curtis, Kathleen and Dillon, In: Sherril, C. (Ed.), *Sport and disabled athletes*, pp. 211-217, 1985.
Eriksson, Peter et al, *Scand. J. Rehab. Med.*, 20: 141-147, 1988.
Forchheimer, Fred, et al, *Scand. J. Rehab. Med.*, 18(2): 59-63, 1986.
Morse, M. I. et al, *Med. Sci. Sports Exerc.*, 20(2), April 1988 Supplement.
van der Woude et al, *Adapted Physical Activity Quarterly*, 6: 109-132, 1989.

Acknowledgements

The development of the *wheelchair-locomotion specific arm-crank ergometer* was partially supported by a grant from the National Wheelchair Athletic Association (NWAA).

KINEMATIC REQUIREMENTS OF HOSPITAL WORKERS USING ON SITE 3D VIDEO ANALYSIS

V.M. Titiloye, N.Xu, L. Lei, M. Parnianpour, F.J. Bejjani
Human Performance Analysis Lab.,New York university
35 West Fourth Street, New York, NY 10003

INTRODUCTION

Low back injury is a common problem that affects more than half of the working population at some time during their working career (1). Lifting methods have frequently been taught in back programs to reduce the incidence of low back injury. However, assessment of lifting capacity have been limited to industries and laboratory settings. In order to design a job to match the physical capabilities of the majority of workers and to place a worker on a job that does not exceed his/her lifting capacity job site lifting requirements need to be established. The purpose of this study is twofold: to determine the kinematic requirements of various lifting tasks in a hospital setting, and to introduce a model for assessing three tasks in the workplace.

REVIEW AND THEORY

Surface electromyography has been widely used to study job requirements (2). Knowledge of the biomechanical profiles of lifting - isometric, isokinetic and isoinertial - have evolved (3,4,5,). Jonsson (3) popularized the use of electromyographic kinesiology and quantified EMG in musculoskeletal performance analysis and ergonomic workplace. Almstrom & Kadefors (4) developed a portable equipment for the measurement of EMG during a normal work situation, consisting of lifting and lowering tasks. Because most muscles move more than one joint, and because most activities involve multiple and complex joint motions in more than one plane, a biomechanical profile of a given task cannot be complete without video analysis, preferably 3-D, in the workplace. Hence the need for the present study.

METHODS

Twelve adults (7 males, 5 females) aged 20-45 (M = 44, SD = .13) participated in the study. Subjects' personal and job related data were acquired via a standard occupational questionnaires. The subjects were asked to randomly freely perform the following lifting tasks, with loads weighing 10% and 20% of their body weight, while being videotaped by 3 cameras in 3 different planes, after calibration:

1. lift symmetrically from the ground to a table height of 52 cm (low Sym.).
2. lift symmetrically from the ground to a table height of 95cm (high Sym.).
3. lift from a table height of 95cm to a standard shopping cart, 35cm deep, located to the left of the subject, perpendicularly to the table(Rotational).
4. repeat 1,2,and 3 times, both in the ground-to-table, or cart to table (Lift Up) and the table-to-ground(cart) (lift down) directions. Kinematic data were recorded by the video cameras . A special software was used to digitize the video data and to obtain a 3-D reconstruction. The kinematic data obtained for the respective joints and for each task were subjected to a multiple analysis of variance.

RESULTS & DISCUSSION

Figures 1 to 6 depicts the findings in this study. Maximum shoulder range of motion was significantly diffferent in all the lifting conditions. Maximum velocity of the shoulder and hip were significantly different both in all lifting conditions and lifting directions. Significant difference existed in maximum shoulder and hip acceleration for all lifting conditions and lifting directions. Knee and ankle acceleration were significantly different only in the lifting directions.Lifting conditions, especially lifting directions, demonstrated the most significant differences between the kinematic variables,primarily their maximum values. Findings indicate that the kinetic requirements of the shoulder and the hip show the greatest difference as compared to the other joints. This might due to the characteristics of the lifting tasks. Velocities were significantly higher at the knee and the hip during lift up, and lower for the shoulder. Maximum accelerations did not exceed 0.4 to 0.5 g(gravity) at all joints.

CONCLUSION

The introduction of portable 3-D videoanalysis in the workplace have numerous applications in the fields of ergonomics, sports, and occupational and rehabilitation medicine. It can have direct therapeutic implementation. Information obtained from the 3-D can be analyzed and programmed into a software of computerized exercise machine that can be used for specific training of workers.

REFERENCES

1.Mayer, T.G., Gatchel, R.J.(1988). Functional Restoration for Spinal Disorders: The Sports Medicine Approach. Philadelphia: Lea and Febiger.
2. Aghazadeh, F.& Ayoub, M.M. (1985). A comparison of dynamic- and static-strength models for prediction of lifting capacity. Ergonomics, 28(10):1009-1417.
3. Jonsson, B.(1978). Kinesiology: With special reference to electromyographic kinesiology. In W.A. Cobb , H. Van Duigh (eds.),Contemporary Clinical Neurophysiology, 34, (pp.417- 428). Amsterdam: Elsevier Science Pub. Co.
4. Almstrom, C. & Kadefors, R. (1985). EMG analysis : Muscle load and fatigue in manual work. In I.D. Brown, R. Goldsmith, K. Combes, M.A. Sinclair (eds.), Ergonomics International 85(pp.901-906). London and Philadelphia: Taylor & Francis.

KINEMATIC LIFTING REQUIREMENTS

Range of Motion

Mean +/- 2 SE

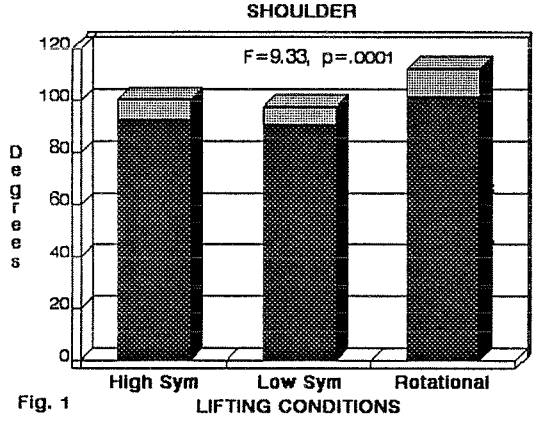

Fig. 1

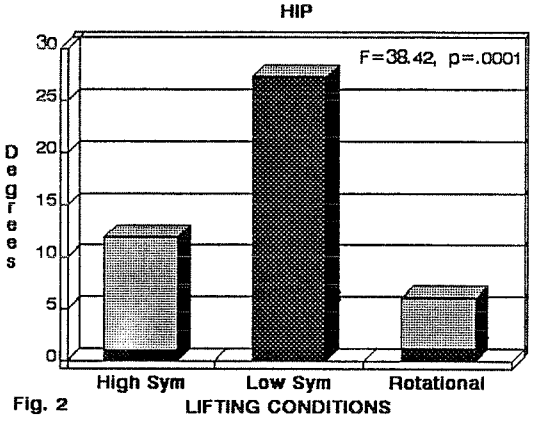

Fig. 2

Maximum Velocity

Mean +/- 2 SE

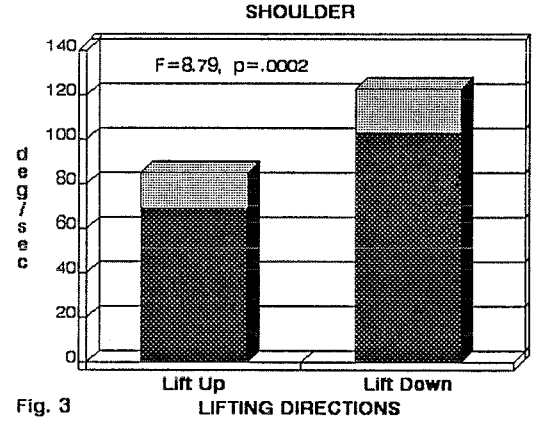

Fig. 3

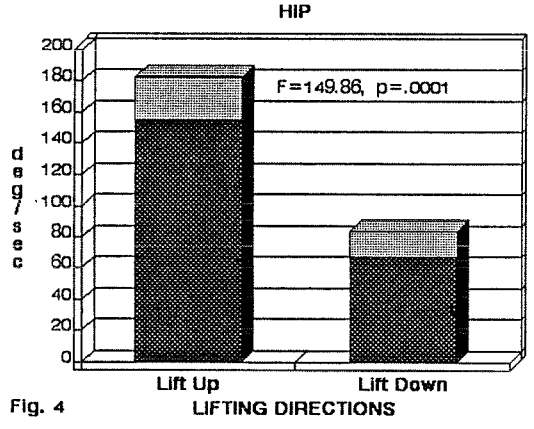

Fig. 4

Maximum Acceleration

Mean +/- 2SE

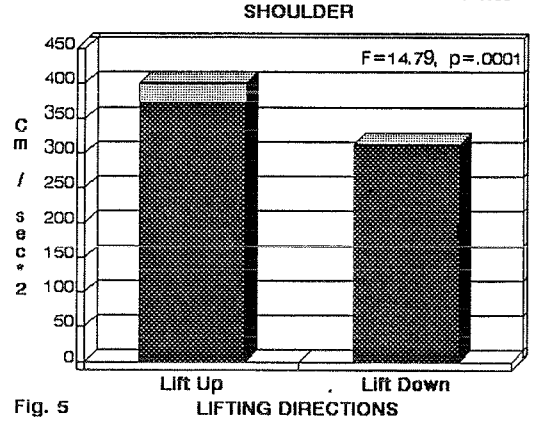

Fig. 5

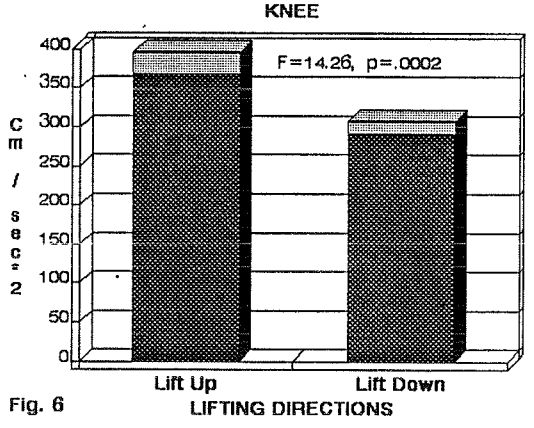

Fig. 6

RELATIONSHIP BETWEEN HUMAN PARAMETERS AND TRUNK FUNCTIONAL ABILITIES IN CHRONIC LOW BACK PAIN PATIENTS

Eileen Diaz, Tarek Khalil, Elsayed Abdel-Moty
Renee Steele-Rosomoff, and Hubert Rosomoff

University of Miami Comprehensive Pain and Rehabilitation Center
Departments of Neurological Surgery and Industrial Engineering
University of Miami, Coral Gables, Florida 33124, USA

INTRODUCTION: A sample of 176 patients with chronic low back pain (CLBP) participated in a study to establishing criteria data for static strength and surface muscle activity (EMG) of the trunk extensors upon rehabilitation. Two age groups, and 3 body weight categories were identified for both males and females. Patients were tested upon admission to a 4-week rehabilitation program. Evaluation was repeated after 2 weeks. All patients increased their strength and EMG significantly. Males had significantly higher strength and EMG than females at evaluation points for both age groups. EMG varied inversely with body weight and age for males and females at both evaluation times. Strength decreased with age, but not with body weight.

BACKGROUND: In rehabilitation programs designed for the restoration of functional capabilities, it is desirable to document patient progress in terms of "achievement". Achievement can be measured by the change in function and by the deviation from target "norms" that reflect scores of healthy individuals. Both these "scales" require the use of stratification that accounts for various human parameters such as age, sex and body weight. Therefore, the objective of this study was to establish such criteria data for the variables of static strength and integrated muscle activity (EMG) of the trunk extensors for patients CLBP upon rehabilitation.

METHODOLOGY: A random sample of 176 patients with CLBP were included in the study. All subjects were selected from the pain patients population of the University of Miami Comprehensive Pain and Rehabilitation Center (CPRC). The CPRC utilizes a multidisciplinary aggressive physical medicine approach to the management of pain condition. To be included in the study all patients had to have medical referrals for low back muscles' strengthening and reeducation exercises. Patients were grouped according to age (<40, $>= 40$ yr), body weight (<150, 150-200, >200 lb) and sex (89 males and 87 females). Assessment of isometric trunk extension strength in the standing posture was based on the concept of Acceptable Maximum Effort, AME (Khalil et al., 1987). AME measures patients' acceptable levels of strength performance as modified by their perception of pain. EMG activity of the right sacrospinalis muscle was measured while the patient was in the prone position. and attempting to raise the upper body off the table and to hold this extension for 10 seconds.

RESULTS AND DISCUSSION: Results of analyzing trunk strength and EMG measures with respect to age, weight, and gender showed that patients were able to increase their strength and EMG significantly over the two week period (Fig. 1-4). Males were found to have significantly higher strength and EMG than females at both evaluation points for all age groups (Fig. 2,4). EMG was found to vary inversely with body weight (Fig. 3) and with age (Fig. 4) for males and females at both evaluation times. Strength decreased significantly with age (Fig. 3), but not with body weight (Fig. 1). The data obtained

provided accurate basis for comparing patients with CLBP and healthy individuals of matched characteristics. Classifying patients according to their personal attributes of age, gender, and body weight assists to determine objective criteria for progress and expectations during treatment and rehabilitation.

Fig. 1

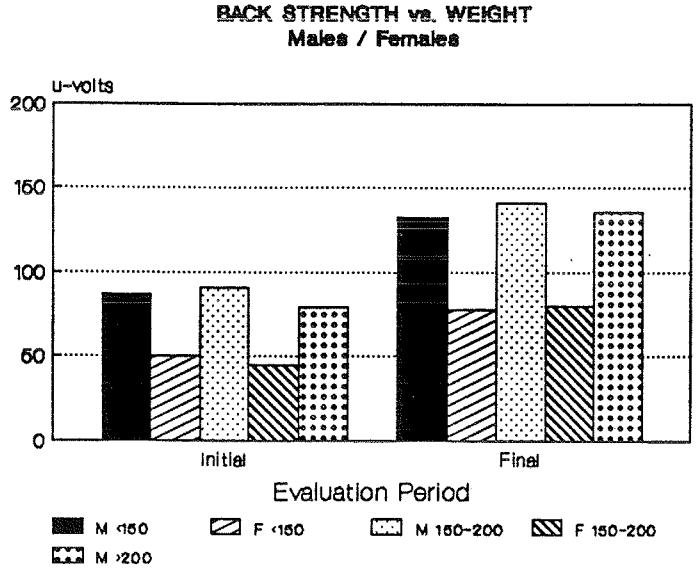

Fig. 2

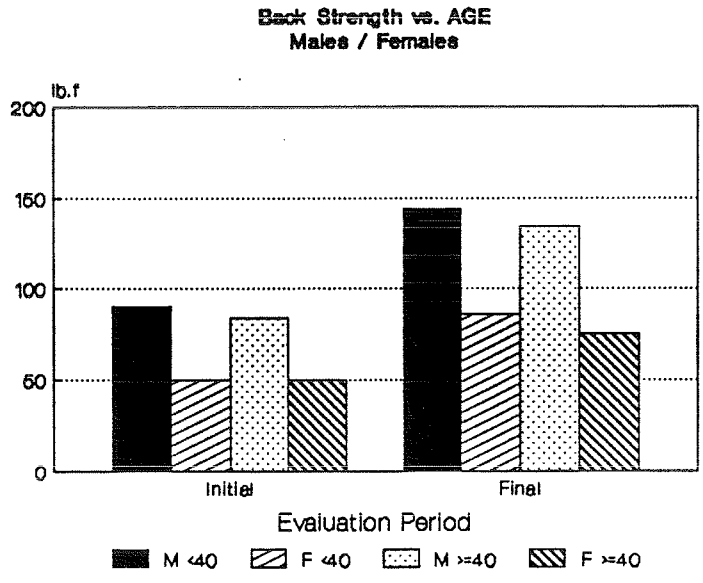

Fig. 3

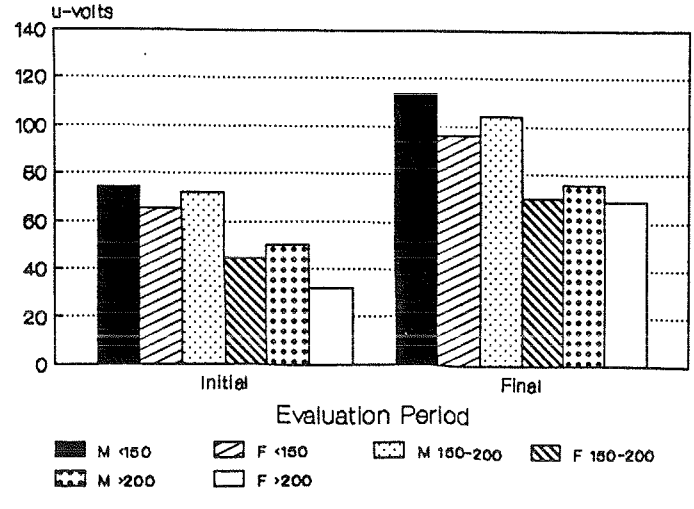

Fig. 4

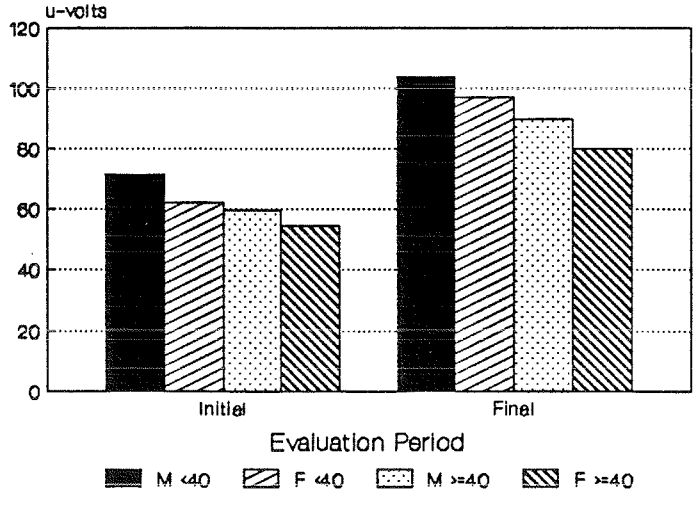

REFERENCES:

Khalil, T.M., Goldberg, M.L., Asfour, S.S., Abdel-Moty, E., Rosomoff, R.S., Rosomoff, H., 1987. Acceptable Maximum Effort (AME): A Psychophysical Measures of Strength in Low Back Pain Patients. Spine, 12, 4, 372-376.

COMPARATIVE DYNAMIC RESPONSE FOR ASSESSING VIBRATION EXPOSURE: HUMAN VS MONKEY

Suzanne D. Smith and Leon E. Kazarian
Armstrong Aerospace Medical Research Lab, WPAFB, OHIO 45433

INTRODUCTION: In studying the potentially harmful effects of chronic vibration exposure, the Rhesus monkey has been considered as a human surrogate candidate for laboratory studies based on gross anatomical and morphological considerations. In assessing the feasibility of extrapolating results from the monkey to the human exposed to vibratory stress, a critical comparison of dynamic response characteristics in the vibration environment is required. The literature presents mechanical response characteristics of the two species exposed to vibration and uses lumped-parameter models to represent major anatomical structures sensitive to particular frequencies or ranges of frequencies. The objective of this study was to compare the mechanical impedance response data previously collected and from the literature for the two species and correlate similarities and differences in response characteristics to anatomical/morphological considerations.

METHODS AND MATERIALS: Driving-point mechanical impedance response data were obtained from several human and Rhesus seated, whole-body vibration studies. The data were collected for sinusoidal exposures between 3-30 Hz at .1-1.0 g's for the Rhesus and 2-31.5 Hz at .1-.5 g's for the human. Specifically, comparisons were made between impedance profile shapes, the mathematical models used to simulate response, and the resultant stiffness, damping and resonance characteristics.

RESULTS AND CONCLUSIONS: Figure 1 illustrates typical impedance magnitude and phase curves for the human (1) and Rhesus (2). The most obvious difference is the higher primary resonance frequency (indicated by the peak in magnitude) in the smaller Rhesus (10-14 Hz) as compared to the human (4-6 Hz), with the human showing a second lower peak between 10-12 Hz, not observed in the Rhesus. For the Rhesus, the primary resonance has been described as due to excitation of the

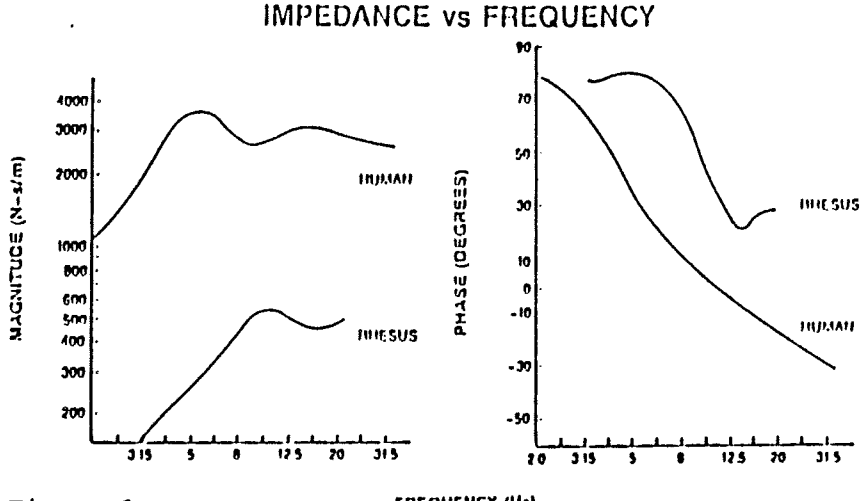

Figure 1

reactive upper torso by the lower torso with significant variations in response being associated with variations in spinal column shape which is supported by modeling analysis (2). Anatomical/morphological influences on the dynamic response of the Rhesus include the hard callosities of the buttocks, the slender pelvis and lack of lumbar lordosis, resulting in a relatively rigid lower torso and supporting the modeling of the region as a rigid mass. Along with the narrow inverted V shape of the rib cage, the Rhesus also presents a more compact and cylindrically arranged viscera which provides for a tightly integrated structure between the viscera and spinal column for transmitting and attenuating loads between the upper and lower torso regions. The models used to describe human response are more complex in defining the major anatomical structures which contribute to the vibration response. As a result, the stiffness and damping coefficients are not easily compared within this species. The damping factors in both species are similar and respresent highly damped systems. The literature attributes the primary resonance in the human to excitation of the thoraco-abdominal region including the visceral masses (3). The human, in constrast with the Rhesus, possesses a short broad pelvis, lumbar lordosis, and an inverted U shaped rib cage leading to greater relative motion between soft tissue organ systems. The transmission/attenuation of loads to the upper body in the human is influenced by significant visera response, the soft buttock tissue, and the potential occurrence of moments about the pelvis.

Other observations of the Rhesus response indicate significant lowering of the resonance frequency and increase in damping behavior associated with increases in thoracic curvature. In the human, the first impedance magnitude peak is decreased and the second peak enhanced both for the relaxed posture and the addition of a corset (4). These results suggest that the relaxed posture and damping of the lower torso may reduce relative visceral motion and act to lower the primary impedance magnitude, but, consequently, can reduce the influence of the viscera on damping of the second resonance associated with the spinal column.

In conclusion, while the human and Rhesus possess similar major anatomical structures and organ systems, the specific morphological or geometrical characteristics of these systems may play an important role in the characteristics and complexity of system response to vibration stress. The effects of these characteristics on transmission/attenuation pathways must be well understood in assessing the effects of chronic vibration exposure using the Rhesus monkey.

REFERENCES:

(1) International Standards Org. (1983), ISO 2631.
(2) Smith (1988) Doctoral Dissertion, University of Vermont.
(3) Guignard and King (1972) AGARD-AG-151, Nov.
(4) Coermann (1961) ASD Tech. Rep. 61-492, WPAFB, OH.

THREE-DIMENSIONAL KINEMATIC ANALYSIS OF THE VOLLEYBALL DIG

Joe F. Garrett and Gregory S. Rash,
United States Sports Academy, Daphne, AL 36526

INTRODUCTION: Defensive skills are highly important to the success of a volleyball team. One defensive skill is the "dig" (Gozansky, 1987). The purpose of this study was to determine the three-dimensional (3D) kinematics of the volleyball dig. Many studies describing the set, pass, spike, and serve skills were found but no literature could be found which described the kinematics of the dig. Only coaches descriptions of the dig could be found in the literature (Bertucci, 1982; Keller, 1977; Rosenthal, 1983; Scates, 1972; Slaymaker and Brown, 1976; and Thigpen, 1974). Therefore, an attempt was made to resolve this problem by analyzing various kinematic parameters involving the dig.

METHODS: Twelve female volleyball players were selected from an elite high school team located in Mobile, AL. They were analyzed in a practice setting. Their average age, height, and weight were 15.67 yrs, 1.70 m, and 63.4 kg respectively. Two cameras were used to collect video images; one camera was positioned at the right side of the subjects and the second camera was positioned directly in front of the subjects. To obtain 3D joint coordinates, the DLT computer program was utilized. Whole body center of gravity (CG) kinematics, segment CG kinematics, and joint kinematics were determined. In addition, the distance and angle between the feet and the ball position were determined at contact. Ball velocity was calculated four fields before and after ball contact.

RESULTS AND DISCUSSION: Table 1 shows that the stance used to "dig" the volleyball was wide. The average distance between the left and right foot was 0.78 m (45.8 % of their height). The average angle between the right and left feet was 23.49o. This was due to the player stepping toward the incoming ball. They moved there CG an average of 0.17 m to get to the ball and their CG was travelling an average velocity of 0.58 m/s at ball contact.

Table 1 shows that the thighs were almost at right angles with the trunk, the knees were flexed, the elbows were slightly bent, and the shoulders were extended about 25o below a right angle with the trunk. The averages for both left and right sides were close. Further investigation showed the subjects who reached to their right were similar to the subjects reaching to their left.

Table 1. Joint angle (degrees) at contact

	LH	RH	LK	RK	LE	RE	LS	RS
AVE	99.39	104.23	120.57	120.02	165.56	170.87	60.98	77.23
STD	36.86	35.03	36.96	23.96	8.04	5.38	21.84	22.32

LH=Left hip, RH=Right hip, LK=Left knee, RK=Right knee, LE=left elbow, RE=Right elbow, LS=Left shoulder, RS=Right shoulder

Both the right and left trunk were bending forward at ball contact to make an average angle of 60.08o and 61.28o respectively with the horizontal.

At ball contact the right and left forearms were angled down 38.37° and 20.79° respectively from the horizontal. The right and left sides showed similar results both in the trunk and the forearms.

Table 2 shows the right and left hip velocities (how fast the thigh moved with respect to the trunk in 3D), right and left knee velocities, the right and left elbow velocities, and the right and left shoulder velocities (how fast the upper arm was moving away from the trunk in 3D) at ball contact. There were large differences in the right and left side velocities due to negative and positive velocities. This was dependent upon whether the ball was hit to the right or left side of the body.

Table 2. Joint angle velocity (deg/sec) at ball contact

	LH	RH	LK	RK	LE	RE	LS	RS
AVE	21.35	115.50	12.59	62.25	8.14	33.44	217.63	162.72
STD	105.58	116.05	110.87	127.86	171.59	177.46	135.52	84.73

LH=Left hip, RH=Right hip, LK=Left knee, RK=Right knee, LE=Left elbow, RE=Right elbow, LS=Left shoulder, RS=Right shoulder

The results presented in this paper may yield a greater understanding into the kinematics of the volleyball dig. This study can help the high school volleyball coach by giving a base from which they can teach. Another possible application of this information concerns injury prevention as poor mechanics often are the mechanism of injury. Similar studies need to be conducted on college and olympic males and females to give a complete database for older and more advanced players of both genders.

REFERENCES:

Bertucci, B. (1982). Championship Volleyball: By the Experts. West Point, New York: Leisure Press.

Gozansky, Sue (1987). Championship Volleyball Techniques and Drills. West Nyack, New York: Parker Publishing Company, Inc.

Keller, V. (1977). Level I: Technical Module. United States Volleyball Association.

Rosenthal, Gary (1983). Volleyball: The game and how to play it. New York: Charles Scribner's Sons.

Scates, Allen E. (1972). Winning Volleyball: Fundamentals, Tactics and Strategy. Boston, Massachusetts: Allyn and Bacon.

Slaymaker and Brown (1976). Power Volleyball. Philadelphia: W. B. Saunders Company.

Thigpen, Janet (1974). Power Volleyball. Dubuque: William C. Brown Publishers.

REGIONAL ORGANIZATION OF ADULT SCOLIOTIC SPINES

J. DIMNET, P. ROUSSOULY, L. CHEZE

In normal subjects each vertebral symmetry plane belongs roughly to the patient's sagittal plane.
Scolioses may be characterized by :

i) a change of spinal shape in frontal view ; it is clinically measured by the COBB-angle.
ii) a change of spinal shape in sagittal view.
and iii) an axial vertebral rotation which may be coupled with lateral vertebral rotation measured in frontal plane.

A great number of teams performed analytical studies in the goal of obtaining accurate location of affixed vertebral frames from two X-ray images. DIMNET et al [1] modified the X-ray protocole so that standard radiographs may be used for 3 dimensional reconstruction and measurements. STAGNARA [2] had a global approach : the spinal changes in both frontal and sagittal projections corresponded to an alteration of global vertebral structure of spines in 3 dimensional space when scolioses. A new radiographic incidence was defined showing maximum spinal curvature.

The goal of this paper is to propose a technique displaying automatically the different regions in scolioses, each region being characterized by showing the maximum regional curvature.

It is assumed that several local vertebral symmetry planes may keep roughly in a planar region, this plane being rotated and tilted versus the patient's pelvis. Planar regions are located in 3 dimensional space and their boundaries corresponding to discontinuities are computed. Local vertebral frames are projected onto corresponding regional set of axis. Then the initial hypothesis may be validated : most adult scolioses are structured in planar regions separated by angular dislocations.

Let $O_v\ X_v\ Y_v\ Z_v$ be the local set of axis. $O_v\ X_v\ Z_v$ being the symmetry plane. The regional plane $O_p\ X_p\ Z_p$ is found through a least-square method acting upon both relative location of vertebral origins O_v and relative orientation of unit vectors Y_v normal to local symmetry planes. A fitting coefficient to the regional plane is computed for each symmetry plane. If this coefficient becomes too great, the corresponding vertebra is claimed belonging to another plane. A dislocated vertebra may belong neither the lower regional plane nor the upper one.

Each vertebral frame $O_v\ X_v\ Y_v\ Z_v$ is projected onto the regional frame $O_p X_p Y_p Z_p$. The regional upper view $O_p\ X_p\ Y_p$ illustrates the fitting of the considered vertebra to regional plane, while regional frontal view $O_p\ Y_p\ Z_p$ shows the regional maximum curvature, and regional sagittal view $O_p\ X_p\ Z_p$ displays regional lordosis or kyphosis. New research findings have been validated through using CAD CATIA 3 dimensional software.

A simplified software has been specially defined for clinical use in a specialized department of a Lyon's hospital. It allows clinicians choosing by themselves the boundaries of regional planes and directly validating the assumption of regional plane organization.

A numerical file, made for each patient, includes : the simplified shape of spine in frontal and sagittal plane, the structuration of whole spine in separate planar regions and corresponding figures in 3 dimensional space, projections of vertebral frames in corresponding regional frame.

These calculations are performed before and after orthopaedic treatment or surgical operations.

When number of medical cases will be judged significant clinical analyses will be proposed.

[1] **J. DIMNET , V. DJORDJALIAN and R. GAERTNER**
A new technique of 3 dimensional reconstruction of the shape of in vivo spines using standard radiographs.
Conference at the American Society of Biomechanics
Congress URBANA-CHAMPAIGN (USA) (Sept. 1988)

[2] **P. STAGNARA**
Les déviations du rachis
Editions MASSON, Paris pp 16-18 (1984).

* Groupe de Biomécanique Fondamentale UCB Lyon 1
et Laboratoire d'Anatomie et de Biomécanique Clinique

** Centre de Réadaptation Fonctionnelle des Massues

ANALYSIS OF PHYSICAL EXERCISES RECOMMENDED FOR VDT USERS

Naomi G. Swanson and Steven L. Sauter
National Institute for Occupational Safety and Health
4676 Columbia Parkway, Cincinnati, OH 45226

Kwan Lee and A. Waikar
Dept. of Industrial Engineering, Louisiana State University
Baton Rouge, LA 70803

M. Mangum
Dept. of Physical Education, Columbus College
Columbus, GA 31993

INTRODUCTION

Widespread study of video display terminal (VDT) users has raised concerns regarding the potential for musculoskeletal disorders among these workers. A review of current literature indicates that the primary emphasis for reducing musculoskeletal strain in VDT/office work has been on improving the ergonomic design of the workstation and work environment. This approach cannot fully correct for static loading and postural constraint, which are primary stressors leading to musculoskeletal discomfort in VDT/office work. Increasingly, physical activity such as exercise breaks during the workday is being proposed as a means to offset these stressors, and a number of exercise programs which purport to reduce the discomforts arising from VDT work are now widely available. While there has been insufficient research of such exercise programs to determine their salutory effects, inspection of available programs reveals numerous characteristics which may influence their efficacy in the workplace. In the present study, exercise programs recommended for VDT users were systematically analyzed with respect to these characteristics.

METHODOLOGY

Over 100 individual exercises from 15 different exercise programs[1] were analyzed along dimensions reflecting their efficacy in terms of acceptance and performance in the workplace. These dimensions included:

---

[1] These included widely disseminated programs such as those by Austin (1984), Gore and Tasker (1986), and Krames Communications (1986), as well as lesser-known programs identified through direct contact with researchers, consultants and clinicians recognized for their work involving musculoskeletal problems in VDT use.

- specificity of instructions;
- suitability for performance at the workstation;
- potential for disruption of the work process;
- requirement for unnatural or conspicuous postures and motions;
- ease of learning and performance.

In addition, it was noted when performance of an exercise posed unanticipated safety or health risks.

RESULTS

Exercises designed for the neck and upper extremities had few attributes which would distract from their acceptance and performance in the workplace. Most were simple to perform, had clear instructions, were inconspicuous, and could be performed in a brief period without leaving the workstation. On the other hand, the majority of the exercises designed for the back, legs, shoulders and trunks were conspicuous and/or involved disruption of the work process (i.e., required standing postures or movements quite different from routine behavior). Approximately one-quarter of the exercises may present safety risks, or biomechanical demands that could aggravate pre-existing health conditions. Most of these exercises were leg and upper extremity exercises, and involved maneuvers which approached physiological limits or reproduced the biomechanical demands of VDT work. Examples include bouncing movements which may place high impact loads on the knees and ankles, and wrist hyperextension/flexion. Additionally, some of the exercises required the use of mobile office furniture as gymnastic supports.

CONCLUSIONS

On the basis of this analysis, it is apparent that some of the exercises recommended for VDT users may be more suitable than others. Ultimately, the utility of these exercises needs to be examined empirically. However, this analysis may provide some guidance for the selection of exercises appropriate to VDT/office workers until empirical data emerges.

Austin, D. Tone Up at the Terminals, Sunnyvale, CA: Verbatim, 1984.

Gore, A. and Tasker, D. Pause Gymnastics: Improving Comfort and Health at Work, North Ryde: CCH Australia Limited, 1986.

Fitness at the Terminal, Daly City, CA: Krames Communications, 1986.

A 3-D KINETIC MODEL FOR LIFTING ACTIVITIES: A GRAPHIC MICRO-COMPUTERIZED-BASED MODEL

Mohamed Zaki Ramadan

Production Engineering Department
Helwan University, Helwan, Egypt

The purpose of this paper is to present a micro-computerized model to analyse the stresses occured at the various articulations while lifting loads manually. The program obtains either measured or estimated anthropometrical data of the individual, and angular velocities accelerations from displacement input. Then, the program determines joint forces and moments including the contribution of each body segment to the whole trajectory of motion. The results are displayed numerically as well as graphically expressed in terms of X, Y, and Z coordinations. The new model proved its capability to study the relationship between posture, type of task, and stresses imposed at various joints and muscles of the human body.

THE MOTION OF THE SHOULDER JOINT DURING THE OVERHAND VOLLEYBALL SERVE

Lisa A. Schaller and Mary C. Verstraete, Ph.D.
Department of Biomedical Engineering
The University of Akron, Akron, OH 44325, USA

INTRODUCTION

The shoulder complex is probably the most challenging region of the human body to study. It has the largest range of motion and is comprised of a collection of ligaments, tendons, muscles and bones. The shoulder joint, or glenohumeral joint consists of the articulation between the head of the humerus and the glenoid cavity of the scapula, along with the associated musculotendinous structures. The shoulder girdle includes the articulations between the scapula and the clavicle. These many components contribute synergistically to control its movements and stability.

The number of studies looking at the motions of the body during volleyball is very small, with only a few of these studies analyzing the serve. The serve is just one of the skilled motions and is a form of attack. Its primary objectives are to hinder the opponent's serve-reception attack or to score an ace. The serving motion can be broken down into four stages: (1) cocking, (2) forward swing, (3) ball contact, and (4) follow-through. In the cocking stage, the upper arm is put into maximum external rotation. In the forward swing, the shoulder extends, which moves the hand over the shoulder, and the extending elbow brings the palm around to contact the ball. At the time of contact, the arm is fully extended and reaching toward the ball. In the follow-through, the arm continues its forward motion and is decelerating.

PURPOSE

The purpose of this study is to quantify the motions of the shoulder joint during the overhand volleyball serve in elite intercollegiate athletes. The results of this study will provide an anatomical description of the motion of the humerus with respect to the scapula.

METHODS

To adequately determine the position of a three-dimensional body segment in space, a minimum of three markers must be placed on the segment. This allows rigid body mechanics to be used for the analysis. For this study, six passive markers covered with "Scotchlite", manufactured by 3M, were attached to the subjects with double-sided tape. The markers were placed on bony landmarks to minimize the error induced by soft tissue motion. The marker locations were: the medial and lateral epicondyles of the humerus, the deltoid tuberosity, the acromion process, the most distal point on the spine of the scapula and the inferior angle.

The motions of the six markers were recorded using a Vicon Motion Analysis System, which was available through the Motion Analysis Laboratory at the University of Akron. Four Vicon cameras were used to capture the positions of the markers at a rate of 50 Hertz. The camera arrangement chosen ensured that each marker could be seen by at least two cameras for every instant. After data collection, the three-dimensional marker positions were computed by the Vicon software through the inclusion of the calibration data.

A total of sixteen subjects from the intercollegiate volleyball squad at the University of Akron were recruited for the study. The six markers were attached to the right shoulder joint at the predetermined bony landmarks and the subject was allowed to practice serving until they felt comfortable with the test environment. The subject was then asked to perform three "good" serves. A "good" trial was defined as a serve that felt "natural" to the subject.

RESULTS

A typical representation of the motion is shown in Figure 1. The two triangular shapes, A and B, represent the motions of the scapula and humerus, respectively, during the four stages of the volleyball serve from a view directly lateral to the subject. From Figure 1, the rotation and translation of the humerus can be clearly seen. Motions of the two segments may be identified by the following characteristics: an even spacing signifies translation, an increasing spacing shows acceleration, a decreasing spacing represents deceleration, and a change in the shape identifies either a rotation or a variation of the projection of the triangle onto the viewing plane. Future analysis will quantify the motion of the humerus relative to the motion of the scapula to provide an anatomically significant relationship. The variation in motion between the subjects will be compared in relation to both the local and global coordinate systems.

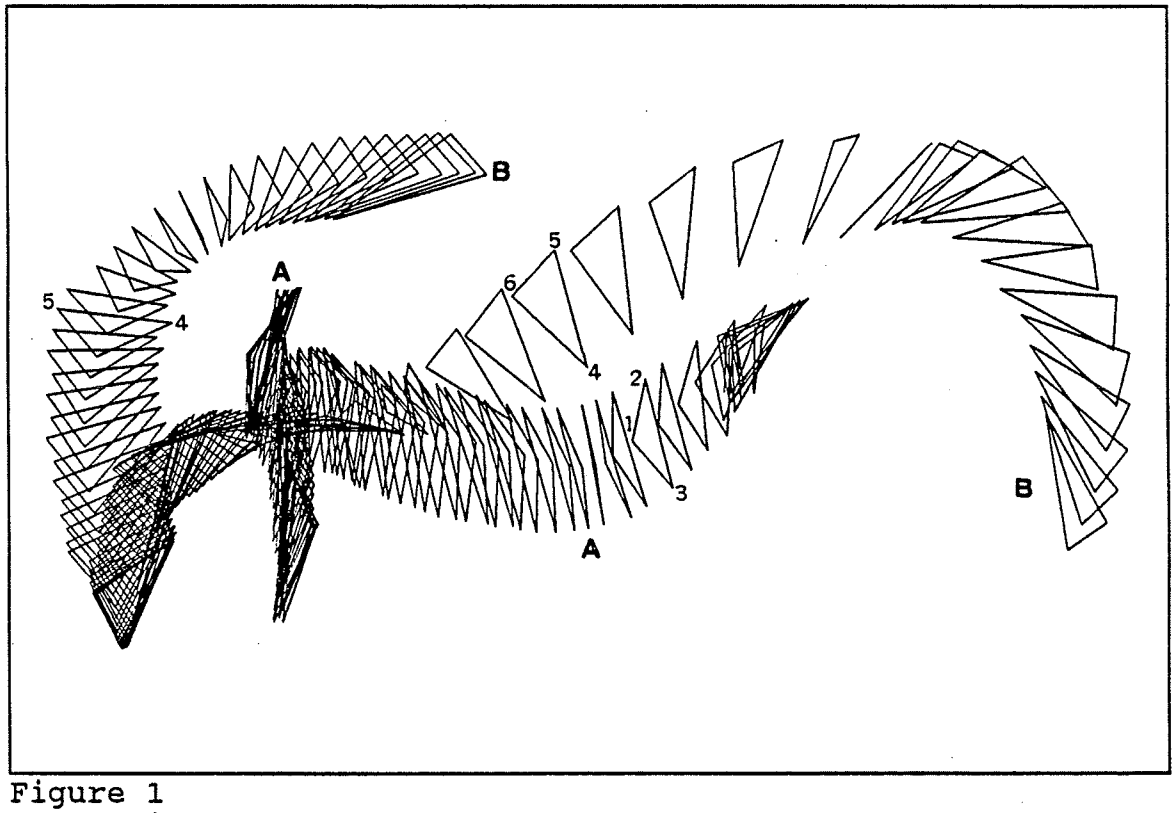

Figure 1
The motion of the scapula and humerus during the overhand volleyball serve.

A TAXONOMY FOR HUMAN DYNAMIC MUSCLE STRENGTH ASSESSMENT

Karl H. E. Kroemer, Virginia Polytechnic Institute and State University, Indus. Ergonomics Lab., IEOR Dept., Blacksburg, VA 24061-0118, William S. Marras, The Ohio State University, Industrial and Systems Engineering Department, Columbus, OH 43210, James D. McGlothlin, University of Cincinnati, Dept. of Indus. and Mechan. Engineering, Cincinnati, OH 45226, Donald R. McIntyre, Isotechnologies, Inc., Hillsborough, NC 27278, and Margareta Nordin, Hospital for Joint Diseases Orthopaedic Institute, New York, NY 10003.

The assessment of "Human Dynamic Musculo-Skeletal Performance" is of much research interest and of great practical importance in biomechanics as well as in medicine, rehabilitation, physical education, physiology, and ergonomics/human factors engineering. In the past, different terminologies, measurement strategies and exertion techniques have been used in the various disciplines. This has led to information which is tailored to the specific areas of interest, hence our knowledge about "dynamic muscle strength" is peacemeal, incomplete, incompatible, even contradictory.

The purpose of this paper is to propose and discuss a standard taxonomy for describing and assessing musculo-skeletal motor performance. For this, independent and dependent variables must be defined, and other variables controlled. In doing so, one can generate a distinct set of experimental conditions, listed in Table 1. It shows a variety of procedures that exist, or are conceivable, by which one can classify and measure human motor performance, both static and dynamic. In each procedure, a specific independent variable is manipulated, possibly accompanied by other secondary independent variables, while changes in the dependent variable(s) are measured. Current assessment techniques can be viewed as having the isometric exertion (static strength) at one end and free dynamic exertions on the other end of the performance continuum.

The table lists various possible human performance measures defined by independent and dependent experimental variables. Specifically, the variables displacement (and its time derivatives) as well as force, mass, and repetition can be assigned to be either independent, dependent, or controlled variables. For example, if one makes "displacement" an independent variable and sets it to zero, one generates the isometric testing condition, where velocity, etc. are also zero, where mass properties are controlled, and where force and/or repetition are dependent variables. By systematically assigning the other listed variables to be either independent or dependent, one generates defined conditions that are (or may be) called isokinetic, isoacceleration, isojerk, isoforce, or isoinertial. If only mass properties and/or repetitions are controlled, the "free dynamic" motor exertion exists. Yet, it is conceivable that experimental variables other than listed in the table may be selected, and be used as either dependent or independent variable. Also, control of a variable may be more complex than simply keeping it constant ("iso..."). Thus, the proposed taxonomy can be expanded as needed.

The taxonomy proposed here is one feasible way to classify muscular activities by variables, using terminology common in engineering and mechanics, which lends itself to computerization. This classification scheme should help to organize and standardize measuring approaches of dynamic musculo-skeletal performance.

Table 1. Independent and Dependent Variables in Several Techniques to Measure Motor Performance

Names of Technique / Variables	Isometric (Static)		Isokinetic		Isoacceleration		Isojerk		Isoforce		Isoinertial		Free Dynamic	
	Indep.	Dep.	Indep.	Dep.	Indep.	Dep.	Indep.	Dep.	Indep.	Dep.	Indep.	Dep.	Indep.	Dep.
Displacement, linear/angular	constant* (zero)		C or X		C or X		C or X		C or X		C or X			X
Velocity, linear/angular	O		constant		C or X		C or X		C or X		C or X			X
Acceleration, linear/angular	O		O		constant		C or X		C or X		C or X			X
Jerk, linear/angular	O		O		O		constant		C or X		C or X			X
Force, Torque	C or X		C or X		C or X		C or X		constant		C or X			X
Mass, Moment of Inertia	C		C		C		C		C		constant		C or X	
Repetition	C or X		C or X		C or X		C or X		C or X		C or X		C or X	

Legend
C = variable can be controlled
* = set to zero
O = variable is not present (zero)
X = can be dependent variable

The boxed constant variable provides the descriptive name.

RADIOGRAPHIC GRADING OF THE DISTAL FEMUR FOR THE DIAGNOSIS OF OSTEOPENIA

D. Jerássy
Univ. of Miami, Dept. of Biomedical Eng., PO 248294, Coral Gables, FL, 33146
E. Milne, S. Saitoh, G. Zych, L. Latta
Univ. of Miami, Ortho. Biomech. Lab., Mt Sinai Med. Ctr., Miami Bch, FL, 33140
Univ. of Miami, Dept. of Ortho. and Rehab., PO 016960, Miami, FL, 33101

INTRODUCTION

A subjective qualitative radiographic grading technique in the distal femur for the clinical assessment of osteoporosis was developed. Anterior-posterior (AP) plane view radiographs of formalin fixed femurs were taken. Distal grade and Singh Index were assigned to each femur. Dual-Photon Absorptiometry (DPA) was used to measure mineral content in the distal femur. Energy required to indent cancellous bone in a transverse slice of the distal femur was used to characterize mechanical strength. Significant correlations between the proposed distal grading technique versus mineral density and indention energy were demonstrated.

REVIEW AND THEORY

Osteoporosis, a common geriatric disease correlates with a higher incidence of fractures in the elderly[1]. As the degree of osteopenia increases, bone strength is reduced and it becomes more difficult to internally fix these fractures[2-5]. The alternative treatments for fracture healing require immobilization which is associated with higher rates of morbidity and mortality in the elderly[6]. A practical and accepted clinical tool for assessing the degree of osteoporosis is the Singh Index [7-9], a radiographic grading technique based on the trabecular patterns in the proximal femur. However, Singh Index is limited by poor radiographic resolution and exhibited no significant correlation to mineral content[6]. Bone density in the distal femur is easier to evaluate radiographically[10] and more consistent with systemic changes than the proximal femur[11]. This radiographic grading technique could be used as a reliable and accurate indicator of mineral density and strength of bone and an effective clinical tool in the diagnosis of degree of osteopenia. Formalin fixed and fresh femurs exhibited consistent mechanical properties[12].

The criteria for trabecular patterns used for distal grade assignment is as follows. Grade IV was assigned if the medial and lateral trabecular columns appeared normal and a dense trabecular pattern coupled them. Grade III was assigned if the columns were intact, but the coupling trabeculae were attenuated. Grade II was given if only one column was intact; and grade I, if neither column remained intact. Grades I and II consistently had markedly thinned cortices compared to Grades III and IV.

METHODOLOGY

Cadaveric femurs were graded by Singh Index proximally and by our method distally. A ten-step x-ray density standard was included with the radiographs for objective calibration of grey scale. Distal gradings by five independent observers were compared to determine repeatability and accuracy.

DUAL-PHOTON ABSORPTIOMETRY TECHNIQUE

A Lunar DPA system was used with a 2" plexiglass thickness placed underneath each bone to simulate soft tissue. The distal femur was scanned and medial, lateral and central region mineral contents were measured.

INDENTION TESTING

Starting 1 cm above the intercondylar notch and proceeding distally, two 1 cm thick transverse slices were taken from each distal femur. A Model 810 MTS was used for indention testing. The more proximal slice was positioned, distal side up, on a rigid metal platform and the five regions were determined using a standard grid. Indentions (5mm diameter) were made in each region at a constant displacement rate of 0.04 mm/sec. Load displacement curves were plotted and energy required to compress 5mm of cancellous bone was measured.

RESULTS AND DISCUSSION

Preliminary results indicated a low correlation between Singh Index and distal grade. Correlations between indention energy (joules) and distal grade were high in the posterior region (table 1). Correlations between regional mineral density (g/cm^2) and distal grade were moderate (table 2).

	L.P.	L.A.	Central	M.P.	M.A.
Distal Grade	0.615	0.014	0.187	0.748	0.373

Table 1. Correlation between indention energy and distal grade in 31 femurs.

	Lateral	Central	Medial
Distal Grade	0.462	0.580	0.570

Table 2. Correlation between mineral content and distal grade in 26 femurs.

CONCLUSION

This subjective radiographic grading method is repeatable, accurate, and a reliable indicator of mineral content and mechanical strength. A larger, more integrated database is necessary to support its clinical viability.

REFERENCES

1. Hansson et al. Acta Orthop. Scand. 53, 721.
2. Giles et al. J. Bone Joint Surg. 64A, 864.
3. Richardson et al. Trans. 32nd Ortho. Res. Soc. 11, 462.
4. Carter et al. J. Bone Joint Surg. 59A, 954.
5. Schatzker et al. Clin. Orthop. 138, 77.
6. Hubbart et al. J. Bone Joint Surg. 56B, 96.
7. Khairi et al. J. Bone Joint Surg. 58A, 221.
8. Kranendonk et al. J. Bone Joint Surg. 54A, 1472.
9. Singh et al. J. Bone Joint Surg. 52A, 457.
10. Inoue et al. J. Jpn. Orthop. Assoc. 57, 1923.
11. Ciarelli et al. Trans. 32nd Ortho. Res. Soc. 11, 42.
12. McElhany et al. J. Ortho. Physio. 19: 1234.

RELATIONSHIP BETWEEN EXPERIMENTALLY DETERMINED MUSCLE PROPERTIES OF M. QUADRICEPS FEMORIS AND JUMPING PERFORMANCE

Rudi Andries, Marc Van Leemputte and Eustachius Willems
Institute of Physical Education, Katholieke Universiteit Leuven,Tervuursevest 101, 3030 Leuven, BELGIUM.

INTRODUCTION

A great number of investigations deal with the response characteristics of muscle in well defined but artificial situations. In these experiments it is clear that a relationship exists between the mechanical output of a muscle and its length, contraction velocity and contraction history. Recent articles (Bobbert 1985, Gregor 1988) have questioned the extent to wich these muscle properties determine complex multisegmental movements. The purpose of this study is twofold: to experimentally determine the muscular properties of m. quadriceps femoris from isolated knee extensions and to compare individual differences in muscle properties with the performance in vertical jumps.

METHODOLOGY

The experiment was carried out on 20 male subjects, aged 21 to 24 years. Data were collected in two separate phases. In the first phase 8 concentric, 3 isometric and 8 eccentric contractions were performed on a computerized isokinetic dynamometer (PROMETT-system). Isometric contractions were measured at knee angles of 110, 130 and 150 degrees. Dynamic contractions were measured at 4 angular velocities: 30°/s, 100°/s, 200°/s and 400°/s. Torque exerted on the lever of the dynamometer was recorded and corrected for the moment of inertia of both lever and leg. In addition, position and velocity of the lever were monitored to mechanically constrain the velocity of the movement.

A geometrical model of m Rectus femoris and mm Vasti was designed to estimate the relative change in muscle length as a function of hip and knee angle. Estimates of the moment arm at the knee joint were taken from Hoy (1990) and were used to compute muscle forces from joint moment. The force-length and force-velocity relation of m quadriceps were determined. The dependence on contraction history was individually expressed as a percentage of the isometric maximum.

In the second phase the subjects performed 2 squat jumps, 2 counter movement jumps, 2 drop jumps starting from 40 cm height and 2 drop jumps starting from 60 cm height on a Kistler force plate. Vertical ground reaction forces were sampled (1 KHz.) and 10 mechanical parameters were calculated: the durations of impact, braking impulse, acceleration impulse and flight phase, the time to reach maximum force, the total impulse, braking impulse and acceleration impulse, the

magnitude of maximum force and the velocity at take off based on duration of flight phase. Jumping performances (maximum height) were statistically compared with the muscular properties obtained in phase 1 and the mechanical parameters obtained in phase 2. Secondly, the muscular properties were statistically compared with the mechanical parameters.

RESULTS

The muscular properties obtained in phase 1 were consistent with the expected dependence of muscle force on muscle length, contraction velocity and contraction history in m. Quadriceps femoris. The results were individually summarized by 3 parameters, namely: the mean isometric muscle force at different knee angles, the mean concentric loss and the mean eccentric enhancement at different contraction velocities.

Results of the jumps revealed the best performance for the counter movement jumps, followed by the two drop jumps. Among the correlations between the 10 parameters calculated in each jump and the jumping performance only those related with the impulse were significant (Table 1). No relationship is found between muscle force characteristics and jumping performance. However, low but significant correlations are found between these force characteristics and impulse related jump parameters.

	SQUATJUMP				COUNTERMOVEMENT			
	I	II	III	IV	I	II	III	IV
Total impulse	.76**	.48*	.46*	.42	.58**	.12	.46*	.49*
Braking impulse	--	--	--	--	.54*	.34	.44	.50*
Acceleration impulse	.78**	.48*	.45*	.41	.58**	.12	.46*	.49*
	DROPJUMP 40 cm				DROPJUMP 60 cm			
	I	II	III	IV	I	II	III	IV
Total impulse	.52**	.62**	.41	.57**	.40	.66**	.48*	.61**
Braking impulse	.18	.62**	.39	.50*	.11	.71**	.46*	.60**
Acceleration-impulse	.71**	.53*	.36	.55*	.61**	.53*	.43	.54*

Table 1 : Pearson correlations between jump characteristics and jumping performance (I), isometric force of m. Quadriceps (II), influence of concentric loss (III) and eccentric enhacement (IV). (* and ** indicate significant correlations at 5 % resp. 1 %)

REFERENCES

Bobbert MF et al. (1985). in: Current interdisciplinary research, Dordrecht: Martinus Nijhoff Publishers, 675-690.
Gregor RJ et al. (1988). J. Biomech. 21: 721-732.
Hoy GH (1990). J. Biomech. 23: 157-169.

A COMPARISON OF THE FORCES PRODUCED BY THE LATERAL AND MEDIAL HEADS OF THE GASTROCNEMIUS IN THE CAT ACROSS A CONTINUUM OF POSTURAL AND MOVEMENT DEMANDS

J. A. Tjoe, R. J. Gregor, K. L. Perell and R.R. Roy
Department of Kinesiology and Brain Research Institute, UCLA, Los Angeles, CA 90024-1568

INTRODUCTION. The medial gastrocnemius (MG) and lateral gastrocnemius (LG), in the past, have been assumed to be functionally identical with respect to load sharing among hindlimb extensors in the cat. However, the muscle heads are architecturally and histochemically different. While the LG is shorter than the MG, its individual fibers are 17.2% longer (2.45 cm for LG vs. 2.09 cm for MG). The fibers of the MG also possess larger angles of pinnation than the LG (21 degrees for MG vs. 17 degrees for LG). These architectural characteristics suggest that the LG is better designed for load contribution during high power activities such as jumping, while the MG is better suited to contribute loads during slower activities requiring high forces. Moreover, because the MG possesses the largest observed angle of pinnation in the cat, 21 degrees, it is only able to exert 93% of its potential speed and tension output at the tendon (Sacks and Roy, 1982). The LG shows only minimal or no indication of recruitment during quiet standing and slow walking, and its electromyographic (EMG) activity increases substantially as gait progresses from a slow walk to a gallop (Smith, *et al.*, 1977). EMG data support the notion of the segregation of fast and slow fibers into two muscle heads representing functional specializations matched precisely to the demands of motor behavior.

Recent presentations have reported the forces in the combined tendon of the entire gastrocnemius, but no data are available on the forces directly measured from the separate heads of the gastrocnemius within the same limb in the same animal. The purpose of this investigation was to compare the division of effort between the medial and lateral heads of the gastrocnemius with respect to the forces produced during standing, walking and jumping.

METHODS. Two adult male cats (weight = 4.65 ± 0.35 kg) were trained to walk and jump (0.62 m) within a plexiglass enclosed walkway. Tendon force transducers were implanted, under sterile conditions, on the individual MG and LG tendons, in each animal (Sherif, *et al.*, 1983)

Force recording and high speed filming occurred one week following surgery. Joint markers were placed on the iliac crest, greater trochanter, approximate knee joint center, lateral malleolus and base of the fifth metatarsal for kinematic analysis. The cat was placed in the walkway containing two concealed force platforms possessing two piezoelectric elements capable of measuring vertical and horizontal components of the ground reaction force. Limb movement was filmed at a rate of 100 fps by a camera placed orthogonal to the plane of movement. Film, tendon forces, and ground reaction forces were synchronized using a DC pulse and light in the camera field of view. Each tendon transducer was calibrated during a terminal experiment *in situ* where the buckle transducer was left undisturbed on the tendon, connected distally to a force lever. The tendon transducer output was then compared to the calibrated lever output during a series of isotonic contractions of varying intensities, and a calibration factor obtained for each transducer (Sherif, et al., 1983). Maximum tetanic tension (P_o) was also determined.

Coordinates (x,y) of skin markers were obtained from serial film frames. Each frame was projected onto a screen and limb position-time data calculated from the digitized coordinates of segment endpoint markers. Ground reaction force records were acquired on line to an IBM PC, multiplied by appropriate conversion factors, and point of force application on the paw calculated. Anthropometric data (segment mass, center of mass, and moment of inertia) were obtained for each segment using regression equations with cat mass and segment lengths as predictor variables (Hoy and Zernicke, 1985). Standard rigid body mechanics were employed to calculate the generalized muscle moment about the ankle (Fowler, *et al.*, 1989).

RESULTS AND DISCUSSION. Exemplar data are shown in Table 1 for cat 1 (weight = 4.4 kg) whose MG and LG were instrumented in separate limbs, and cat 2 (weight = 4.9 kg) whose MG was instrumented in one limb . While MG forces in cat 2 (X = 13.0 N) were slightly greater than those for cat 1 (X = 10.5 N), the average forces produced by the MG during level walking were consistently at least 62% greater than the forces produced by the LG. Moreover, the percentage of P_0 produced by the MG was greater than that of the LG during level walking. These findings are supported by previously reported data (Fowler, *et al.*, 1989), which depict the MG as being the larger contributor of the two gastrocnemius heads to the peak generalized muscle moment at the ankle during standing, level and incline walking.

During jumping, a higher demand activity, the average forces produced by the LG and MG greatly increased and were nearly identical. However, the maximum tetanic tension produced by the LG (108 N) was greater than that produced by the MG (93.2 N). Hence, the remaining resources available to the muscle for recruitment, expressed as a percentage of P_0 appear greater for the LG (a reserve of 17.4% of P_0 for LG vs. a reserve of 4.0% of P_0 for MG). These findings are consistent with the architecture and histochemical profile differences of the two heads of the gastrocnemius muscle in the cat.

Table 1. Muscle forces, percentages of maximum tetanic tension, and ground reaction forces for two cats during walking and jumping.

	WALKING			JUMPING		
	Muscle Forces (N)	$\%P_0$ (%)	GRF (N)	Muscle Forces (N)	$\%P_0$ (%)	
$LG_{cat\ 1}$	6.3	5.8	6.4	$LG_{cat\ 1}$	91.5	84.7
$LG_{cat\ 1}$	6.6	6.1	7.8	$LG_{cat\ 1}$	88.1	81.6
	X = 6.5	X = 6.0	X = 7.1	$LG_{cat\ 1}$	88.6	81.5
					X = 89.4	X = 96.0
$MG_{cat\ 1}$	9.8	10.5	7.4			
$MG_{cat\ 1}$	11.2	12.0	9.3			
	X = 10.5	X = 11.3	X = 8.4			
$MG_{cat\ 2}$	10.0	7.2	21.5	$MG_{cat\ 1}$	86.1	92.4
$MG_{cat\ 2}$	18.1	13.0	21.2	$MG_{cat\ 1}$	90.0	96.6
$MG_{cat\ 2}$	14.9	10.7	21.3	$MG_{cat\ 1}$	92.3	99.1
$MG_{cat\ 2}$	8.8	6.3	18.7		X = 89.5	X = 82.6
	X = 13.0	X = 9.3	X = 20.7			

REFERENCES

Fowler, E. G., Gregor, R. J., Hodgson, J. A., Roy, R. R., and Broker, J. P. (1989). The Contribution of Individual Muscles to the Ankle Moment Produced in the Cat Hindlimb. *J. Biomechanics. 22*:1011.

Hoy, M. G. and Zernicke, R. F. (1985). Modulation of Limb Dynamics in the Swing Phase of Locomotion. *J. Biomechanics. 18*(1): 49-60.

Sacks, R. D. and Roy, R. R. (1982). Architecture of the Hindlimb Muscles of Cats: Functional Significance. *J. Morphol. 173*:185-195.

Sherif, M. H., Gregor, R. J., Liu, L. M., and Roy, R. R. and Hager, C. L. (1983). Correlation of Myoelectric Activity and Muscle Force During Selected Cat Treadmill Locomotion. *J. Biomechanics. 16*(9):691-701.

Smith, J. L., Edgerton, V. R., Betts, B., and Collatos, T. C. EMG of Slow and Fast Ankle Extensors of Cat During Posture, Locomotion, and Jumping. (1977). *J. Neurophysiol.* 40(3):503-513.

THE PRIMORDIAL STRUCTURE

Stephen M. Levin
Potomac Back Center, 5021 Seminary Road, Alexandria, VA 22311

INTRODUCTION

Structure defines biology. From DNA, to drosophila, to diplodocus a biologic entity is dependent on its structure for its function. The mechanical forces that shape clusters (Duncan and Rouvray, 1986), DNA, proteins, subcellular structures, flora and fauna, vertebrates and invertebrates are constant and invariable. That whitch is true for the macro is true for the micro and vice versa. In evolution, mechanics and structure are integral, form follows function and each structure evolved from a previous construct. For every structure there is an homologous structure that preceded it. Homologous structures, the arm of a man, the wing of a bat, the leg of a horse, are structurally and mechanically related to some preceding form, as well as to each other. In both evolution and embryonic development each physical structure develops from a previously existing structure that rigidly obeys natures mechanical laws. At any point in time a structure exists only if it can physically exist. Escher-like constructions that can only exist on paper or in the mind of a computer are intolerable to mother nature.

REVIEW AND THEORY

There are only three naturally existing structures as only fully triangulated constructs are inherently stable (Fuller, 1975). They are the tetrahedron, the octahedron and the icosahedron. All biologic constructions must be some combination or permutation of these structures. The icosahedron is the most efficient volume per unit of structural material. It is also the most efficient volume controlling device of nature and the most suitable for biologic constructs.

Closely linked with structural evolution is the concept of close-packing of spheres. Architects(Pearse, 1978), physicists (Weare and Rivier, 1984; Kroto, 1988), and biologists (Pyshnov, 1980) recognize this concept as a fundamental element in the development of self generating structures. Close-pack four spheres as a cluster and the stable configuration is a tetrahedron. Eight spheres pack as an octahedron, and twelve spheres around a smaller thirteenth, or an empty space, generate an icosahedron [Fig. 1]. More spheres will only close pack as stable clusters when their outer shell is some frequency of an icosahedron, forty-two, ninety-two etc.. Any other configuration is unstable and cannot exist as a structure. To be consistent with the second law of thermodynamics nature would continually seek the lowest energy configuration, always tending toward the tetrahedral-icosahedral form. Icosahedra can be linked by mechanical bonding so that a chain of icosahedra may function as one icosahedron. This would allow for an infinite variety of shapes built from icosahedra as the finite element but still conforming to the laws of close-packing and of structure.

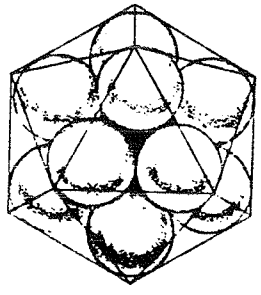

Fig. 1. Twelve spere close-packed icosahedron.

There is a variation of the icosahedron where the compression elements internalize as an endoskeleton (Snelson, 1965). Six compression struts separate the twelve vertices of the icosahedron with none of the struts passing through the center or touching one another[Fig. 2]. The compression elements "float" within a tension outer shell. These, too, can be linked through several mechanisms to form an infinite variety of forms with an internalized, floating, endoskeletal system held together by a continuous tension outer shell [Fig. 3]. Each sub-unit icosahedron can function as an independent icosahedron or as part of an ever increasing icosahedron in a hierarchical pattern. Vertices,

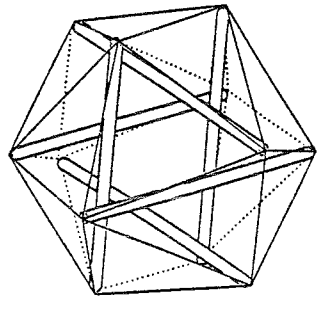

Fig. 2. Endoskeletal icosahedron.

tension elements, or compression elements, may be shared so that icosahedra may nest within one another. The patterns that develop, three dimensional tiling, would be best formulated as fractals (Mandebroit, 1983; Barnesley et al., 1987).

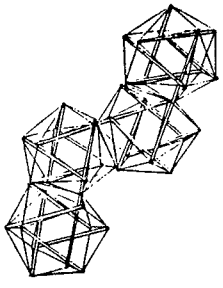

Fig. 3. Linked icosahedra.

RESULTS AND DISCUSSION

Many biologic entities are already recognized, or are easily recognizable as conforming to this structural pattern. The proteins of viruses close pack as icosahedra. The intracellular structure, clathrin, the cell wall of leukocytes, many amoebae, the marine organisms radiolaria and volvox, the compound eyes of insects, alveoli of lungs, fat cells, and puff balls of dandelions are all icosahedral structures. Amino acids, proteins such as DNA and similar structures must conform to these patterns as well.

The Mechanics of endoskeletal, tension-shell icosahedra are apparently unique. When loaded the whole structure shrinks or expands and so becomes more or less dense as a factor of the square of the radius. This produces a non-linear stress-strain curve. This type of curve is very common, if not a *sine qua non*, in biologic structures (Gordon 1978).

With the icosahedron as the primordial structure and finite element we can build clusters of sub-cellular aggregates, cellular structures that in higher frequencies could hollow out blastomere or vesicle like, and complex organisms that can evolve phylogenetically and/or embryologically with exo or endo skeletons. The same structure would demonstrate hierarchical constructs that are least energy structures, stable with flexible hinges and have non-linear mechanical behavior. Soft bodied structures such as earthworms, frogs tongues and elephants trunks, would utilize the incompressible property of fluids as the compression resisting elements of the icosahedra. Internally vectored endoskeletal icosahedra would model the neck of a swan, the knee of an ostrich or cat, the tail of a monkey, which could be rigid at one instant of time, flexible the next, always maintaining its lowest energy state [Fig. 4].

As are other fractal constructions the icosahedral structures would be self-generating, self-organizing, self-similar and recursive non-linear dynamical systems, ideally suited for biologic modeling. Since it is the least energy system there is no need for multiple systems to explain biologic evolution or structure.

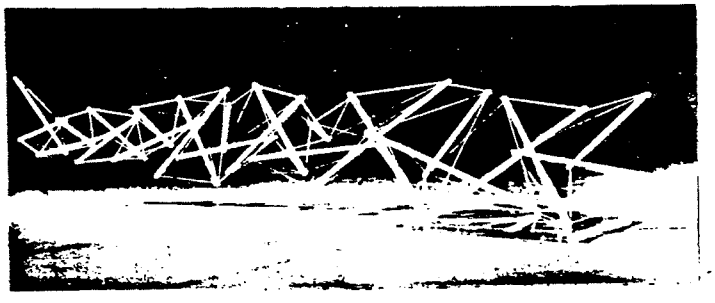

Fig. 4. Model for Easy K. (Snelson)

REFERENCES

Barnesley, M. P., Massopust, P., Strickland, H. and Sloan, A.D. (1987) Fractal modeling of biologic structures. *Annals of the New York Academy of Science* **504**:179-194.

Duncan, M.A., Rouvray, D.H. (1986)Microclusters. *Scientific American* **261**, 110-115.

Fuller, R.B. (1975) *Synergetics* 314-431. McMillan Publishing Co., New York.

Gordon, J.E. (1978) *Structures*. Harmondsworth: Penguin Books, London.

Kroto H. (1988) Space, stars, C60, and soot. *Science* **242**:1139- 1145.

Mandelbrot, B.B. (1983) *The fractal geometry of nature*. Wm. Freeman & Co. San Francisco.

Pearce, P. (1978) *Structure in nature as a strategy for design*. MIT Press, Cambridge, MA.

Pyshnov, M.B. (1980) Topological solution for cell proliferation in intestinal crypt. *Journal of Ther. Biol.* **87** 189-200.

Snelson, K. (1965) Discontinuous compression structures. *U.S. Patent* #3169611.

Weaire, D. and Rivier, N. (1984) Soap, cells and statistics. *Contemp. Phys.* **25** 59-99.

SURFACE-HEPARINIZATION AND TEMPORARY PLATELET INHIBITION PRESERVE PLATELETS DURING EXTRACORPOREAL CIRCULATION

George M. Palatianos, M.D.
University of Miami School of Medicine
Miami, Florida

INTRODUCTION

In an effort to produce non-thrombogenic artificial surfaces heparin has been bonded with several techniques onto various biomaterials. Surface-heparinization, however, in extracorporeal circulation systems, has not resulted in complete platelet preservation. To evaluate the effect of surface heparinization on platelet consumption during cardiopulmonary bypass (CPB) 8 pigs with platelets labeled with Indium-111 were placed on CPB. Improved platelet preservation was found in pigs which received the platelet inhibitor Iloprost (ZK36374).

REVIEW AND THEORY

Gott et al reported heparin binding to colloidal graphite surfaces in 1963. Since then surface heparinization has been tested in several extracorporeal circulation models (2-4). Improved platelet preservation and prevention of thrombosis were observed during two-hour perfusion with a surface-heparinized left ventricular assist device in non-heparinized sheep receiving Prostacyclin (PGI 2) (5). In this pilot study we tested the hypothesis that surface-heparinization in combination with temporary platelet inhibition could preserve platelets during extracorporeal circulation with a hollow-fiber membrane oxygenator.

METHODOLOGY

Eight healthy adult female Yorkshire pigs were anesthetized with ketamine hydrochloride (20 mg/kg i.m.) and sodium pentothal (5-7 mg/kg i.v.), were intubated and ventilated with a Harvard ventilator. Anesthesia was maintained with 0.25% sodium pentothal. Arterial pressure, heart rate and electrocardiogram were continuously monitored. CPB (right atrium to ascending aorta) was established via a median sternotomy, with a barely occlusive roller pump, a hollow-fiber membrane oxygenator (HFMO, Bentley CM-50) and an arterial filter (AF, Bentley 1025). All components of the CPB system in each pig were surface-heparinized with Duraflo-II (TM) heparin coating complex (Baxter/Bentley Laboratories, Irvine, CA). Four pigs were systemically heparinized prior to cannulation for CPB (Group A). Their Activated Coagulation Times were maintained longer than 400 sec throughout CPB. In the remaining 4 pigs (group B) heparin was not administered; instead, the prostacyclin analog Iloprost (ZK36374) (Berlex Laboratories, Cedar Knolls, NJ) was infused at 1 ng/kg/min beginning 30 min prior to CPB and lasting

throughout CPB (7). All pigs had their platelets labeled with Indium-111 the day before CPB (8). At 3 hours of extracorporeal circulation, CPB was terminated and the pigs were sacrificed by exsanguination. The CPB system was disconnected from each pig, was drained and flushed with 1 litter of Plasma-Lyte (Travenol Laboratories, Deefield, IL) with a very low pump rotation. Platelet deposits in HFMO, AF, tubing, cannulas, and reservoir were imaged with a gamma camera (Siemens, Gammasonics V, LFOV, Des Plains, IL). The percentage of injected radioactivity in the various components of the CPB system were calculated with a Lotus 123 and an IBM-PS/2 computer (8).

RESULTS AND DISCUSSION

Platelet counts decreased by 34.4% of control value at 3 hours of CPB in group A pigs, whereas in group B pigs a 2.3% (mean) reduction was noted. There was no significant difference in intraoperative bleeding between the two groups. Percentage of injected radioactivity (mean $\pm$ SD) in components of CPB system is presented in the following table.

TABLE

Component	Group A (n=4)	Group B (n=4)	p
HFMO	3.11 $\pm$ 1.82	0.65 $\pm$ 0.67	0.057
AF	0.76 $\pm$ 0.37	0.31 $\pm$ 0.16	0.11

Minimal radioactivity was traced in the remaining components of CPB system (cannulas,tubing, reservoir).

Preservation of platelet counts and minimal platelet deposition in the HFMO were observed during CPB with surface-heparinized extracorporeal perfusion systems, especially in the pigs which were receiving Iloprost. Improvement in platelet inhibition in combination with surface-heparinization may prevent thrombosis and coagulation in extracorporeal perfusion systems without systemic heparinization.

REFERENCES

1. Gott VL et al, Science 142:1297-1298,1963.
2. Merker RL et al, U.S. Government Printing Office PB 188548, 1969.
3. Grode G et al, U.S. Government Printing Office PB 195727, 1970 and PB 205475, 1971.
4. Larson R et al, Thromb Res 19:43-54,1980.
5. Palatianos GM et al, Ann Thorac Surg 35:504-515, 1983.
6. Toomasian JM et al, Trans Am Soc Artif Intern Organs 34:410-414, 1988.
7. Schrör K et al, Naunyn-Schmiedeberg's Arch Pharmacol 316:252-255, 1981.
8. Palatianos GM et al, Trans Am Soc Artif Intern Organs 35:667-670, 1989.

AUTHOR INDEX